Evolution of an active metamorphic core complex, Suckling-Dayman Massif, eastern PNG

by Peter Caffi, BSc

Farewell Dance from Biniguni Village, Milne Bay Province, PNG.

Presented to the Department of Earth and Planetary Sciences,
Division of Environmental and Life Sciences
in Partial Fulfilment of the Requirements
for the Degree of

Honours, BSc

Macquarie University, Sydney

June, 2008

Statement of Originality

All the work submitted in this thesis is the original work of the author except where otherwise acknowledged. No part of this thesis has been previously submitted to any other university or institution.

Signed:

Peter Caffi

Date:

Dedication

To the people of Pumani and Biniguni.

Acknowledgements

First and above all, I would like to thank my supervisor, Nathan Daczko. His dedication to this project has been admirable. His help has been invaluable, his enthusiasm, a driving force and his patience beyond belief. He sacrificed many nights and week-ends to accommodate my time schedule to make sure that I was on the right track and on time. During the field work in Papua New Guinea he endured an ulcerated oesophagus and malaria to allow me to collect all the information necessary for my project. I will always be indebted for the opportunity that he gave me to participate in such a project in such an amazing place, and I am glad to have shared this experience in the jungle of PNG with him. Nathan, thank you.

I would like to thank the following people: Stephanie Carroll for her help in the field; Nicole Harb for her assistance with the SEM at the Electron Microscopy Unit at Sydney University; Steve Craven, Manal Bebbington and Luke Milan from Macquarie University and Rad Flossman from The University of NSW for their support in the production of thin sections; Luke Strotz, Briony Mamo and Tony Allan (CSIRO) for assisting with the palaeontologic specimens; Paul Mann from The University of Texas Institute for Geophysics for his assistance and manipulation of SRTM data and Melissa Murphy for providing the ^{206}Pb-^{238}U dating.

I thank all the people involved in the review and editing of this thesis: Nathan Daczko, Dick Flood, Kelsie Dadd and Mark Lackie.

A special thankyou goes to all the people that believed in me, supported and tolerated me: my beautiful friends, Angela and Leo, for their unbelievable and unshakable belief in me; my dearest friend, Pip, for his unconditional support; to Vincenzo and Dalia for their enthusiastic support, and all the people at AC Butchery, in particular, Carlo, Angela, Jo, Brian, Sara and Primo for putting up with me during my undergraduate study.

Finally, I want to thank my fantastic wife, Laura, who has been my greatest believer, supporter and the most patient of all. She endured all the tough times with composure and understanding and took care of the household to allow me to concentrate on my studies. Laura helped me to remain focused when my mind was wandering. These five lines do not do justice to what she really meant for me. I will be forever grateful.

Abstract

A shallow-dipping ductile mylonitic shear zone is the dominant geological structure that controls the orientation of dip slopes on the flanks of Mount Dayman, eastern Papuan Peninsula, Papua New Guinea. The dip slopes dip in all directions from the peak of Mount Dayman and form a domed landform that is much less dissected by streams compared to the adjacent Mount Suckling domed landform. The orientation of megamullions on the domed surface of Mount Dayman is consistent with NNE-directed transport of the hanging wall block. Though previously documented as a thrust surface, the geometry and style of structures and map relations presented in this study indicate an extensional origin for the domed mylonitic foliation (S1) and mineral stretching lineation (L1). The field relationships are consistent with the domed landform comprising the core of a kilometre-scale metamorphic core complex. Observations of dominantly NNE-trending regional lineaments in aerial photography and shuttle radar topography mission (SRTM) data correlate with detailed field analysis of mineral stretching lineations (L1) in the main metamorphic core complex-bounding shear zone. Field relationships show a cross cutting sequence of structures that includes: (i) ductile S2 folia with ESE-plunging riebeckite mineral stretching lineations; (ii) narrow steeply dipping ductile D2 shear zones; and (iii) semi-brittle to brittle fault zones. S-C' fabrics, mantled porphyroclasts and fault drag indicate a top down to the NNE sense-of-shear for most structures. Kinematic vorticity analysis of the highest-grade ductile deformation indicates a kinematic vorticity number (Wk) between 0.34 and 0.56, suggesting general shear for the early stage of deformation (D1). Metamorphic mineral assemblages of the metabasite ductile mylonitic rocks record greenschist facies conditions. The presence of pumpellyite-actinolite facies assemblages in the core of the complex indicates peak metamorphic pressures of 6-9.5 kbar, demonstrating exhumation of the core from 20-30 km depth. The NNE-directed structural lineaments and L1 mineral stretching lineations are consistent with the Australia-Woodlark Eulerian pole for periods between 0.52-3.6 Ma. This observation is consistent with 3.3 Ma granite and monzonite intrusions that cut the mylonitic fabrics and limit the age of the mylonitic fabrics to older than 3.3 Ma. A SE dipping sedimentary sequence (Gwoira Conglomerate) characterises the hanging wall of the metamorphic core complex. Petrography of the clasts within the sedimentary rocks indicates that metabasite rocks were the dominant source. The unit is in fault contact with the metabasite footwall across prehnite-bearing D3 brittle fault zones. The rotation direction of bedding is consistent with NW-directed extension as predicted by the 0-0.52 Ma Australia-Woodlark Eulerian pole.

Table of Contents

Chapter 1 INTRODUCTION 1

1.1 Tectonic setting of Eastern Papua 1

1.2 The Suckling-Dayman Massif 4

1.2.1 Geomorphology 4

1.2.2 Metamorphic geology 6

1.2.3 Structural geology 8

1.3 Neighbouring localities 9

1.4 Geological synthesis 9

1.5 Objectives of the project 10

Chapter 2 REMOTE SENSING: Aerial Photographs, Google Earth and Shuttle Radar Topography Mission (SRTM) Data 11

2.1 Introduction 11

2.2 Aerial Photographs 11

2.3 Google Earth™ images 13

2.4 Shuttle Radar Topography Mission (SRTM) data 16

2.5 Discussion 20

Chapter 3 FIELDWORK: Logistics and Methodology 24

3.1 Introduction 24

3.2 Logistics 25

3.3 Methodology 26

3.3.1 Pumani 26

3.3.2 Biniguni 28

Chapter 4 SEDIMENTARY GEOLOGY: Gwoira Conglomerate 31

4.1 Introduction 31

4.2 Regional setting 32

4.3 Gwoira Conglomerate 32

4.3.1 Pebble/cobble breccia 36

4.3.2 Sandstone 39

4.3.3 Mudstone 44
4.3.4 Fossiliferous sandstone and limestone 44
4.3.5 Quaternary alluvium 48
4.5 Mineral chemistry 48
4.6 Discussion 52
Chapter 5 STRUCTURAL GEOLOGY 56
5.1 Introduction 56
5.2 Ductile shallowly dipping S1 and S2 fabric 56
5.2.1 Pumani: East flank of Dayman Dome 57
5.2.2 Biniguni: North flank of Dayman Dome 57
5.2.3 Kinematics 61
5.2.4 Kinematic vorticity 65
5.3 Narrow steeply dipping S2 shear zones 67
5.4 Folds and semi-brittle to brittle overprint 67
5.5 Veins 69
5.6 Dykes 69
5.7 Gwoira Conglomerate 73
5.8 Discussion 78
Chapter 6 METAMORPHIC GEOLOGY 81
6.1 Introduction 81
6.2 Ductile shallowly dipping S1 and S2 fabric 81
6.2.1 Pumani: East flank of Dayman Dome 83
6.2.2 Biniguni: North flank of Dayman Dome 83
6.3 Narrow steeply dipping S2 shear zones 86
6.4 Folds and semi-brittle to brittle overprint 86
6.5 Veins 89
6.6 Dykes 89
6.7 Mineral Chemistry 93
6.8 Discussion 96
Chapter 7 DISCUSSION and CONCLUSIONS 102
7.1 Geological Synthesis 102

7.2 Conclusions 109

7.3 Directions for Further Research 109

References **111**

Appendices

Appendix A: Aerial Photographs and SRTM Structural Measurements

Appendix B: Sample Locations, Lithologies and Catalogue Numbers

Appendix C: Electron Microprobe (EMP) Data

Appendix D: Field Structural Measurements

Appendix E: Vorticity Measurements

Figures

1.1 Tectonic Setting of Eastern Papua New Guinea 2

1.2 Geological Map of Suckling-Dayman Massif 5

2.1 Aerial Photograph Interpretation 12

2.2 Google Earth™ Image of Dayman and Suckling Domes 14

2.3 Google Earth™ Image of Gwoira Conglomerate 14

2.4 Google Earth™ Image of Dayman Dome Looking South 14

2.5 Google Earth™ Image of Dayman Dome Looking Southwest 15

2.6 Google Earth™ Image Between Dayman and Suckling Domes 15

2.7 Google Earth™ Image Between Dayman and Suckling Domes 15

2.8 Google Earth™ Image of Dayman Dome and Biman Dip Slope 17

2.9 Google Earth™ Image of East Flank of Dayman Dome 17

2.10 Google Earth™ Image of Southeast Flank of Dayman Dome 17

2.11 Google Earth™ Image of South Flank of Dayman Dome 18

2.12 SRTM Image of the Dayman Dome 18

2.13 SRTM Image of the Dayman Dome with Profiles 19

2.14 SRTM Image of the Dayman Dome and Rose Diagram 21

3.1 Location of Rivers and Creeks in the Area of Study 27

3.2 Oriented Sample 30

4.1 View of the Gwoira Conglomerate Looking Southwest 33

4.2 View of the Gwoira Conglomerate and Biman Dip Slope 33

4.3 View of the East Flank of Dayman Dome 33

4.4 View of Mt. Gwoira 34
4.5 Google Earth™ Image of the Gwoira Fault 34
4.6 Erosion Pattern of the Gwoira Conglomerate 34
4.7 View of the Gwoira Conglomerate Looking South 35
4.8 Location of Rivers and Creeks in the Pumani Area 35
4.9 Breccia in the Gwoira Conglomerate 37
4.10 Interbedded Breccia and Sandstone 37
4.11 Metabasalt Clast in Breccia 37
4.12 Paraconglomeratic Breccia in the Gwoira Conglomerate 38
4.13 Photomicrographs of Blastogabbroic Texture 38
4.14 Photomicrographs of Blastodoleritic to Blastobasaltic Texture 38
4.15 Mylonitised Cobble in the Gwoira Conglomerate 40
4.16 Photomicrographs of Granophyric Texture 40
4.17 Photomicrographs of Clinopyroxenite Clast in Breccia 40
4.18 Photomicrographs of Reworked and Rounded Mudstone Clast 41
4.19 Photomicrographs of Metabasite Rock Fragments 41
4.20 Back-Scattered Electron (BSE) Images of Metabasite Rock 42
4.21 Stratigraphic Log of Sedimentary Rock 43
4.22 Sandstone Beds in the Gwoira Conglomerate 43
4.23 Lens of Mudstone in Breccia 45
4.24 Mudstone of Gwoira Conglomerate 45
4.25 Concretion in Mudstone of the Gwoira Conglomerate 45
4.26 Concretion with Laminations 46
4.27 Back-Scattered Electron (BSE) Images of Sample 0617A 46
4.28 Fossiliferous Coral in Dare Creek 47
4.29 Fossiliferous Coral in Dare Creek 47
4.30 Photomicrographs of Blastobasaltic Texture 47
4.31 Echinoderm Spine in the Gwoira Conglomerate 49
4.32 Photomicrographs of Benthic Foraminifera Fossils 49
4.33 Coralline Red Algae in the Gwoira Conglomerate 50
4.34 Back-Scattered Electron (BSE) Images of Fossils 50

4.35 Unconsolidated Quaternary Alluvium, Dare Creek 51
4.36 Shallow Cross-Bedding in Unconsolidated Quaternary Alluvium 51
4.37 Mineral Chemistry Classification Plots (Sedimentary Ch) 53
5.1 Equal Area, Stereograms for S1, L1 and S2, L2 of Dayman Dome 58
5.2 Foliation Planes and Shear Bands, Aro Creek 58
5.3 Narrow bands of Blue Amphibole (riebeckite), Yatap Creek 59
5.4 Elongate and Aligned Blue Amphibole, L2, Biyawap Creek 59
5.5 S2 Foliation Plane and Blue Amphibole that Defines L2, Biyawap Creek 59
5.6 S1 Foliation Planes, Biniguni River 60
5.7 S1 Foliation Plane and L1, Biniguni River 60
5.8 S1 Foliation Plane and L1, Gwariu River 60
5.9 Schematic Diagram of Mylonite Shear Zone and Nomenclature 62
5.10 Shear Bands (C'-Planes), Ampae Creek 63
5.11 Shear Bands (C'-Planes), Yatap Creek 63
5.12 Lenticular Shaped Parts of the Outcrop Enveloped by Foliation 63
5.13 Photomicrograph of Sigma Type Mantled Porphyroclast 64
5.14 Photomicrograph of Quartz Antitaxial Fibrous Overgrowths 64
5.15 Photomicrograph of Actinolite 'Fish' 64
5.16 Kinematic Vorticity 66
5.17 S2 Shear Zone, Biniguni River 68
5.18 S2 Shear Zone, Ampae River 68
5.19 Photomicrograph of Steeply Dipping S2 Folia 68
5.20 Gentle Fold of S1, Yuga Creek 70
5.21 Open Fold of S1, Gwariu Creek 70
5.22 Equal Area, Stereograms for Folded S1 and L1 Data 70
5.23 Photomicrograph of Crenulated S1 71
5.24 S3 Semi-Brittle to Brittle Fault Zone, Pumani River 71
5.25 Prehnite (prh) and Epidote (ep) Veins in S3 Fault Zone, Pumani River 71
5.26 Photomicrograph of Grain Scale Fault 72
5.27 S2 Shear Zone Filled with Veins, Ampae Creek 72
5.28 Photomicrograph of Boudinaged Vein 72

5.29 Mafic Dykes that Cut S1, Biniguni River 74
5.30 Mafic Dykes Showing Lacks of Chilled Margins, Biniguni River 74
5.31 Equal Area, Stereograms for S1, L1 and Dykes 74
5.32 Mafic Sill that Cut S1, Gwariu Creek 75
5.33 Equal Area, Stereograms for S0 75
5.34 Google Earth™ Image of Gwoira Conglomerate with Fault and S0 75
5.35 Brittle Normal Fault Cutting S0, Kwekweme Creek 76
5.36 Oxidised Brittle Fault Zone, Dare Creek 76
5.37 Brittle Fault Zone Cutting Gwoira Conglomerate, Sisipoa Creek 76
5.38 Equal Area, Stereograms for Fault Planes and Slikensides 77
5.39 Equal Area, Stereograms for S1 from Davies and Smith (1974) 77
6.1 Photomicrograph of Coarse Grain S1, Sample 0668A 82
6.2 Photomicrograph of S2 bands of Blue Amphibole 82
6.3 Photomicrograph of S1, Sample 0629 82
6.4 Photomicrograph of S1, Sample 0605 84
6.5 Back-Scattered Electron (BSE) Images, Sample 0605 84
6.6 Photomicrograph of S1 with Albite Ribbons, Sample 0668A 85
6.7 Photomicrograph of S1, Sample 0677G 85
6.8 Photomicrograph of a Optically Zoned Epidote 85
6.9 Photomicrograph of a Epidote Mineral Cluster 87
6.10 Photomicrograph of S2, Sample 0677A 87
6.11 Photomicrograph of Fine Grain Gauge 87
6.12 Photomicrograph of F2 Folds of S1 88
6.13 Photomicrograph of Axial Planar Microfault with Epidote 88
6.14 Photomicrograph of Epidote and Prehnite 88
6.15 Photomicrograph of Fine Grain Gauge in Fault Zone 90
6.16 Photomicrograph of a Pre- to Sin-S1 Quartz 90
6.17 Photomicrograph of. A Folded Calcite 90
6.18 Photomicrograph of Partially Recrystallised Calcite 91
6.19 Photomicrograph of a Post-S1 Calcite 91
6.20 Photomicrograph of a Multiple Generation of Veins 91

6.21 Photomicrograph of a Partially Recrystallised Dyke 92
6.22 Photomicrograph of a Fine-Grained Domain within the Dyke 92
6.23 (a-d) Mineral Chemistry Classification Plots (Metamorphic Ch) 94
6.23 (e-g) Mineral Chemistry Classification Plots (Metamorphic Ch) 95
6.24 Distribution of Metamorphic Facies and P-T Diagram 97
6.25 Geological Map and Metamorphic Zone of Suckling-Dayman Massif 99
7.1 Schematic Cross Section of the Evolution of the Suckling-Dayman Massif 108

Table

2.1 Euler Poles for Woodlark Basin Seafloor Spreading 23

Chapter 1 INTRODUCTION

1.1 Tectonic setting of Eastern Papua

The Eastern Papuan region (Fig. 1.1) is characterised by a series of interacting microplates related to the oblique collision of the Indo-Australian plate and the Pacific Plate (Fig. 1.1; Davies and Smith, 1971; Baldwin *et al*., 1993). Two important tectonic events shaped the current geology: (i) a Palaeogene collisional event between Papuan continental crust and a magmatic arc to the north that resulted in obduction of the Papuan Ultramafic Belt (PUB) over the Owen Stanley Metamorphic belt (Fig. 1.1a), and (ii) a Pliocene extensional event that initiated the development of a sequence of metamorphic core complexes (MCC) that characterise eastern Papua (Baldwin *et al*., 1993: Martinez *et al*., 2001).

The Palaeogene arc-continent collision thickened continental crust in large part by overthrusting the PUB (Davies, 1980; Davies and Jaques, 1984) and led to the deep subduction of continental crust (>100 km; Baldwin and Ireland, 2005). Subduction stalled following the attempted subduction of buoyant felsic material of the Australian plate margin and the convergence was subsequently taken up in the newly formed New Britain arc (Davies and Jaques, 1984). Subsequent extension in eastern PNG during the Early Miocene exhumed the deeply subducted Australian margin in MCC of the D'Entrecasteaux Islands that are correlated to sialic units of the Owen Stanley metamorphic belt from the Papuan Peninsula (Baldwin *et al*., 1993). The Suckling-Dayman Massif on the peninsula represents an exhumed less deeply subducted part of the failed subduction system (Davies, 1980). The uplift of the massif accompanied a reversal of movement in the former subduction system (Davies and Jaques, 1984). The emplacement of granite such at those exposed in the cores of the Suckling or Goodenough Island domes may have contributed to driving uplift of the MCC (Davies and Warren, 1988).

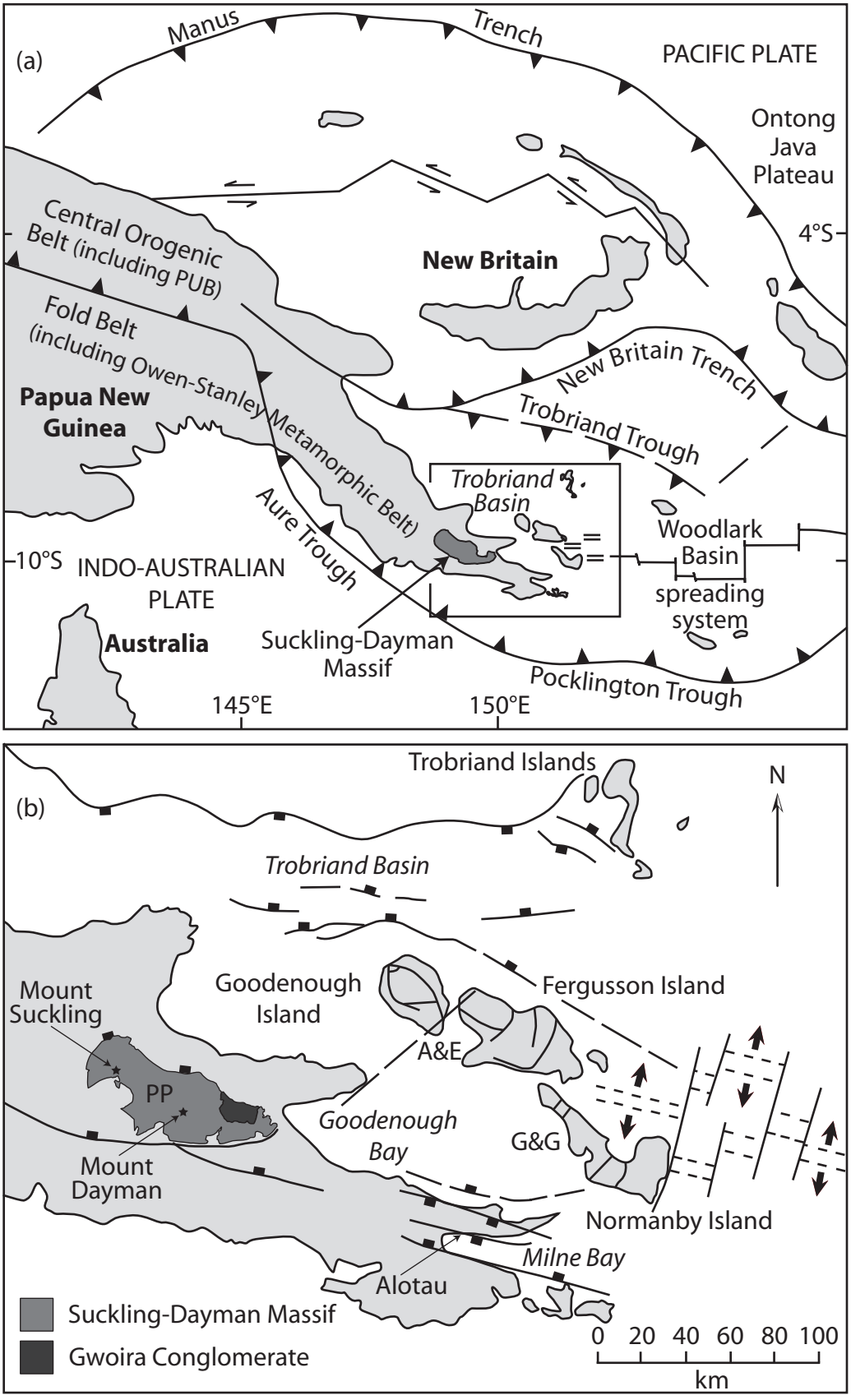

Figure 1.1 (a) Regional tectonic setting of Eastern Papua New Guinea. (b) Detailed map of Eastern Papua New Guinea and the D'Entrecasteaux Islands (Goodenough, Fergusson and Normanby). PP – Prehnite-Pumpellyite; A&E – Amphibolite and Eclogite; G&G – Granulite and Greenschist facies (modified from Hill and Baldwin, 1993).

Recent seismic activity indicates that the region around the D'Entrecasteaux Islands is presently undergoing N-S extension and seafloor spreading full rates of 6 cm/yr are recorded in the Woodlark Basin seafloor to the east of the line of MCC (Hill, 1994; Fig. 1.1). Seafloor spreading initiated in the Woodlark Basin at ~20 Ma (Early Miocene), but the main rifting phase did not begin until ~3.5 Ma (Davies and Smith, 1971; Baldwin *et al*., 1993; Hill, 1994). The active westward propagating tip of sea-floor spreading is located in the Woodlark Basin between Ferguson Island and Normanby Island (Fig. 1.1; Baldwin *et al*., 1993; Hill, 1994) and the rift is currently propagating into continental crust (Baldwin *et al*., 1993). Evidence of recent extension is exemplified by the presence of graben-bounding E-W faults along Goodenough Bay and Milne Bay on the Papuan Peninsula (Fig. 1.1b; Baldwin *et al*., 1993; Hill and Baldwin, 1993; Hill, 1994), and E-W normal faulting on the Trobriand Platform (Fig. 1.1; Hill and Baldwin, 1993; Hill, 1994).

The three MCC of the D'Entrecasteaux Islands share similar dimensions and domal fold structures and styles (Davies, 1980) as well as similar stratigraphic sequences (Davies and Warren, 1988) to the MCC of the Suckling-Dayman Massif, but the rocks of the Suckling-Dayman Massif are of lower metamorphic grade (Davies, 1980). On a broad scale, the metamorphic rocks that make up eastern Papua show a zonation from prehnite-pumpellyite and greenschist facies in the Suckling-Dayman Massif area to amphibolite and eclogite facies in the Goodenough and Fergusson Islands area (Fig. 1.1b; Davies and Warren, 1988). The difference in metamorphic grade is consistent with the two areas representing different stages of exhumation of the subducted north Australian margin (Davies, 1980). The similarity of the MCC of eastern Papua led Ollier and Pain (1981) to suggest that all the MCC ("gneiss domes" in their terminology) can be aligned if strike slip faults are restored in the D'Entrecasteaux Islands and if the Goodenough Bay graben is closed. These authors also suggested that the aligned gneiss domes lie above and indeed were caused by the emplacement of an elongate granite batholith at depth. However, Martinez *et al*. (2001) show that Goodenough Bay is underlain by ~25 km of PUB above a further ~10 km of hydrated continental crust. Therefore, it is unlikely that a single continuous batholith existed.

1.2 The Suckling-Dayman Massif

The Suckling-Dayman Massif that is the focus of this study is situated in southeastern Papua New Guinea (PNG) and forms two well-defined elongate dome-shaped mountains trending NW-SE (Fig. 1.1b). The area is covered by the Tufi-Cape Nelson geological sheet SC/55-8, 4 (Davies and Smith, 1974). The Suckling-Dayman Massif is ~ 60 km by ~25 km (Fig. 1.1b); it reaches an elevation of 2850 m at Mount Dayman and 3676 m at Mount Suckling (Davies and Smith, 1974; Davies, 1980). The Suckling-Dayman Massif is part of the Owen Stanley Range which is a ~500 km long mountain range consisting mostly of felsic (Kagi Metamorphic) and mafic (Emo Metamorphic) metamorphic units and ophiolite.

1.2.1 Geomorphology

Mount Suckling is the highest, steepest and most dissected of the two main peaks. The north and west flanks of the mountain fall steeply to the alluvial plains and on the south it comes together with other less outstanding mountains. The east slope of Mount Suckling merges with the west slope of Mount Dayman forming a watershed divide at about 1800 m elevation continuing to a gradual rise to the broad top of the Dayman Dome (Fig. 1.2; Davies, 1980). All the slopes of Mount Dayman have dips at ~20˚ and are occupied by numerous subparallel streams. The lower north slope of the mountain is characterised by a fault scarp, the Mai'iu fault, which marks a sharp contact between the metamorphic rocks and alluvial plains (Davies, 1980; Ollier and Pain, 1981). Ollier and Pain (1981) point out that the reduced dissection by streams of the fault scarp at the base of the north face of the dome is evidence of recent and current movement.

The northeast flank of Mount Dayman terminates in the Gwoira embayment (Fig. 1.1b), which is composed of Pliocene (1.8-5.3 Ma) conglomeratic sediments (Davies, 1980). The dome rose through unconsolidated sediment in the Gwoira embayment

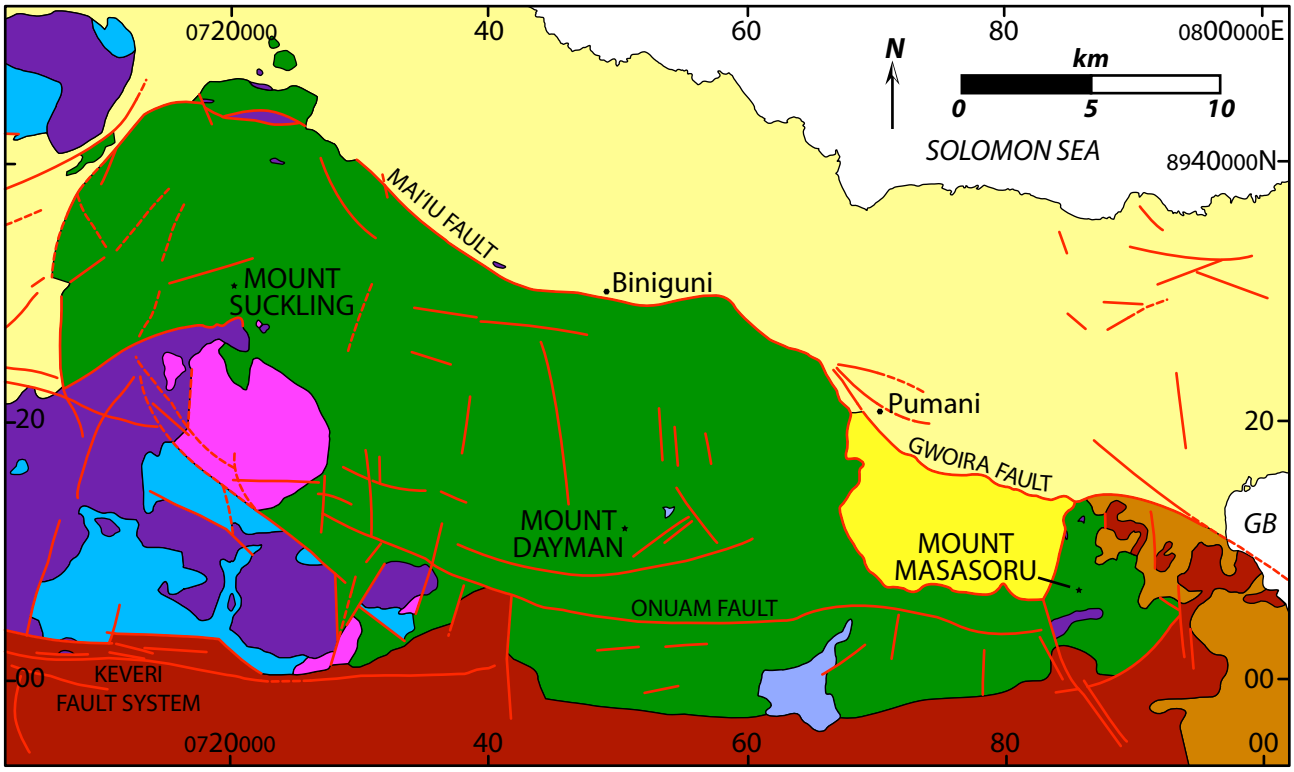

KEY:

PLIOCENE TO HOLOCENE	Undifferentiated Quaternary and Tertiary Volcanic and Sedimentary Rocks
PLIOCENE	Uga Sanstone (sandstone, siltstone; minor conglomerate)
	Gwoira Conglomerate (conglomerate, poorly sorted sandstone and siltstone)
UPPER MIOCENE TO PLIOCENE	Undifferentiated Tertiary Felsic Plutonics (granite; granodiorite, monzonite; microdiorite, micromonzonite porphyry)
UPPER CRETACEOUS TO MIDDLE EOCENE	Kutu Volcanics (basalt lava and pillow lava; minor tuff, limestone)
UPPER CRETACEOUS	Goropu Metabasalt (including Bonenau Schist Member) (variably schistose meta-basalt, -dolerite, -gabbro and -limestone; hornfels)
	Yau Gabbro (gabbro, diorite, granophyric tonalite: *prehnite-pumpellyite facies*)
JURRASIC? TO CRETACEOUS {Papuan Ultramafic Belt (PUB) Gabbro and Ultramfic zones}	Undifferentiated Gabbro (gabbro with ophitic, allotriomorphic/hypidiomorphic or cumulus textures)
	Undifferentiated Ultramafics (ultramafic rock with cumulus or tectonite fabric)

Figure 1.2 Geological map of the Suckling Dayman Massif and surrounding areas (modified from Davies and Smith, 1974). GB = Goodenough Bay.

that later moved down the surface of the dome (Ollier and Pain, 1981). The Gwoira embayment is bounded to the north by the Gwoira Fault (Fig. 1.2), which appears to be the present focus of rift propagation in eastern PNG, sustaining an extension of about 11 mm/yr (Mann and Taylor, 2002).

1.2.2 Metamorphic geology

The Suckling-Dayman Massif consists mostly of Cretaceous meta-basalt (Goropu Metabasalt) and minor limestone (Bonenau Schist Member) overthrust by ultramafic rocks (called the Tectonite ultramafics on the Tufi-Cape Nelson geological sheet SC/55-8, 4; Davies and Smith, 1974) and minor conglomerate (Davies and Smith, 1971; Davies, 1980; Ollier and Pain, 1981). The metamorphic grade varies from prehnite-pumpellyite to pumpellyite-actinolite facies (with minor high P assemblages including lawsonite, glaucophane and metamorphic aragonite), to greenschist facies (Davies and Smith, 1971; Davies, 1980; Ollier and Pain, 1981).

The *prehnite-pumpellyite facies* rocks are located mostly at the eastern end of the massif, south of the Onuam Fault (Fig. 1.2) apparently transitional southward into unmetamorphosed basalt (Davies, 1980). The rocks show only weak deformation and maintain a massive primary basalt texture. Some other occurrences of low-grade metamorphic rocks are situated along the north flank of Mt Suckling (Fig. 1.2; Davies, 1980). The *pumpellyite-actinolite facies* rocks have an assemblage of chlorite-pumpellyite-epidote-albite-actinolite with rare sericite, blue amphibole, lawsonite, stilpnomelane, titanite, calcite and quartz but not all together in one sample. The schistosity is not pervasive and there is some preservation of pillow structures. Rocks of this metamorphic grade constitute the largest percentage of the Suckling-Dayman Massif and occur throughout the massif (Davies, 1980). *Greenschist facies* rocks underwent a complete recrystallisation process, resulting in a metamorphic assemblage consisting of chlorite-albite-epidote-actinolite with some sericite, quartz, titanite, hematite and stilpnomelane. Greenschist rocks occur in thrust shear zones at the boundary with overlying ultramafic rocks south of Mount Suckling and at the northern and southern

perimeter of the Suckling-Dayman Massif (Fig. 1.2; Davies, 1980). *Metamorphosed limestone* (Bonenau Schist Member, Fig. 1.2) occurs as small lenses within the metabasites and also as a 1 km thick unit to the east and southeast of the Suckling-Dayman Massif (Kutu Volcanics; Fig. 1.2). Most limestone is completely recrystallised to calcite-muscovite-quartz-albite schist. In some parts of the eastern side of the massif the metamorphosed limestone contains metamorphic aragonite and dolomite (Davies, 1980). In the areas where the rocks underwent prehnite-pumpellyite grade metamorphism (in the east of the Massif) the limestone preserves original bedding and microfossils (Davies, 1980).

Ultramafic rocks of the PUB (Tectonite ultramafics) overlie all the different metamorphic units of the Suckling-Dayman Massif. The ultramafic rocks are typically well-foliated harzburgite with evident mylonitization near the contact of the metabasalts. These rocks occur south of the Suckling-Dayman Massif, on Mount Masasoru and as inliers within the alluvial plains north of the Mai'iu Fault (Fig. 1.2; Davies, 1980).

The Suckling Granite and Mai'iu Monzonite intrude the Tectonite ultramafics and Goropu Metabasalt, suggesting they intruded post movement on the shear zone between the ultramafics and metabasalts. Gravity lows were identified by Davies and Warren (1988) over the Suckling-Dayman Massif, suggesting the presence of felsic material beneath the metamorphosed sequence of the complex. This may indicate that more extensive felsic intrusions occur beneath the complex similar to the felsic batholith proposed by Ollier and Pain (1981).

The overall metamorphic grade gradually increases toward the north, from a prehnite-pumpellyite facies to pumpellyite-actinolite and blueschist. Greenschist facies rocks are confined to near the thrust plane. This scenario reflects the likelihood of a greater and deeper underthrusting of the northern rock units, and an increase of temperature and strain in the proximity of the thrust plane (Davies, 1980).

1.2.3 Structural geology

The most imposing structure of the Suckling-Dayman Massif is the broad domal fold defined by the foliation in the metamorphosed basalt and limestone (Goropu Metabasalt; Fig. 1.2). The flanks of the massif are generally shallow and lie sub-parallel to the bounding shear zones of the domes with minor variation between the two main mountains (Suckling and Dayman; Fig. 1.2). Mount Dayman has consistent dip slopes where the shear zone foliation dips 10˚ to 30˚ on all flanks of the dome, except on the south, where the slope is steeper and the determination of the slope is obscured by faults and talus accumulations (Davies, 1980; Ollier and Pain, 1981). Mount Suckling is higher and the dip slopes are steeper, with shear zone foliations controlling slopes of 30˚ and up to 60˚ (Davies, 1980).

Davies (1980) suggests that the metabasite thrust foliation is parallel to and controls the relatively shallow slopes of the Dayman Dome. This foliation cuts the steeply dipping calcareous schistosity in tectonic windows exposed along some creeks. This discordance could indicate a more complex deformation history or, perhaps more simply, an expression of the less competent environment of the calcareous rocks underneath the more competent mafic assemblages. Shear zone foliations are parallel to the surface of the dome, which may or may not be parallel to bedding, and metamorphic lineations plunge in the dip direction of the schistosity (Davies, 1980; Ollier and Pain, 1981).

The Suckling-Dayman Massif is bounded by thrust faults that are exposed south of Mount Suckling and near Mount Masasoru (Davies, 1980) where bodies of ultramafic rocks overlie metabasalt on relatively shallow angle faults (Fig. 1.2). Other implied thrust faults include the Mai'iu Fault in the north (Fig. 1.2) and faults along the south of the massif, and also, through the Biman dip slopes directly south of the Gwoira Conglomerate, which preserve strongly foliated greenschist facies rocks (Fig. 1.2; Davies, 1980). Other faults, which contributed to further vertical displacement, include the Gwoira and Onuam Faults (Fig. 1.2) that developed during the horst-and-graben tectonics of the Quaternary (Davies, 1980).

1.3 Neighbouring localities

In contrast to the paucity of research on the Suckling-Dayman Massif, there has been considerable recent research into the MCC of the D'Entrecasteaux Islands to the northeast of the Papuan Peninsula. The Islands consist of a series of MCC with amphibolite and some eclogite facies rocks exposed on the northern islands (Goodenough and Fergusson) and mostly granulite and greenschist facies on the southeastern island (Normanby) (Davies and Warren, 1988). Each of these MCC have a similar structure consisting of felsic metamorphic rocks at the base, mafic metamorphic rocks in the central zone and ultramafic and mafic rocks at the top (Davies and Warren, 1988). The protoliths of the felsic and mafic metamorphic rocks were probably Cretaceous sedimentary and felsic volcanic deposits for the former and calcareous sedimentary rocks and basaltic ocean crust for the latter. The ultramafic and mafic rocks represent part of the obducted PUB ophiolite (Davies and Warren, 1988; Hill and Baldwin, 1993).

All of the MCC are bounded by faults that are parallel to compositional layering and schistosity (Davies and Warren, 1988). Peak metamorphic pressures were reached during the Palaeogene arc-continent collision. Rifting reactivated the former subduction thrust as a normal fault detachment system (Davies and Warren, 1988; Baldwin and Ireland, 2005). The most recent study of the mechanism of uplift concludes that the MCC were uplifted by vertical extrusion of ductile lower crustal material driven by a crustal density inversion (Marinez *et al*., 2001). Previous studies have inferred that crustal thinning, plutonism and isostatic response to rapid erosion as additional important driving mechanisms for the uplift (Davies and Smith, 1971; Davies, 1980; Davies and Warren, 1988; Hill and Baldwin, 1993; Baldwin *et al*., 1993; Hill, 1994).

1.4 Geological synthesis

The Woodlark Basin spreading centre rift (Fig. 1.1a) is propagating westward into eastern PNG. The extensional environment has exhumed deeply subducted high- and low-grade metamorphic rocks in the D'Entrecasteaux Islands and Suckling-Dayman Massif MCC

respectively (Fig. 1.1b). A zonation from high- to low-T from east-northeast to west-southwest suggests that the protoliths of all the MCC were once part of the same mid-Tertiary subduction complex.

1.5 Objectives of the project

The specific objectives of the project are as follows:

1. Interpret regional structural lineaments in aerial photography and Shuttle Radar Topography Mission (SRTM) data to place the detailed field analyses into a regional context.
2. Record the structural and metamorphic relationship of the hanging wall sedimentary sequences of the Gwoira Conglomerate and the metabasite footwall of the Dayman Dome.
3. Document the fabric development and kinematics of shear zones that bound the Dayman Dome.
4. Determine the metamorphic evolution of the Suckling-Dayman Massif by conducting petrographic analyses of mineral assemblages and rock textures and characterising mineral chemistry of key assemblages to document the P-T path of the Dayman Dome.
5. Synthesise field observations, petrographic analyses, and structural measurements to develop a tectonic model for the evolution of the Suckling-Dayman Massif.

Chapter 2 REMOTE SENSING: Aerial Photographs, Google Earth and Shuttle Radar Topography Mission (SRTM) Data

2.1 Introduction

Aerial photography, Google Earth™ images and Shuttle Radar Topography Mission (SRTM) data are examined to delineate major structures so as to place the detailed fieldwork that follows into a regional context. The specific observational aims of this analysis are to define (1) regional lineaments that may demarcate major structures or geological boundaries, (2) areas of the Suckling-Dayman Massif where the topography is controlled by the dip of shear zones (i.e. metabasite dip slopes), and (3) drainage patterns across the dome to compare to dip slopes and megamullions (very large corrugations on a fault plane) identified in the SRTM data.

2.2 Aerial Photographs

Six aerial photograph stereo-pairs were analysed using a Topcon mirror stereoscope. Figure 2.1 shows a mosaic of the interpretation. Green shaded areas represent interpreted metabasite dip slopes. Blue lines represent waterways. Red lines represent structural lineaments commonly observed as straight streams on dip slopes. The analysis shows that the Suckling-Dayman Massif may be divided into the Suckling and Dayman Domes (Fig. 2.1). The Dayman Dome is nearly complete in the north, having been dissected by the Gwariu and Biniguni rivers (Fig. 2.1). The Nowandowan River on the southeast flank and the Bonua River on the south and southwest flanks have eroded a large proportion of the southern half of the Dayman Dome (Fig. 2.1). The Suckling Dome is largely eroded and dip slopes are limited to the east flank. Therefore aerial photographs west of the Mai'iu River (Fig. 2.1) were not interpreted as no lineaments were observed. The Biman dip slopes east of the Dayman Dome are relatively small and are restricted to the lower hills south of the Gwoira Conglomerate. A sharp topographic change from alluvium to the

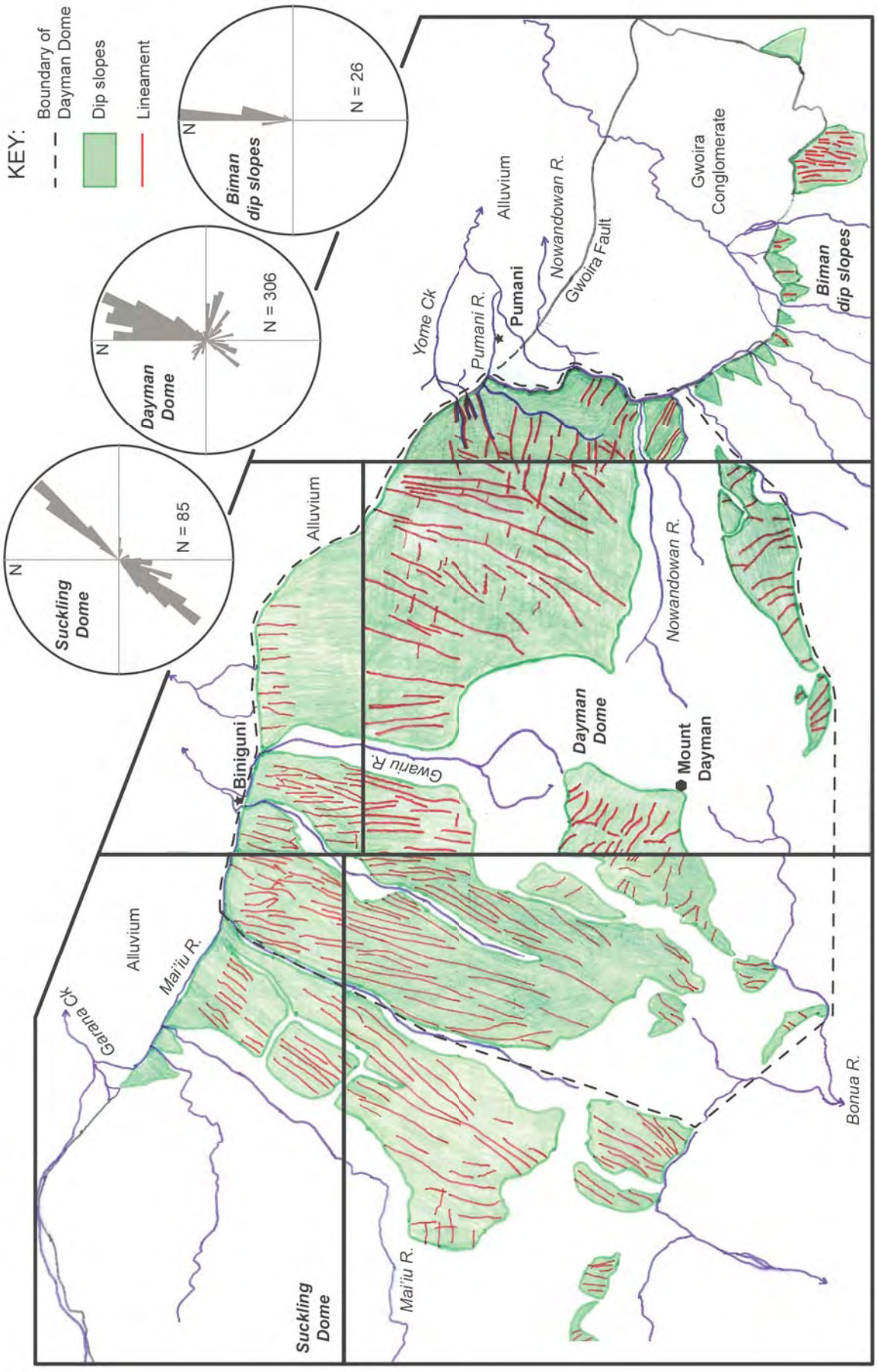

Figure 2.1 Aerial photograph interpretation. Rose diagrams show structural lineaments (red lines) for three domains.

irregular hills of the Gwoira Conglomerate mark the location of the Gwoira Fault (Fig. 2.1) that marks the northern boundary of the Gwoira Conglomerate.

Over 400 orientation measurements were made of the structural lineaments observed on metabasite dip slopes of the Suckling-Dayman Massif (red lines, Fig. 2.1, Appendix A). These were divided into three domains: Suckling Dome, Dayman Dome and Biman dip slopes (Fig. 2.1). Structural lineaments of the east flank of the Suckling Dome trend northeast and southwest, whereas those of the Dayman Dome dominantly trend north to NNE. Minor sets of structural lineaments on the Dayman Dome trend east, ESE, southeast, south, southwest and northwest. Two sets of nearly orthogonal lineaments are observed on the east flank of the Dayman Dome. Structural lineaments of the Biman dip slopes trend north (Fig. 2.1).

2.3 Google Earth™ images

Google Earth™ images were examined to supplement and test the aerial photograph interpretation as the three-dimensional view provides an extra dataset to interpret and compare with. The figures with Google Earth™ images are presented to help the reader visualise the structure of the massif. Figure 2.2 contrasts the largely dissected Suckling Dome with the less dissected Dayman Dome and shows the sharp northern boundary of the Suckling-Dayman Massif (Mai'iu Fault). Figure 2.3 shows the Gwoira Conglomerate bounded by the Gwoira Fault in the north and the Biman dip slopes in the south. The topographically highest parts of the Dayman Dome are the most dissected by streams, whereas the least dissected parts lie closest to the Mai'iu Fault and are highlighted in Figure 2.4. The Mai'iu Fault trace has a scalloped pattern at the surface (Fig. 2.5). A topographic saddle divides the Suckling and Dayman Domes (Fig. 2.6). Dip slopes are less common on the southern flanks of both domes and are heavily dissected by streams (Fig. 2.7). The Mai'iu Fault changes orientation from an east-west strike to a north-south strike between the northern and eastern flanks of the Dayman Dome. The fault switches

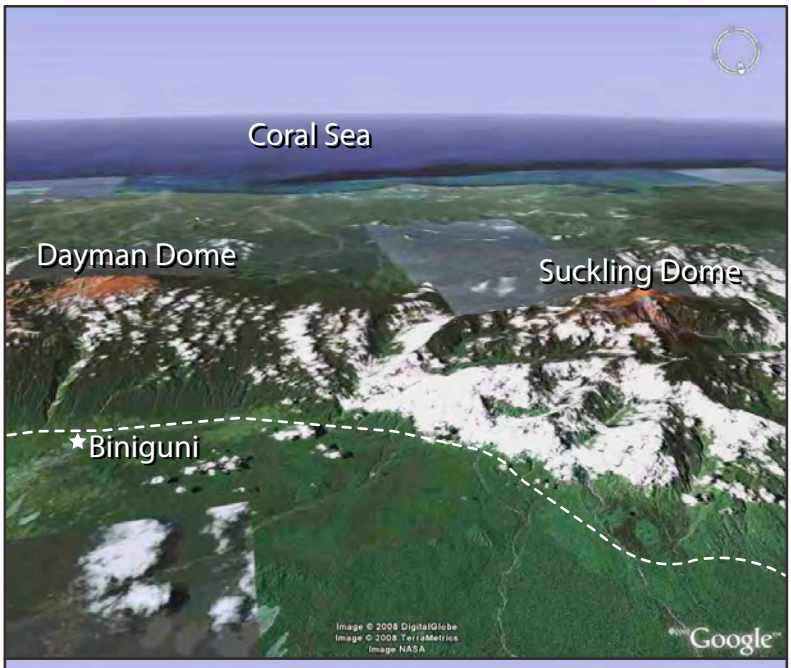

Figure 2.2 Google Earth™ image view looking south of the Dayman and Suckling domes. The Mai'iu Fault is marked by a dashed line.

Figure 2.3 Google Earth™ image view looking southwest of the Gwoira Conglomerate (GC, centre) with the Biman dip slopes (left). The Mai'iu Fault is marked by a dashed line. The Gwoira Fault is marked by a solid line.

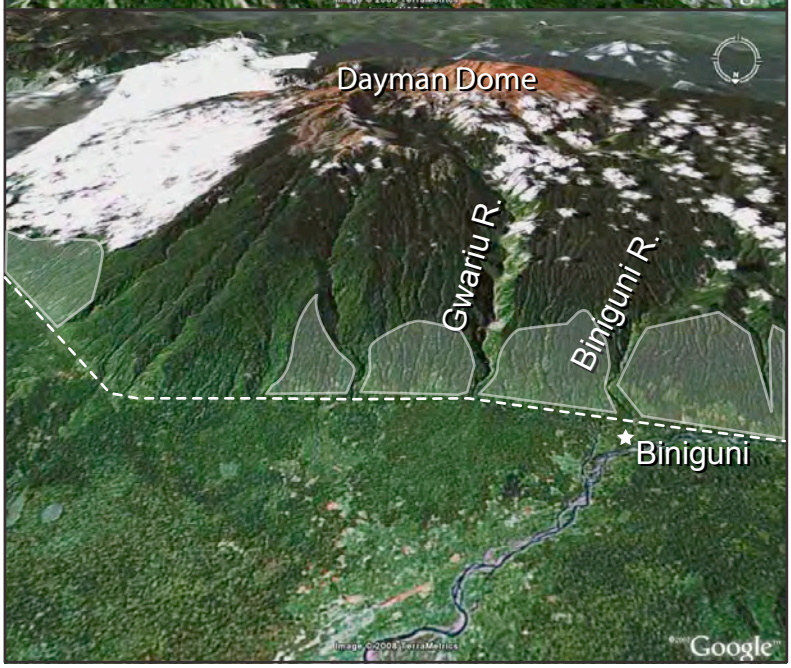

Figure 2.4 Google Earth™ image view looking south of the Dayman Domes. The Mai'iu Fault is marked by a dashed line. The parts of the dome that are least dissected by streams are highlighted.

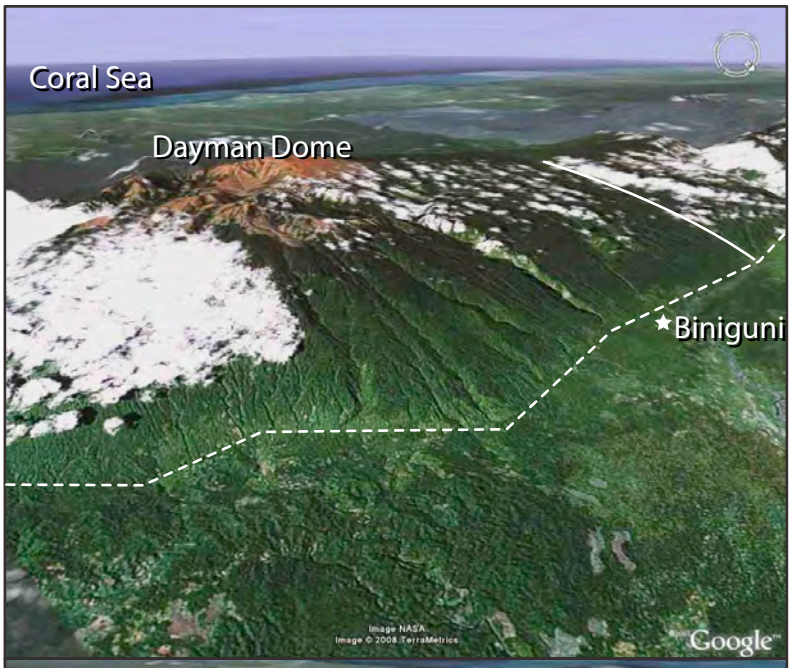

Figure 2.5 Google Earth™ image view looking southwest of the Dayman Dome. The Mai'iu Fault is marked by a dashed line. The boundary between the Dayman and Suckling domes is marked by a solid line.

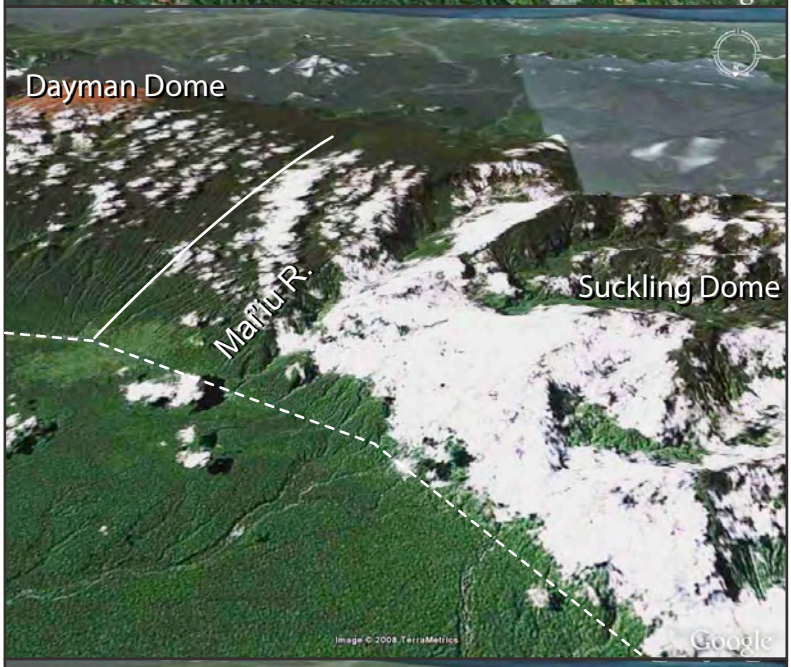

Figure 2.6 Google Earth™ image view looking south of the topographic saddle between the Dayman and Suckling domes (the boundary is marked by a solid line). The Mai'iu Fault is marked by a dashed line.

Figure 2.7 Google Earth™ image view looking south of the topographic saddle between the Dayman and Suckling domes (the boundary is marked by a solid line). The south-dipping dip slopes of the east flank of the Suckling Dome are highlighted.

back to an east-west strike along the Biman dip slopes (Fig. 2.8). The least dissected parts of the east flank of the Dayman Dome again lie closest to the Mai'iu Fault (Fig. 2.9). The southeast and southern flanks of the Dayman Dome are highly dissected by streams and the dip slopes are generally steeper than those of the northern flanks (Fig. 2.10 & 2.11).

2.4 Shuttle Radar Topography Mission (SRTM) data

The Shuttle Radar Topography Mission (SRTM) obtained elevation data on a near-global scale (SRTM Project: http://www.jpl.nasa.gov/srtm/) and consisted of a specially modified radar system that flew onboard the Space Shuttle Endeavour during an 11-day mission in February 2000. SRTM is an international project spearheaded by the National Geospatial-Intelligence Agency (NGA) and the National Aeronautics and Space Administration (NASA). SRTM data is sampled at 3 arc-seconds, which is 1/1200th of a degree of latitude and longitude, or about 90 m. The STRM data provides a detailed digital elevation model of the topography and is very useful as it "sees through" cloud cover and vegetation bypassing a key limitation of the above datasets. Lineaments are also visible in the STRM data that are coincident with north-draining streams, even on the east-dipping flank of the Dayman Dome (Fig. 2.12). A topographic profile oriented east to west across the SRTM data for the Dayman Dome shows a corrugated surface of broadly spaced ridges and troughs (Fig. 2.13), these are called megamullions. The analysis identified three broad megamullions on the Dayman Dome with wavelengths of approximately 10 km. The parallel drainage pattern across the dome is dominantly controlled by these north-trending structural megamullions. The corrugated topography of the megamullions has been accentuated by fluvial incision of the megamullion troughs following subaerial exposure of the Dayman Dome. A second topographic profile oriented south to north across the SRTM data for the lower north flank of the Dayman Dome shows the structural dip of the dip slope changing from ~21° at the base (200-600 m elevation) to ~18° slightly higher up the dome flank (700-1000 m elevation).

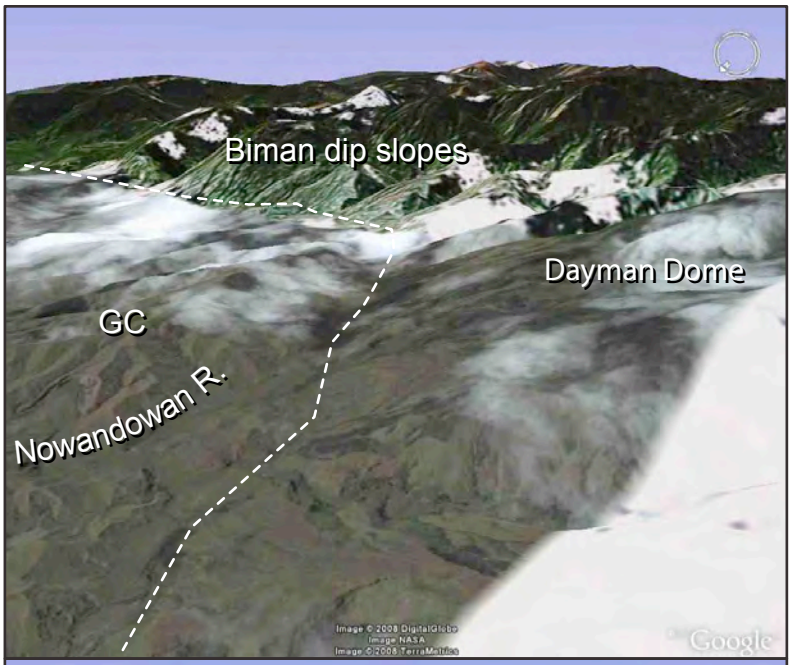

Figure 2.8 Google Earth™ image view looking southeast of the east flank of the Dayman Dome and Biman dip slopes. The Mai'iu Fault is marked by a dashed line. GC = Gwoira Conglomerate.

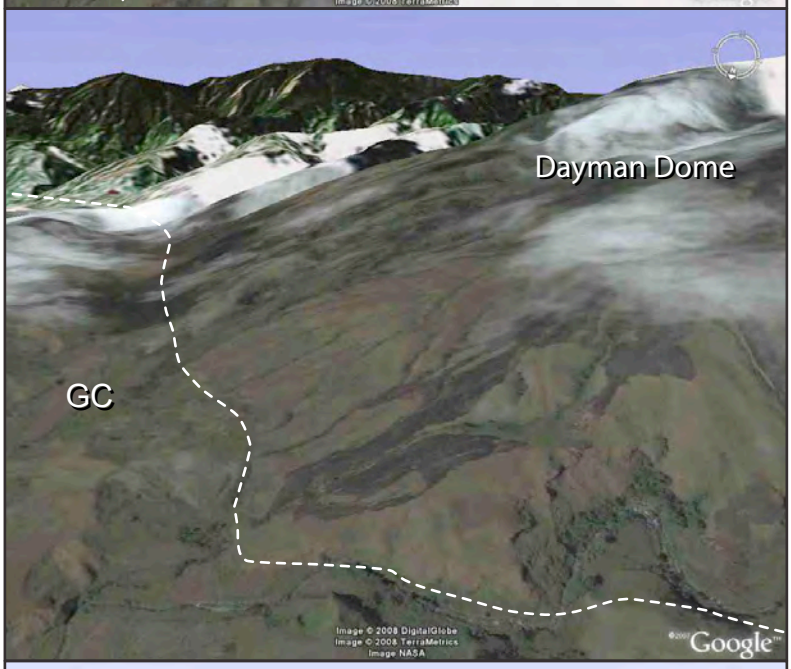

Figure 2.9 Google Earth™ image view looking south of the east flank of the Dayman Dome. The Mai'iu Fault is marked by a dashed line. GC = Gwoira Conglomerate.

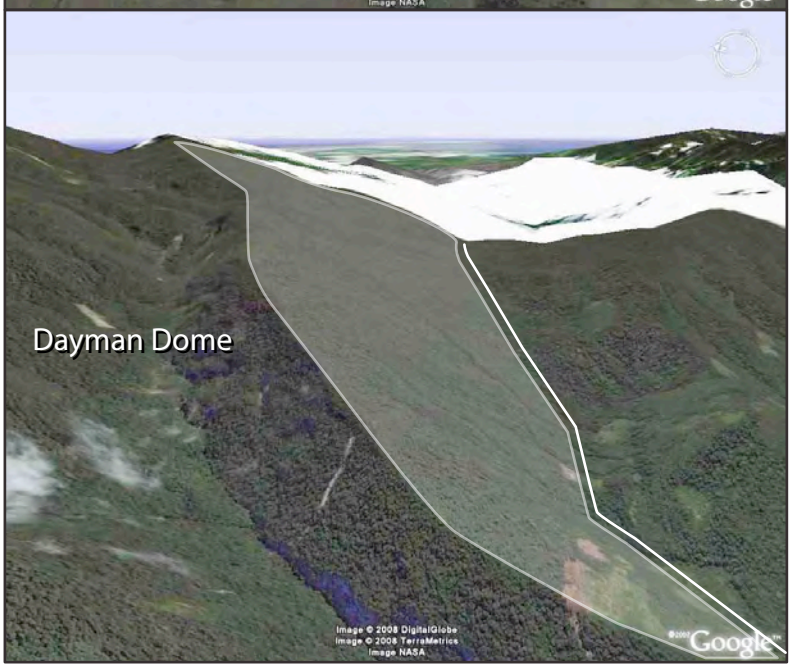

Figure 2.10 Google Earth™ image view looking ENE of the southeast flank of the Dayman Dome. The boundary of the dome is marked by a solid line. The southeast dip slope is highlighted.

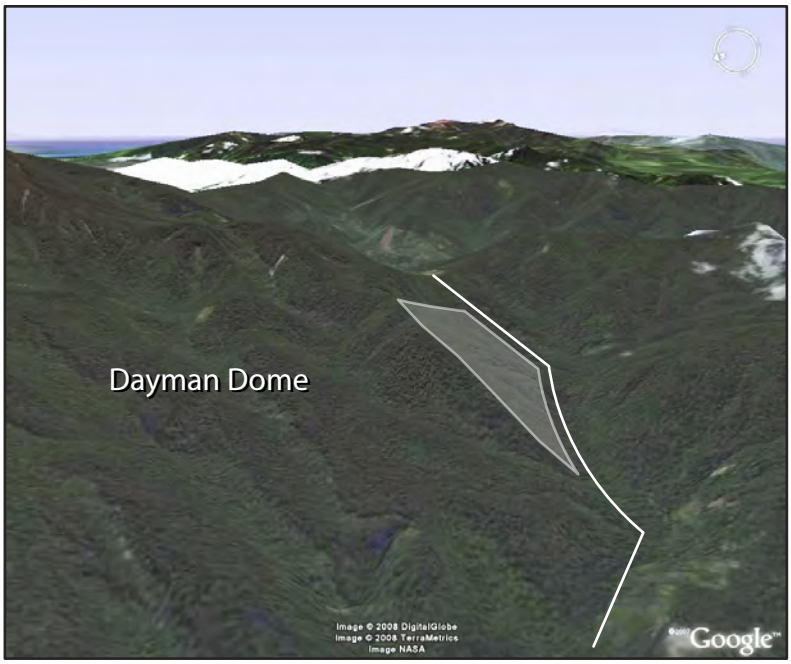

Figure 2.11 Google Earth™ image view looking ESE of the south flank of the Dayman Dome. The boundary of the dome is marked by a solid line. The southeast dip slope is highlighted.

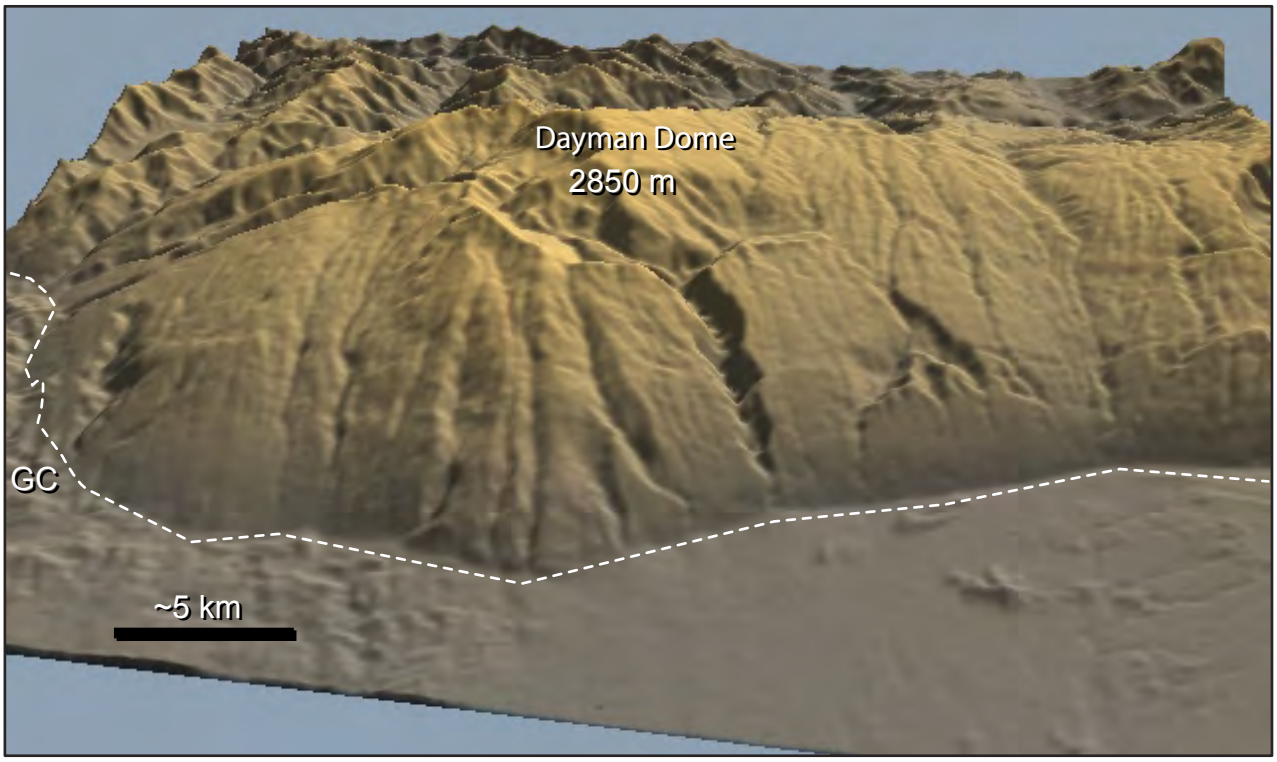

Figure 2.12 SRTM image view looking south of the Dayman Dome. The Mai'iu Fault is marked by a dashed line. GC = Gwoira Conglomerate.

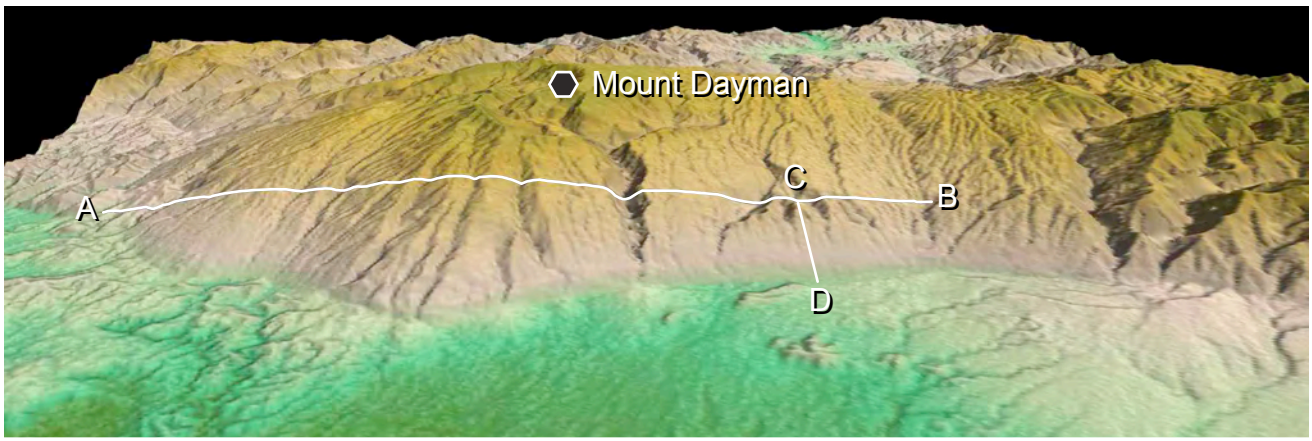

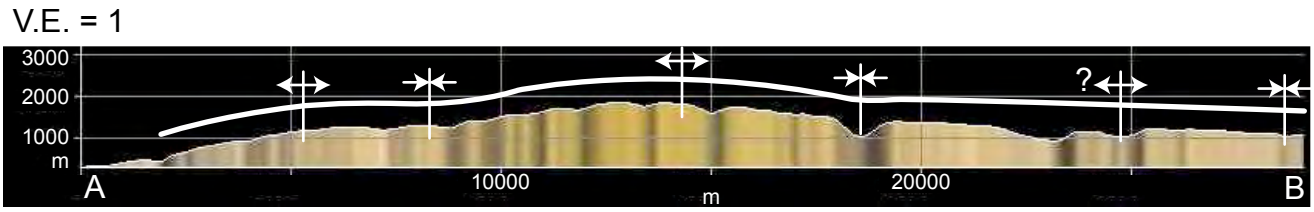

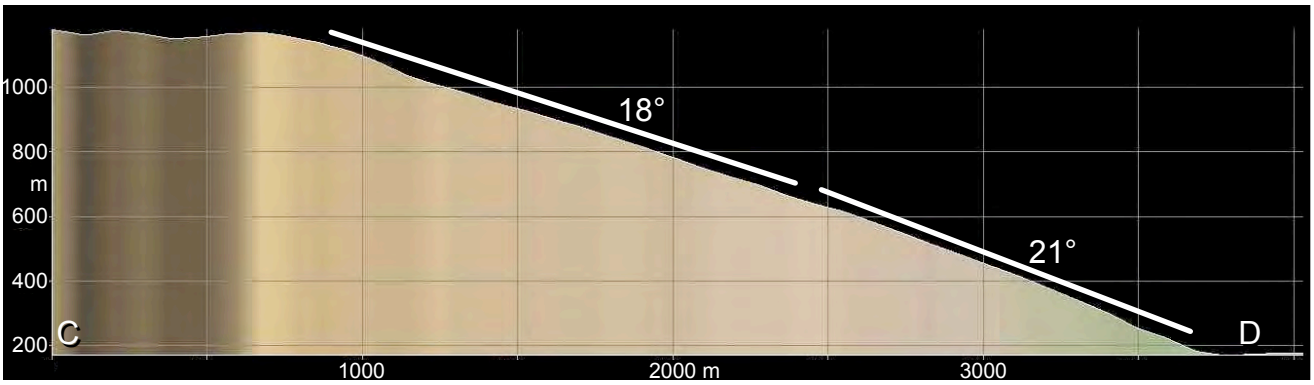

Figure 2.13 SRTM image for the Dayman Dome (view looking south) showing the location of two topographic profiles. Profile A-B shows a ridge and trough morphology to the Dayman Dome surface that defines megamullions. Profile C-D shows a prominent dip slope on the lower north flank of the Dayman Dome that is little dissected by streams.

The SRTM data was also used to further explore the two sets of lineaments identified in aerial photography on the east flank of the Dayman Dome (section 2.2). Figure 2.14 shows the interpretation of topographic lineaments on a plan view shaded relief image (illuminated from the west) of the Dayman Dome. The orientation of lineaments is presented in Appendix A. Black lines define the outline of the dip slopes, major valleys and lineaments. Blue lines represent major waterways following the troughs of the megamullions, whereas red lines represent ridges or the interpreted crests of the megamullions. The six megamullion crests and troughs are oriented NNE (Fig. 2.14b). Thirty-nine orientation measurements of the structural lineaments on the east flank of the Dayman Dome (Fig. 2.14c) fall into two main orientation groups: (i) a minor set oriented ESE to ENE and (ii) a major set oriented NNE to N. The first group trend down the dip slope of the east flank and are spatially concentrated on the lowermost east flank, whereas the second group are oriented similarly to the dominant NNE structural lineaments identified across the majority of the Dayman Dome in aerial photography (Fig. 2.1). A notable feature of the drainage pattern of the eastern flank is a stepped pattern of some streams (Fig. 2.14c). The steps comprise long segments oriented NE with shorter N to NNE oriented segments.

2.5 Discussion

At the broadest scale, the Suckling-Dayman Massif is a twin domal shape elongated east to west that may be subdivided into the Dayman and Suckling domes. Remote-sensed information is difficult to gain from the Suckling Dome due to the high degree of dissection by streams. The analysis of the Dayman Dome identified three broad megamullions on the northern flank of the dome oriented NNE. The megamullions create a scalloped range front and curved fault trace of the Mai'iu Fault. The orientation of the broad megamullions correlates with the structural lineaments identified in aerial photography on the Dayman Dome. Detailed analysis of the STRM data on the east flank of the Dayman Dome shows a large number of streams oriented NNE to N, at a high

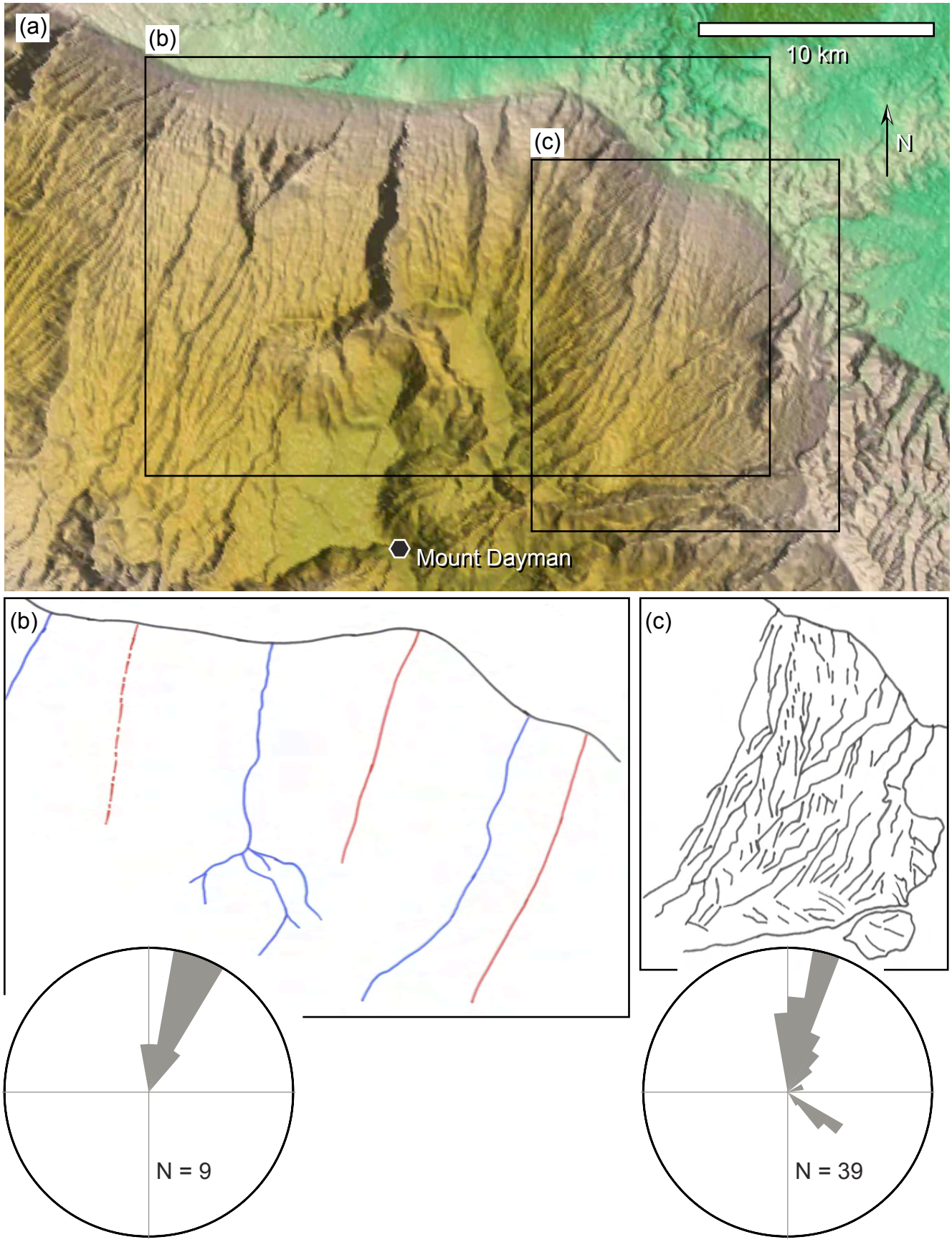

Figure 2.14 (a) SRTM image for the Dayman Dome. (b) Orientation of megamullion ridges (red - dashed = inferred) and troughs (blue) plotted onto a rose diagram. (c) Structural lineaments on the east flank of the Dayman Dome plotted onto a rose diagram.

angle to the dip slope. The unusual along strike orientation of these streams is consistent with a structural control such as fault surface mullions, corrugations or striations. The orientation of stepped streams is consistent with a combination of typical down-dip and structural controls on the flow direction of the streams.

The megamullions and lineaments on the Dayman Dome are oriented differently to the lineaments on the Suckling Dome and Biman dip slopes. Although streams heavily dissect the Suckling Dome, the Mai'iu River comprises a long straight segment (Fig. 2.1) that may be controlled by a Suckling Dome megamullion oriented parallel to NE lineaments identified in the aerial photography.

The structural data may be compared to orientations predicted by Euler poles for the extension in this area. The oldest magnetic anomaly picked for the Woodlark Basin is anomaly 3A.1 indicating that continental rifting initiated prior to approximately 6 Ma (Taylor *et al*., 1999). Analysis of fracture zone orientations and magnetic anomalies identifies two major changes in the location of the Euler poles for rifting between the Indo-Australian and Woodlark plates as presented in Table 2.1 (Taylor *et al*., 1999). The Euler poles may be used to predict the orientation of extension within the rifting crust at a given location. The Euler poles indicate NNW-directed extension for periods younger than approximately 0.5 Ma, whereas for periods between 0.52-3.6 Ma a NNE-directed extension is predicted (Table 2.1). The remote-sensed data analysed above shows no evidence of NW-directed structural lineaments and best matches the extension direction predicted by the oldest Eulerian pole. Therefore, the exposed sections of the dome contain structures formed greater than half a million years ago. This is consistent with erosion of any young NW-directed extensional structures that would have likely formed a carapace of brittle fault gouge overlying the exposed zone of ductile mylonites that now form dip slopes with NNE-directed linear structures.

Table 2.1 Euler poles for Woodlark Basin seafloor spreading from Taylor *et al*. (1999). The orientation of extension is calculated for the Biniguni-Pumani region.

Age (Ma)	Latitude	Longitude	Rate (°/Myr)	Orientation of extension
0 - 0.08	10.8°S	145.2°E	1.86 ± 0.03	344-346°
0.08 - 0.52	12°S	144°E	3.437	336-338°
0.52 - 3.6	9.3°S (±0.2°)	147°E (+1°,-2°)	4.234	9-11°

Chapter 3 FIELDWORK: Logistics and Methodology

3.1 Introduction

Fieldwork locations were selected on the basis of regional structural analysis of aerial photographs, Google Earth images and Shuttle Radar Topography Mission (SRTM) digital elevation data (Chapter 2). Specifically, the Pumani (0770200E, 8920500N) and Biniguni villages (0749100E, 8929900N; Figs 1.2 and 2.1) were selected as fieldwork bases as they are near the northern flank of the Dayman Dome and, in the case of Pumani, it is close to sedimentary units that unconformably overlie and form the hanging wall to the dome. These two locations of study permitted the examination of the metabasite dome, its bounding shear zone and the overlying sedimentary rocks. There has been very little previous research in this area. Hence, the broad scope of the fieldwork was to document all geological features, with a particular focus on collecting structural data and rock samples, and photographically documenting key field relations at outcrop scale.

In addition to features of geological interest, care was taken in noting and documenting any geomorphologic characteristics visible from the helicopter and from the ground. Photographs and field notes were taken to supplement the aerial photography, Google Earth and SRTM data analyses and to broaden the general understanding of this little studied area.

The location of rivers and rock samples were recorded with a Garmin GPS 72 (Global Positioning System) using AGD66 datum, zone 55, with an accuracy of ±10-50m. Samples are listed in Appendix B showing locations and lithologies. Bearings and structural data in the field were measured using Brunton® and Freiberg® compasses. A subsequent declination adjustment for true north of 7.5° was applied to all structural measurements.

3.2 Logistics

This study was logistically very challenging. The unexpected time taken to obtain a research visa from the PNG government delayed the fieldwork by five months. The field area is remote and largely inaccessible. There are no telephone lines or postal service and hence our first contact with the villagers was when we arrived by helicopter. Of the three weeks spent "in the field", many days were lost while: (i) in transit between Sydney and Alotau, (ii) preparing logistics in Alotau, (iii) dealing with malaria prevention and minor health issues in Alotau, (iv) waiting for helicopter repairs prior to flying into the field, and particularly significant loss of research time took place while (v) in the villages, as we needed to wait for approval for the party to carry out the fieldwork from the local elders and local customs limited the help of our guides to a daily schedule of approximately between 9 am and 3 pm. However, all this being said, the fieldwork was exciting and enjoyable, and we had tremendous support from the local villagers.

Fieldwork was carried out in eastern PNG, on the north flank of the Dayman Dome and Gwoira Conglomerate (Fig. 1.2). The Pumani area is located on the east flank of the Dayman Dome and north flank of the Gwoira Conglomerate (Fig. 2.1). The Biniguni area is located on the north flank of the Dayman Dome (Fig. 2.1). Both the Pumani and Biniguni villages were reached by helicopter from Alotau (Fig. 1.1), Milne Bay Province. The entire duration of the fieldwork extended from the 21st of April 2006 to the 14th of May 2006. The party reached the Pumani village on the 25th of April and returned to Alotau on the 2nd of May, and departed for Biniguni on the 4th of May and returned on the 12th of May 2006. Once in the villages, all the rivers and locations were reached by foot and long periods of time were spent walking inside the watercourses, which was the best way to find good outcrop and avoid the thick tropical jungle.

3.3 Methodology

Local guides were relied upon to lead the field party along foot tracks across the alluvial plain and through the jungle. As we worked, the guides showed the field party the locations of waterways on the topographic map and supplied their names. The local information did not always match the waterway names on the topographic and geological maps. For example, locals call the Gwadi Creek on the topographic map the Gwariu River. The names (and spelling) of waterways provided by the local guides are presented in Fig 3.1. Each outcrop was delimited and examined as the guides lead the field party to and along each waterway. Outside the narrow waterways the territory was completely covered by very thick tropical jungle vegetation and no outcrop was observed in these areas. The different methods used for documentation of geological features, structural data and sample collection were dictated by the position and condition of the outcrop along waterways. All the waterways selected for analysis generally flow north or northeast off the Dayman Dome, with the exception of the Mai'iu River that flows east along the foot of the dome. The small channels cut by the waterways provided excellent windows into and sections across the shallowly to moderately dipping sedimentary strata of the Gwoira Conglomerate unit and shear zone fabric of the Dayman Dome.

3.3.1 Pumani

The aims of the fieldwork in the Pumani Area were to: (i) document sedimentary assemblages, forms, fabrics (orthoconglomeratic, paraconglomeratic and preferred orientations), textures (clast sizes and sorting) and relation between adjacent different sedimentary and non-sedimentary units within the Gwoira Conglomerate, and (ii) examine the metabasite shear zone beneath the unconformity at the base of the Gwoira Conglomerate. Particular attention was dedicated to the collection of in-situ rock samples that were indicative of particular sedimentary units or structural features. "Float" rock samples were also collected from waterways that drained off the

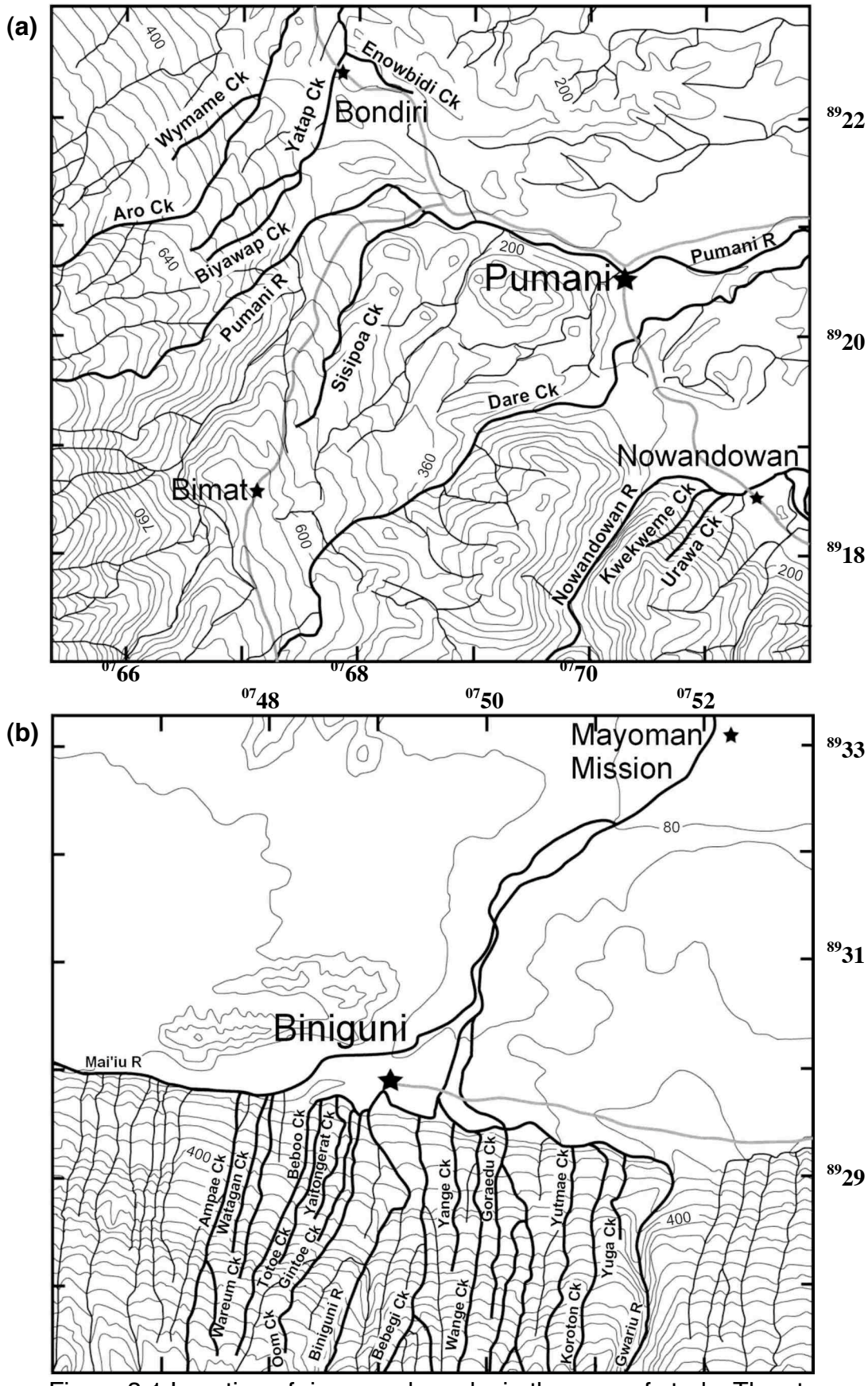

Figure 3.1 Location of rivers and creeks in the area of study. The streams used for traverses are labelled. (a) Pumani area, Gwoira Conglomerate. (b) Biniguni area, Dayman Dome. Map projection is AGD66 and scale is in km.

Gwoira Conglomerate and metabasite dome. These samples are indicative of rock units inaccessible to us but still of interest to the study, as they are from stratigraphically higher sections within the Gwoira Conglomerate unit or from sections of metabasite higher up the flanks of the dome. The collection of rock samples facilitates accurate mineralogical and petrologic analyses of the sedimentary complex and an understanding of the key mineralogical parageneses and structural progression of the metabasite rocks. Of 48 rock samples collected, 35 were in-situ and include seven oriented structural samples of the shear zone flanking the Dayman Dome, one fossiliferous mudstone of the Gwoira Conglomerate and 32 other sedimentary rocks of the Gwoira Conglomerate. Thirteen float samples include four fossiliferous and 8 other sedimentary rocks of the Gwoira Conglomerate. Of the 11 waterways selected for analysis, five drain the hills of the Gwoira Conglomerate (Urawa, Kwekweme, Dare and Sisipoa creeks and the Nowandowan River) and 6 drain the Dayman Dome (Pumani River and Biyawap, Yatap, Aro, Wymame and Enowbidi creeks).

Numerous photographs were also taken, mostly illustrating the various sedimentary structures (e.g. graded beds and boundaries), textures and fossiliferous materials in sedimentary units and structural fabrics in metabasite units.

3.3.2 Biniguni

The aim of the fieldwork in the Biniguni area was to document the metabasite shear zone, its sense of movement and relation with low strain rocks at the outcrop scale. Particular attention was paid to collecting plenty of structural measurements of the shear zone fabrics. Approximately 590 measurements of foliation and mineral lineation were taken.

An important aspect of the fieldwork was to collect rock samples for mineralogical, geochemical and structural analyses. The collection was undertaken for the identification of metamorphic assemblages, determination of metamorphic facies and history, and the

presence of kinematic indicators for vorticity analyses to establish a more qualitative and quantitative sense of movement.

In total 40 samples were collected, of which 12 are float and 28 in-situ samples of the metabasite unit. All the rivers investigated in the Biniguni area have their origin within the northern slope of the Dayman Dome. Seventeen out of the 28 in-situ samples are oriented. The orientation was determined by taking the strike and dip of a flat rock face with a compass and clinometer and writing the measurement on the face with permanent marker. Subsequent careful removal of the sample from the outcrop resulted in a sample that could be re-oriented in the laboratory for detailed structural analysis (Fig. 3.2).

Figure 3.2 Orientation of a flat face of a rock sample, Ampae Ck. Measurement is of a foliation plane in metabasite.

Chapter 4 SEDIMENTARY GEOLOGY: Gwoira Conglomerate

4.1 Introduction

The ductile Mai'iu Fault plane largely defines the present-day surface of the northern flank of the Suckling-Dayman Massif. The hanging wall block is either (i) largely eroded with minor exposures immediately south of Mt Suckling and Mt Masasoru where ultramafic rocks of the Papuan Ultramafic Belt (PUB) overlie sheared greenschist facies metabasite (Fig. 1.2; Davies, 1980), or (ii) is buried beneath Quaternary alluvium to the north of Mt. Dayman and Mt. Suckling (Fig. 1.2). However, the hanging wall block located on the east flank of the Dayman Dome and north of the Biman dip slopes comprises the Gwoira Conglomerate (Figs 1.2 & 2.1). The literature is unclear as to the timing of deposition of the sediment in the Gwoira Conglomerate relative to movement on the Mai'iu Fault. However, a Pliocene deposition age suggests that the unit postdates at least some of the movement on the Mai'iu Fault. The broad aim of examining the structure and sedimentology of the Gwoira Conglomerate is to document the structural and metamorphic relationship of the hanging wall sedimentary rocks to the metabasite footwall by examining the contact between the two units (i.e. the Mai'iu Fault). The more specific observational and analytical aims were to: (1) analyse and document the textural characteristic of the component clasts; (2) document any sedimentary structures and fabrics in the unit in order to reconstruct the sedimentary processes that emplaced the unit; (3) determine the sedimentary environment of deposition; and (4) explore the possibility that the source for the sediment in the Gwoira Conglomerate may have included the actively exhuming metabasite dome (i.e. Dayman Dome). A detailed sedimentological analysis of the Gwoira Conglomerate has not proven possible because of the high degree of weathering and poor outcrop of the unit. Consequently, this chapter presents an overview of the key sedimentological characteristics of the Gwoira Conglomerate and explores its petrographic makeup. These observations will be incorporated into the geological synthesis.

4.2 Regional setting

The Gwoira Conglomerate is situated east of the Dayman Dome and north of the Biman dip slopes (Figs 1.2, 2.1 & 4.1); it covers an area of approximately 25-30 km^2 and has a rectangular outcrop area (Fig. 1.2) because the unit is fault-bounded. It is faulted against the Goropu metabasalt to the east, south and west, and Quaternary alluvium to the north (Figs 1.2 & 4.1). The ductile Mai'iu Fault along the Biman dip slopes and Dayman Dome forms the southern (Fig. 4.2) and western (Fig. 4.3) boundaries of the unit. The Gwoira Fault, a younger brittle north-dipping normal fault, marks the northern boundary (Figs 4.4 & 4.5) and Mann and Taylor (2002) suggested that it is the most recently active rift propagation fault in the Papuan Peninsula. The border with Mt. Masasoru is a fault that may be the curved continuation of the Mai'iu Fault based on the map pattern (Fig. 1.2).

Analysis of aerial photographs (Chapter 2) shows that the Gwoira Conglomerate is more weathered and eroded than the adjacent Goropu Metabasalt (compare Figs 4.1 & 4.3). Trees are confined to small valleys that dissect the Gwoira Conglomerate (Figs 4.6 & 4.7). It remains unclear as to why the ridges are bare, however, this pattern is common in the area. The extensive erosion defines the tone of the Gwoira Conglomerate on aerial photographs and permits delineation of its boundaries. Previous erosional surfaces that have been recently uplifted (peneplains) are exposed as flat-topped hills within the Gwoira Conglomerate (Fig. 4.7).

4.3 Gwoira Conglomerate

Davies and Smith (1974) described the Pliocene Gwoira Conglomerate as comprising conglomerate and poorly sorted sandstone and siltstone with an estimated stratigraphic thickness of 1000 m. The Gwoira Conglomerate unconformably overlies the Upper Cretaceous Goropu Metabasalt and Jurassic-Cretaceous ultramafic rocks of the Papuan Ultramafic Belt, and was deposited in a high-energy marine environment

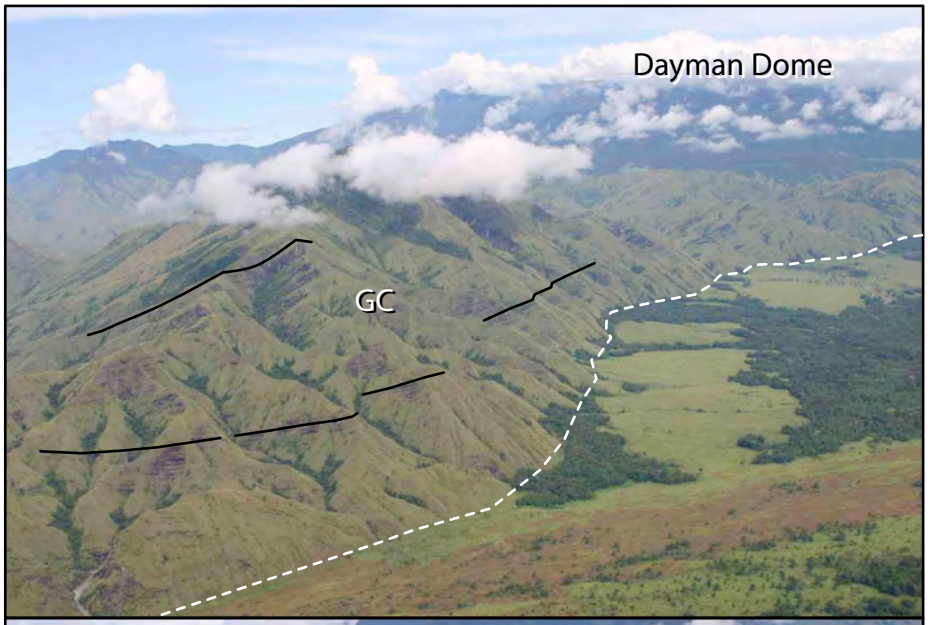

Figure 4.1 View of the Gwoira Conglomerate looking southwest. Note southeast dipping beds of the Gwoira Conglomerate (GC) highlighted by black lines. The Gwoira Fault is marked by a dashed line.

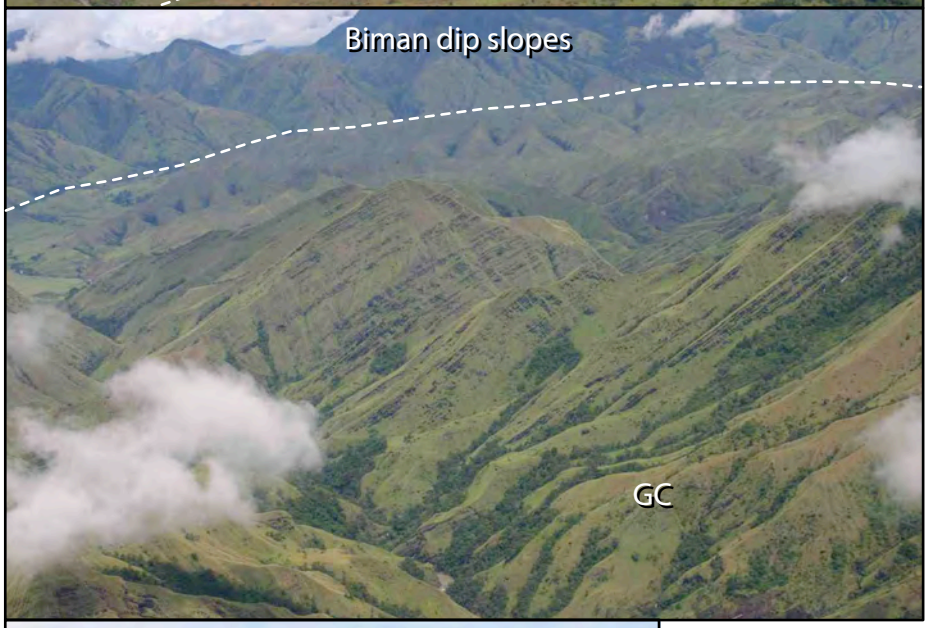

Figure 4.2 View looking SSW of the Gwoira Conglomerate with Biman dip slopes in background separated by the Mai'iu Fault marked by a dashed line.

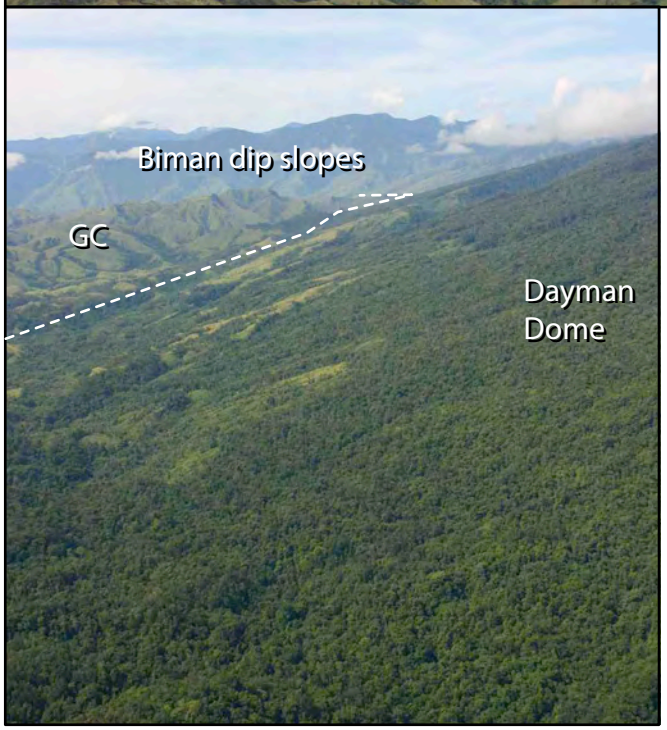

Figure 4.3 View looking south of the east flank of the Dayman Dome. Mai'iu Fault marked by a dashed line.

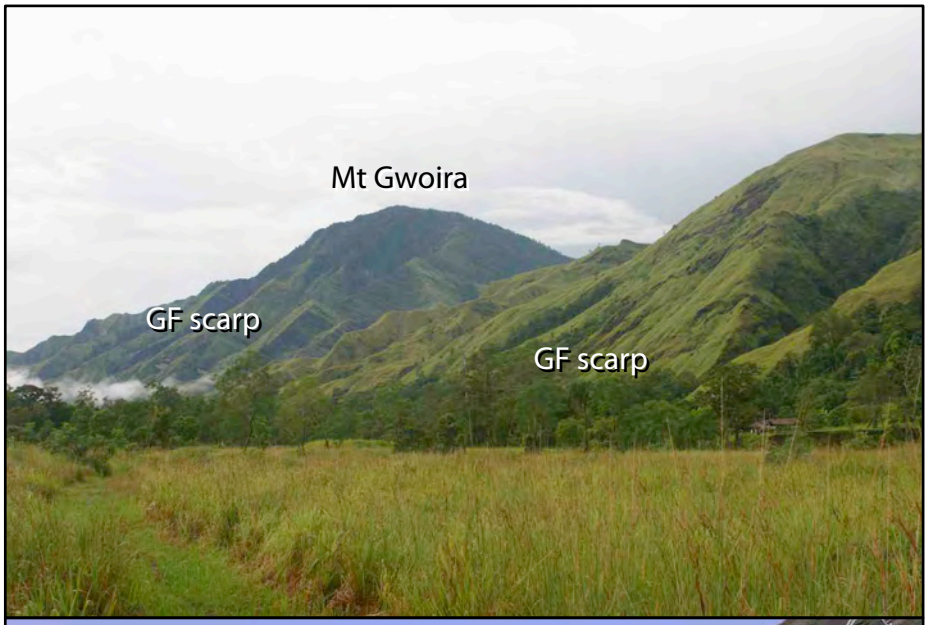

Figure 4.4 View looking southeast toward Mt Gwoira. Note the brittle moderately to steeply north-dipping Gwoira Fault (GF) scarp along the northern side of the hills.

Figure 4.5 Google Earth™ image view looking east of the Gwoira Fault marked by a dashed line.

Figure 4.6 Erosion pattern of the Gwoira Conglomerate. Note the vegetation is confined to the narrow valleys.

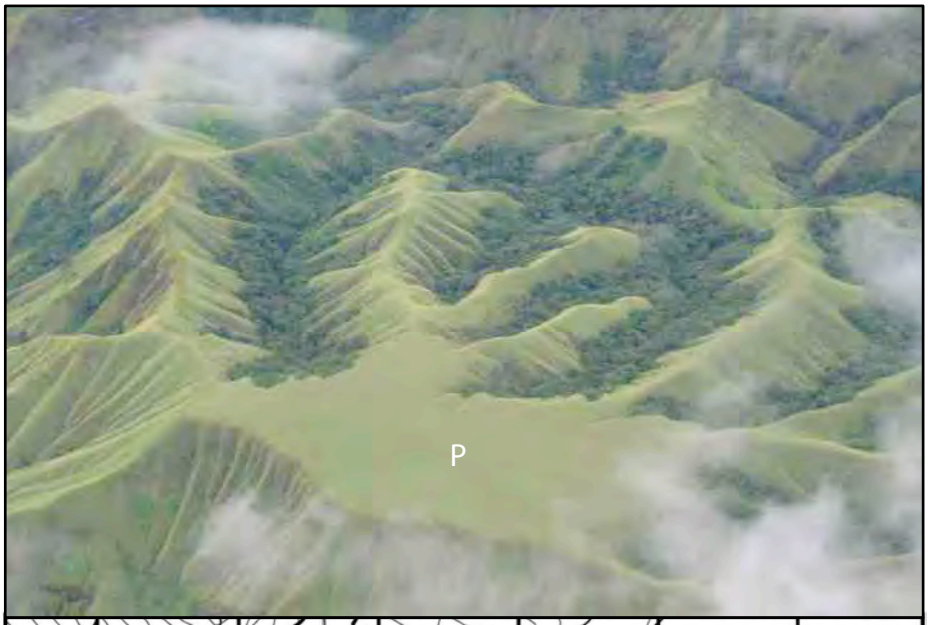

Figure 4.7 View of the Gwoira Conglomerate looking south. A peneplain (P) is in the foreground.

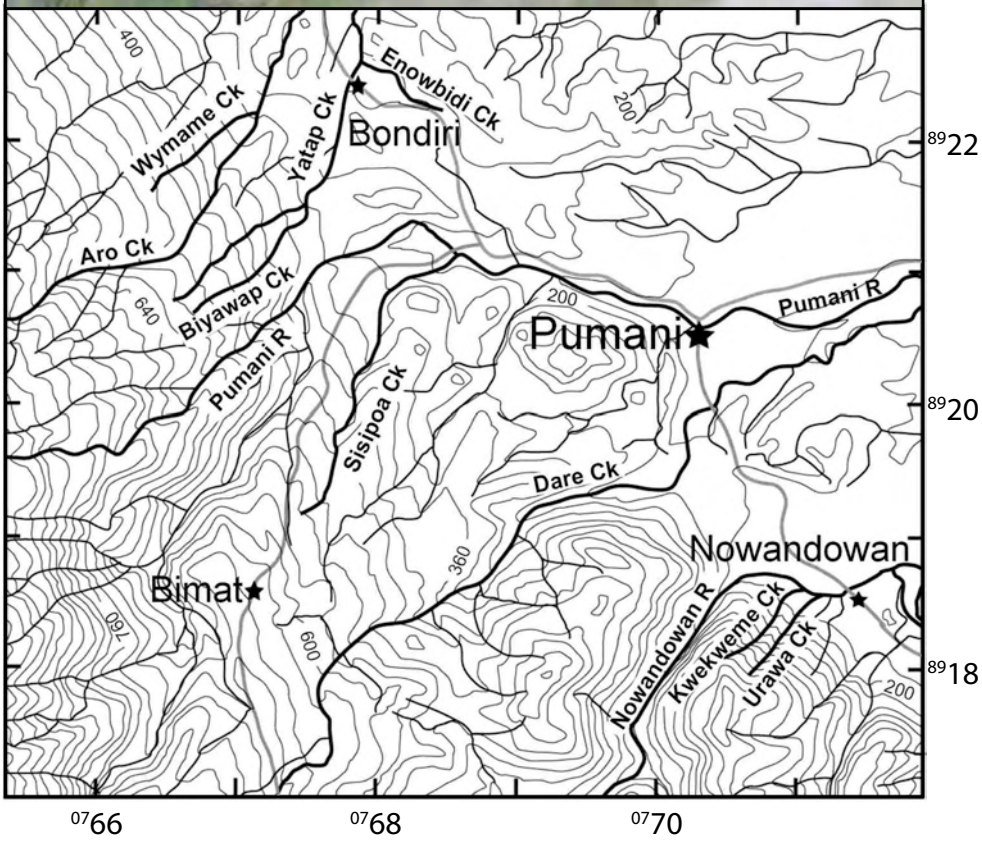

Figure 4.8 Map showing locations discussed in text. Map projection is AGD66 and scale is in km.

(Davies and Smith, 1974). This study has recognised sandstones within the Gwoira Conglomerate that are fossiliferous (see below).

Deep weathering and tropical vegetation limit outcrop of the Gwoira Conglomerate to the rivers and streams that dissect the unit. Traverses were completed along a number of rivers and streams including Urawa, Kwekweme, Dare, Sisipoa, Biyawap, Aro, Yatap, Wymame and Enowbidi creeks and Nowandowan and Pumani rivers (Fig. 4.8). The outcrop along traverses is discontinuous as thick vegetation and landslide debris commonly cover it. Loose boulders and cobbles in the shorter streams provide examples of the nearby lithologies. All rudite examined along the traverses is dominated by angular pebble- and cobble-sized clasts and is therefore defined as breccia rather than conglomerate.

4.3.1 Pebble/cobble breccia

The breccia occurs as a green-grey coloured outcrop extending up to a few metres across (Fig. 4.9) but the poor outcrop does not allow determination of true thickness. The breccia is typically massive, although graded sequences of breccia to coarse sandstone and rarely to mudstone over less than one metre are present. Commonly, the interbedded breccia and sandstone units have sharp contacts (Fig. 4.10). Breccia units are poorly sorted to very poorly sorted. A coarse lithic sandstone matrix forms more than 50% of the breccia and consists of green-grey subangular rock fragments (Fig. 4.9). The size of the breccia clasts varies between 3-60 mm with rare boulders (Fig. 4.11). The majority of clasts have low sphericity and are angular to sub-angular (Fig. 4.9). Sparse well-rounded clasts have a highly polished, reddish-brown iron-oxide exterior (Fig. 4.12).

The matrix and smaller pebble clasts were examined in thin-section under petrographic and scanning electron microscopes. The majority of clasts are low-grade thermal and dynamothermal metabasite rock fragments that preserve igneous textures such as euhedral and lath-like to tabular plagioclase feldspar grains (i.e. displaying

Figure 4.9 Breccia of the Gwoira Conglomerate, Nowandowan River. Massive bedding runs from left to right and way up is up the page. Lens cap is 60 mm across.

Figure 4.10 Interbedded breccia (B), coarse and fine sandstone (S), Pumani River. Bedding runs from top to bottom and way up is to the right. Hand lens is 65 mm long.

Figure 4.11 550 mm long metabasalt clast in breccia outlined by dashed line, Sisipoa Creek. Hammer is 400 mm long.

Figure 4.12 Paraconglomeratic breccia of the Gwoira Conglomerate, Dare Creek. Lens cap is 60 mm across.

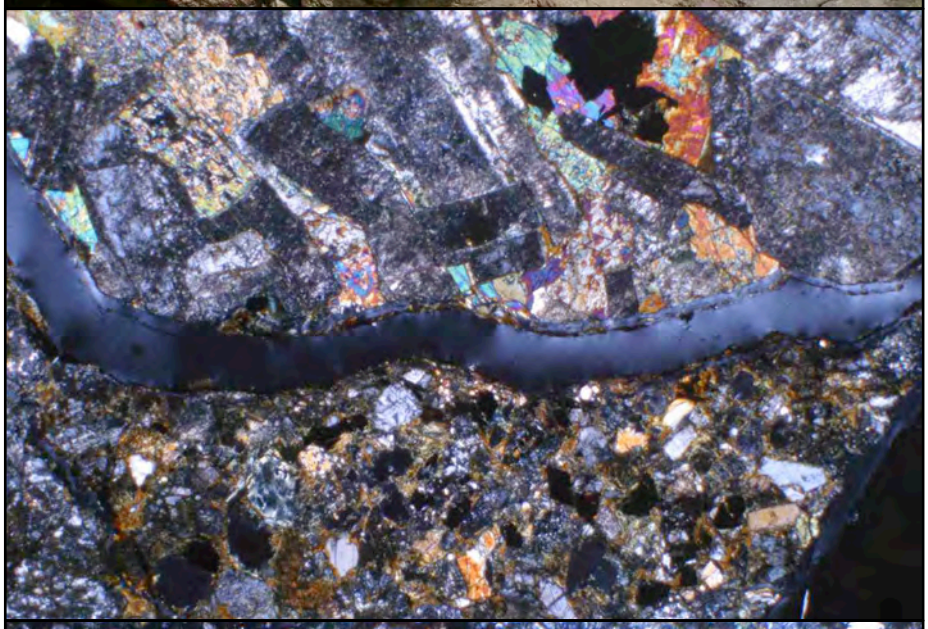

Figure 4.13 Photomicrograph showing blastogabbroic texture in upper clast, sample 0618A, Urawa Creek. Field of view is 1.75 mm across.

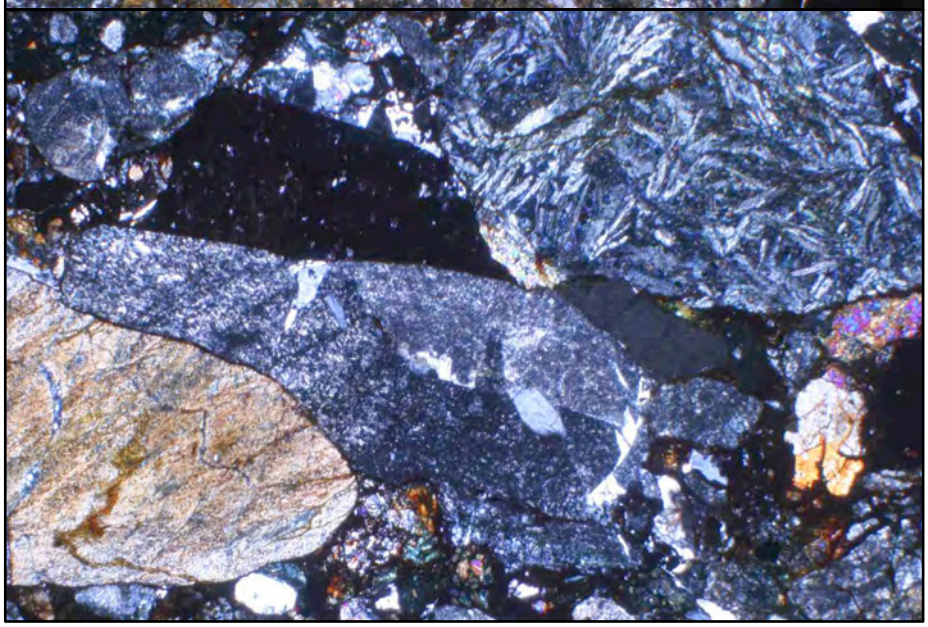

Figure 4.14 Photomicrograph showing blastodoleritic to blastobasaltic texture in upper right and middle clasts, sample 0607, Dare Creek. Field of view is 3.5 mm across.

blastogabbroic (Fig. 4.13) to blastodoleritic to blastobasaltic textures (Fig. 4.14)). The dynamothermal rock fragments are mylonite to ultramylonite (Fig. 4.15). Other rock fragments include (i) granophyric microgranites (with micrographic intergrowth of quartz and potassium feldspar; Dare and Urawa creeks; Fig. 4.16; sample 0608), (ii) clinopyroxenites (up to 5mm across; Dare Creek; Fig. 4.17), and (iii) sedimentary rocks (including rounded mudstone fragments up to 3 mm across; Dare Creek; Fig. 4.18). The metabasite rock fragments in both the matrix and clasts contain prehnite, pumpellyite, chlorite, albite, epidote, titanite and quartz (Figs 4.19 & 4.20). Igneous clinopyroxene and ilmenite are preserved in some clasts and plagioclase is commonly albitised or replaced by the above metamorphic minerals. The matrix also contains monomineralic grains of plagioclase and clinopyroxene (Fig. 4.19e). Minor pressure solutions features are evident between clasts as concavo-convex contacts between grains. Authigenic clay, including smectite (identified by electron microprobe), is observed filling cavities and replacing plagioclase (Fig. 2.20d).

4.3.2 Sandstone

Sandstone outcrops within the Gwoira Conglomerate are mostly green-grey outcrops with a reddish tinge. The true thickness of sandstone beds is difficult to ascertain due to the dense vegetation, but sequences at least a few metres thick are exposed. The sandstone units are typically massive or interbedded with breccia/conglomerate and mudstone or as part of the graded sequences (Figs 4.21 & 4.22). The sandstone is commonly highly friable, possibly reflecting a high degree of weathering. Most of the sandstone is clast supported with the exception of the graded sequences, which tend to be slightly more matrix supported. The sandstone varies from very fine to very coarse and most are poorly sorted. The reddish tinge is more common in graded units.

The sandstone grains are similar to those described in the breccia unit and include low-grade thermal and dynamothermal metabasite rock fragments. Microscopic analysis indicates the sand size fraction is similar to that of the breccia unit and includes the same metabasite mineral assemblages as described above.

Figure 4.15 Mylonitised cobble (pale green) in the Gwoira Conglomerate, Pumani River. Foot is 300 mm long.

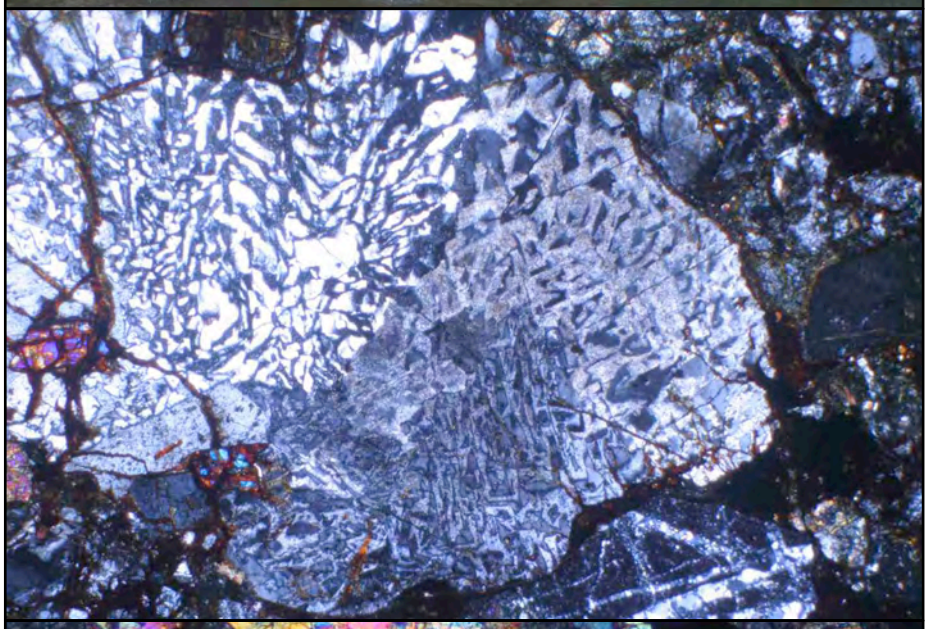

Figure 4.16 Photomicrograph showing granophyric texture, sample 0608, Dare Creek. Field of view is 1.75 mm across.

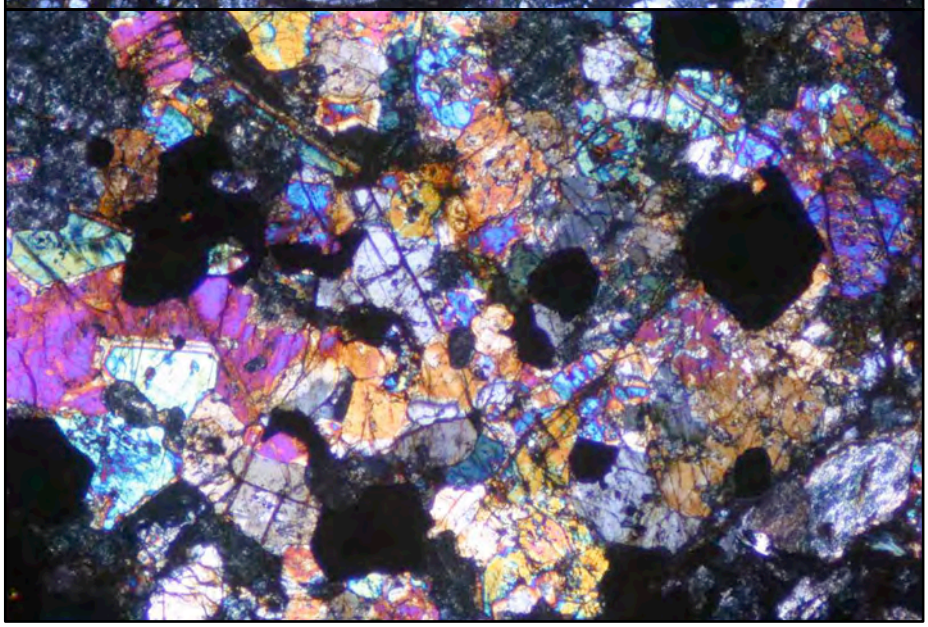

Figure 4.17 Photomicrograph showing clinopyroxenite clast in breccia, sample 0614, Dare Creek. Field of view is 1.75 mm across.

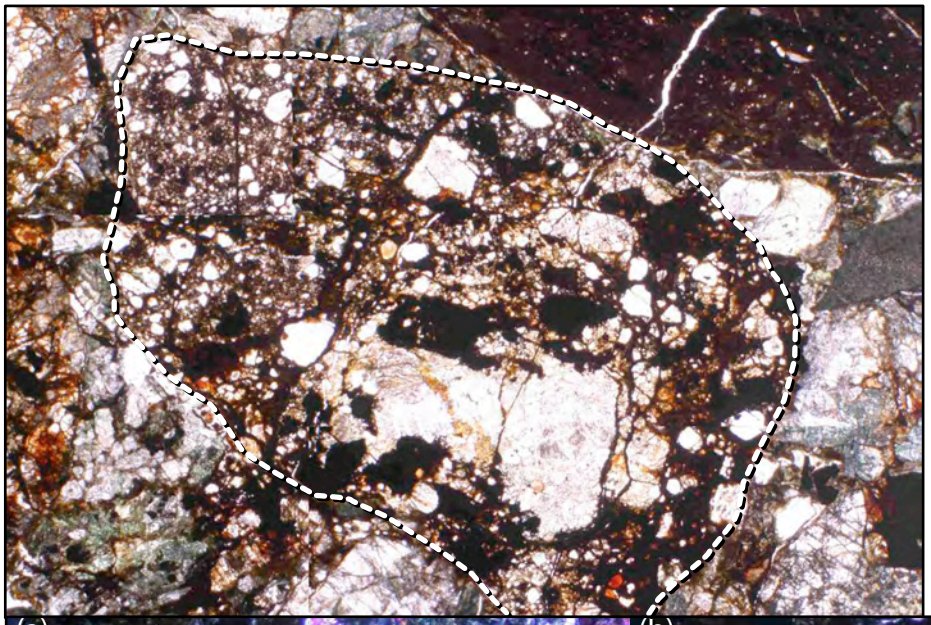

Figure 4.18 Reworked and rounded mud-stone clast outlined by a dashed line in the Gwoira Conglomerate, sample 0612B, Dare Creek. Field of view is 3.5 mm across.

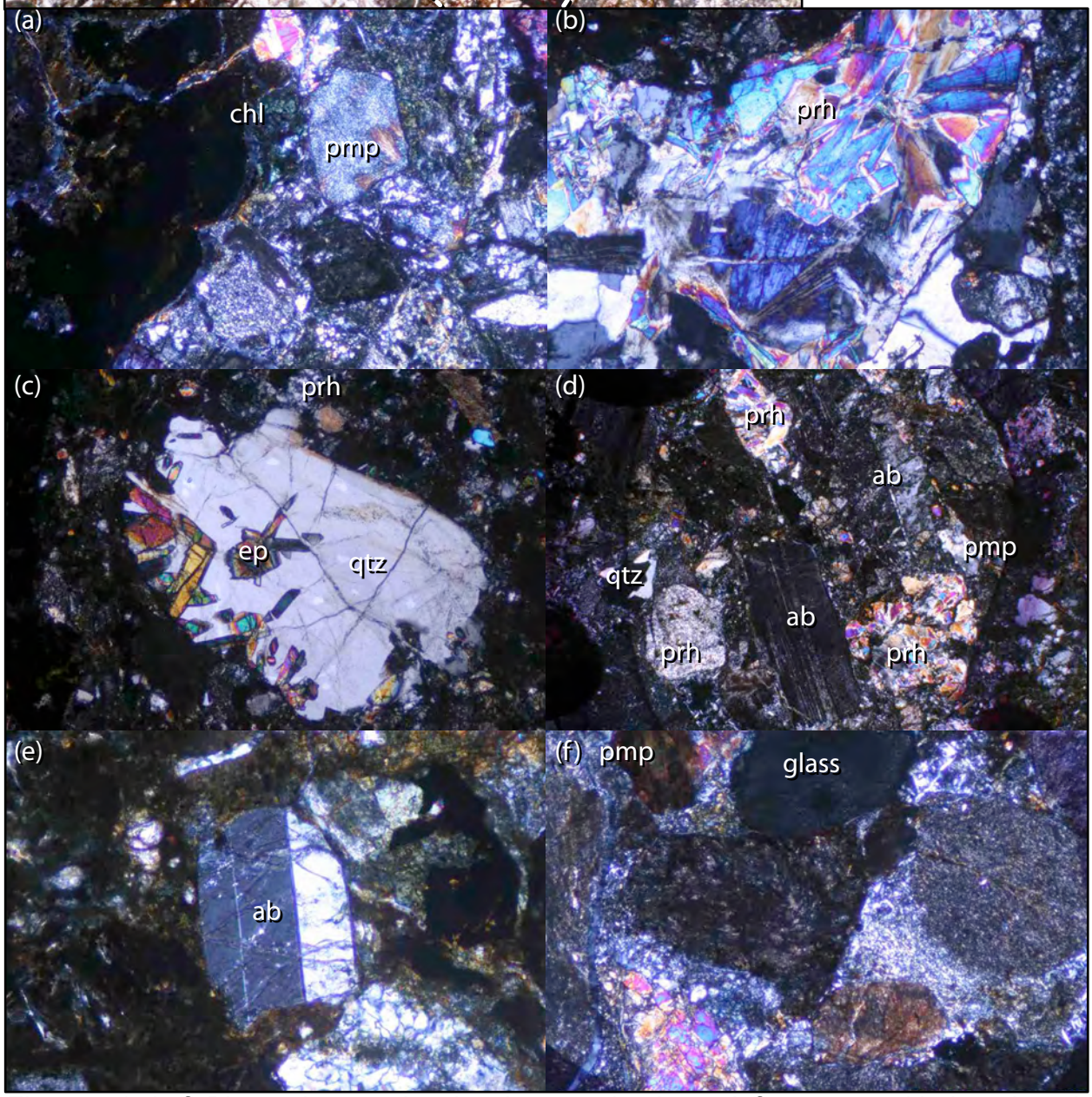

Figure 4.19(a-f) Photomicrographs showing metabasite rock fragments with the minerals prehnite (prh), pumpellyite (pmp), chlorite (chl), albite (ab), epidote (ep) and quartz (qtz), sample 0602A, Pumani River. Field of view is 1.75 mm across (a-c,e,f); 3.5 mm (d).

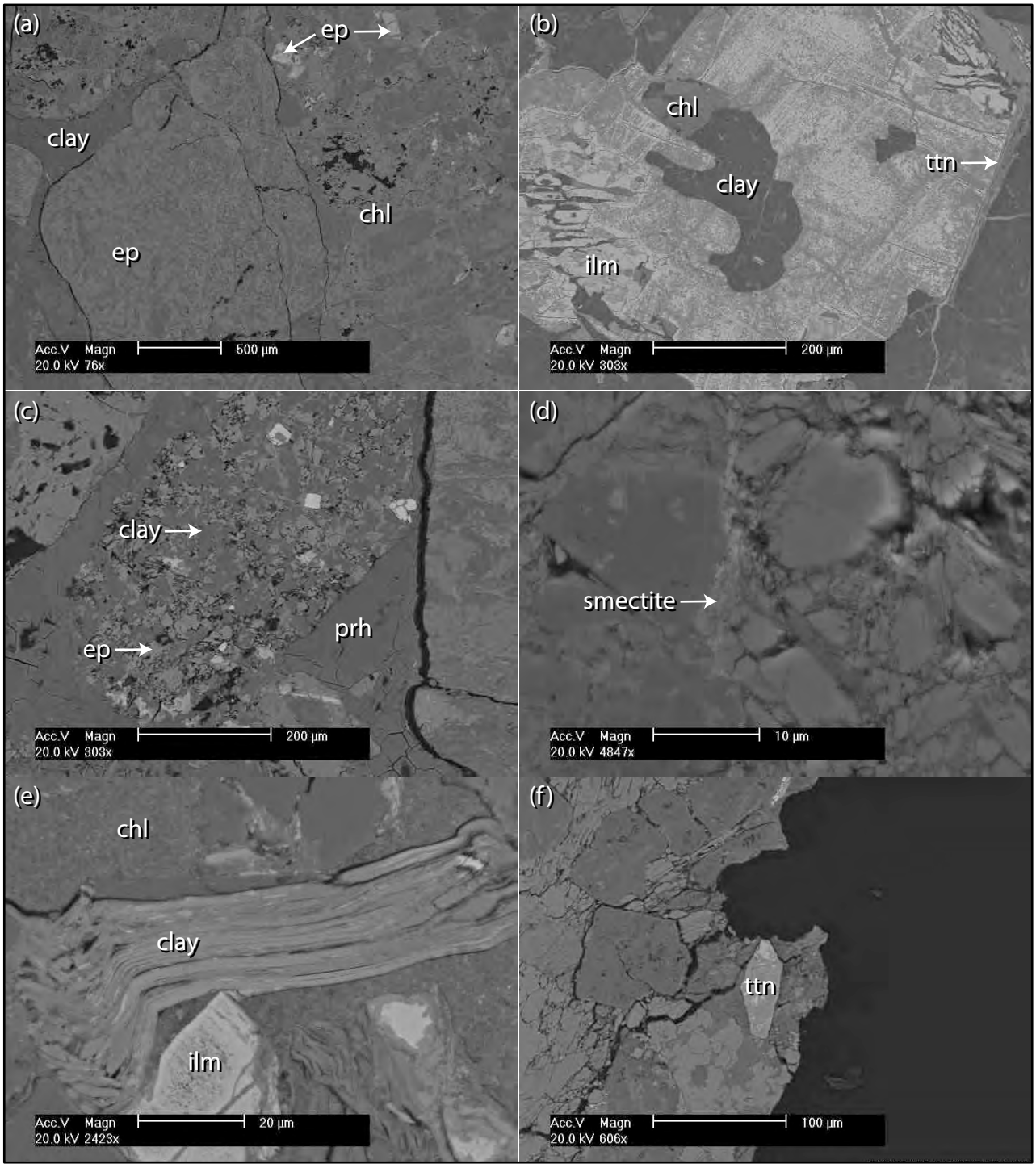

Figure 4.20(a-f) Back-scattered electron (BSE) images showing the key mineralolgy of metabasite rock fragments with the minerals prehnite (prh), chlorite (chl), epidote (ep), clay, smectite, titanite (ttn) and ilmenite (ilm) in sample 0614, Dare Creek. Scales as shown on images.

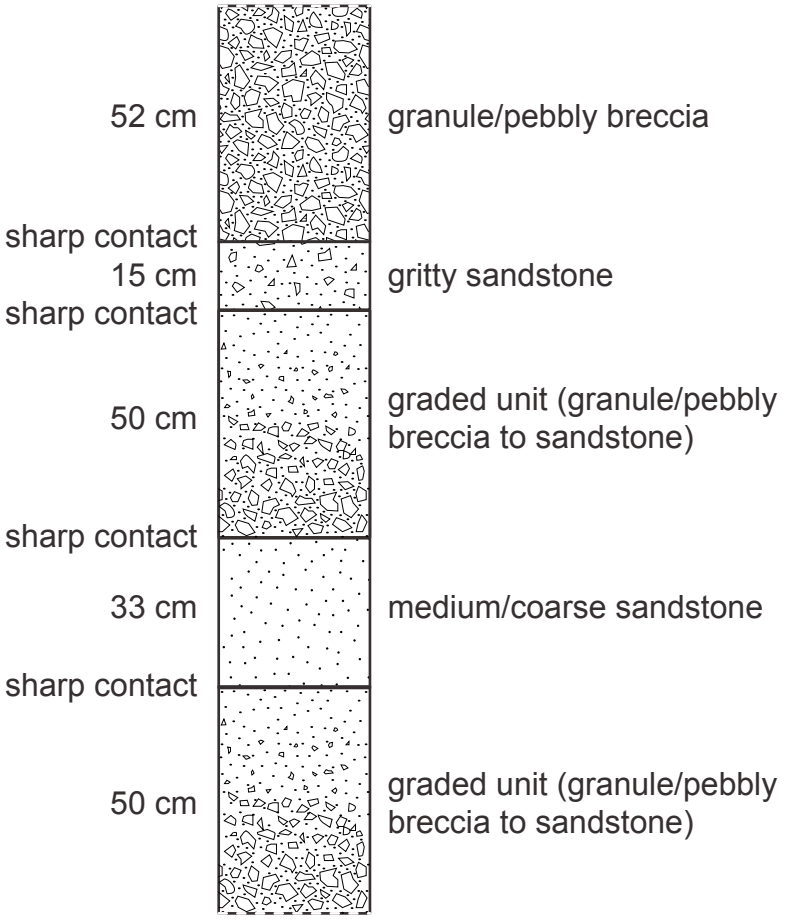

Figure 4.21 Simple stratigraphic log of sedimentary rocks at the junction of Sisipoa Creek and the Pumani River GR685212. Dashed lines indicate unexposed base and top of section.

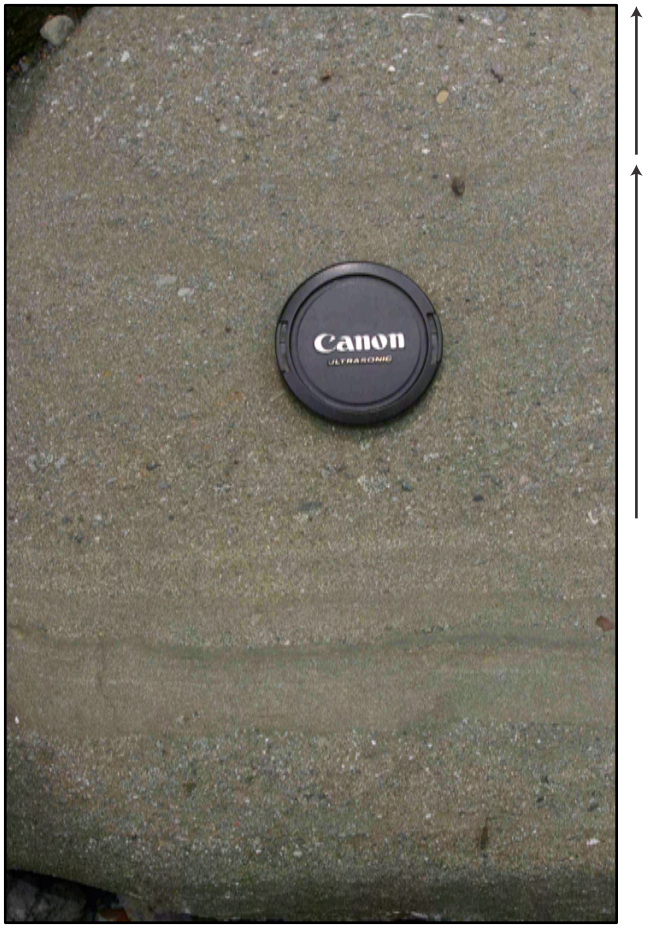

Figure 4.22 Typical sandstone beds in the Gwoira Conglomerate, Dare Creek. Fining upward cycles indicated by black arrows to the right of image. Lens cap is 60 mm across.

4.3.3 Mudstone

Mudstone is rare and occurs as thin lenses within sandstone or breccia beds (Fig. 4.23) or at the top of graded beds. The best exposure of mudstone is located in the southern section of Dare Creek. This outcrop is a 5m thick layer of mudstone (Fig. 4.24) containing bivalve shells and symmetrical ripple marks at the top of the underlying graded breccia, sandstone and mudstone bed. Carbonate concretions are common within mudstone (Fig. 4.25) and some preserve lamination and bedding (Fig. 4.26). The mudstone comprises medium-coarse silt and clay; it is moderately to well sorted (Fig. 4.24). Analysis by SEM of the coarser grains within the mudstone indicates the silt-size fraction is similar to that of the breccia and sand units and includes the same metabasite mineral assemblages as described above; that are monomineralic clasts of plagioclase, clinopyroxene, chlorite and minor titanite (Fig. 4.27). Other grains include authigenic framboidal pyrite, deformed and undeformed fossilised woody debris and abundant calcite cement within the concretions (Fig. 4.27).

4.3.4 Fossiliferous sandstone and limestone

The vast majority of the Gwoira Conglomerate examined in this study is absent of fossils with a single bivalve cast found in only one sample of mudstone (0617B). However, loose stream rubble ('float') in Dare Creek, which was most likely carried downstream from stratigraphically higher components of the Gwoira Conglomerate, includes fossiliferous sandstone and limestone. The float samples contain a diverse group of fossils that are dominated by coral rubble and include solitary (Fungidae), branching and massive corals (Scleractinia; Fig. 4.28 and 4.29). Minor fossils identified in hand sample include *Tridacna* (giant clam, 20-30 cm across), gastropods, pectin bivalves and bryozoans. The coral rubble shows evidence of abrasion, whereas some fossils preserve delicate ornament (for example the costae of the calices of the Fungidae and shells of bivalves). Rare 2-3 mm granule size grains that preserve basaltic texture are present

Figure 4.23 Lens of mudstone in breccia of the Gwoira Conglomerate, Nowandowan River. Lens cap is 60 mm across.

Figure 4.24 Mudstone of the Gwoira Conglomerate, Dare Creek. Lens cap is 60 mm across.

Figure 4.25 Concretions in mudstone of the Gwoira Conglomerate, Dare Creek. Lens cap is 60 mm across.

Figure 4.26 Concretion with laminations preserved, Dare Creek. Lens cap is 60 mm across.

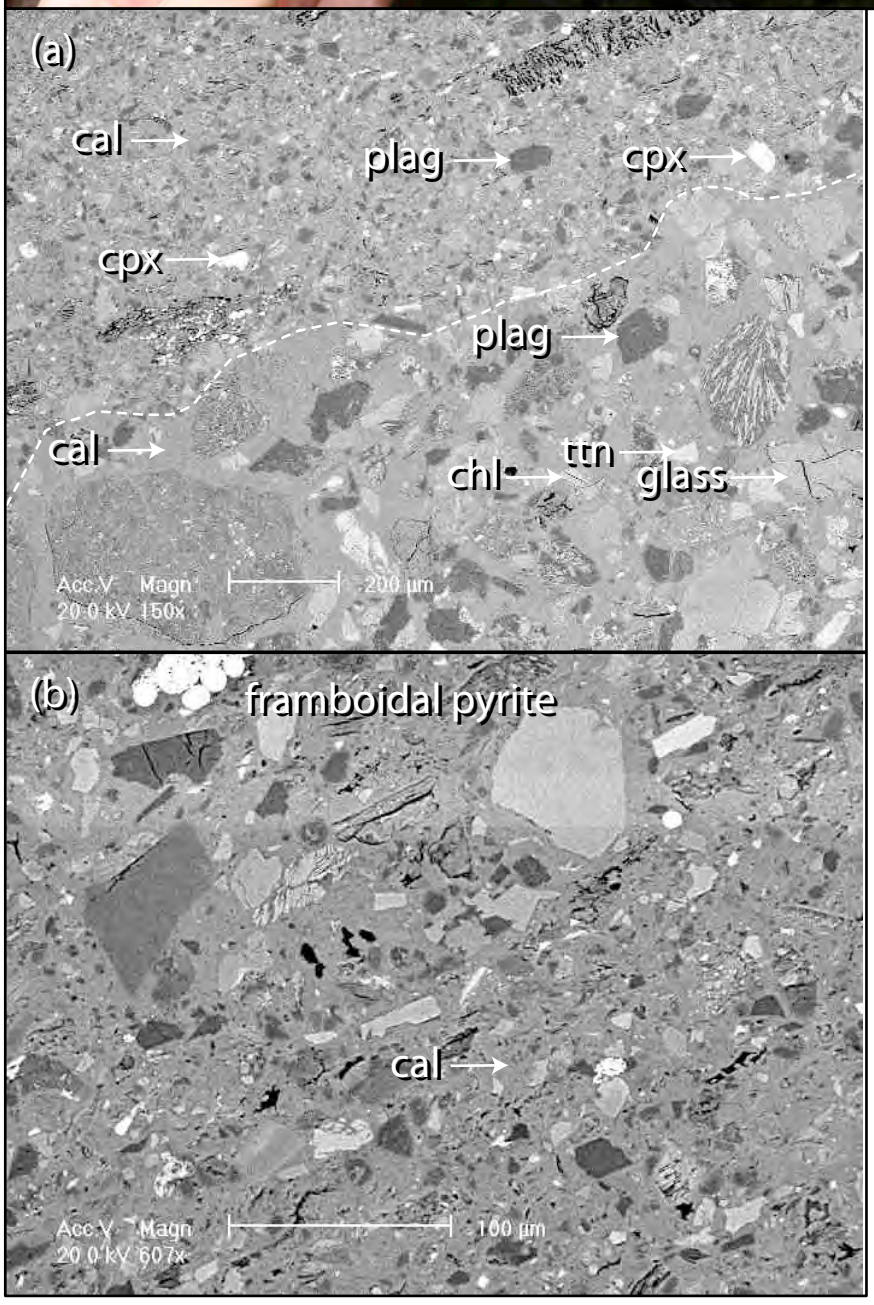

Figure 4.27 Back-scattered electron (BSE) images of sample 0617A showing (a) the boundary between a concretion (lower) and mudstone (upper) marked by a dashed line, and (b) representative concretion, Dare Creek. Monomineralic clasts include plagioclase [anorthite-rich] (plag), clinopyroxene (cpx), calcite (cal), chlorite (chl) and titanite (ttn). Scales as shown on images.

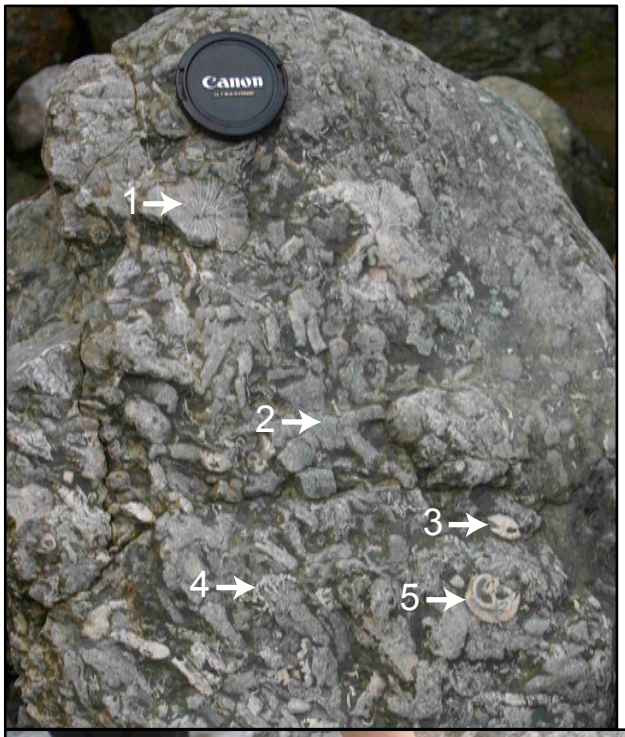

Figure 4.28 Fossiliferous coral rubble boulder in Dare Creek. Fossils include 1. solitary coral (Fungidae); 2. branching coral; 3. bivalves; 4. massive coral; and 5. gastropods. Lens cap is 60 mm across.

Figure 4.29 Fossiliferous coral rubble boulder in Dare Creek. Fossils are dominated by corals.

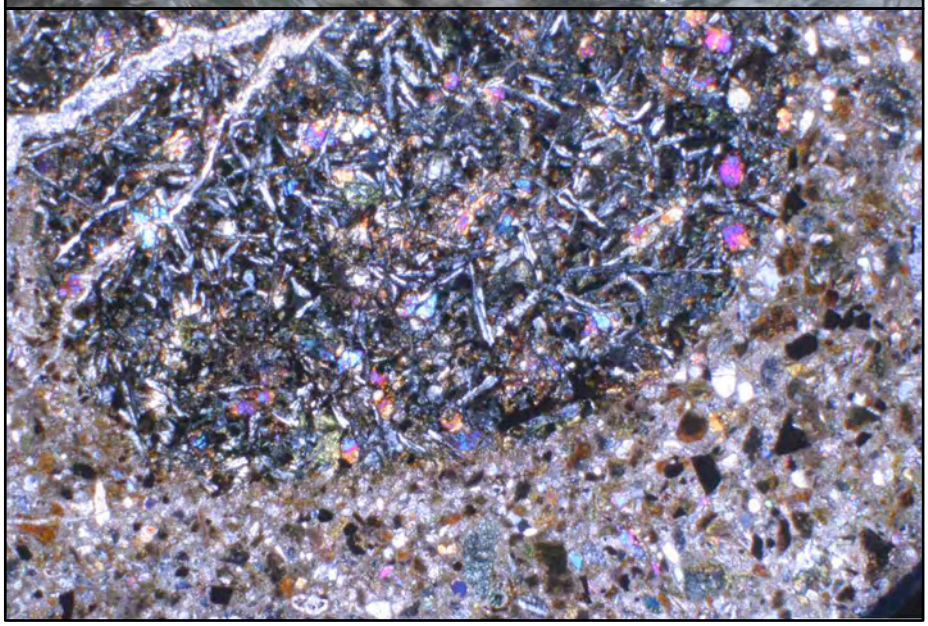

Figure 4.30 Photomicrograph showing blastobasaltic texture in a pebble-sized clast in fossiliferous fine-grained sandstone, sample 0624B, Dare Creek. Field of view is 3.5 mm across.

in some samples (Fig. 4.30). The limestone rudite samples are fossil clast-supported, poorly to very poorly sorted and very immature. The cement is invariably calcite and may comprise up to 15%. The fossils range from microscopic up to 130 mm across. The matrix is poorly sorted silt to fine sand and includes rare echinoderm spines (Fig. 4.31) and foraminifera (~800 μm across; Fig. 4.32) along with fragmented coralline red algae (Fig. 4.33). The foraminifera includes trochospiral (Fig. 4.32a), biserial (Fig. 4.32b) and triserial (Fig. 4.32c) forms and in particular species belonging to Buliminidae (Fig. 4.42b) and Elphididae (*Elphidium*; Fig. 4.32d). The fossil assemblage does not tightly constrain the age of the Gwoira Conglomerate, as these fossils are all common throughout the Tertiary. SEM analysis indicates that the matrix is similar to that of the sandstone and mudstone units described above (Fig. 4.34a) and includes plant fossils (Fig. 4.34b). Authigenic framboidal pyrite is common (Fig. 4.34c).

4.3.5 Quaternary alluvium

The lower Dare Creek (north) cuts through a section of Quaternary alluvium. The semi-consolidated sedimentary wall is 15 m high and contains layers of poorly-sorted cobbles, pebbles and medium-size sand in addition to layers of well-sorted coarse and very coarse sand (Fig. 4.35). The clasts are mostly angular to sub-angular metabasite with low sphericity (Fig. 4.35), but rare clasts show well-rounded shape and high sphericity. The bedding consists of shallow cross bedding (Fig. 4.36) and more commonly horizontal layers.

4.5 Mineral chemistry

The minerals of the clasts were analysed by electron microprobe (EMP) in order to determine their major element compositions and to classify the mineralogy of the different metamorphic assemblages within clasts. All EMP analyses are presented in Appendix C. The main aim of the EMP study is to use the mineral chemistry data to better understand the provenance of the various clasts that make up the Gwoira Conglomerate.

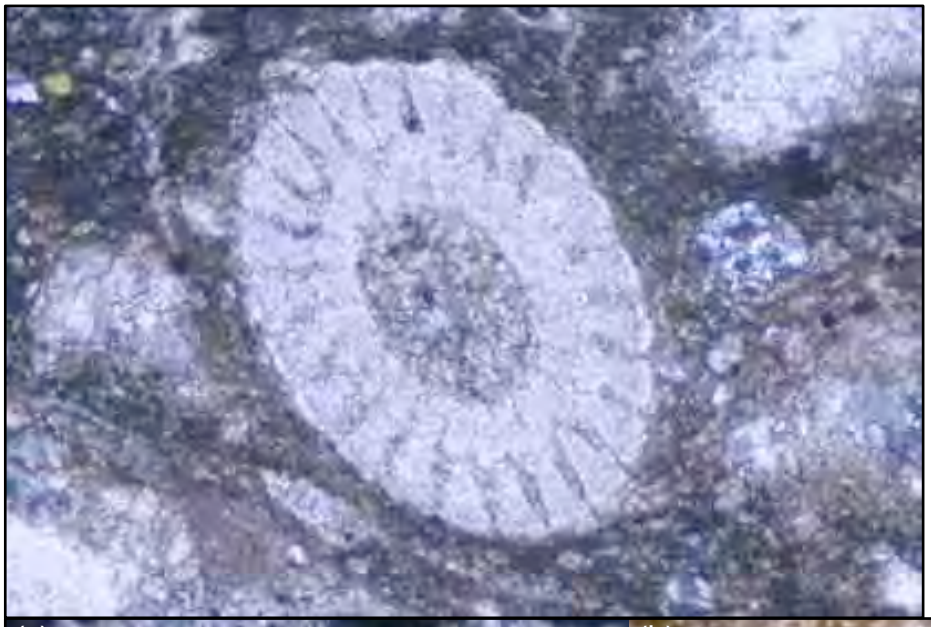

Figure 4.31 Echinoderm spine in the Gwoira Conglomerate, sample 0601D, Dare Creek. Field of view is 1.75 mm across.

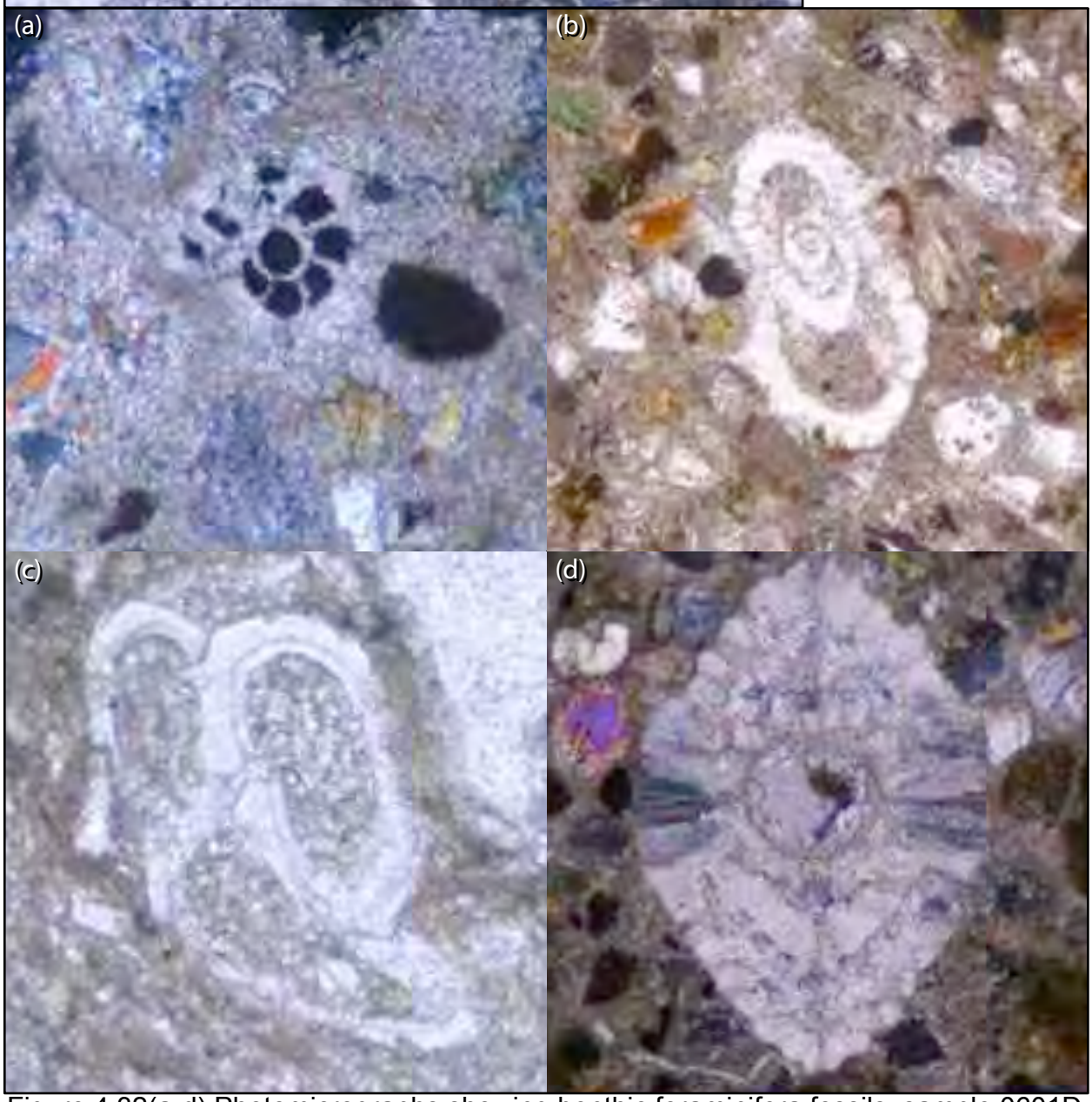

Figure 4.32(a-d) Photomicrographs showing benthic foraminifera fossils, sample 0601D, Dare Creek. Field of view is 1 mm across. (a) trochospiral form; (b) biserial form (Buliminidae); (c) trierial form; (d) Elphididae (*Elphidium*).

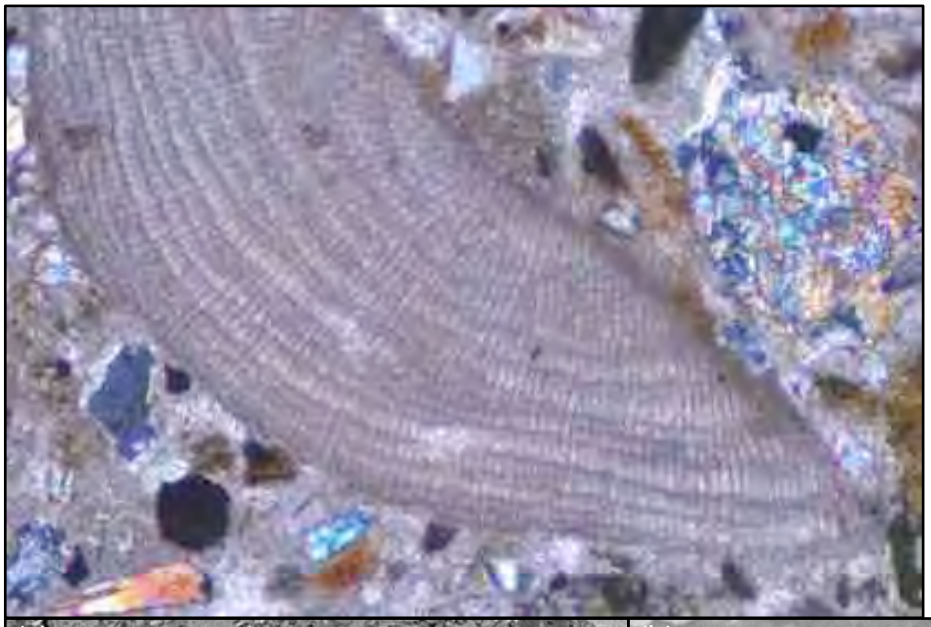

Figure 4.33 Coralline red algae in the Gwoira Conglomerate, sample 0624B, Dare Creek. Field of view is 1.75 mm across.

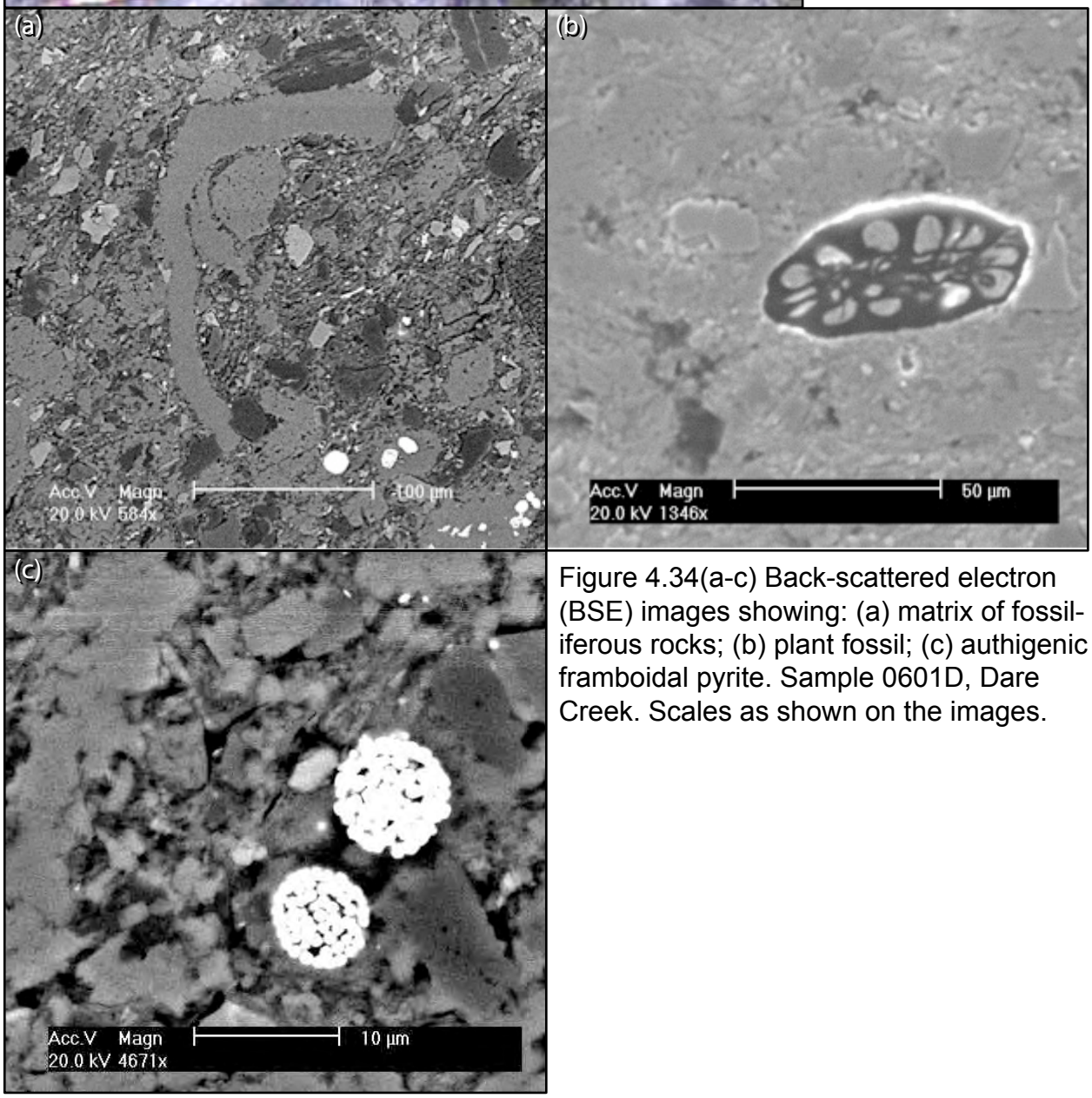

Figure 4.34(a-c) Back-scattered electron (BSE) images showing: (a) matrix of fossiliferous rocks; (b) plant fossil; (c) authigenic framboidal pyrite. Sample 0601D, Dare Creek. Scales as shown on the images.

Figure 4.35 Unconsolidated Quaternary alluvium, Dare Creek. Note rare rounded cobble horizons.

Figure 4.36 Shallow cross-bedding in unconsolidated Quaternary alluvium, Dare Creek. Field of view is approximately 5 m.

The main mineral constituents of the various metamorphic lithic fragments include albite, chlorite, epidote, prehnite and pumpellyite. Minerals of possibly mixed igneous or metamorphic origin include clinopyroxene and plagioclase. Minor volcanic glass was also analysed. Plagioclase feldspar is albite with X_{An} = Ca/(Ca+Na) = 0.02-0.04, where Ca and Na are the number of calcium and sodium cations per formula unit (Fig. 4.37a). The chlorite classifies as penninite or talc-chlorite (Hey, 1954) with X_{Fe} = Fe/(Fe+Mg) = 0.20-0.24, where Fe and Mg are iron and magnesium cations per formula unit (Fig. 4.37b). The recalculation of pumpellyite from EMP analyses is problematic as (i) substantial (OH) may substitute for O, which is not determined, and (ii) O may substitute for (OH) accompanying the introduction of trivalent ions into the X positions (Coombs *et al*., 1976). Therefore, an assumption of filled cation sites and a Fe^{2+}:Fe^{3+} ratio that fills the X site allows a recalculation on the basis of 8 cations per formula unit. Pumpellyite is Fe- and Al-rich and is classified as Pu-(Fe) (Fig. 4.37c; Coombs *et al*., 1976). Epidote shows appreciable substitution of Al by Fe^{3+}. Epidote with high Fe^{3+} content is called pistacite and epidote with low Fe^{3+} content is called clinozoisite (Fig. 4.37d). Epidote in these samples is Fe^{3+}-rich pistacite with Fe^{3+} = 1.57-1.94 cations on the basis of 25 oxygen (Fig. 4.37d). Prehnite may also show appreciable substitution of Al by Fe^{3+}. Prehnite is Fe^{3+}-poor with X_{Fe3+} = Fe^{3+}/(Fe^{3+}+Al) = 0.00-0.15, where all FeO is recast as Fe_2O_3 and Fe^{3+} and Al are the number of cations of ferric iron and aluminium cations per formula unit. The clinopyroxene classification was determined using the spreadsheet PX-NOM (Sturm, 2002). Monomineralic clinopyroxene grains classify as aluminian or aluminian chromian augite, have X_{Fe} = 0.17-0.27 and plot as augite (Fig. 4.37e). Analyses of hydrated volcanic glass have totals of 92-96 wt% oxide, consistent with palagonitisation and alteration of the primary glass. However, the compositions are generally Fe-Mg-Ca-rich and Si-Al-Na-K-poor, consistent with a mafic source.

4.6 Discussion

The poor outcrop precludes an analysis of systematic across- and along-strike variation in the Gwoira Conglomerate. Way-up structures were not observed, however, aerial

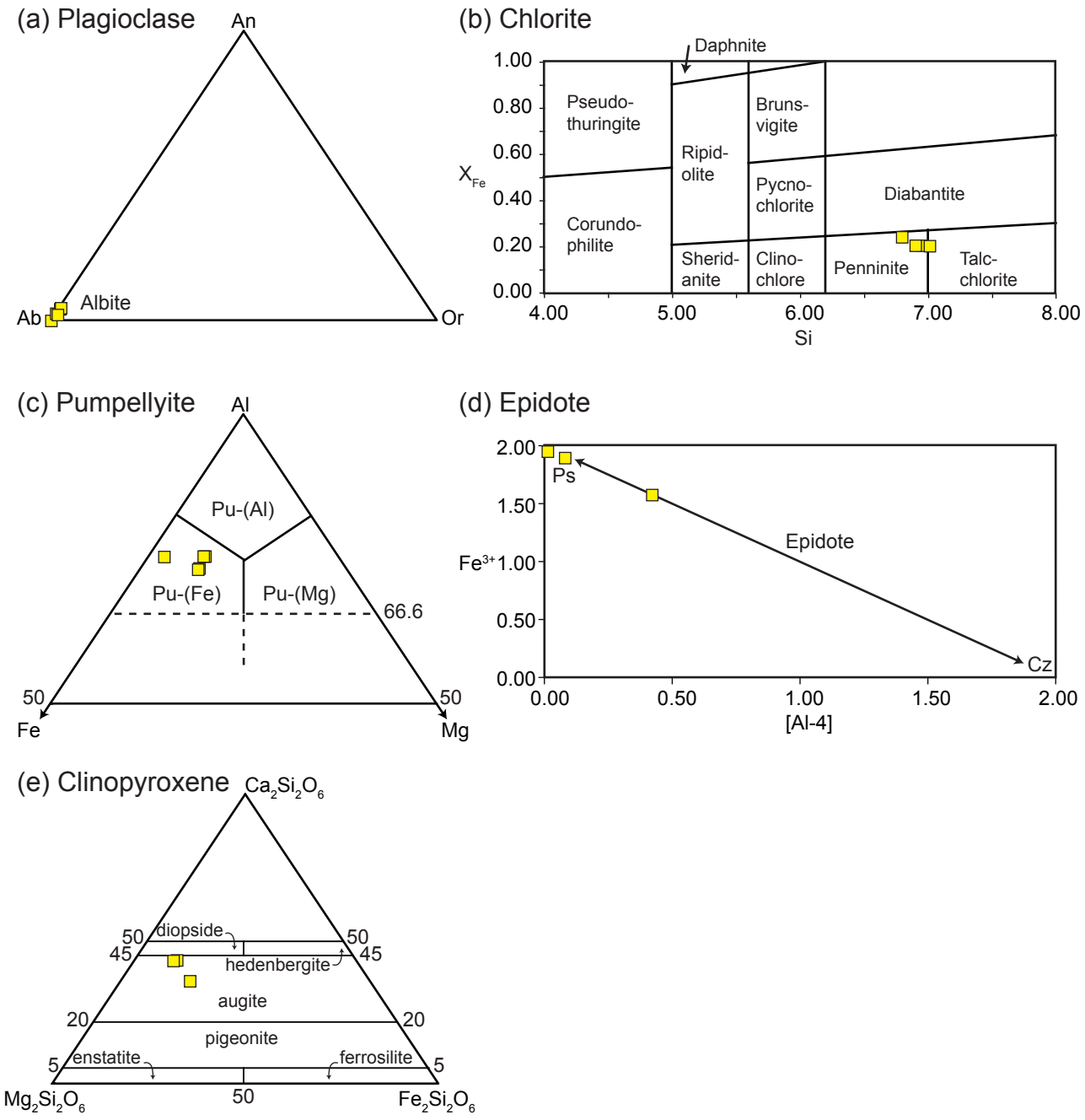

Figure 4.37 Mineral chemistry classification plots for (a) plagioclase [An = anorthite, Ab = albite, Or = orthoclase]; (b) chlorite [X_{Fe} = Fe/(Fe+Mg), Si = number of silicon cations recalculated for 28 oxygen]; (c) pumpellyite [Pu-(Al), Pu-(Fe) and Pu-(Mg) are the Al, Fe and Mg-rich end members]; (d) epidote [Fe^{3+} and Al = number of ferric iron and aluminium cations respectively recalculated for 25 oxygen, Ps = pistacite (2 Fe^{3+}), Cz = clinozoisite (0 Fe^{3+})]; and (e) clinopyroxene.

photographs and Google Earth images (Chapter 2) show bedding in the Gwoira Conglomerate generally dips southeast with no evidence of overturned beds and therefore the graded beds are interpreted as normal. Key observations of the Gwoira Conglomerate include massive bedding and rare normal grading, poor sorting, and very angular to moderately rounded clasts supported by matrix. These characteristics are consistent with sediment gravity flows in general (Middleton and Hampton, 1976). Poorly sorted and massively bedded units are more typical of cohesive debris flows (Fisher, 1971; Coussot and Meunier, 1995), whereas rare graded beds indicate low-particle concentration usual for turbidity currents (Lowe, 1976). Very rare rounded clasts within massively bedded units may indicate fluvial processes were active in the sedimentary cycle prior to reworking by sediment gravity flows. Many of the fossils are of species that contain algae within their tissue and therefore lived in the photic zone (shallow water < 5-20 m). The size of the *Tridacna* (giant clam) examined is most likely found in low-energy shallow reef environments. The pectin bivalves are commonly found in shallow water inner shelf environments. The rare in-situ bivalve cast found within the thick mudstone unit (sample 0617B) is of a bivalve that is much coarser grained than the enclosing mud and the cast shows excellent preservation of costae. Therefore, it is likely that the bivalve experienced little transport prior to deposition and that the mudstone was deposited within a shallow marine environment. This is consistent with plant fragments and a lack of planktonic and deep-water fauna within the fossil assemblage. Therefore the fossils suggest that sediment transport and deposition was largely within the shallow marine environment near to the coast of mainland PNG.

Low-grade metabasite that preserves igneous textures dominate (>80%) the lithic fragments. Minor constituents include igneous and sedimentary rock clasts and fossils. Monomineralic grains are derived from all these rock types. Petrologic analysis of the Gwoira Conglomerate shows a possible minor metamorphic overprint indicated by pressure solution, euhedral titanite, authigenic framboidal pyrite and altered basaltic glass. However, pressure solutions may be caused by an increase in pressure and fluid circulation within the complex and hence the penetration of the fabric is possibly a diagenetic feature. The occurrence of euhedral titanite may be due to an increase of

temperature and pressure caused by burial diagenesis (Morad and Aldahan, 1982). Authigenic framboidal pyrite is common throughout the complex and its presence may be due to leaching of precursor iron sulphides and an increase in fluid circulation due to burial (Neumann *et al*., 2006). In sample 0617A, undeformed fossils and the limited presence of framboidal pyrite and anhedral titanite in the concretions suggest that the strong calcite framework in the concretion protected these features during burial. This is inconsistent with a metamorphic overprint to explain the presence of abundant framboidal pyrite and deformed fossils elsewhere in the mudstone. A metamorphic overprint may be expected to form dolomite, talc or muscovite within the concretions and these are not observed. The presence of smectite around hydrated glass indicates a temperature limit for the diagenesis of ~120°C (Gifkins *et al*., 2005) and the absence of zeolite supports the burial diagenesis interpretation and not a burial metamorphic overprint. This interpretation suggests that all the metabasite lithic fragments within the Gwoira Conglomerate originated from the Dayman Dome during exhumation.

Chapter 5 STRUCTURAL GEOLOGY

5.1 Introduction

A pervasively developed mylonitic L-S tectonite defines a shear zone that forms the dominant structure on the flanks of the Dayman Dome. The shear zone foliation planes dip shallowly and contain a well-developed mineral stretching lineation. Low strain areas or pre-existing fabrics were not observed due to the pervasive nature of the fabric. Rare cross-cutting features include narrow ductile shear zones, veins, brittle to semi-brittle faults, and mafic dykes.

Field observations and nearly eight hundred structural measurements presented in this chapter establish the tectonic significance of and geometric relationship between the mapped structures. All field structural measurements are presented in Appendix D. Measurement of kinematic vorticity (Means *et al*., 1980; Lister & Williams, 1983; Passchier, 1986) for the dominant L-S tectonite permits an interpretation of the flow regime for the shear zone including the sense of displacement. All vorticity measurements are presented in Appendix E. Sense-of-shear indicators are analysed to further document the movement history of the shear zone. The aim of this chapter is to integrate detailed structural analyses to determine the evolution and kinematic significance of the shear zone that bounds the Dayman Dome.

5.2 Ductile shallowly dipping S1 and S2 fabric

All metabasite samples of the Dayman Dome examined in this study (excluding the dykes) are greyish green and contain a well developed S1 foliation and L1 lineation. S1 is defined by aligned actinolite, albite and chlorite, whereas elongate actinolite and albite grains define L1 at the outcrop scale. Very rare blue amphibole is restricted and concentrated in narrow bands (up to 3 mm wide) of S2 folia oriented sub-parallel to S1. The metabasite samples are fine-grained (< 0.5 mm).

5.2.1 Pumani: East flank of Dayman Dome

S1 on the east flank of the Dayman Dome is a coarse continuous foliation that strikes NNW and dips shallowly toward the ENE (average S1 orientation is 152 / 20 / ENE; Fig. 5.1a). S1 foliation planes contain a shallowly plunging L1 mineral lineation on the east flank that trends NNE (average L1 orientation is 14 -> 028). S1 foliation planes anastomose between extensional shear bands forming an S-C' fabric (Fig. 5.2).

Narrow bands of S2 also define a coarse continuous foliation oriented sub-parallel to S1 (Fig. 5.3) that strikes NNE and dips shallowly toward the ESE (average S2 orientation is 015 / 32 / ESE; Fig. 5.1b). The blue amphibole is riebeckite (see Chapter 6); it is aligned with S2 and is elongate to define L2 (Fig. 5.4 & 5.5). The L2 mineral lineation on the east flank is shallowly plunging and trends ESE at a high angle to L1 (average L2 orientation is 29 -> 105). An oxidised iron staining may be associated with S2 folia. The rare S2/L2 fabric was observed in Biyawap and Aro creeks.

5.2.2 Biniguni: North flank of Dayman Dome

S1 on the north flank of the Dayman Dome also defines a coarse continuous foliation that strikes ESE and dips shallowly toward the NNE (average S1 orientation is 106 / 17 / NNE; Fig. 5.1a). Albite ribbons (up to 1mm long) are aligned with S1 in coarse-grained samples. Undulose extinction is common in albite grains. S1 foliation planes (Fig. 5.6) contain a shallowly plunging L1 mineral lineation on the north flank that variably trends between NNW to NE with an average trend of NNE (average L1 orientation is 18 -> 016). L1 mineral lineations are commonly defined by elongate actinolite and albite grains (Fig. 5.7) and may be defined by stretched vein minerals such as calcite (Fig. 5.8). Blue amphibole was not observed on the north flank.

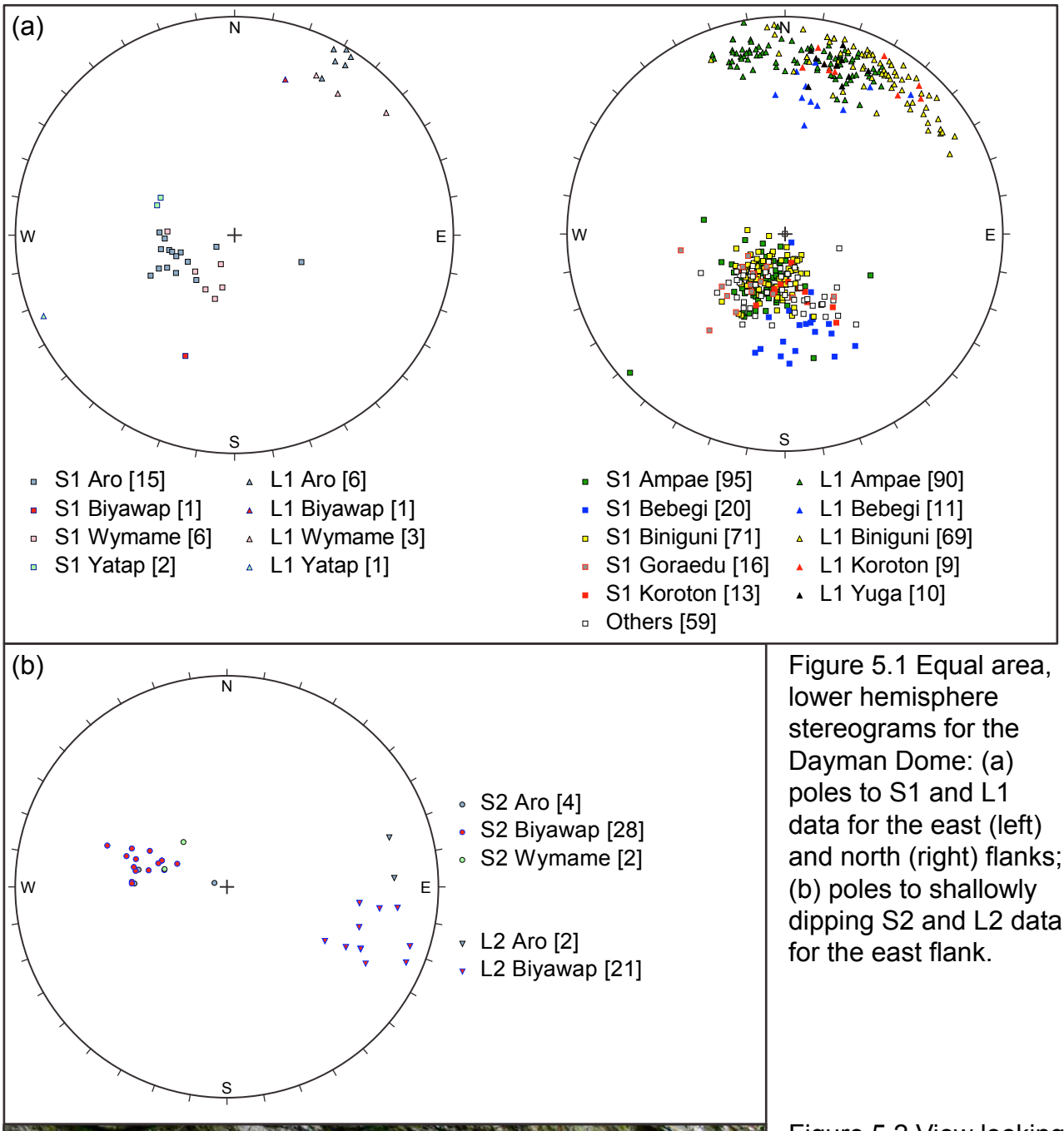

Figure 5.1 Equal area, lower hemisphere stereograms for the Dayman Dome: (a) poles to S1 and L1 data for the east (left) and north (right) flanks; (b) poles to shallowly dipping S2 and L2 data for the east flank.

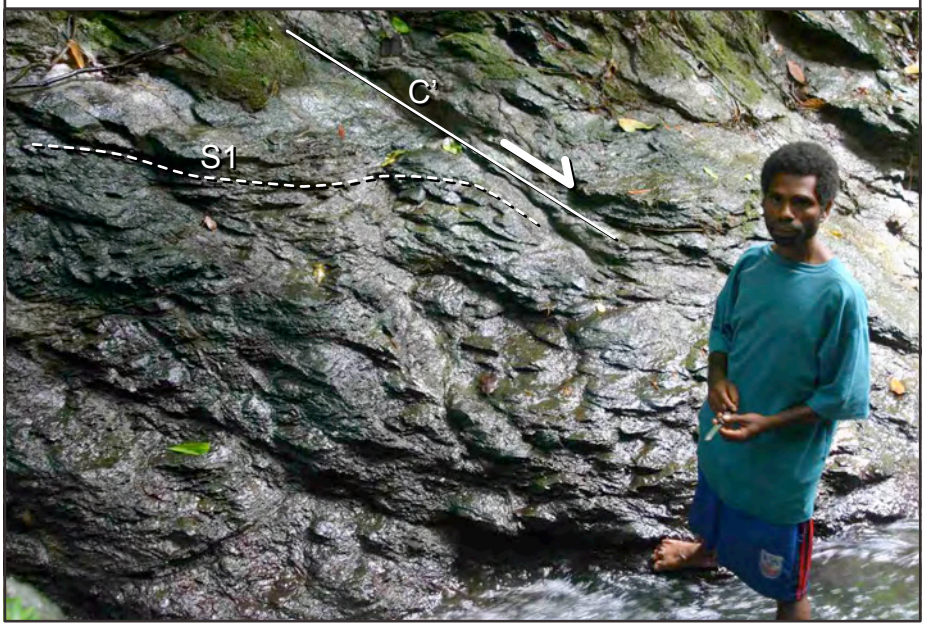

Figure 5.2 View looking WNW of S1 foliation planes (S; dashed line) that anastomose between extensional shear bands (C', solid line) forming an S-C' fabric. The curvature of S-planes indicates top down to the NNE sense-of-shear. Site 0627, Aro Creek.

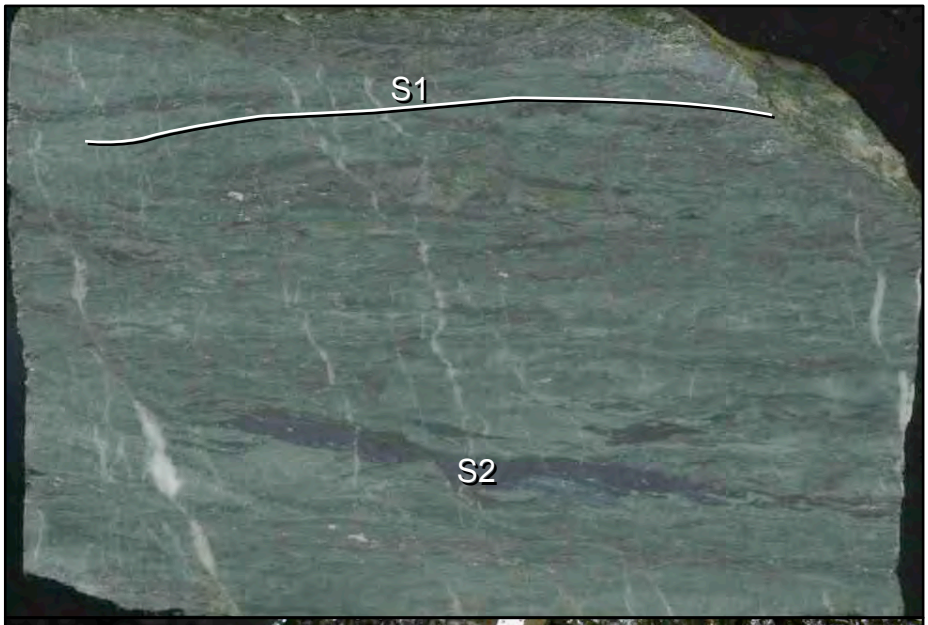

Figure 5.3 Flatbed scan of a sawn rock face of sample 0630 cut parallel to L2, perpendicular to S2. Narrow bands of blue amphibole (riebeckite) define the shallowly dipping S2 folia that lie sub-parallel to S1 (solid line), Yatap Creek. Field of view is 80 mm.

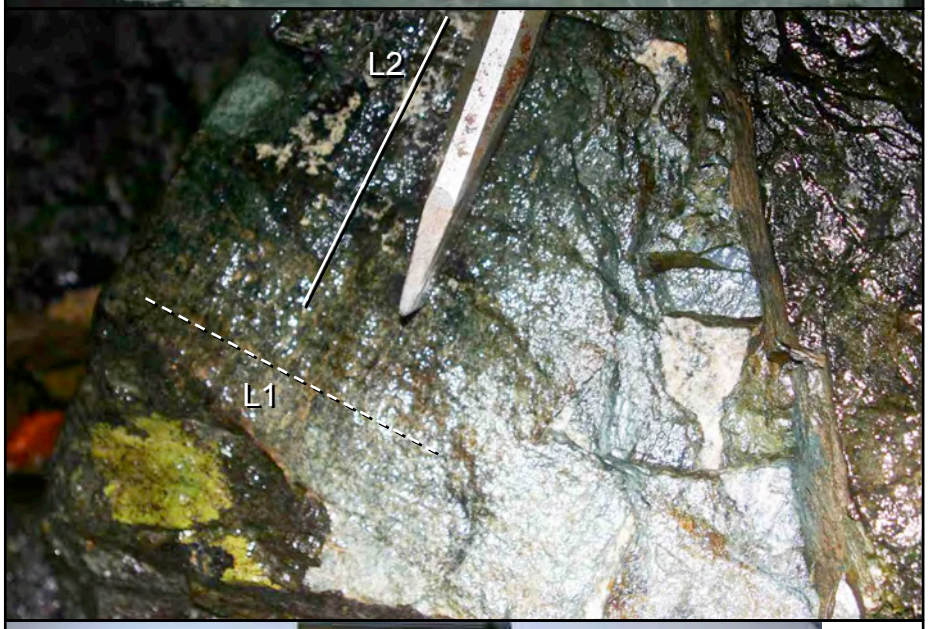

Figure 5.4 View looking W of elongate and aligned blue amphibole that defines L2 (solid line) that lies at a high angle to L1 (dashed line), site 0605, Biyawap Creek. End of chisel shown is 75 mm long.

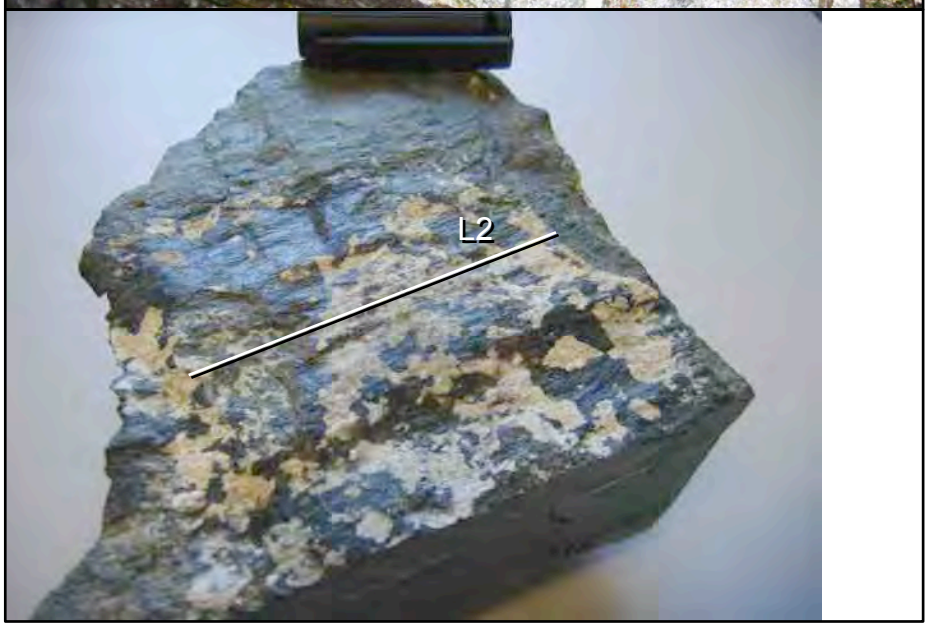

Figure 5.5 View onto S2 foliation plane of elongate and aligned blue amphibole that defines L2 (solid line), sample 0605, Biyawap Creek. Black pen lid is 40 mm long.

Figure 5.6 View looking NNE of S1 foliation planes, site 0660, Biniguni River.

Figure 5.7 View onto S1 foliation plane of elongate and aligned actinolite and albite grains that define L1 (solid line), site 0660, Biniguni River. Pencil is 140 mm long.

Figure 5.8 View onto S1 foliation plane of elongate and aligned vein minerals that define L1 (solid line), boulder in Gwariu Creek. Lens cap is 60 mm across.

5.2.3 Kinematics

The determination of the sense-of-shear during D1 was completed on both thin section and outcrop scale. Thin sections used to determine sense-of-shear were cut parallel to the stretching lineation (L1) and perpendicular to the foliation (S1; Fig. 5.9). At outcrop scale extensional shear bands (S-C' fabrics) are common (Fig. 5.10 & 5.11). The shear bands are spaced from ~30 mm (Fig. 5.10) up to 1.5 m (Fig. 5.11) apart. The more broadly spaced C'-planes are rare and were observed at Yatap Creek, whereas the more finely spaced C'-planes are common and the best exposures were observed at Aro, Ampae and Yuga creeks. The angle between S- and C'-planes varied between 25° and 44°, but was commonly 30-35°. The curvature of S-planes near C'-planes indicates a top to the NNE sense-of-shear (Fig. 5.10 & 5.11). Outcrop scale mantled porphyroclasts were rare. Yuga Creek contains 200-250 mm long parts of the outcrop with coarse foliation enveloped by fine-grained foliation (Fig. 5.12). The parts of the outcrop with coarse foliation form lenticular shapes analogous to sigma mantle porphyroclasts. The asymmetry of the tails of fine-grained foliation indicates a top to the NNE sense-of-shear.

Mantled porphyroclasts were the most common kinematic indicator in thin section. The best examples are in sample 0677G where large elliptical single mineral grains or mineral clusters of epidote are enveloped asymmetrically by S1 (Fig. 5.13). The stair-stepping sense of the asymmetry commonly indicates a top to the NNE sense-of-shear. However, elliptical porphyroclasts with their long axis oriented upstream (see section 5.2.4) show the opposite sense of asymmetry and indicate a top to the SSW sense-of-shear. This observation indicates a component of pure shear for the flow regime and this will be explored in section 5.2.4. Rare antitaxial fibrous overgrowths on pyrite porphyroclasts have grown normal to the crystal faces of the pyrite grains (Fig. 5.14). As a pyrite grain behaves rigidly relative to the surrounding ductile matrix, the pyrite particle boundary and the matrix tend to separate along a surface at a high angle to the maximum instantaneous stretch. Minerals in solution diffuse towards the low stress area and precipitate. Figure 5.14 shows quartz fibres growing normal to the crystal faces

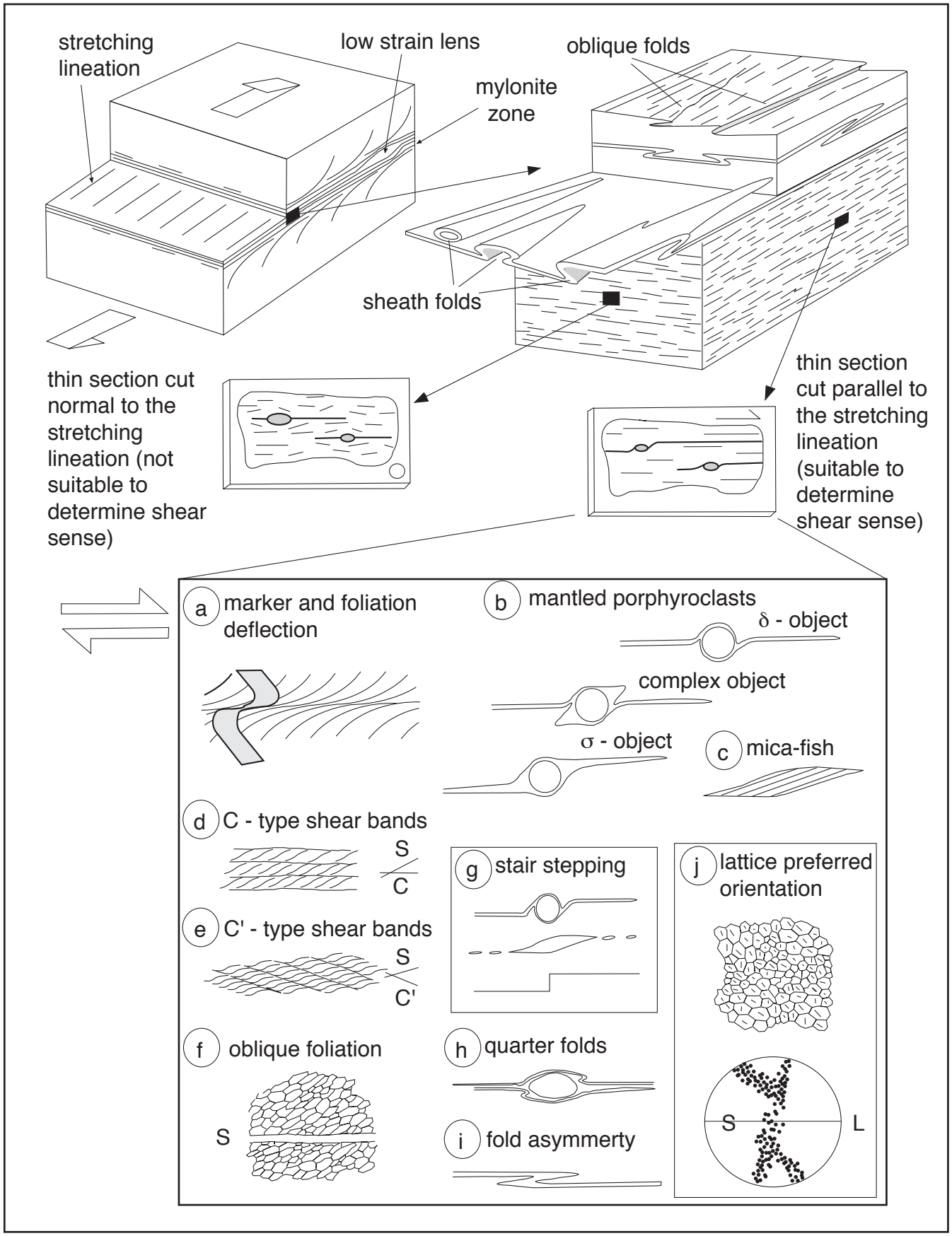

Figure 5.9 Schematic diagram showing the geometry of a mylonite shear zone and the nomenclature used. For sense-of-shear determination on thin-section-scale, thin-sections must be cut parallel to the stretching lineation. (a)-(j) are different systems within naturally deformed rocks that may indicate the sense-of-shear (from Passchier & Trouw, 1996).

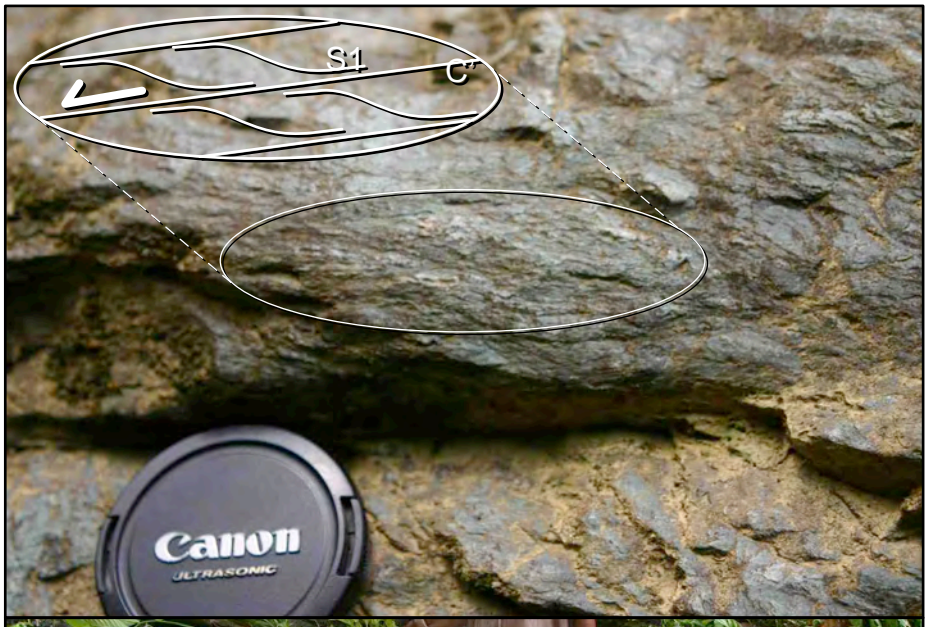

Figure 5.10 View looking ESE of S1 folia (S-planes) that anastomose between extensional shear bands (C'-planes) spaced 20-30 mm apart, site 0677, Ampae Creek. Curvature of S-planes indicates top down to the NNE sense-of-shear. Lens cap is 60 mm across.

Figure 5.11 View looking WNW of S1 folia (S-planes) that anastomose between extensional shear bands (C'-planes) spaced 1-2 m apart, site 0630, Yatap Creek. Curvature of S-planes indicates top down to the NNE sense-of-shear.

Figure 5.12 View looking WNW of 200-250 mm long lenticular shaped parts of the outcrop with coarse foliation enveloped by fine-grained foliation, analogous to sigma mantle porphyroclasts, site 0669, Yuga Creek. The asymmetry of the σ-tails indicate top down to the NNE sense-of-shear. Lens cap is 60 mm across.

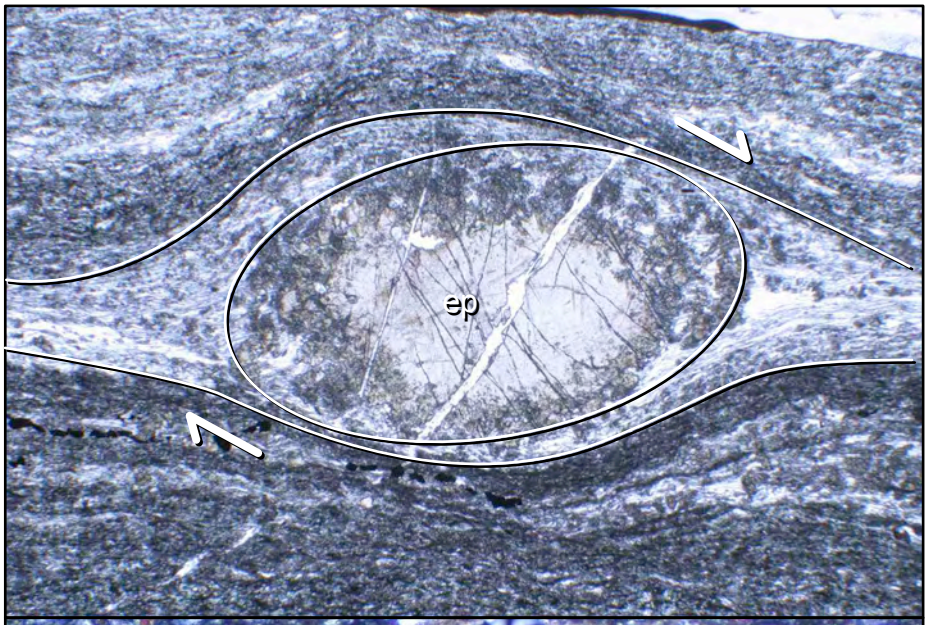

Figure 5.13 Plain polarised light photomicrograph of sigma-type mantled epidote (ep) porphyroclast, sample 0677G, Ampae Creek. The asymmetry of the sigma tails indicates a top down to the NNE sense-of-shear. Field of view is 3.5 mm across.

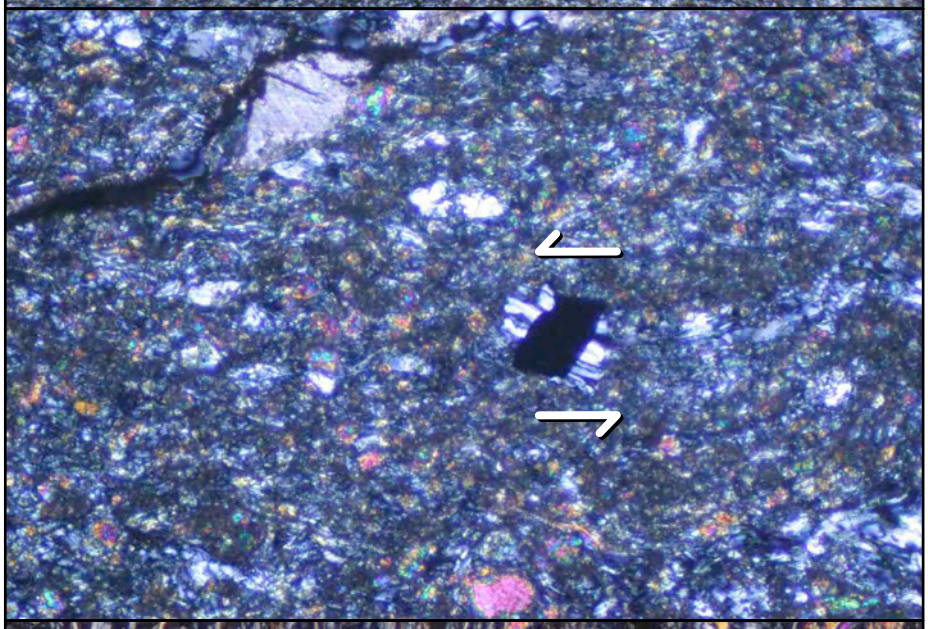

Figure 5.14 Crossed polarised light photomicrograph of quartz antitaxial fibrous overgrowths normal to the crystal faces of a pyrite grain in its strain shadow, sample 0677D, Ampae Creek. The quartz fibres show an asymmetry that indicates a top to the NNE sense-of-shear. Field of view is 0.9 mm across.

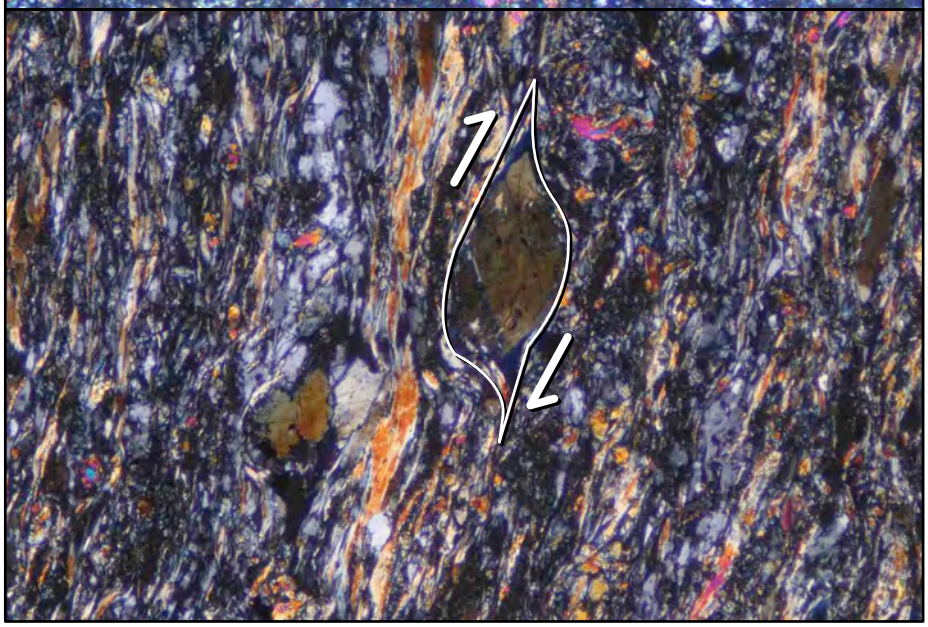

Figure 5.15 Crossed polarised light photomicrograph of actinolite ‘fish’, sample 0677H, Ampae Creek. The tails on the actinolite ‘fish’ indicate a top down to the NNE sense-of-shear. Field of view is 1.75 mm across.

of a pyrite grain in its strain shadow. The geometry and shape of the quartz fibres indicates Coble creep was the principle diffusion mechanism. The quartz fibres show an asymmetry that indicates a top to the NNE sense-of-shear. Other weakly developed kinematic indicators observed in thin section include asymmetric actinolite grains (Fig. 5.15) that are shaped similarly to mica fish. The asymmetry indicates a top to the NNE sense-of-shear.

5.2.4 Kinematic vorticity

There exist two end-members of flow in shear zones: pure shear (irrotational) and simple shear (rotational; Fig. 5.16a). Vorticity is the amount of rotation that a flow type possesses (Means *et al*., 1980). The aim of kinematic vorticity analysis is to determine the ratio of pure to simple shear. The kinematic vorticity number (W_k) represents this ratio and ranges from 0 to 1, representing wholly pure shear or simple shear respectively. Simpson & De Paor (1993) illustrate how the hyperbolic net (Fig. 5.16b) may be used for derivation of the kinematic vorticity number. It involves determination of the sense-of-shear as indicated by the position and direction of the stair stepping of tails on mantled porphyroclasts, coupled with measurement of the finite axial ratio (R_f = X/Z; Fig. 5.16c) and inclination (ϕ) of the elliptical porphyroclasts. The initial inclination of the porphyroclasts will control whether the porphyroclasts rotate forward or backward (Fig. 5.16d). The sense of rotation is determined in the analysis by the sense of stair stepping of the mantled porphyroclasts (Fig. 5.16e). The finite axial ratio (R_f = X/Z) and inclination (ϕ) are plotted onto the hyperbolic net using different symbols for forward versus backward rotated porphyroclasts. The backward rotated porphyroclasts with define a field on the plot (Fig. 5.16f, g). The hyperbola that envelops the field of backward rotated porphyroclasts has two asymptotes that lie parallel to the two eigenvectors of flow; one is parallel to the shear zone boundary. The cosine of the angle between the two eigenvectors is the kinematic vorticity number ($W_k = \cos(\alpha)$; Bobyarchick, 1986).

Figure 5.16

(a) The axes of pure shear (dashed lines) remain in the same orientation after deformation. Pure shear is therefore irrotational. The axes of simple shear (dashed lines) rotate during deformation. Simple shear is therefore rotational. The diagonal fine dashed lines in the centre square represent an object orientated at an angle to the axes of shearing. During narrowing (see d) pure shear, the diagonal line that runs from top left to bottom right rotates anti-clockwise and the diagonal line that runs from top right to bottom left rotates clockwise. During dextral (see e) simple shear, both diagonal lines rotate clockwise. A combination of pure and simple shear results in an angle less that 90° that defines a felid of backward rotation (see d).

(b) The hyperbolic net (from De Paor, 1988) contains the complete set of θ curves (Lisle, 1977) for all values of R_f. The acute hyperbolas represent θ = 45° (50%-of-data) curves for every value of R_f from 1.0 to 8.0.

(c) The finite axial ratio (R_f) is determined by dividing the long axis length by the short axis length of an elliptical object. The finite orientation (φ) is determined by the acute angle the long axis makes with an arbitrary reference line. Orientation data ranges from -90° to 90°.

(d) Clasts with -90° < orientation < 0° are incline d upstream in a dextral shear zone. Clasts inclined upstream at a shallow angle in a shear zone with a combination of compressional pure shear and dextral simple shear will rotate 'backward' (anticlockwise).

(e) Grains with wedge-shaped tails are sigma(∫)-grains. Grains with very narrow tails that cross the foliation are delta(™)-grains. Combinations of the two are complex sigma-delta(∫–™)-grains. The asymmetry of the tails or wings on the clasts indicate the sense-of-shear. Dextral tails step up to the right. Sinistral tails step up to the left.

(f,g) Plots of kinematic vorticity data on a hyperbolic net. Using the shear zone boundary, or foliation trace in narrowing shear zones, as an asymptote, a hyperbola is traced from the hyperbolic net (see b) to enclose the field of back-rotated (see d) grains and then the hyperbola's other asymptote is drawn. The cosine of the angle between the two asymptotes yielded the kinematic vorticity number (W_k) for two thin sections o sample 0677G.

(h) Plot showing paths of constant kinematic vorticity number in simple shear (γ) - pure shear (k) space for plane strain combinations of pure and simple shear. The non-linearity of W_k paths is a result of the finite strain caused by the pure shear component increasing faster than the simple shear component (from Tikoff and Fossen, 1995).

(a) Pure versus simple shear

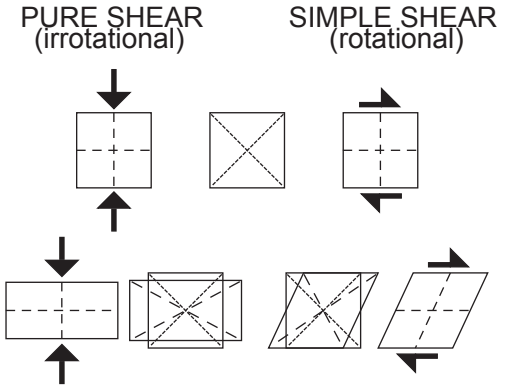

(b) Hyperbolic net

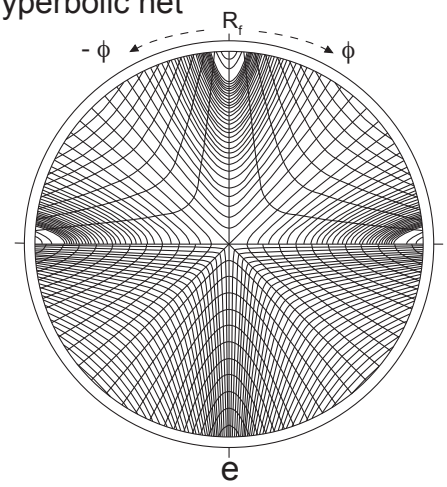

(c) Axial ratio (R_f) & Orientation (ϕ)

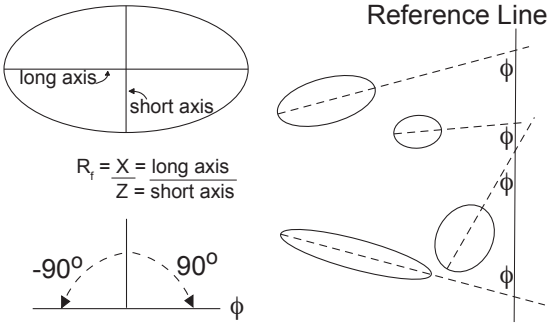

(d) Inclined clasts

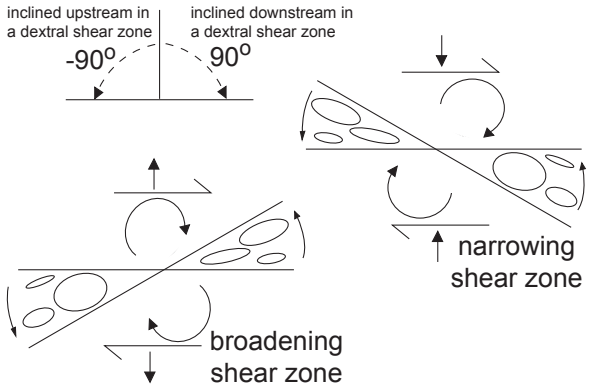

(e) Sense-of-shear, Tails on clasts

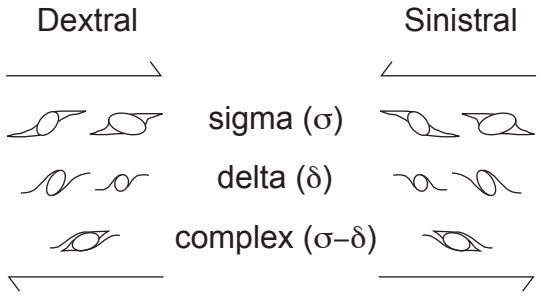

(f) Results 1 for 0677G

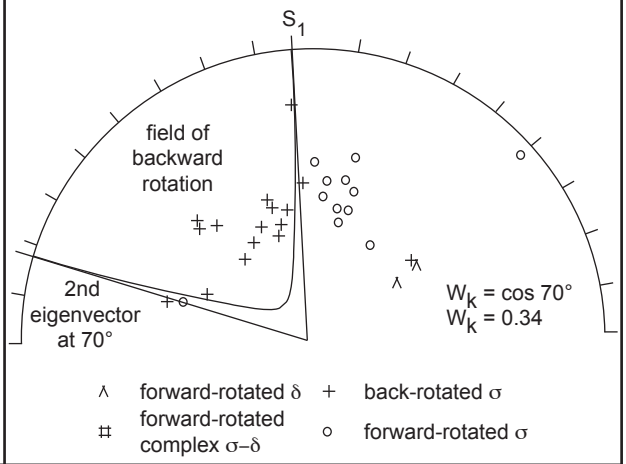

(g) Results 2 for 0677G

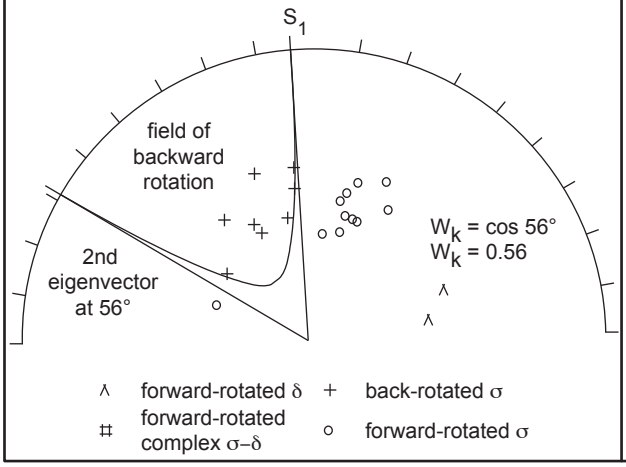

(h) Type of flow

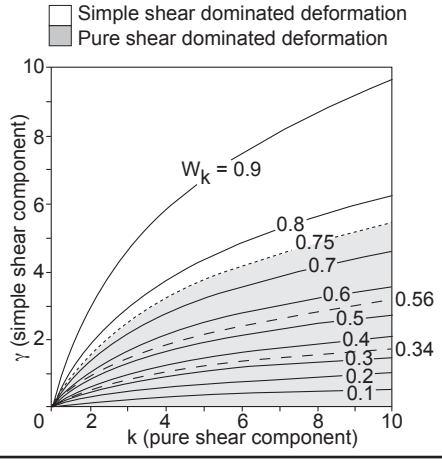

Potential problems with this technique include: (i) a large population of grains is needed; and (ii) the finite axial ratio data should be random and follow a normal distribution. Porphyroclasts that are oblique or impinge on their neighbours must be rejected.

Only one sample (0677G) had enough mantled porphyroclasts to attempt the determination of the kinematic vorticity number. Two thin sections were cut parallel to lineation and perpendicular to foliation. Sixteen out of thirty grains and eight out of twenty-one grains were identified as backward rotated in the two thin sections. The analysis determined kinematic vorticity numbers of 0.34 and 0.56 for the two thin sections (Fig. 5.16f, g). Both analyses indicate that the flow type that produced the D1 fabrics was dominated by a strong component of pure shear (Fossen & Tikoff, 1993; Fig. 5.16h).

5.3 Narrow steeply dipping S2 shear zones

Narrow (< 100 mm) steeply dipping shear zones are rare and were observed at Biniguni River and Ampae Creek (Fig. 5.17 & 5.18). S2 in steeply dipping shear zones is a moderately rough foliation with ductile to semi-brittle character. S2 strikes E-W and dips steeply toward the N. Steeply dipping S2 foliation planes contain a shallowly plunging L1 mineral lineation that trends NE. Steeply dipping S2 foliation planes anastomose around microlithons with that preserve the S1 foliation enveloped by the S2 foliation (Fig. 5.19). The sense of curvature and transposition of the S1 foliation into the S2 foliation indicates a top down to the NE sense-of-shear (Fig. 5.17). Narrow steeply dipping S2 shear zones contain abundant veins that are concentrated within the shear zones and are deformed by them (see below).

5.4 Folds and semi-brittle to brittle overprint

Rare gentle to open folds of S1 (interlimb angle (*i*) = 70-180°) were observed at the

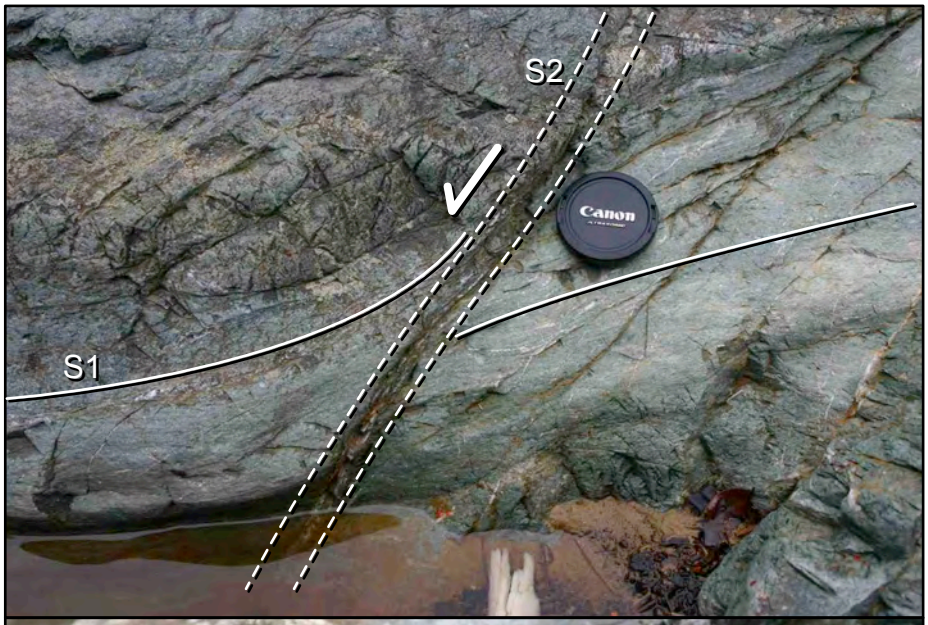

Figure 5.17 View looking ESE of a narrow steeply dipping S2 shear zone, site 0664, Biniguni River. The sense of curvature and transposition of S1 into S2 indicates a top down to the NNE sense-of-shear. Lens cap is 60 mm across.

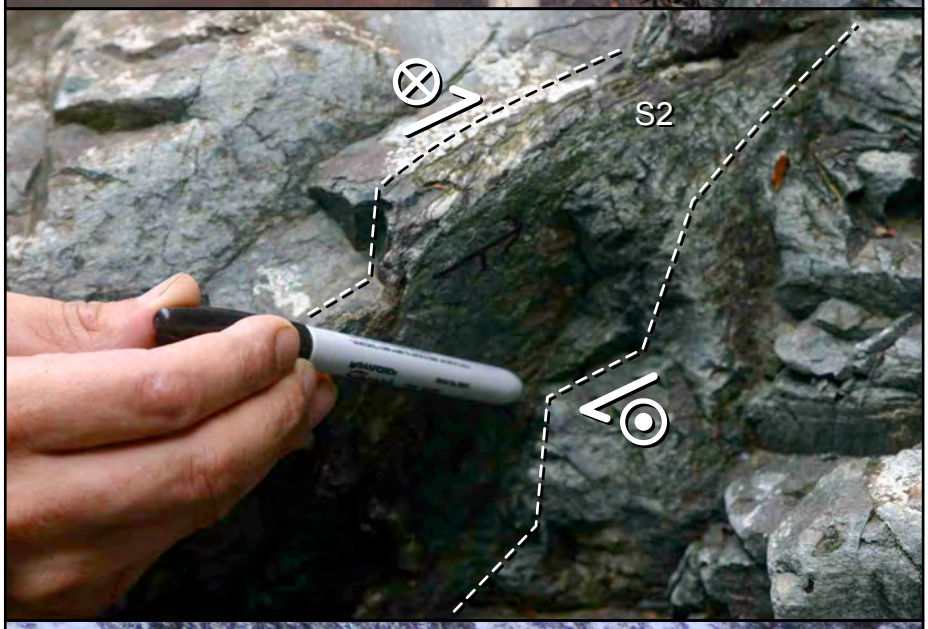

Figure 5.18 View looking N of a narrow steeply dipping S2 shear zone, site 0677A, Ampae Creek. The marker pen is held in the orientation of L2 and is 135 mm long.

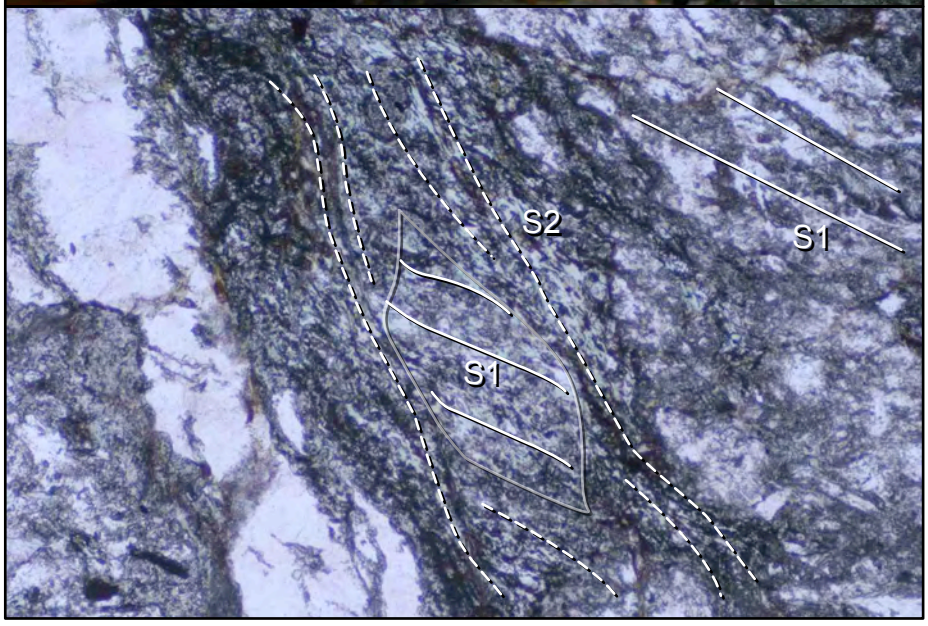

Figure 5.19 Plain polarised light photo-micrograph of steeply dipping S2 folia that anastomoses around microlithons that preserve the S1 folia-tion, sample 0677A, Ampae Creek. Field of view is 1.75 mm across.

outcrop scale (Fig. 5.20 & 5.21). Detailed measurements of folded S1 at Gwariu River show crenulations that plunge very shallowly toward the SE. At this location, S1 is openly folded (i = 104°) and differently oriented to elsewhere on the northern flank. Stereographic determination of the attitude of the fold indicates it is gently plunging (22°->253°) and upright (85°; Fig. 5.22). Zonal crenulation cleavages were mostly observed at thin section scale (Fig. 5.23). The crenulations range from close to open to gentle with chevron to sinusoidal shapes. They are commonly weakly asymmetric.

A rare semi-brittle to brittle overprint (D3) of the S1 and S2 foliations was observed in the Pumani River at the contact between the Gwoira Conglomerate and Goropu Metabasalt (Fig. 5.24). The fault zone is approximately 2 m wide, dips moderately toward the SE and is rich in veins (Fig. 5.25). Extensional shear bands (S-C' fabric) indicate a top down to the SE sense-of-shear (Fig. 5.24 and 5.25). Rare narrow fault zones that contain very fine-grained gouge also define a rare semi-brittle to brittle overprint of the S1 and S2 foliations. The gouge is associated with an oxidised iron staining. Grain scale faults show top down to the NNE sense-of-shear (Fig. 5.26)

5.5 Veins

Narrow veins (< 3 mm wide) commonly contain calcite, less commonly quartz and rarely epidote and prehnite. Field relationships indicated that the veins are common within the narrow D2 shear zones and brittle structures (i.e. post-S1; Fig. 5.27), although rare veins were observed strung out in the S1 foliation and along L1. Rare boudinage of veins was observed in sample 0605 from Biyawap Creek (Fig. 5.28). Epidote and prehnite were only observed within the semi-brittle to brittle structures (D3).

5.6 Dykes

Rare mafic dykes cut the S1/L1 fabric at the Biniguni River waterfall (Fig. 5.29). Chilled dyke margins were not evident and the dykes are very weakly deformed (Fig. 5.30). The

Figure 5.20 View looking W of a gentle fold of S1, site 0669, Yuga Creek.

Figure 5.21 View looking N of an open fold of S1, site 0668, Gwariu Creek.

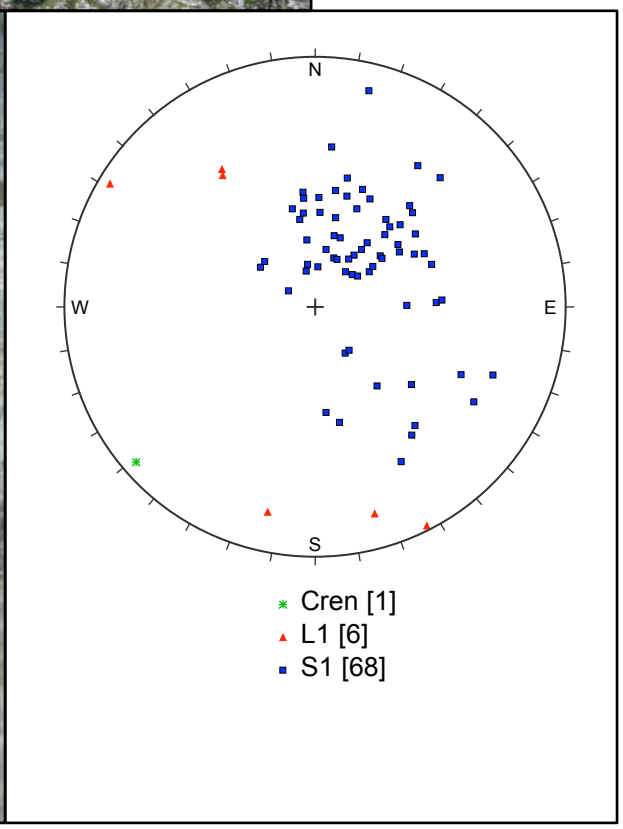

Figure 5.22 Equal area, lower hemi-sphere stereogram for poles to folded S1 and L1 data, and one crenulation measure-ment at site 0668, Gwariu Creek.

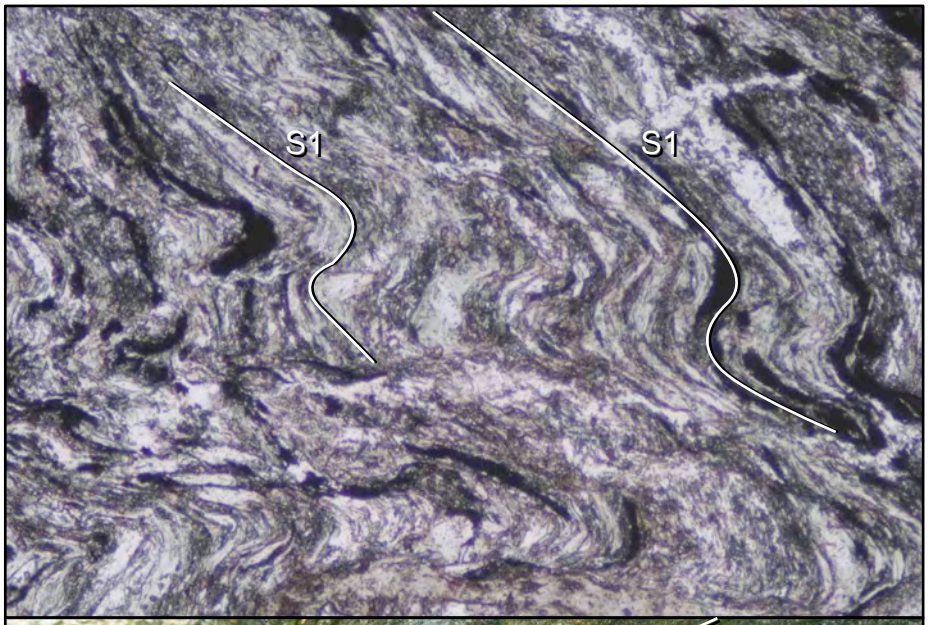

Figure 5.23 Plain polarised light photomicrograph of crenulated S1, sample 0677C, Ampae Creek. Field of view is 1.75 mm across.

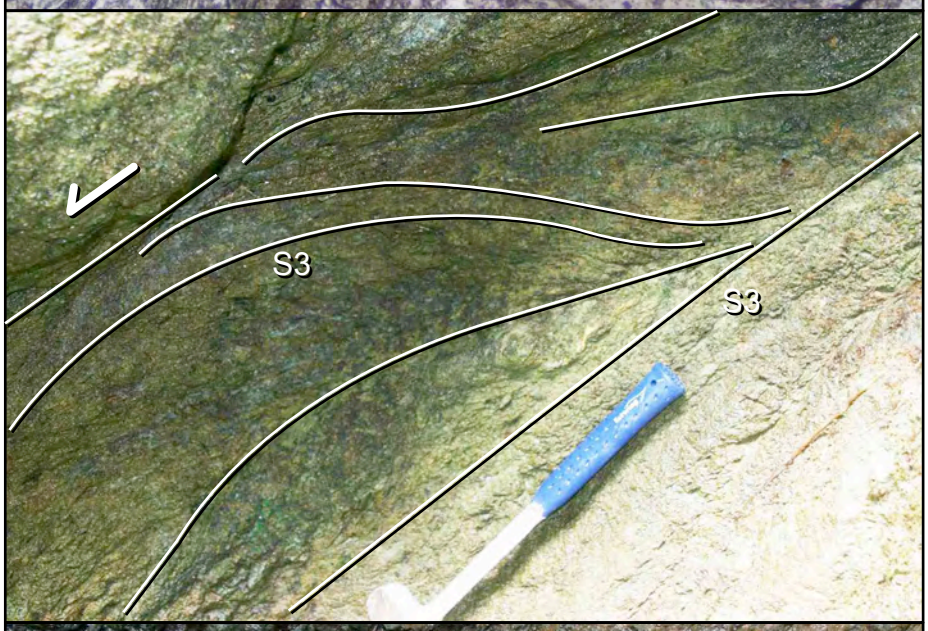

Figure 5.24 View looking E of a S3 semi-brittle to brittle fault zone, site 0604, Pumani River. Long handle crack hammer is 400 mm long.

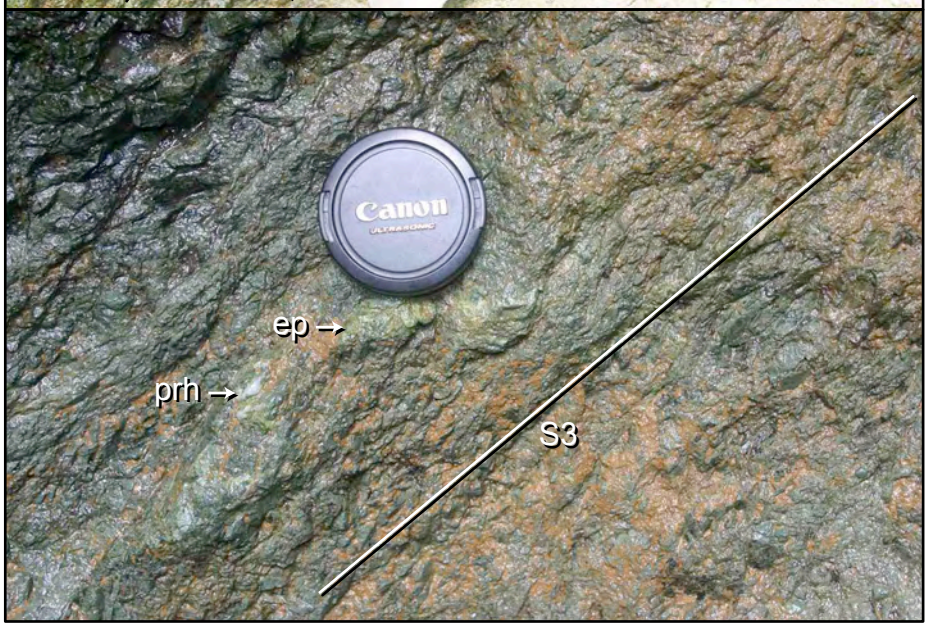

Figure 5.25 View looking E of prehnite (prh) and epidote (ep) veins in the S3 fault zone above, site 0604, Pumani River. Lens cap is 60 mm across.

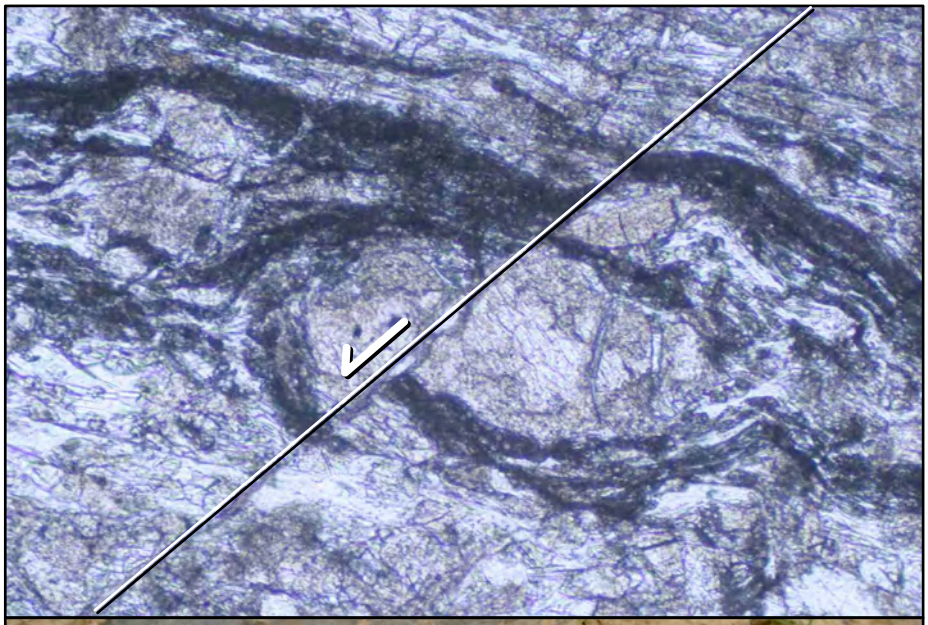

Figure 5.26 Plain polarised light photo-micrograph of a grain scale fault, sample 0669, Yuga Creek. Field of view is 0.9 mm across.

Figure 5.27 View looking W and down onto an outcrop with a S2 shear zone filled with veins, site 0677, Ampae Creek. Lens cap is 60 mm across.

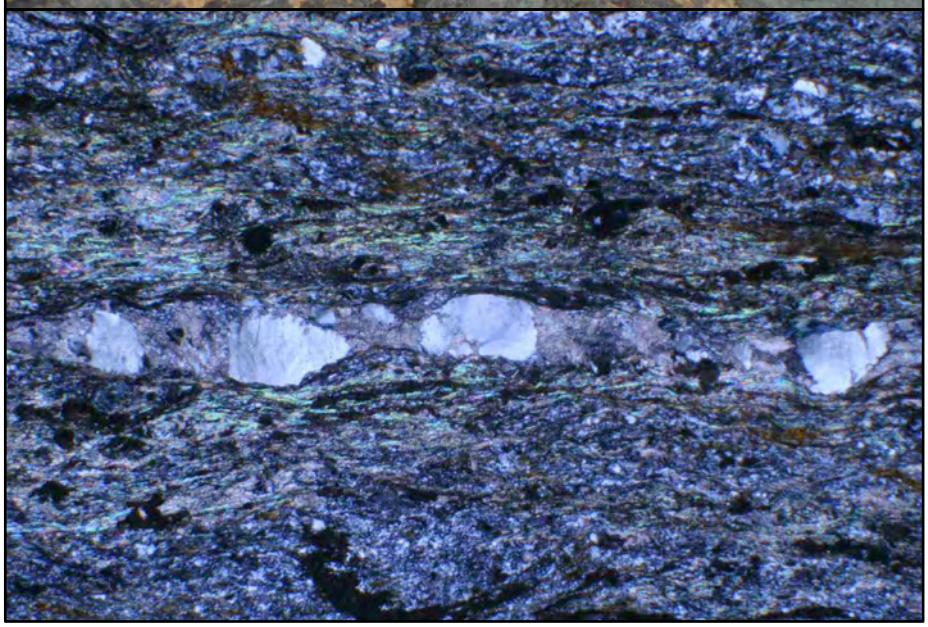

Figure 5.28 Crossed polarised light photo-micrograph of a boudi-naged vein, sample 0605, Biyawap Creek. Field of view is 3.5 mm across.

dykes strike NW to NNW and dip moderately to steeply towards the SW (Fig. 5.31). One sub-horizontal mafic sill was observed in Gwariu Creek with no evidence of chilled margins (Fig. 5.32). The sill truncates the S1 foliation.

5.7 Gwoira Conglomerate

The bedding in the Gwoira Conglomerate dips moderately toward the SE (Chapter 4; Fig. 4.1). This study examined the Gwoira Conglomerate within 4 km of the contact with the Goropu Metabasalt. Measurements of the orientation of S0 furthest from the contact in Kwekweme and Urawa creeks strike N to NE and dip shallowly to moderately E or SE (Fig. 5.33). S0 closer to the contact with the Goropu Metabasalt is more variable in orientation (Fig. 5.33). No outcrop-scale folding was observed in the Gwoira Conglomerate, however faults are common. The most striking boundary of the Gwoira Conglomerate is marked by the Gwoira Fault, an approximately 30 km long brittle north-dipping normal fault (Figs 4.4 & 4.5). Google Earth™ images of the Gwoira Conglomerate rarely show evidence of variation in the orientation of the bedding. Figure 5.34 shows folded bedding that is interpreted to be drag folding adjacent to a normal fault. Outcrop-scale faults are generally very narrow (~10 mm) brittle faults (Fig. 5.35) that commonly display oxidation of the adjacent sedimentary rocks in zones up to 200 mm across (Fig. 5.36). However, rare fault zones may be up to 2 m wide (e.g. Urawa and Sisipoa creeks) with anastomosing foliation (Fig. 5.37). Where determined, faults show a normal with minor sinistral and dextral oblique sense of motion with sedimentary bedding offset by up to ~100 mm (Fig. 5.35). Fault gouge is commonly weathered to clay. Measurements of the orientation of fault planes indicate they are highly variable in strike and dip (Fig. 5.38).

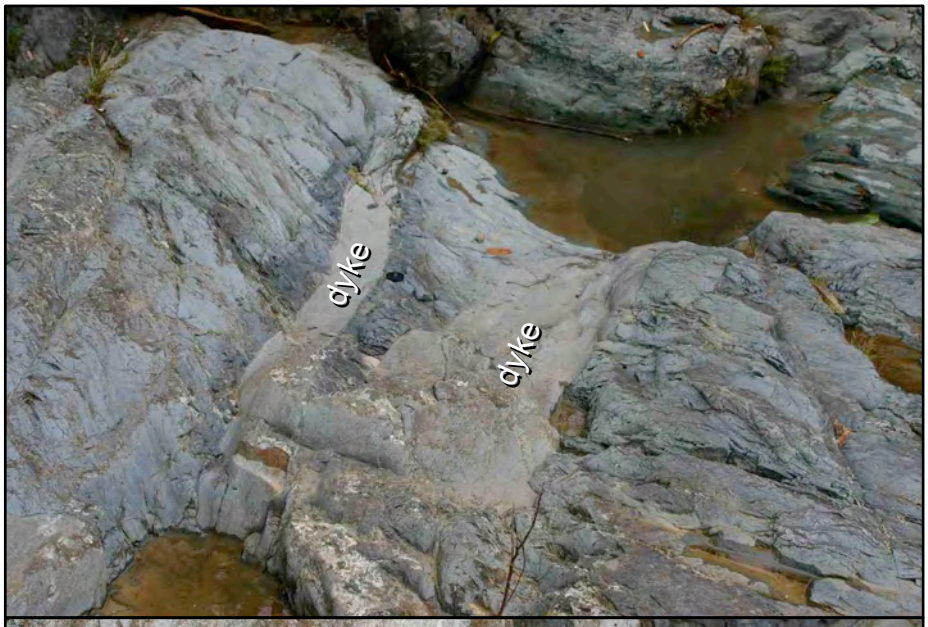

Figure 5.29 View looking WNW of steeply dipping mafic dykes that cut S1, site 0665, Biniguni River. Lens cap is 60 mm across.

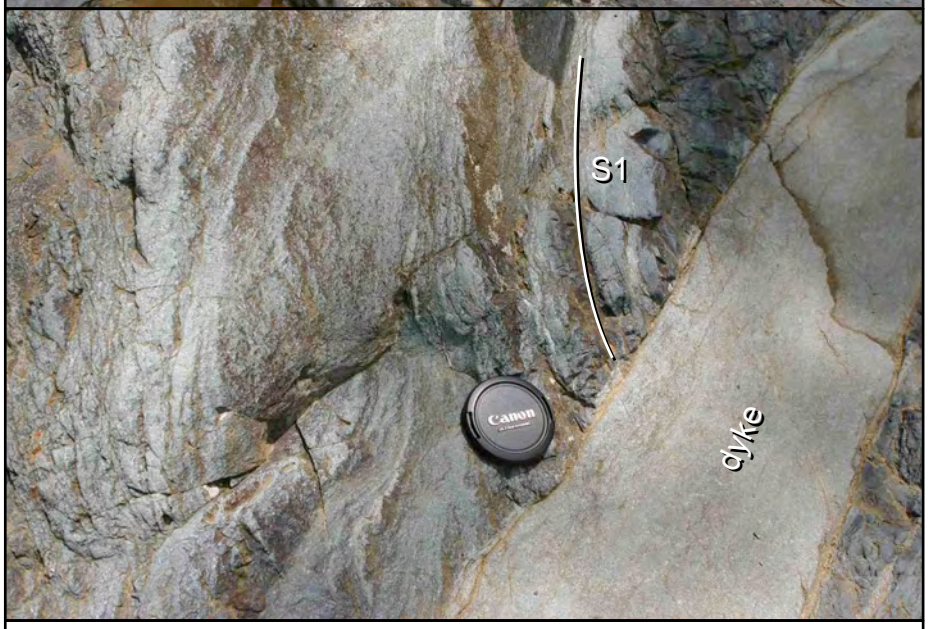

Figure 5.30 View looking down onto an outcrop with a dyke cutting S1, site 0665, Biniguni River. The dyke lacks chilled margins. Lens cap is 60 mm across.

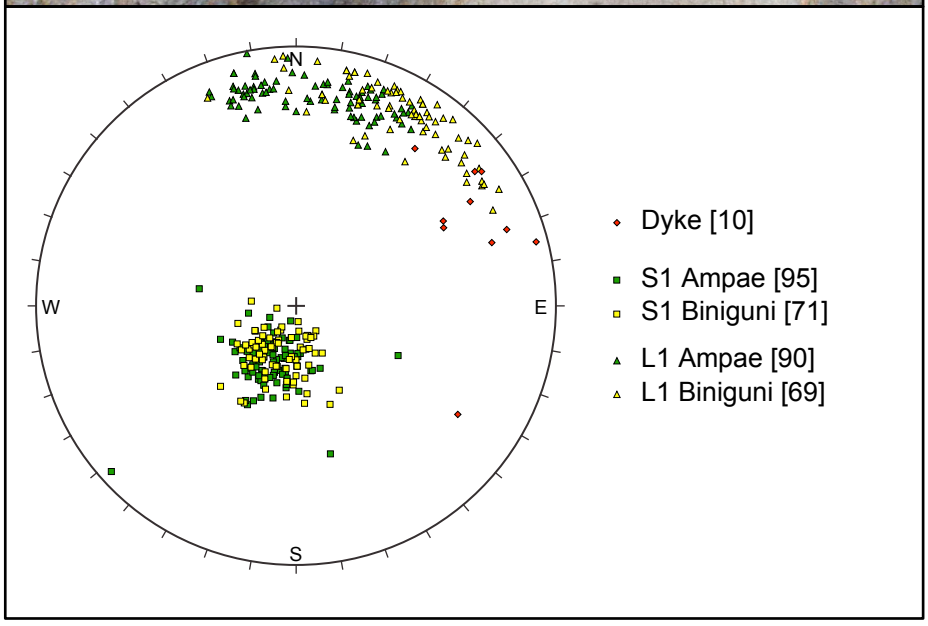

Figure 5.31 Equal area, lower hemi-sphere stereogram comparing poles to S1 and L1 data to poles to dykes for the Dayman Dome.

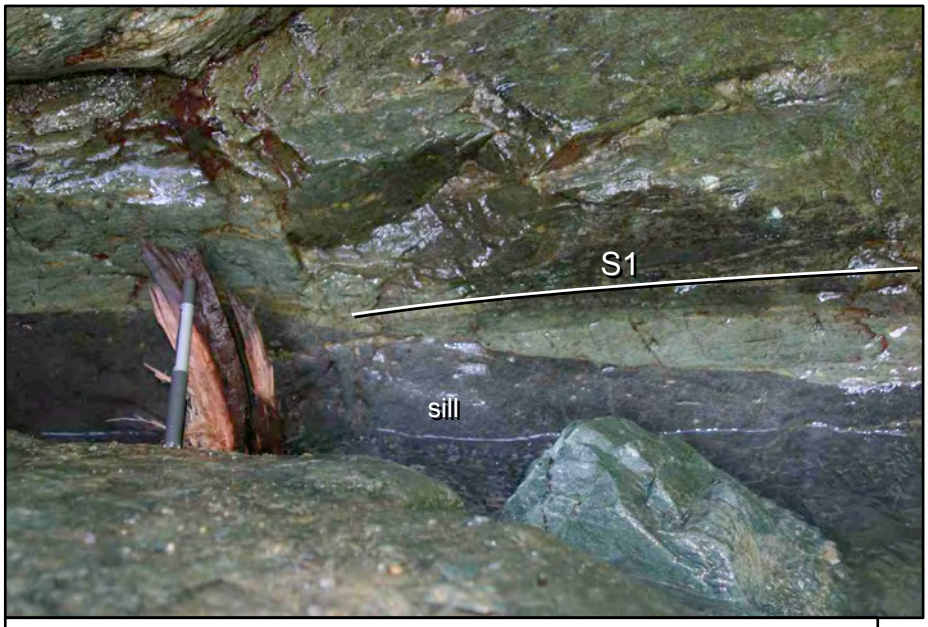

Figure 5.32 View looking E of a mafic sill that cuts S1, site 0668, Gwairiu Creek. Pen is 135 mm long.

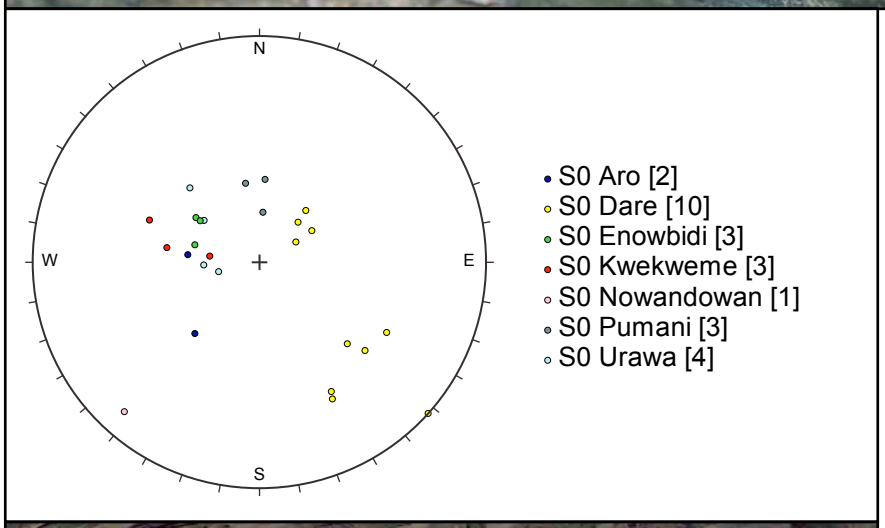

Figure 5.33 Equal area, lower hemi-sphere stereogram of poles to S0 for the Gwoira Conglomerate.

Figure 5.34 Google Earth™ image view looking SE of the Gwoira Conglomerate. A normal fault is marked by a solid line. S0 is marked by a dashed line.

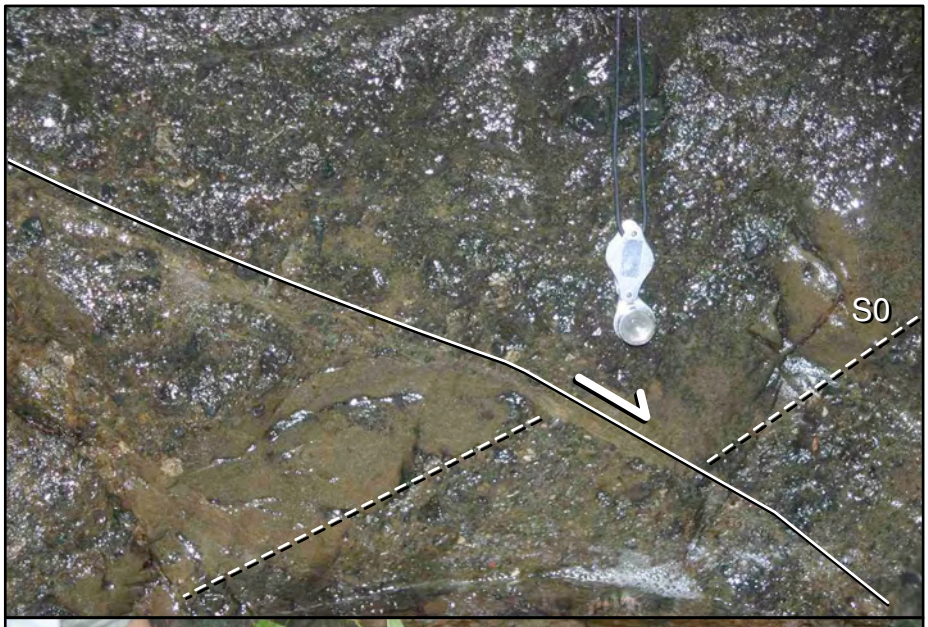

Figure 5.35 View looking E of a brittle normal fault cutting bedding (S0) in the Gwoira Conglomerate, site 0619, Kwekweme Creek. Hand lens is 70 mm long.

Figure 5.36 View looking W of an oxidised brittle fault zone, Dare Creek. The long handle crack hammer is 400 mm long.

Figure 5.37 View looking E of a brittle fault zone cutting the Gwoira Conglomerate, site 0603, Sisipoa Creek. Hand lens is 70 mm long.

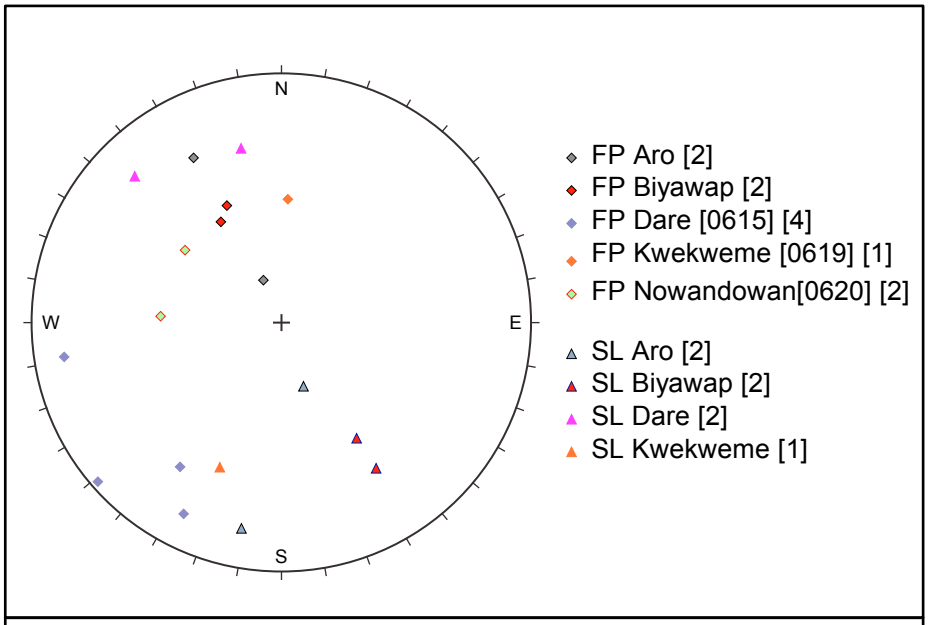

Figure 5.38 Equal area, lower hemisphere stereogram of fault planes (FP) and slickensides (SL) for the Gwoira Conglomerate.

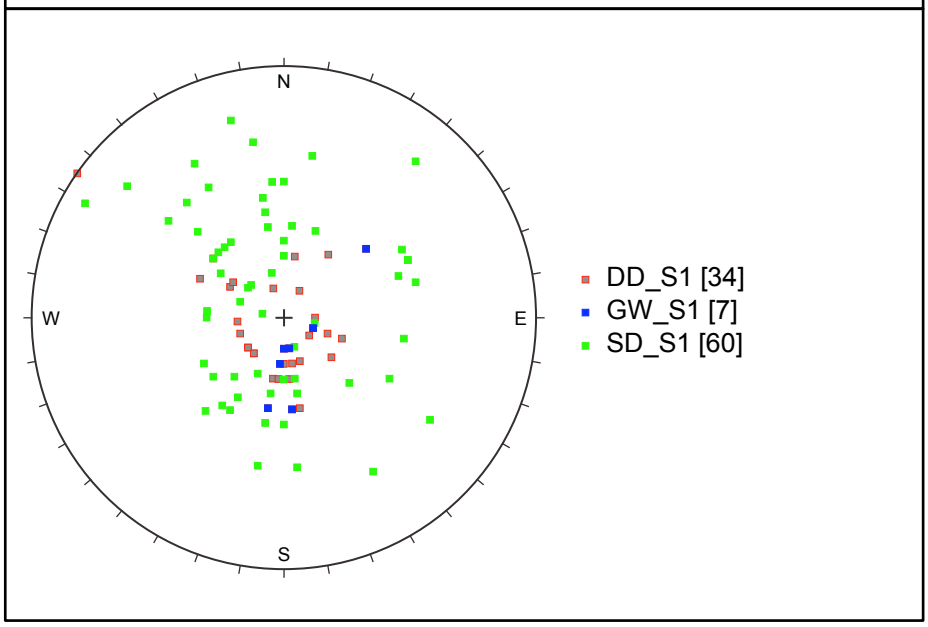

Figure 5.39 Equal area, lower hemisphere stereogram of poles to S1 for the Dayman Dome (DD), Gwariu Gorge (GW) and Suckling Dome (SD). Data from Davies and Smith (1974).

5.8 Discussion

The dominant structure examined in this study is a mylonite ductile shear zone with top to the NNE transport. The overprinting sequence of structures in the Dayman Dome includes: (i) ductile S2 folia with ESE-plunging riebeckite mineral lineations that are oriented at a high angle to the D1 transport direction; (ii) narrow steeply dipping ductile D2 shear zones; and (iii) semi-brittle to brittle fault zones. The structural progression records exhumation of the massif from ductile to brittle deformation conditions. The ductile nature of the S1/L1 fabric is inconsistent with the D1 mylonite zones controlling the exhumation of the massif all the way to the surface. Brittle faults must control the final stages of exhumation of both the massif and mylonite zones. The scarcity of brittle fault zones suggests that these faults that control the final stages of exhumation are largely eroded. Only one large brittle fault zone was observed at the Pumani River (Fig. 5.24). This zone is located near the contact with the Gwoira Conglomerate and may be protected by the overlying sedimentary carapace.

The extension direction recorded by the opening of the mafic dykes is oriented similarly to L1 extension lineations (Fig. 5.30). This observation suggests that the dykes intruded under the same stress regime as that active during the development of the S1/L1 fabric. This implies the dykes were emplaced shortly following cessation of ductile movement in the mylonitic shear zone, prior to any change in regional stress and is consistent with the lack of chilled margins on the dykes and limited deformation of the dykes. The steep to moderate dip of the dykes toward the SW implies rotation of the northern flank about a NW-trending horizontal axis. This may have taken place during flexure of the mylonite zone to form the domal shape of the massif. This is also consistent with a gentle southward dip of the sill observed at Gwariu Creek (Fig. 5.31).

The mylonitic lineations (L1) define a NNE-directed transport direction and are parallel to the aerial photograph lineaments and fault surface megamullions on the Dayman Dome (Chapter 2). Plate motions are recorded in seafloor spreading data in the Woodlark basin since ~6 Ma (Taylor *et al*., 1999). The L1 stretching lineations closely parallel the

Woodlark-Australia spreading vector for the Pliocene to early Pleistocene (0.5-3.6 Ma; Table 2.1), but are not parallel to the late Pleistocene to recent Woodlark-Australia spreading vector (<0.5 Ma; Table 2.1). This suggests that deformation in the D1 mylonite zone is > 0.5 Ma. The rare 2 m-wide semi-brittle to brittle overprint (D3) observed in the Pumani River at the contact between the Gwoira Conglomerate and Goropu Metabasalt (Fig. 5.24) contains a SE-trending lineation and two other orientations of fault slickensides measured on brittle fault planes in the Gwoira Conglomerate (Dare Creek; Fig. 5.37) are also consistent with tectonic transport parallel to the younger Woodlark-Australia spreading vector. It is predicted that slickensides on brittle faults, were they better exposed, would trend NNW-SSE parallel to the late Pleistocene to recent Woodlark-Australia spreading vector.

Structural data presented on the geology map (Davies and Smith, 1974) was plotted onto a stereogram to compare to the measured data presented here (Fig. 5.39). Figure 5.39 shows a much broader set of orientations than those presented in figure 5.1a. The data from Davies and Smith (1974) cover the whole massif and hence the stereogram shows a domal pattern of dominantly shallowly dipping structure. These orientations are consistent with those presented here for the north and east flanks of the Dayman Dome. Hill (1994) presents a similar structural scheme to that presented here for the bounding-shear zones of the Goodenough, Mailolo and Oiatabu domes on Goodenough and Fergusson islands. Her structural scheme includes (i) several hundred-metre thick pervasive shear zone fabrics; (ii) narrow shear zones (a few tens of centimetres or a few centimetres thick) that extend for several hundred metres or less than one metre; and (iii) zones of schistosity, crenulation and brecciation. This structural scheme matches the S1/L1 mylonitic fabric, narrow D2 shear zones and D3 brittle fault zones presented here. The mineral lineations reported by Hill (1994) for the numerous bounding shear zones on Goodenough and Fergusson islands include sets that trend N, NE and E, broadly similar to the L1 lineations of this study. Also similar to this study NW-plunging mineral lineations are not reported by Hill (1994). Little *et al*. (2007) examined the Provost Range massif (dome) on Normanby Island and documented NNE-SSW oriented megamullions and mineral lineations similar to those reported here.

The analysis of vorticity of the shear zone deformation indicates a W_k between 0.34 and 0.56, suggesting general shear deformation. The strong component of pure shear suggests that the shear zone evolved with a stress comprising a strong overburden component (Bailey and Eyster, 2003). Many authors describe the coexistence of coaxial and non-coaxial shear in MCC irrespective of their lithology or environment (Wells and Allmendinger, 1990; Wawrzenitz and Krohe, 1998; Bestmann *et al*., 2000; Bailey and Eyster, 2003; Little *et al*., 2007). Bailey and Eyster (2003) and Bestmann *et al*. (2000) describe an evolving combination of pure and simple shear in MCC at different stages of uplift. Bailey and Eyster (2003) describe the overall deformation as general shear that evolves from ductile pure shear dominated early in the deformation to brittle simple shear dominated as the load on the footwall block (i.e. the overburden) is reduced during exhumation of the core. The evolving flow regime may show overprinting relationships where pure shear dominated shear zones are cut by simple shear dominated ones (Bailey and Eyster, 2003). The high pressures recorded by metamorphic assemblages (see Chapter 6) in the core suggest that the overburden would have been very significant during the early stages of shear (D1), consistent with the determination of W_k. Simple shear dominated shear zones most likely formed a carapace over the pure shear dominated shear zone now exposed and may include the D3 fault zone observed at the contact between the Goropu Metabasalt and Gwoira Conglomerate. The friable nature of the more brittle simple shear dominated deformation makes these zones more susceptible to erosion and perhaps explains their absence from the study area.

Figure 4.1 suggests that the Gwoira Conglomerate consistently dips moderately toward the SE. However, the measurements of S0 presented here are somewhat variable. This structural complexity may be due to the proximity of this study to the contact with the Suckling-Dayman Massif. The overall moderate dip toward the SE for the Gwoira Conglomerate is consistent with tilting of a hanging-wall block above a major listric normal fault at depth and suggests that the Biman dip slopes extend beneath the Gwoira Conglomerate in listric geometry. This exposure of the hanging wall is rare amongst the eastern PNG metamorphic core complexes.

Chapter 6 METAMORPHIC GEOLOGY

6.1 Introduction

Thin sections of metabasite rock samples from the Dayman Dome were analysed under a petrographic microscope to (1) characterise the metamorphic mineralogy of key structures documented in Chapter 5; (2) examine metamorphic textures; (3) determine the mineralogy of vein assemblages and (4) determine the extent of metamorphism of the dykes. 68 thin sections were mounted and polished to 30 microns on 46 x 26 mm glass slides. Each thin section was examined using a Nikon Eclipse E400 Pol binocular petrographic microscope.

The highest-grade shear zone foliation (S1) is best preserved on the northern flank of the dome and is defined by actinolite-bearing greenschist facies metamorphic assemblages. The greenschist facies S1 assemblages are rarely overprinted by two distinct foliations: (i) rare riebeckite-bearing shallowly-dipping S2 foliations on the eastern flank of the dome and (ii) ductile to semi-brittle recrystallisation in narrow steeply dipping D2 shear zones on the northern flank of the dome. Rare mafic dykes show evidence of minor recrystallisation.

6.2 Ductile shallowly dipping S1 and S2 fabric

All metabasite samples of the Dayman Dome examined in this study (excluding the dykes) contain a well developed S1 foliation and L1 lineation. S1 is defined by aligned actinolite, albite and epidote (e.g. sample 0668A; Fig. 6.1). Chlorite, titanite, calcite and quartz are commonly also part of the S1 assemblage. Accessory phases include apatite, pyrite, muscovite, potassium feldspar, chalcopyrite, rutile and zircon. Very rare blue amphibole is restricted and concentrated in narrow bands (up to 3 mm wide) of S2 folia oriented sub-parallel to S1 (e.g. sample 0605; Fig. 6.2). The metabasite samples are fine-grained (commonly 0.1-0.3 mm but up to 1.5 mm).

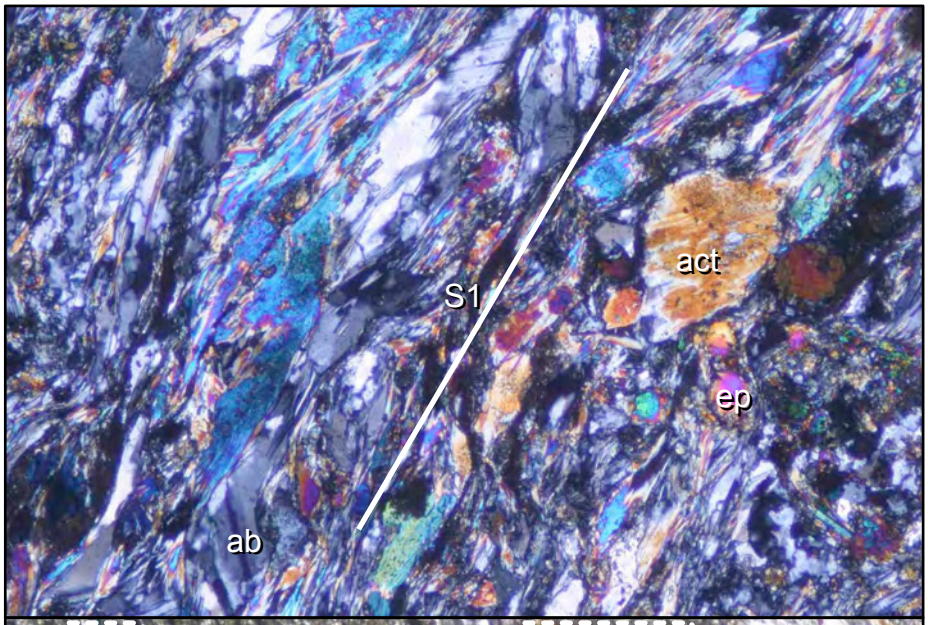

Fig. 6.1 Cross polarised light photomicrograph of coarse-grained S1 (white line) running diagonally from top right to bottom left, sample 0668A, Gwariu River. S1 is defined by aligned actinolite (act), albite (ab) and epidote (ep). Field of view is 1.75 mm.

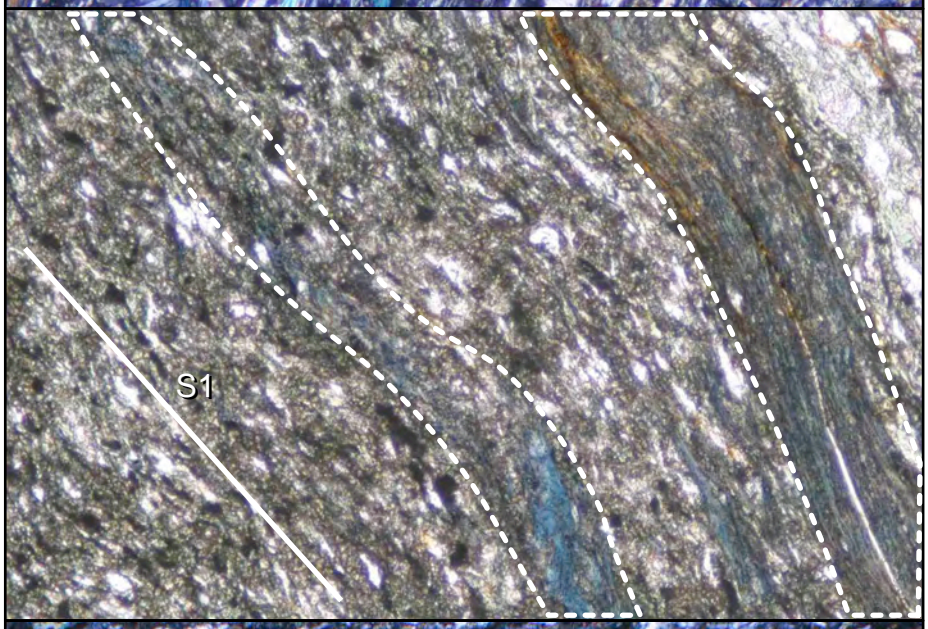

Fig. 6.2 Plain polarised light photomicrograph of S2 bands of blue amphibole (outlined by dashed lines) running sub-parallel to S1 (white line) diagonally from top left to bottom right, sample 0605, Biyawap Creek. Field of view is 1.75 mm.

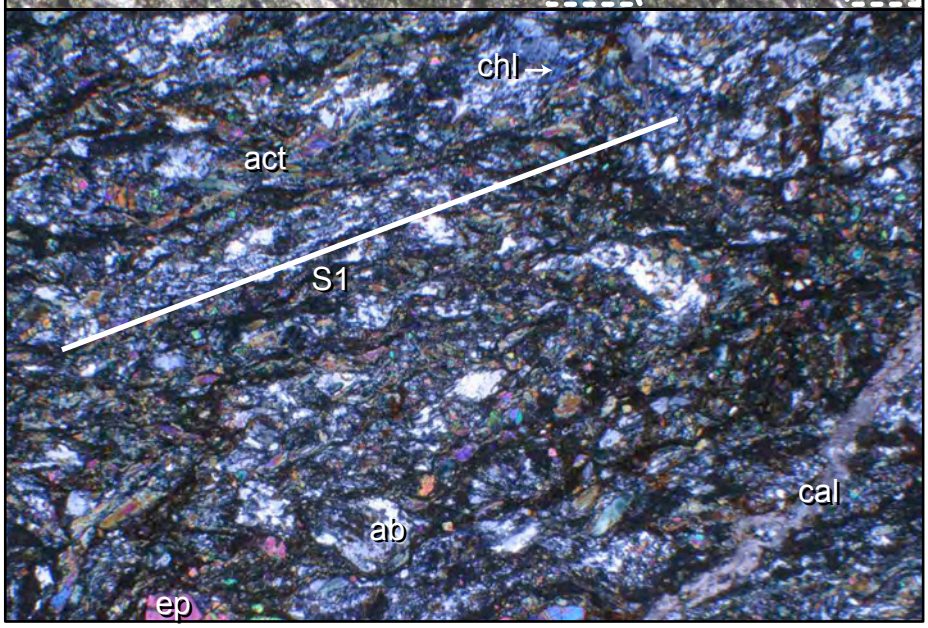

Fig. 6.3 Cross polarised light photomicrograph of S1 (white line) running diagonally from top right to bottom left, sample 0629, Aro Creek. S1 is defined by aligned actinolite (act), albite (ab) and epidote (ep). Field of view is 3.5 mm.

6.2.1 Pumani: East flank of Dayman Dome

Samples 0627 to 0630 are representative of the S1 foliation on the east flank of the Dayman Dome and contain actinolite, albite, epidote, chlorite, titanite, calcite and quartz. The actinolite and epidote vary in grainsize from 0.1 to 0.2 mm across (e.g. sample 0629; Fig. 6.3). Chlorite may partially pseudomorph epidote and the S1 foliation commonly envelops the larger actinolite and epidote grains (e.g. sample 0605; Fig. 6.4). Minor calcite and quartz veins (up to 2 mm across) may be deformed and aligned with S1 (see below).

Sample 0605 is unusual. It contains S1 defined by the common actinolite-albite-epidote assemblage described above (Fig. 6.4). Rare blue amphibole is concentrated in narrow bands of S2 that are sub-parallel to S1 (Fig. 6.2). The blue amphibole is riebeckite (see below) and is aligned with S2 in the interior of the bands but may also form random splays that cut S1 adjacent to the bands (Fig. 6.5a). Chlorite may be pseudomorphed by the blue amphibole. Accessory muscovite, calcite and very rare zircon (< 10 μm across) are associated with the blue amphibole textures (Fig. 6.5a). Titanite partially replaces rutile grains (~200 μm) where the rutile is left as many small remnants enveloped by titanite (Fig. 6.5b). An oxidised iron staining may be associated with S2 folia.

6.2.2 Biniguni: North flank of Dayman Dome

Samples 0668A, 0672 and 0677H show the largest grainsize for S1 with actinolite grains up to 0.7 mm long, albite ribbons up to 1 mm long and epidote grains ~0.4 mm across (e.g. sample 0668A; Fig. 6.6). Sample 0676 and the majority of samples from site 0677 contain generally smaller grains defining S1 (~0.1-0.2 mm), similar to those of the eastern flank (e.g. sample 0677G; Fig. 6.7). Large round to elliptical single grains or mineral clusters of epidote (up to 1.5 mm across) are enveloped by the fine-grained S1. The single grains of epidote are optically zoned (e.g. sample 0676; Fig. 6.8)

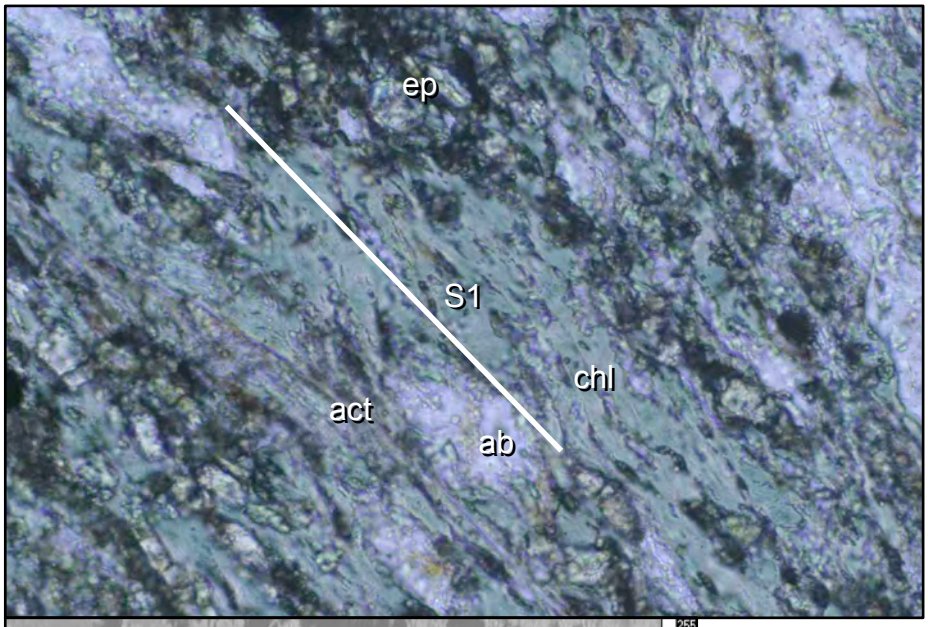

Fig. 6.4 Plain polarised light photomicrograph of S1 (white line) running diagonally from top left to bottom right, sample 0605, Biyawap Creek. S1 is defined by aligned chlorite (chl) that envelops aligned actinolite (act), albite (ab) and epidote (ep). Field of view is 0.5 mm.

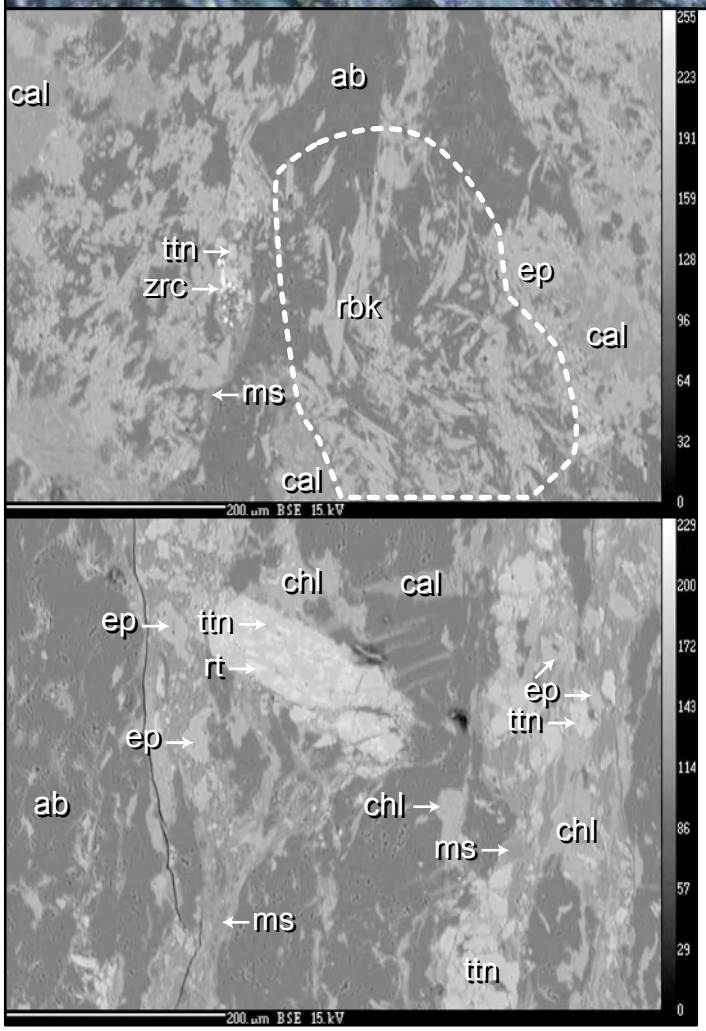

Fig. 6.5(a,b) Back-scattered electron (BSE) images showing: (a) random splays of riebeckite (rbk; outlined by dashed line), very rare zircon (zrc), and minor S2 phengitic muscovite (ms); and (b) titanite (ttn) pseudomorphs of rutile (rt), sample 0605, Biyawap Creek. Scales as shown on the images.

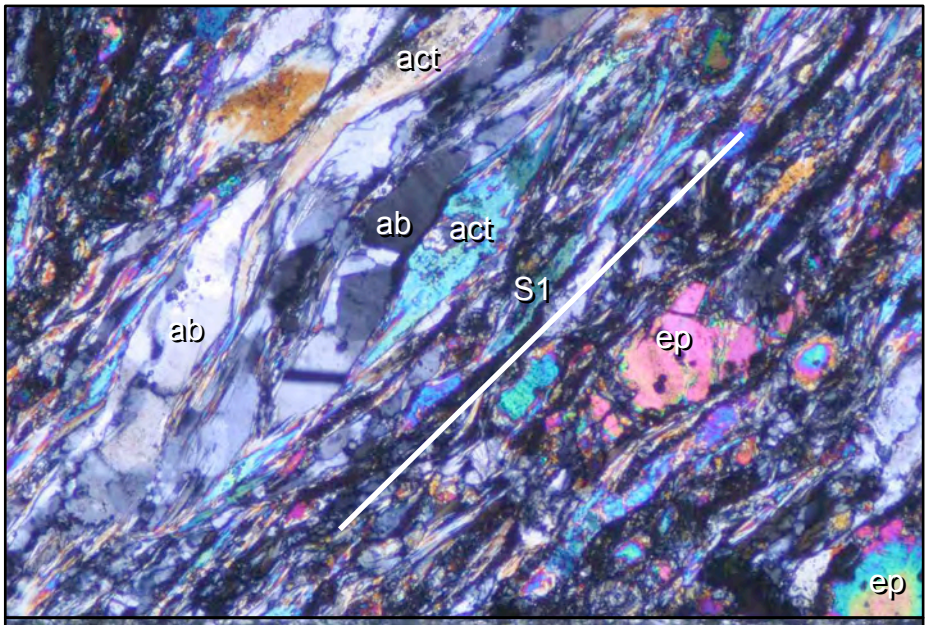

Fig. 6.6 Cross polarised light photomicrograph of coarse-grained S1 (white line) running diagonally from top right to bottom left, sample 0668A, Gwariu River. S1 is defined by aligned actinolite (act), albite (ab) ribbons and epidote (ep). Field of view is 1.75 mm.

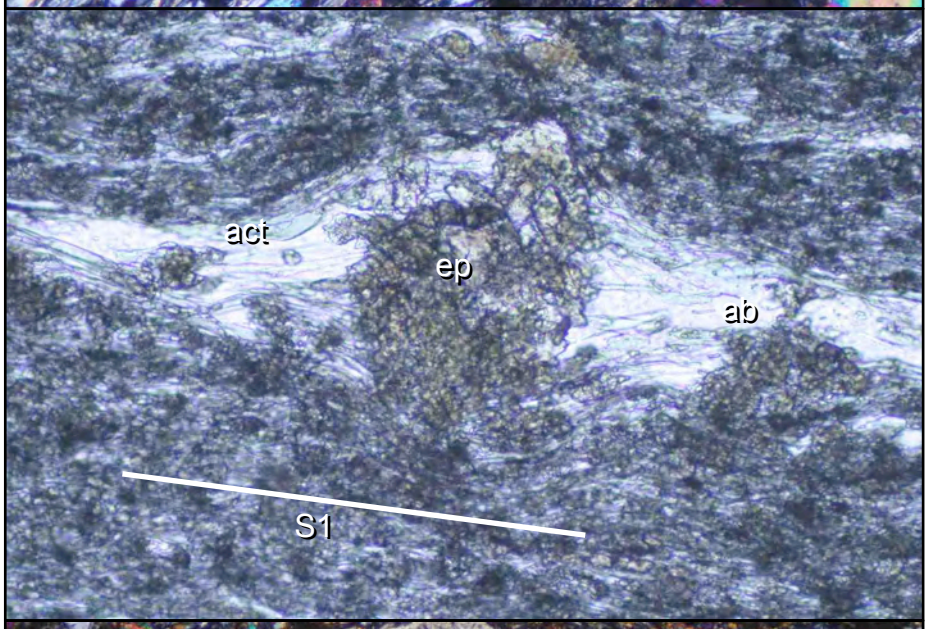

Fig. 6.7 Plain polarised light photomicrograph of S1 running left to right (white line) , sample 0677G, Ampae Creek. Field of view is 3.5 mm.

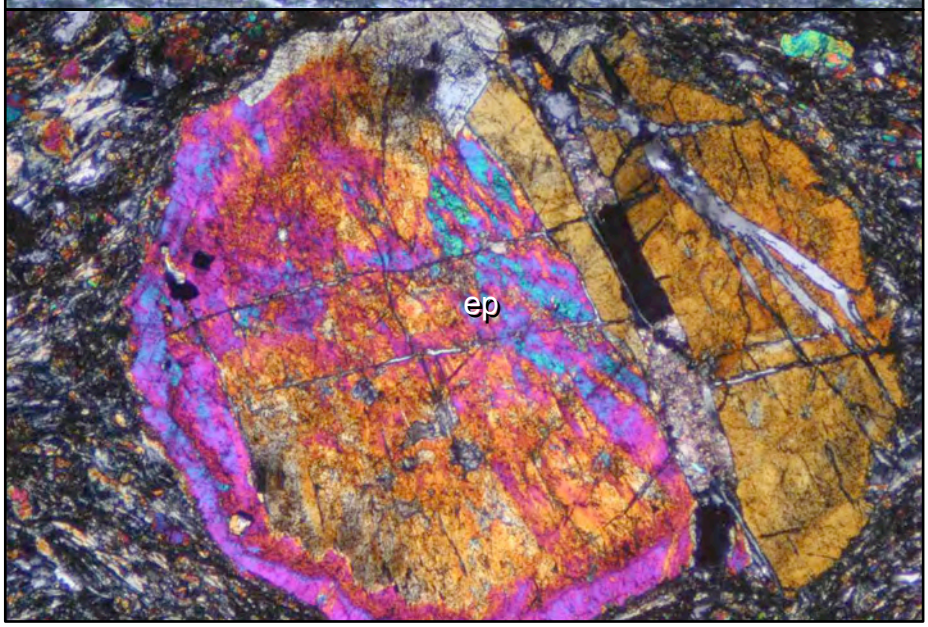

Fig. 6.8 Cross polarised light photomicrograph of a large optically zoned epidote grain, sample 0676, Yutmae Creek. Field of view is 1.75 mm.

and the mineral clusters of epidote (e.g. sample 0677G; Fig. 6.9) are zoned from a pale green coarse-grained core to a pale brown fine-grained rim. Chlorite and albite are common minerals in the strain shadows of the coarse epidote grains or clusters (Fig. 6.7). Minor calcite and quartz veins (up to 2 mm across) may be deformed and aligned with S1 (see below).

6.3 Narrow steeply dipping S2 shear zones

Samples 0677A and 0677I are representative of the narrow S2 shear zones. The deformation mode within the narrow shear zones spans ductile to semi-brittle. The ductile S2 foliation is defined by very fine-grained chlorite, epidote and albite (<0.02 mm; e.g. sample 0677A; Fig. 6.10), whereas the semi-brittle S2 foliation is defined largely by very fine-grained epidote and fine-grained gouge (sub-microscopic; e.g. sample 0664; Fig. 6.11). The gouge contains common angular lithic and monomineralic clasts derived from the host rock (Fig. 6.11). Abundant calcite and quartz veins are deformed and aligned with the S2 foliation (see below).

6.4 Folds and semi-brittle to brittle overprint

Samples of folded S1 were examined under the microscope and found not to contain any recrystallisation or new minerals growing axial planar to the folds (e.g. sample 0677C; Fig. 6.12). Rare axial planar micro-faults contain epidote and calcite mineralisation (e.g. sample 0628; Fig. 6.13).

A 2 m wide semi-brittle to brittle fault zone at the contact between the Gwoira Conglomerate and Goropu Metabasalt (site 0604) contains veins of epidote and prehnite (e.g. sample 0604; Fig. 6.14). Elsewhere, narrow fault zones that contain very fine-grained gouge define a rare semi-brittle to brittle overprint of the S1 and S2 foliations (e.g. sample 0664; Fig. 6.15). The gouge is associated with an oxidised iron staining and

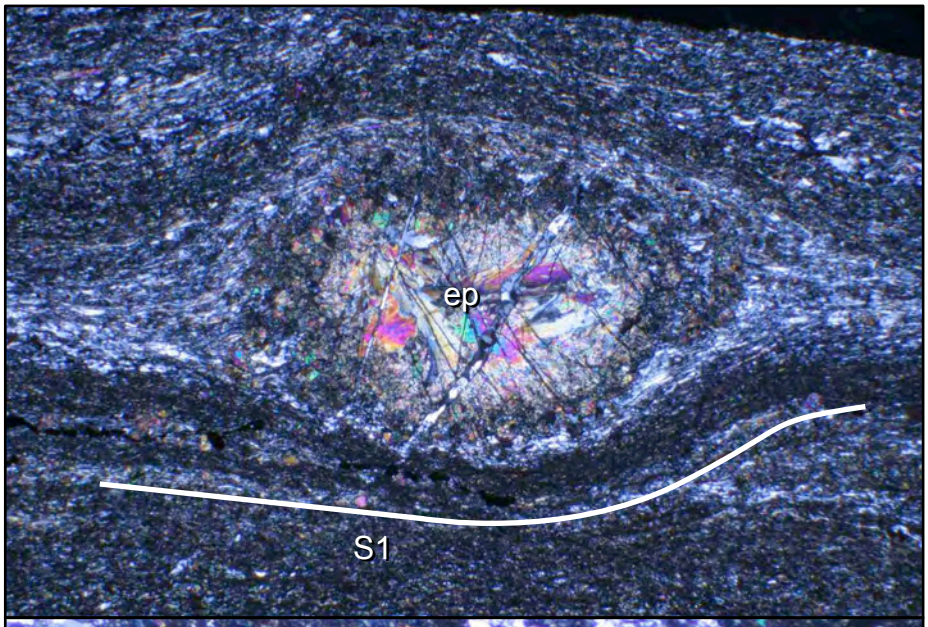

Fig. 6.9 Cross polarised light photomicrograph of an epidote (ep) mineral cluster enveloped by S1 (white line) running left to right, sample 0677G, Ampae Creek. Field of view is 3.5 mm.

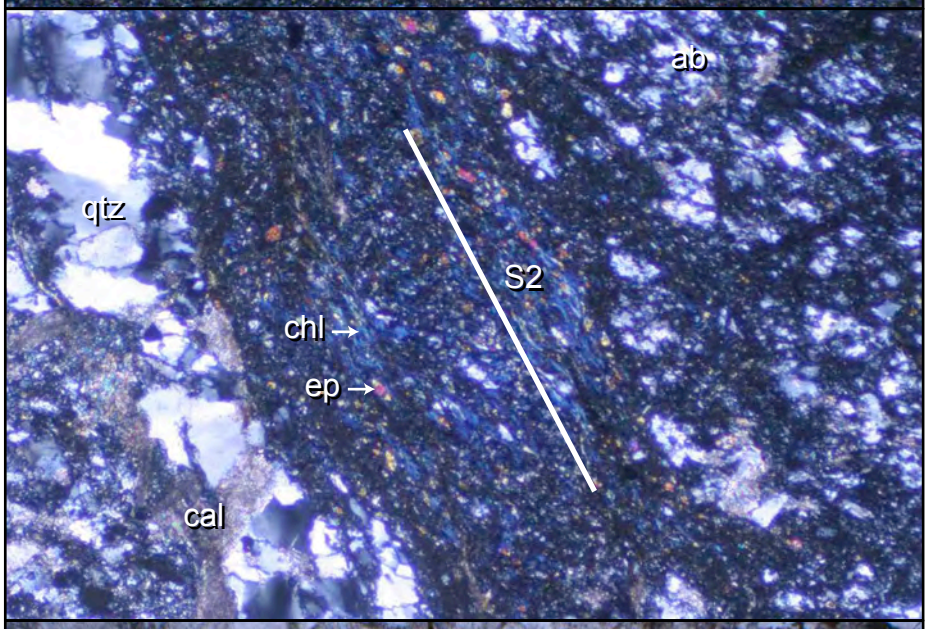

Fig. 6.10 Crossed polarised light photomicrograph of S2 defined by chlorite (chl), epidote (ep) and albite (ab), running top to bottom (white line), sample 0677A, Ampae Creek. Quartz (qtz) and calcite (cal) veins are oriented sub-parallel to S2. Field of view is 1.75 mm.

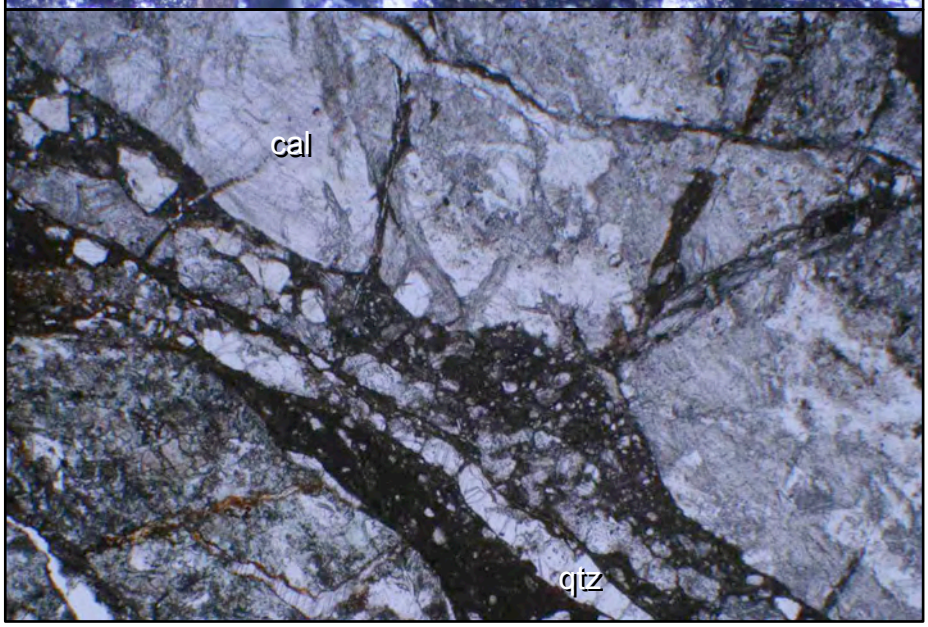

Fig. 6.11 Plain polarised light photomicrograph of fine-grained gouge in semi-brittle S2 fault zone, sample 0664, Biniguni River. Field of view is 3.5 mm.

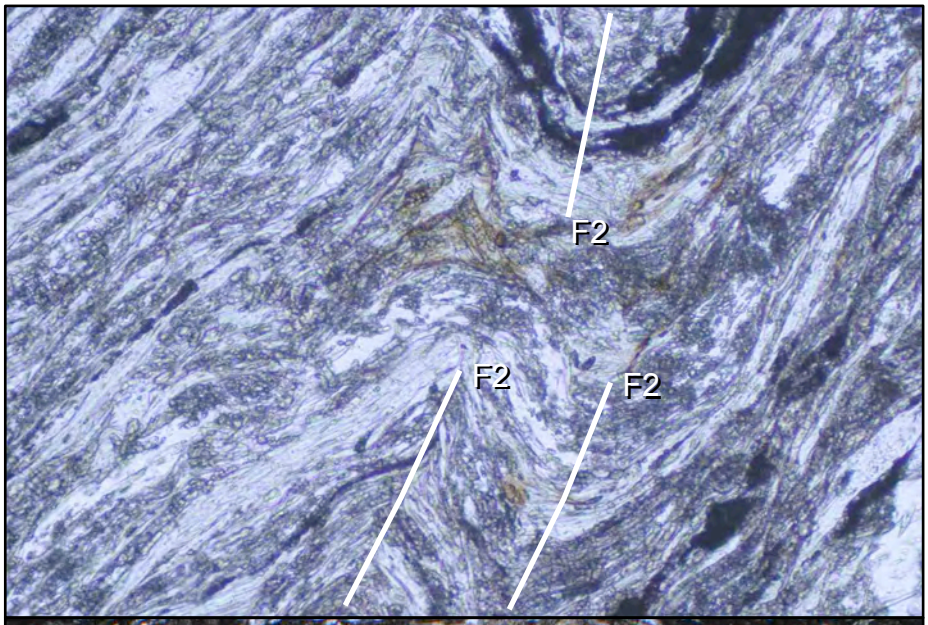

Figure 6.12 Plain polarised light photomicrograph of F2 folds of S1 (axial trace marked by a white line), sample 0677C, Ampae Creek. Field of view is 0.9 mm.

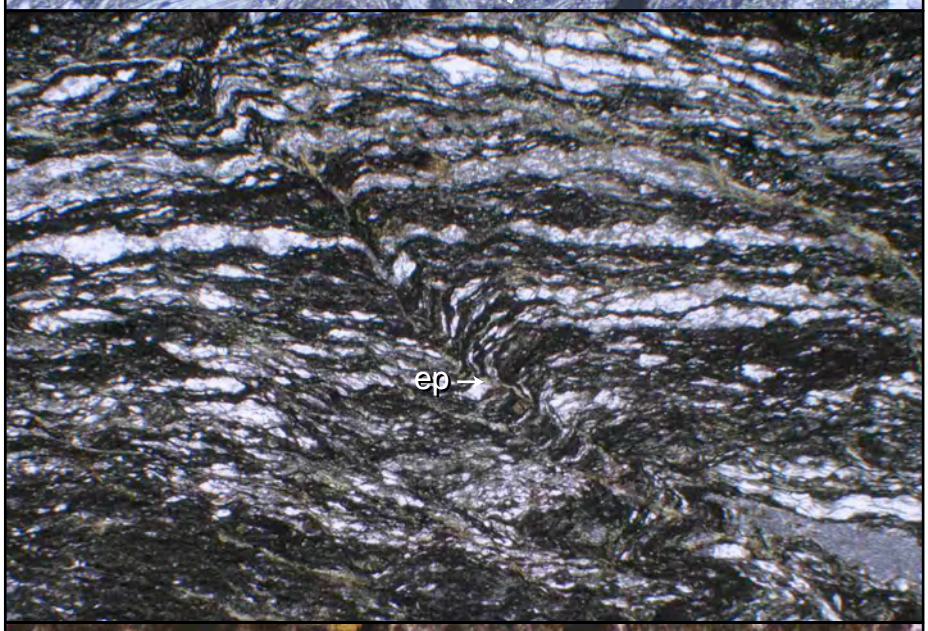

Figure 6.13 Plain polarised light photomicrograph of axial planar microfault with epidote (ep) mineralisation, sample 0628, Aro Creek. Field of view is 3.5 mm.

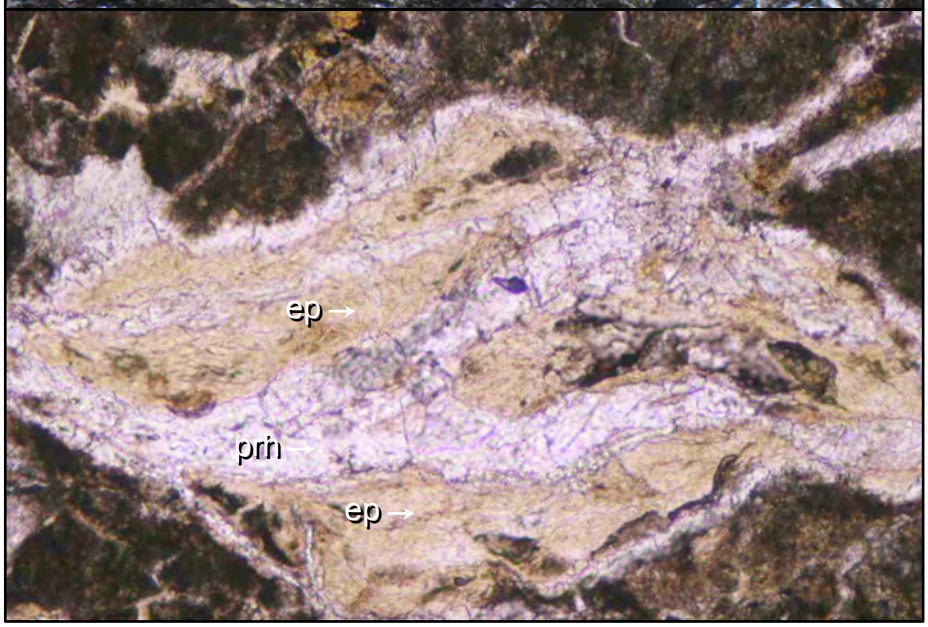

Figure 6.14 Plain polarised light photomicrograph of epidote (ep) and prehnite (prh) veins, sample 0604, Pumani River. Field of view is 0.9 mm.

contains common angular lithic and monomineralic clasts derived from the host rock (Fig. 6.15). Rare epidote and prehnite veins are typically associated with semi-brittle to brittle faults (e.g. sample 0604; Fig. 6.14).

6.5 Veins

Veins range from 0.03 to 3 mm wide and commonly contain calcite, less commonly quartz and rarely epidote and prehnite. The timing of the veins spans the entire deformation history. They are both deformed by and cut S1, S2 and the semi-brittle to brittle overprint. The calcite and quartz veins formed throughout the deformation history, whereas the epidote and prehnite veins are restricted to the semi-brittle to brittle overprint. Pre- to syn-S1 veins are recrystallised with sub-grains aligned with the S1 foliation (e.g. sample 0627; Fig. 6.16) and those at a high angle to S1 are folded and recrystallised (e.g. sample 0674; Fig. 6.17). Some veins show partial recrystallisation by S1 at the margins of the veins (e.g. 0668A; Fig. 6.18). Post-S1 veins show sharp contacts (e.g. sample 0628; Fig. 6.19). These show either concentrations of chlorite at the vein margins or little new mineral growth (e.g. samples 0677A and 0628 respectively). Chlorite may also pseudomorph epidote adjacent to veins (e.g. sample 0629). Samples commonly show multiple generations of veins (e.g. sample 0630; Fig. 6.20). For example, in sample 0630, pre-S1 quartz veins are recrystallised and cut by post-S1 calcite veins. In addition, the post-S1 calcite veins are cut by epidote veins, which are in turn cut by further calcite veins. The prehnite veins are commonly in the centre of epidote veins (e.g. sample 0604; Fig. 6.14).

6.6 Dykes

The dykes preserve a doleritic texture defined by elongate and randomly oriented augite grains (e.g. sample 0661C; Fig. 6.21). The augite grains are euhedral and mineral chemistry data (see below) indicate that they are the only igneous minerals unaffected by the thermal metamorphism of the dykes. Plagioclase is pseudomorphed

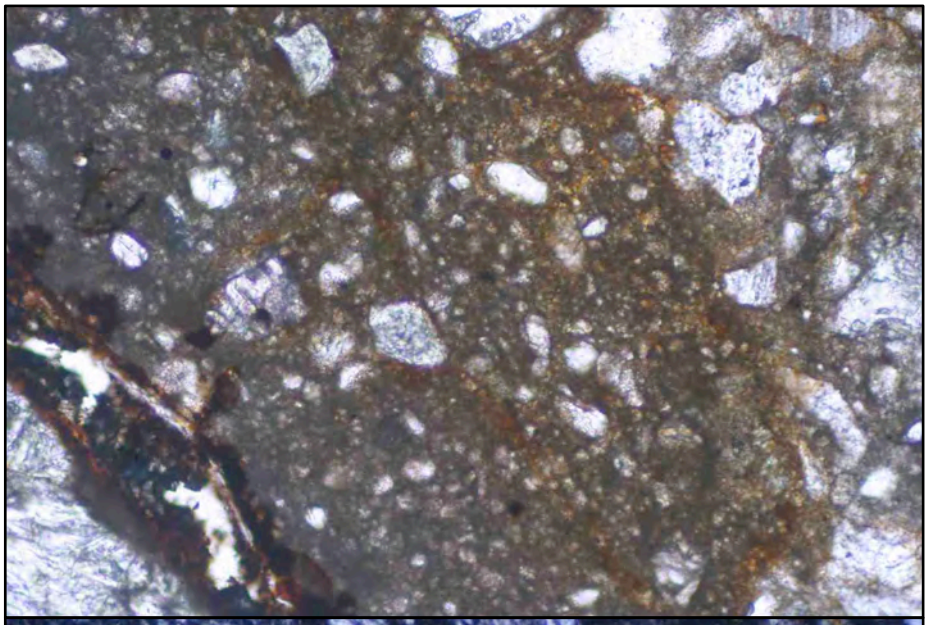

Figure 6.15 Plain polarised light photo-micrograph of fine-grained gouge in a late fault zone, sample 0664, Biniguni River. Field of view is 0.9 mm.

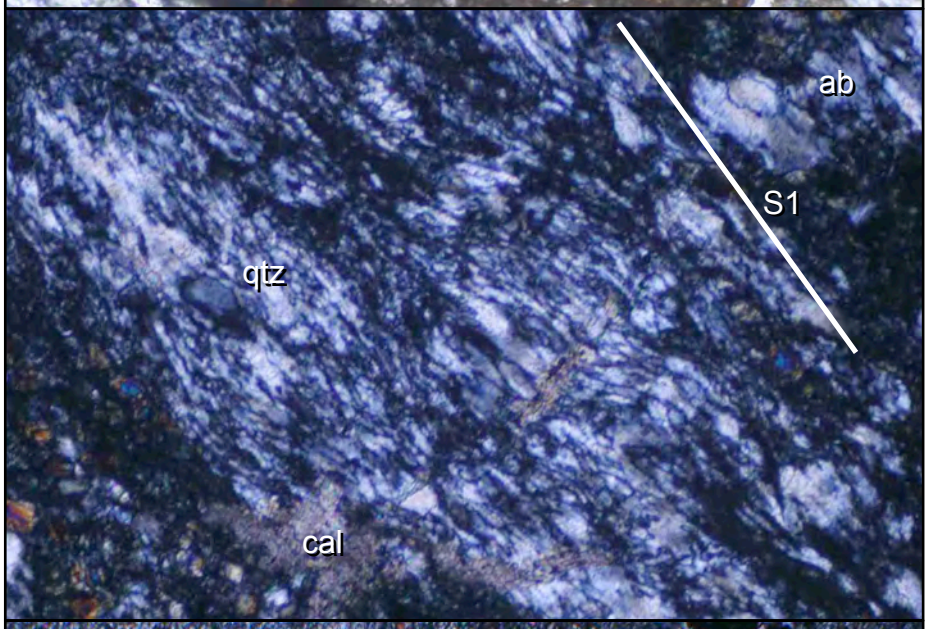

Figure 6.16 Crossed polarised light photo-micrograph of a pre- to syn-S1 quartz (qtz) vein with recrystallised sub-grains of quartz aligned with S1 (white line), sample 0627, Aro Creek. Field of view is 0.9 mm.

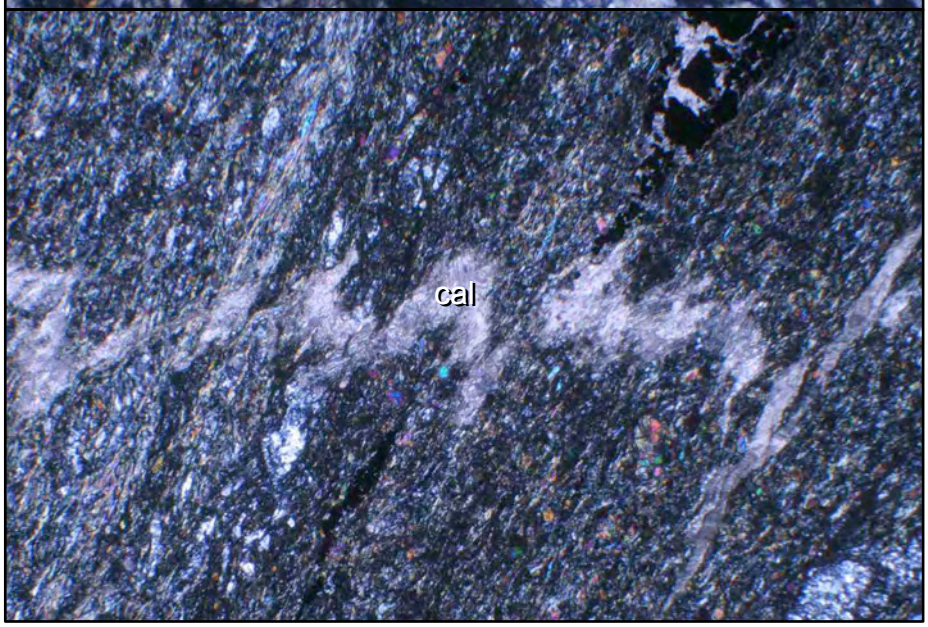

Figure 6.17 Crossed polarised light photo-micrograph of a folded calcite (cal) vein, sample 0674, Wange Creek. Field of view is 3.5 mm.

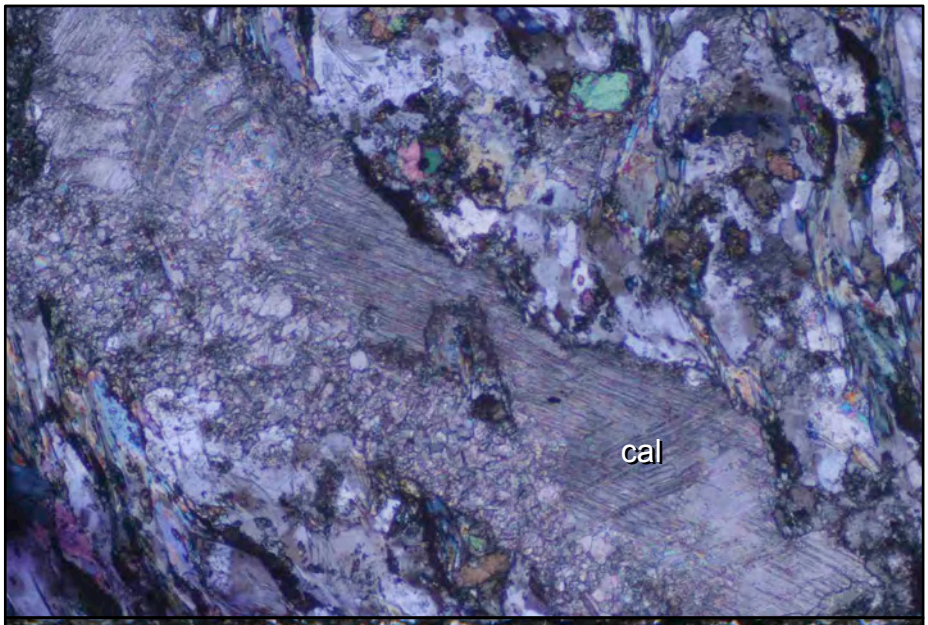

Fig. 6.18 Cross polarised light photomicrograph of partially recrystallised calcite (cal) vein, sample 0668A, Gwariu River. Field of view is 1.75 mm.

Fig. 6.19 Crossed polarised light photomicrograph of a post-S1 calcite (cal) vein with sharp contacts, sample 0628A, Aro Creek. Field of view is 3.5 mm.

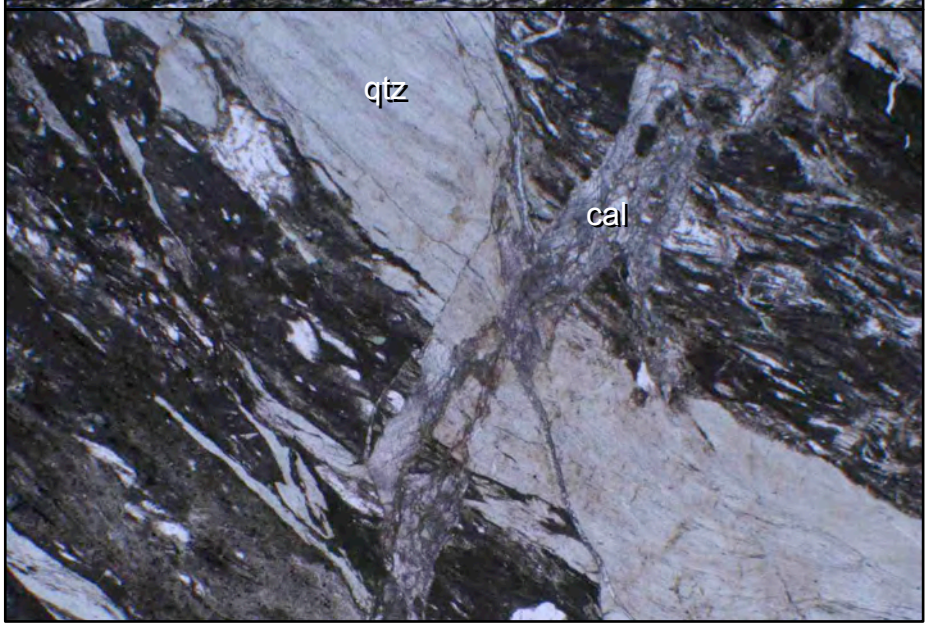

Fig. 6.20 Plain polarised light photomicrograph of multiple generations of veins, sample 0630, Yatap Creek. Field of view is 3.5 mm.

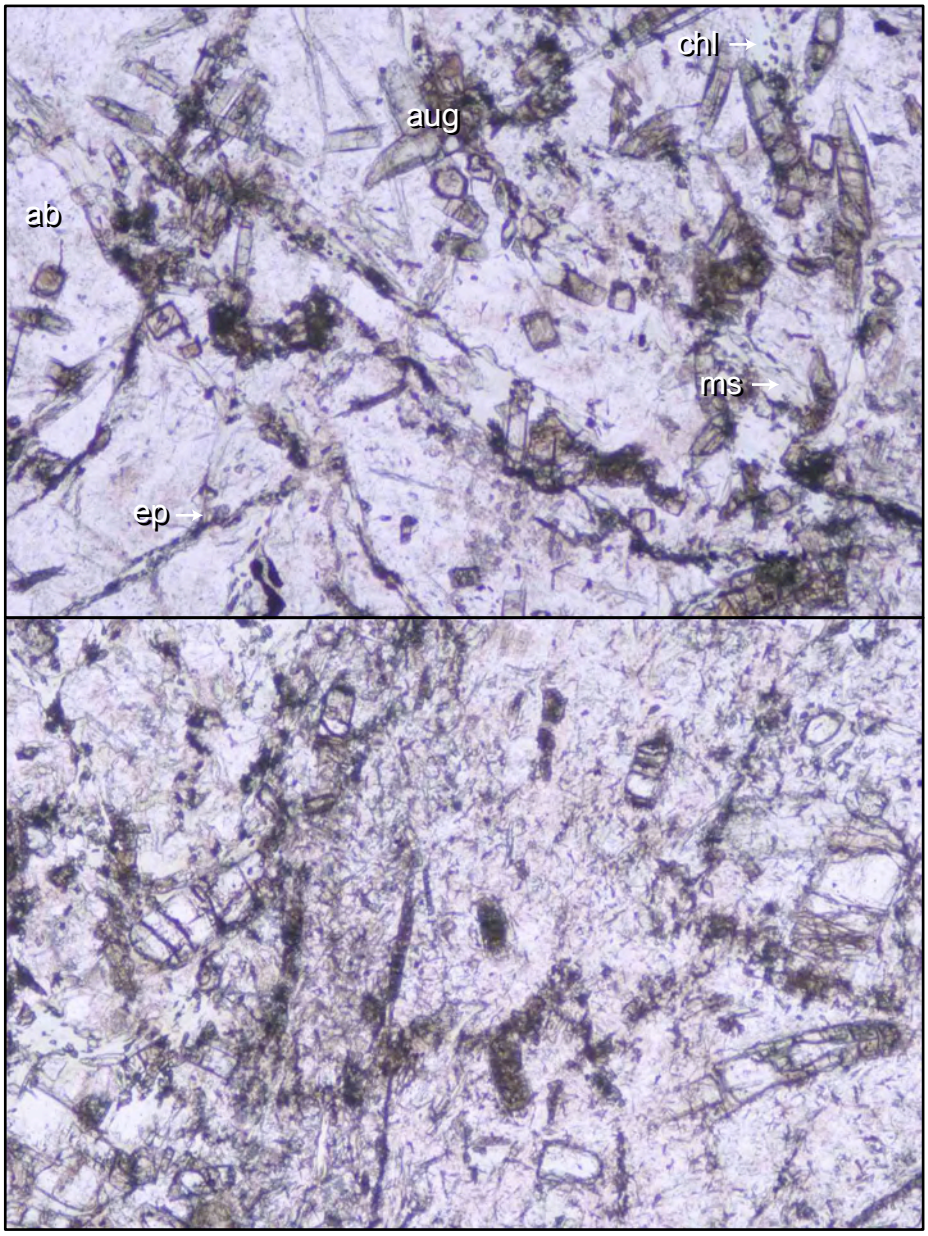

Fig. 6.21 Plain polarised light photomicrograph of partially recrystallised dyke with randomly oriented augite (aug) grains. Plagioclase domains are pseudomorphed by albite (ab), chlorite (chl), muscovite (ms) and epidote (ep), sample 0661C, Biniguni River. Field of view is 1.75 mm.

Fig. 6.22 Plain polarised light photomicrograph of a fine-grained domain within the dyke that shows similar texture to Fig. 6.21, sample 0661C, Biniguni River. Field of view is 1.75 mm.

by albite with randomly oriented chlorite, muscovite and fine-grained acicular epidote (Fig. 6.21). Fine-grained domains show the same texture and mineralogy as the domains with larger grain size (e.g. sample 0661C; Fig. 6.22).

6.7 Mineral Chemistry

The minerals of the metabasite rocks were analysed by electron microprobe (EMP) in order to determine their major element compositions and to classify the mineralogy of the different metamorphic assemblages. All EMP analyses are presented in Appendix C.

Plagioclase feldspar displays little variation in composition and is albite with XAn = Ca/(Ca+Na) < 0.02, where Ca and Na are the number of calcium and sodium cations per formula unit (Fig. 6.23a). Very rare potassium feldspar included within plagioclase has XOr = K/(K+Ca+Na) = 0.95, where K, Ca and Na are the number of potassium, calcium and sodium cations per formula unit (Fig. 6.23a). S1 chlorite classifies mainly as pycnochlorite with minor brunsvigite (Hey, 1954) with XFe = Fe/(Fe+Mg) = 0.51-0.59 for all samples except 0676 which has slightly lower XFe = 0.42-0.47, where Fe and Mg are iron and magnesium cations per formula unit (Fig. 6.23b). Chlorite grains within the mafic dyke (sample 0661C) classify as talc-chlorite (Hey, 1954) with XFe = 0.29 (Fig. 6.23b). The clinopyroxene classification of grains within the mafic dyke (sample 0661C) was determined using the spreadsheet PX-NOM (Sturm, 2002). The clinopyroxene grains classify as aluminian or aluminian ferrian diopside, or aluminian or chromian augite, have XFe = 0.22-0.49 and plot as either diopside or augite (Fig. 6.23c). Epidote shows appreciable substitution of Al by Fe3+. Epidote with high Fe3+ content (up to two Fe3+ cations) is called pistacite and epidote with low Fe3+ content (zero Fe3+) is called clinozoisite (Fig. 6.23d). S1 epidote is Fe3+-rich pistacite with Fe3+ = 1.01-1.99 cations on the basis of 25 oxygen (Fig. 6.23d). However, the least Fe3+-rich grains are from a coarse-grained S1 fabric (sample 0672) and the most Fe3+-rich grains include both samples from the eastern flank of the Dayman Dome (samples 0605 and 0628) and finer grained samples from the northern flank.

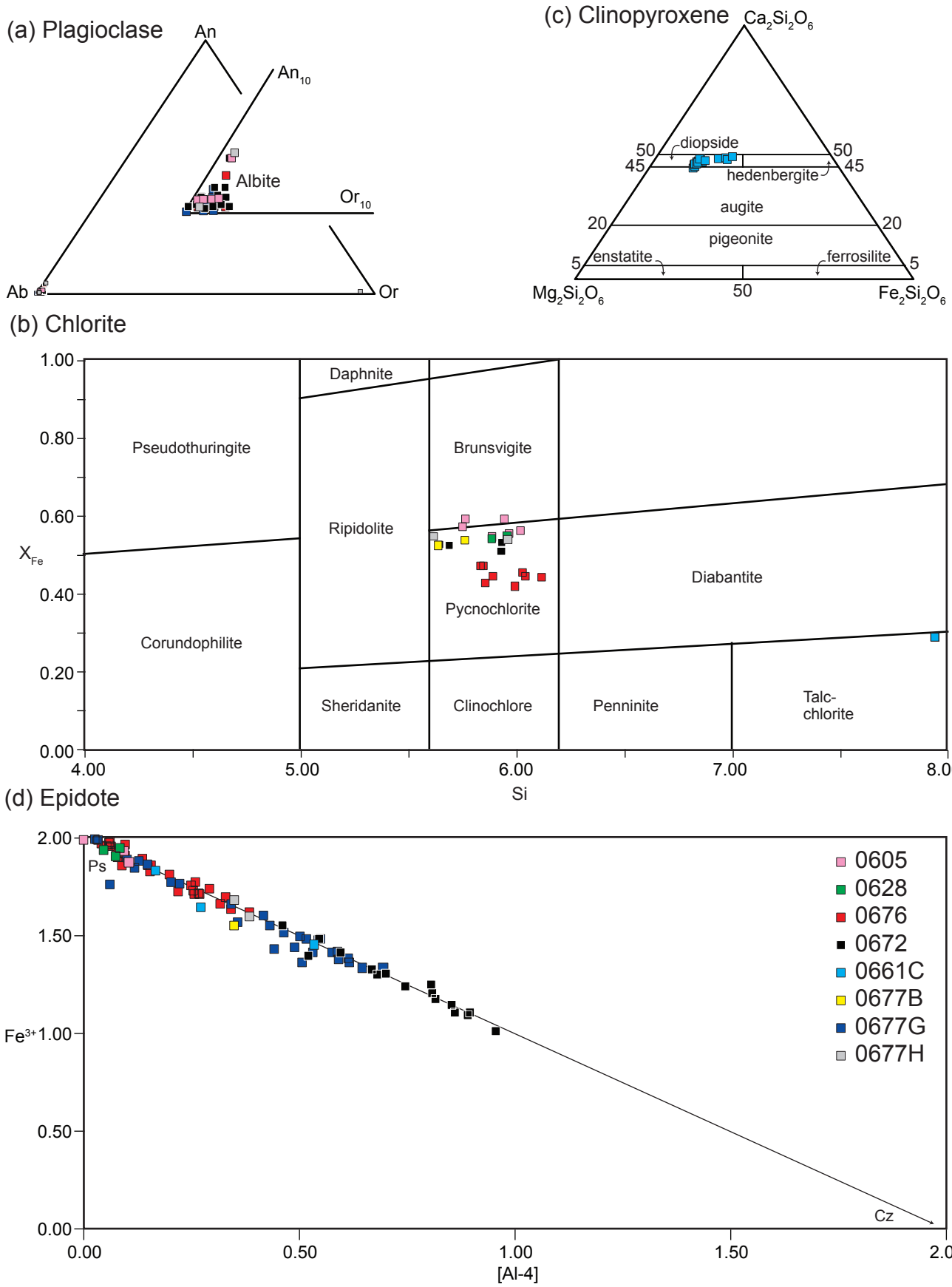

Figure 6.23(a-d) Mineral chemistry classification plots for (a) plagioclase [An = anorthite, Ab = albite, Or = orthoclase]; (b) chlorite [X_{Fe} = Fe/(Fe+Mg), Si = number of silicon cations recalculated for 28 oxygen]; (c) clinopyroxene; (d) epidote [Fe^{3+} and Al = number of ferric iron and aluminium cations respectively recalculated for 25 oxygen, Ps = pistacite (2 Fe^{3+}), Cz = clinozoisite (0 Fe^{3+})].

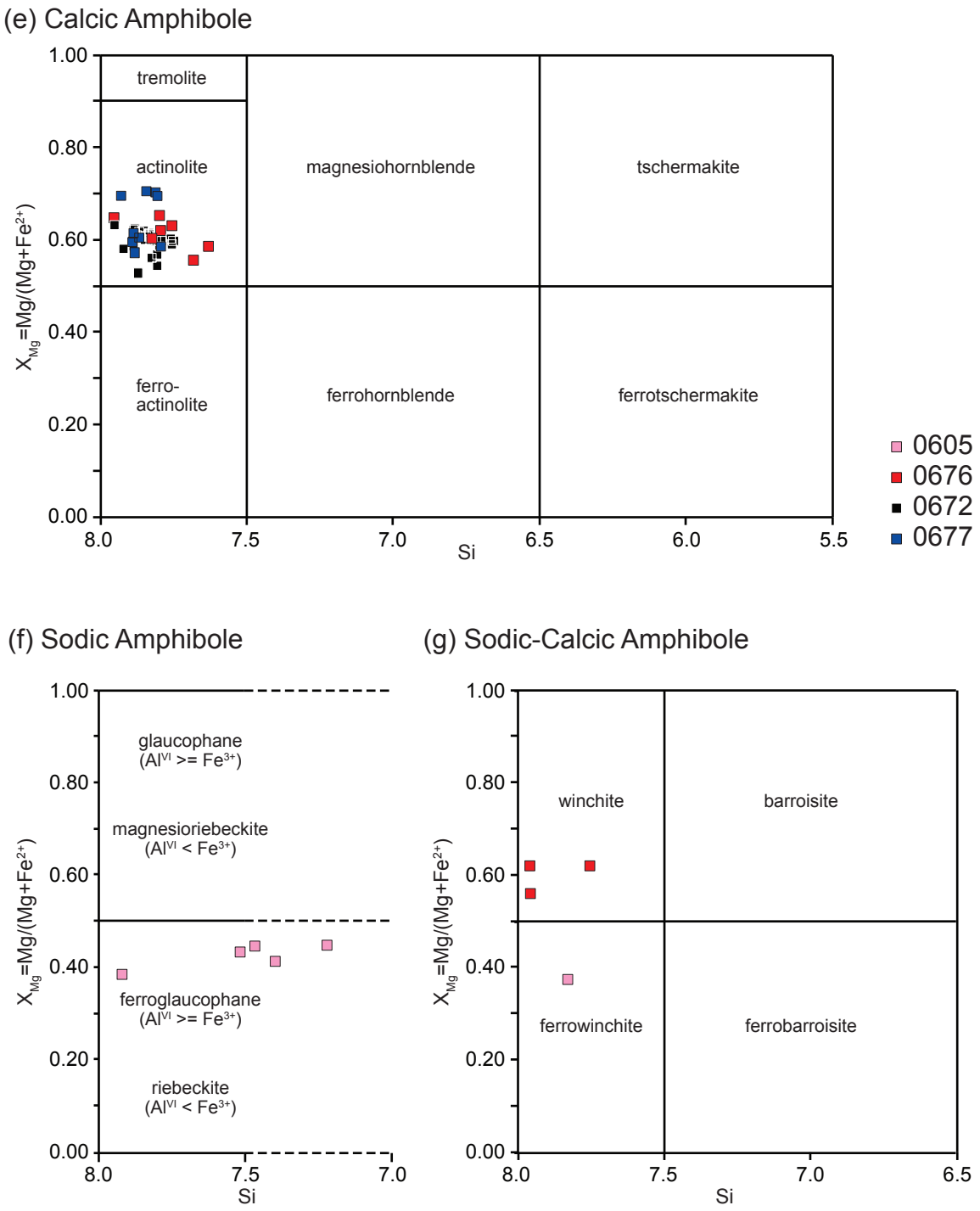

Figure 6.23(e-g) Mineral chemistry classification plots for (e) calcic, (f) sodic and (f) sodic-calcic amphiboles. [Mg, Fe^{2+} and Si = number of magnesium, ferrous iron and silica cations respectively recalculated for 23 oxygen].

All samples contain S1 calcic amphibole that classifies as actinolite using the classification scheme of Leake *et al*. (1997, 2004) with XFe = 0.29-0.47 (Fig. 6.23e). Rare blue S2 sodic amphibole grains in sample 0605 classify as riebeckite with XFe = 0.55-0.61 (Fig. 6.23f). One analysis of a blue-green sodic-calcic amphibole in sample 0605 classifies as ferrowinchite with XFe = 0.63 (Fig. 6.23g). In addition to the common actinolite, sample 0676 also contains rare sodic-calcic amphibole that classifies as winchite with XFe = 0.38-0.44 (Fig. 6.23g).

6.8 Discussion

The S1 assemblage includes actinolite, albite, epidote, chlorite, titanite, calcite and quartz. This assemblage indicates that the conditions of metamorphism that accompanied the development of S1 lay in either the greenschist or epidote blueschist facies (Fig. 6.24a). The lack of prehnite or pumpellyite in association with S1 actinolite excludes the prehnite-pumpellyite facies. The lack of hornblende and plagioclase feldspar with XAn > 0.20 excludes the amphibolite facies. The lack of lawsonite excludes the lawsonite blueschist facies and suggests the metamorphic temperature of recrystallisation that accompanied the development of S1 was on the high-T side of the lawsonite to epidote transition (Fig. 6.24a). Although the pressure of recrystallisation is poorly constrained by the greenschist facies assemblage, the temperature lies between T = 330-430 °C at P = 3 kbar to T = 500-550 at P = 15 kbar (Fig. 6.24a). However, the pressure of metamorphism was likely P = 6.5-9 kbar as discussed below and therefore the temperature was likely approximately T = 450 °C (Fig. 6.24b).

The low Na content of S1 actinolite is consistent with greenschist facies conditions (P < 9 kbar) and suggests that epidote blueschist facies conditions were unlikely during the development of S1. Although blue amphibole is typically associated with high-P metamorphism of the blueschist facies, Fe3+ rich blue amphiboles may form at low-P under oxidising conditions (Brown, 1977; Jun *et al*., 1995). Fe3+ is calculated for all S1 actinolite grains at less than 0.4 wt% oxide (Fe2O3) using the IMA-favoured procedure (dependant upon composition) of adjusting the sum (Si + Al + Cr + Ti + Fe

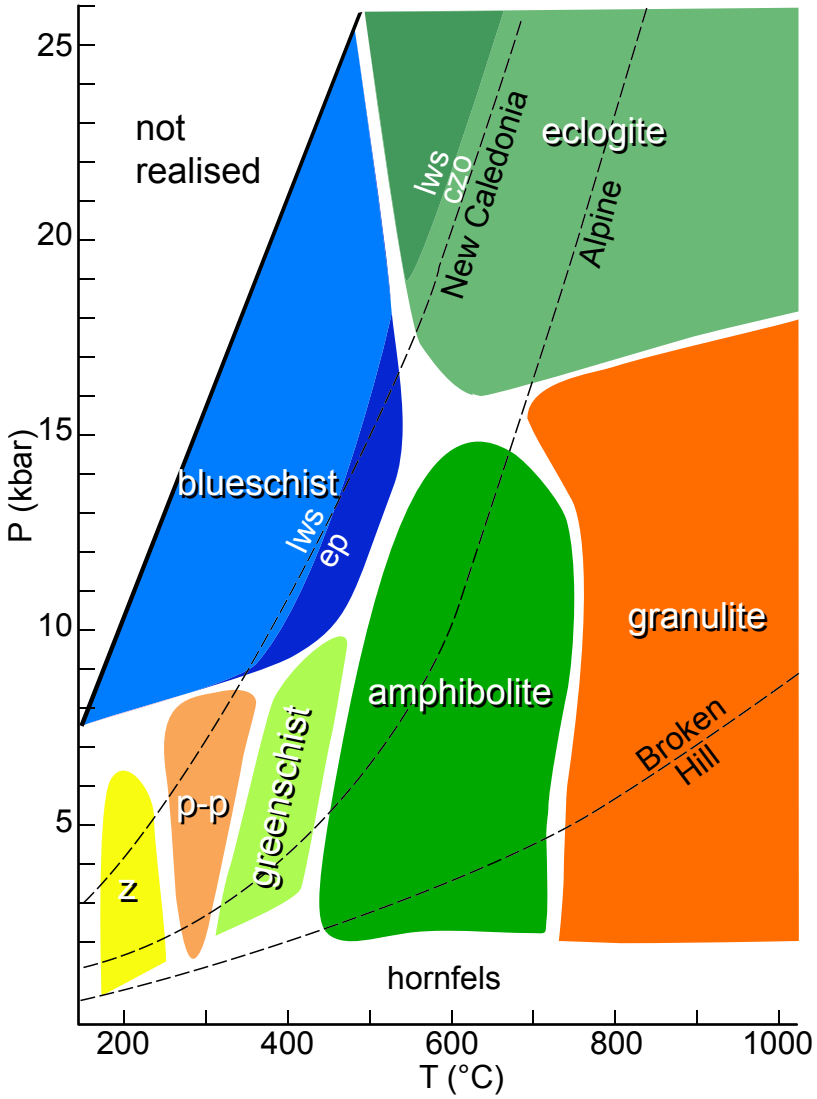

Figure 6.24(a) P-T diagram showing the generalized distribution of the various metamorphic facies. The blueschist and eclogite facies may be subdivided on the basis of the breakdown reaction of lawsonite (lws) to form epidote (ep) or clinozoisite (czo). Representative geotherms are shown for: subduction (New Caledonia), convergent continent (Alpine) and exceptionally high heat flow (Broken Hill). Abbreviations: z = zeolite; p-p = prehnite-pumpellyite. From Vernon & Clarke (2008).

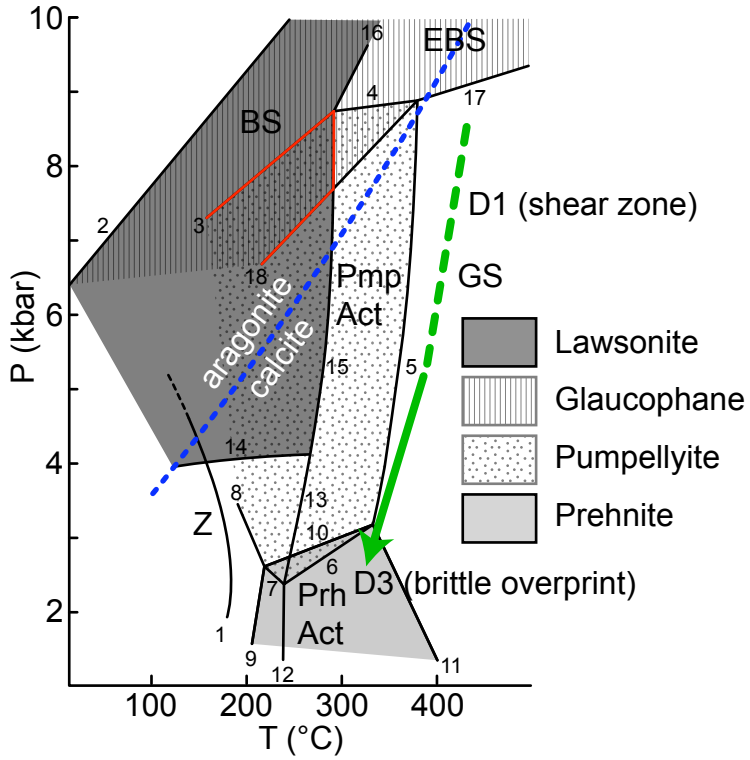

Figure 6.24(b) Schematic P-T diagram for low grade metabasites. Facies abbreviations: Z = zeolite, Prh Act = prehnite-actinolite, Pmp Act = pumpellyite-actinolite, GS = greenschist, BS = blueschist, EBS = epidote blueschist. From Beiersdorfer & Day (1995). The filled regions represent the stability of prehnite, pumpellyite, glaucophane and lawsonite. The red lines highlight the P-T region where pumpellyite, glaucophane and lawsonite are all stable. The argonite to calcite transition is shown (blue dashed line). The green line represents the P-T path between D1 and D3.

1. analcime (anl) + quartz (qtz) = albite (ab)
2. jadeite (jd) + qtz = ab
3. glaucophane (gln) + lawsonite (lws) = pumpellyite (pmp) + chlorite (chl) + ab + qtz
4. gln + epidote (ep) + H2O = pmp + chl + ab
5. pmp + chl + qtz = ep + tremolite (tr) + H2O
6. pmp + qtz = prehnite (prh) + ep + chl + H2O
7. pmp + qtz + H2O = prh + chl + laumontite (lmt)
8. pmp + chl + qtz + H2O = tr + lmt
9. tr + lmt = prh + chl + qtz + H2O
10. pmp + qtz = prh + chl + H2O
11. tr + ep + H2O = prh + chl + qtz
12. prh + lmt = ep + qtz + H2O
13. pmp + lmt = ep + chl + qtz + H2O
14. lws + qtz + H2O = lmt
15. pmp + lws = ep + chl + qtz + H2O
16. gln + law = ep + chl + ab + qtz + H2O
17. ep + gln + qtz + H2O = tr + chl + ab
18. pmp + gln + qtz + H2O = tr + chl + ab

+ Mg +Mn) to 13 by varying the Fe3+ and Fe2+ appropriately in the amphibole recalculation on the basis of 23 oxygen (Leake *et al*., 1997, 2004). Fe3+ in S2 riebeckite in sample 0605 is calculated at up to 7 wt% oxide (Fe2O3). This is consistent with a change in oxidation state controlling the development of the blue amphibole rather that an increase in pressure.

Davies (1980) defined metamorphic zones across the Suckling-Dayman Massif including large areas of pumpellyite-actinolite facies schist with spot occurrences of glaucophane, lawsonite and/or aragonite (respectively G, L and A on Fig. 6.25). Greenschist facies rocks are restricted to a 500 m-thick shear zone (Mai'iu Fault) best exposed on the northern and eastern flanks of the Dayman Dome and along the Biman dip slopes (Fig. 6.25). In addition, minor greenschist facies rocks outcrop near the summit of Mt Suckling. The data presented here confirms the interpretation of greenschist facies conditions for the development of S1 on the northern and eastern flanks of the Dayman Dome. S1 cuts the footwall pumpellyite-actinolite facies schists with minor pods of prehnite-pumpellyite facies rocks (Davies, 1980; Fig. 6.25). Although these units were not sampled in this study, pumpellyite-actinolite assemblages are stable at $P < 9$ kbar, whereas glaucophane-lawsonite assemblages are stable at $P > 6.5$ kbar (Fig. 6.24b; Beiersdorfer & Day, 1995) suggesting that the Suckling-Dayman Massif has been exhumed from a depth of 20-30 km. This is consistent with observations of aragonite (Fig. 6.24b) mainly in pumpellyite-actinolite facies schist (Davies, 1980) and calcite in slightly higher-T greenschist facies rocks of this study.

Prehnite-pumpellyite facies rocks include a large area south of the Onuam Fault and rare pods within the pumpellyite-actinolite facies schists mapped by Davies (1980). Coexisting prehnite and pumpellyite suggest these metabasites likely recrystallised at approximately $P < 3$ kbar and $T = 250$ °C (Fig. 6.24b). This may represent a maximum burial depth of approximately 10 km for the large area south of the Onuam Fault as these rocks grade into unmetamorphosed basalt of the Kutu Volcanics (Davies, 1980; Fig. 6.25). The rare pods of prehnite-pumpellyite facies rocks within the pumpellyite-

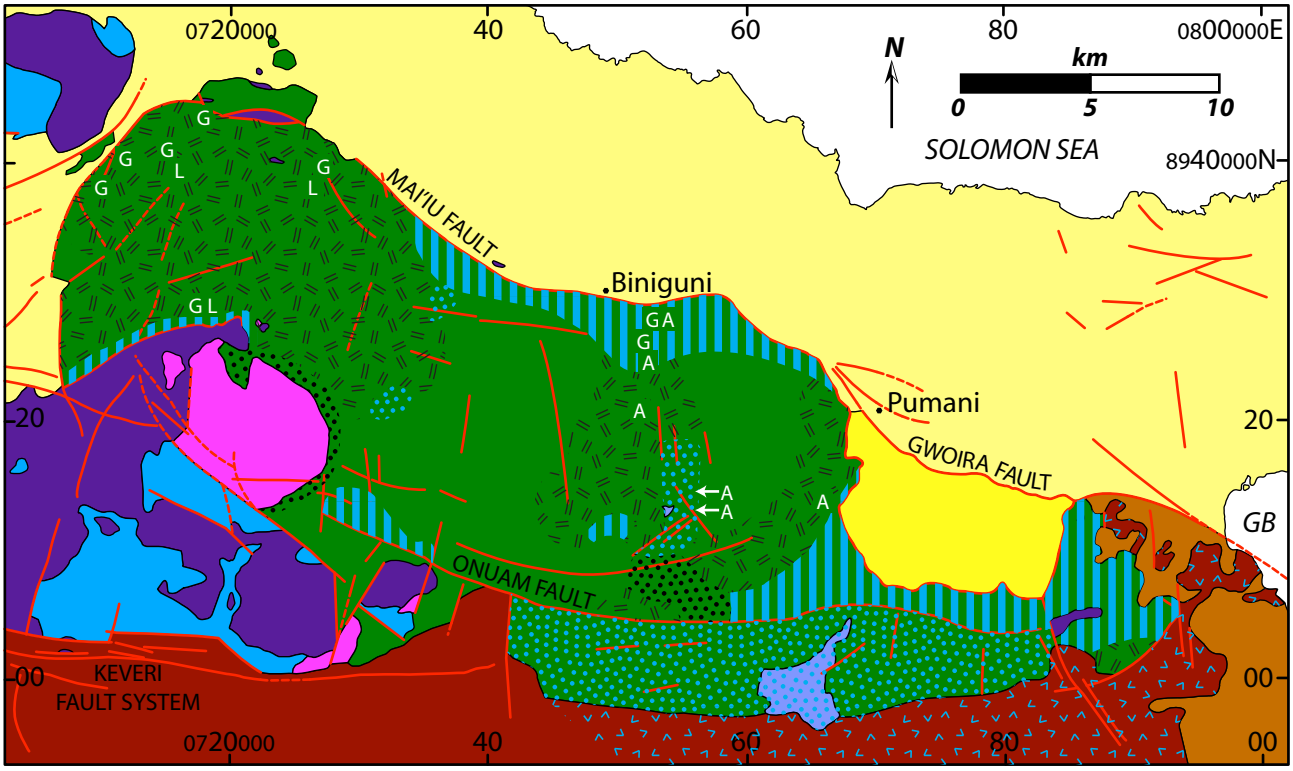

KEY:

Geological units:

- Undifferentiated Quaternary and Tertiary Volcanic and Sedimentary Rocks
- Uga Sanstone (sandstone, siltstone; minor conglomerate)
- Gwoira Conglomerate (conglomerate, poorly sorted sandstone and siltstone)
- Undifferentiated Tertiary Felsic Plutonics (granite; granodiorite, monzonite; microdiorite, micromonzonite porphyry)
- Kutu Volcanics (basalt lava and pillow lava; minor tuff, limestone)
- Goropu Metabasalt (including Bonenau Schist Member) (variably schistose meta-basalt, -dolerite, -gabbro and -limestone; hornfels)
- Yau Gabbro (gabbro, diorite, granophyric tonalite: *prehnite-pumpellyite facies*)
- Undifferentiated Gabbro (gabbro with ophitic, allotriomorphic/hypidiomorphic or cumulus textures)
- Undifferentiated Ultramafics (ultramafic rock with cumulus or tectonite fabric)

Metamorphic zones:

- Kutu Volcanics (unmetamorphosed)
- Goropu Metabasalt and Yau Gabbro (prehnite, pumpellyite)
- Goropu Metabasalt (pumpellyite-actinolite)
- Goropu Metabasalt (greenschist)
- Goropu Metabasalt (hornfels)
  - G = glaucophane
  - L = lawsonite
  - A = aragonite

Figure 6.25 Geological map and metamorphic zones of the Suckling Dayman Massif and surrounding areas (modified from Davies and Smith, 1974 and Davies, 1980). GB = Goodenough Bay.

actinolite facies schists north of the Onuam Fault (Fig. 6.25) may represent low strain zones that did not recrystallise at the higher-P pumpellyite-actinolite facies metamorphic conditions experienced by the majority of the Goropu Metabasalt. The prehnite identified within the D3 semi-brittle to brittle fault zone at site 0604 is consistent with exhumation of the Goropu Metabasalt between D1 and D3 (see green arrow on Fig. 6.24b).

Davies (1980) also mapped a contact aureole hornfels facies in the Goropu Metabasalt around felsic plutonic rocks near the summit of Mt Suckling (Fig. 6.25). Metamorphic mineral assemblages reported by Davies (1980) include garnet-mica schists with andalusite and staurolite. These assemblages suggest a depth of recrystallisation within the stability field of andalusite (i.e. P < 4 kbar; depth < ~12 km). This observation suggests that the felsic pluton intruded following significant uplift of the pumpellyite-actinolite facies schists. Davies mapped a second hornfels facies domain south of Mt Dayman (Fig. 6.25) that he interpreted to predate the regional metamorphism, however the pluton (heat source) is not exposed.

There is widespread agreement that Fe3+ in epidote decreases with increasing metamorphic grade (Beiersdorfer & Day, 1995). The correlation between coarse-grained samples and relatively lower Fe3+ in S1 epidote compared to fine-grained samples supports this general relationship. Beiersdorfer & Day (1995) conclude that compositions of pumpellyite, prehnite and chlorite are commonly unreliable indicators of metamorphic grade, consistent with the lack of a trend observed in the mineral chemistry data for chlorite.

The round to elliptical shaped single grains or mineral clusters of epidote (up to 1.5 mm across) are unusually coarse-grained compared to the enveloping fine-grained S1. These grains may reflect porphyroblasts of epidote, however this is inconsistent with the fine grainsize of matrix epidote common in all samples. A second possible explanation is that the large single grains or mineral clusters of epidote pseudomorph a mineral that filled vesicles of the protolith basalt. This explanation is consistent with the round to elliptical shape of the epidote grains or clusters and the observation that they are common in

restricted samples. The mafic dykes cut S1, lack chilled margins and are partially recrystallised. These observations are consistent with intrusion of the dykes shortly following the cessation of D1 shear, but prior to significant cooling of the greenschist facies rocks. This short timeframe is consistent with the orientation of the dykes reflecting a similar extension direction to the L1 mineral lineation (Chapter 5).

Chapter 7 DISCUSSION and CONCLUSIONS

7.1 Geological Synthesis

The Suckling-Dayman Massif is characterised by an elongate twin dome shape that is subdivided into the Dayman and Suckling domes (Chapter 2). Several similarities exist between the Suckling-Dayman Massif and metamorphic core complexes (MCC) of the North American Cordillera, Aegean Sea region near Greece and indeed the nearby D'Entrecasteaux Islands: (1) a thick mylonitic ductile shear zone, (2) elongate domed landforms of the core, (3) igneous activity associated with progressive uplift, and (4) progressive deformation from ductile to brittle conditions. These other settings also commonly show late low-angle faults overlain by unmetamorphosed rocks and these structures proved elusive in the Pumani and Biniguni areas visited for this study. The D3 fault zone identified in Chapter 5 may be one such structure.

Much of the Papua New Guinea literature describes the basal contact of the Papuan Ultramafic Belt (PUB) as a thrust surface (e.g. Davies, 1980), which undoubtedly it was on the basis of the juxtaposition of mantle rocks over continental rocks. However, no evidence of this thrust history was observed in shear zones examined in this study, suggesting pervasive recrystallisation of this boundary during later extensional deformation. The geometry and style of structures and map relations presented in this study indicate an extensional origin for the mylonitic foliation (S1) and mineral lineation (L1) of the Dayman Dome. Chapter 5 presents several lines of evidence that demonstrate an extensional origin for the mylonites in the Dayman Dome: (1) kinematic indicators in the footwall shear zone show a NNE directed down-dip, or normal, sense-of-shear, and (2) footwall rocks exhibit a progression from ductile to brittle structures at both the microscopic and mesoscopic scale. These structural relations and metamorphic constraints suggest that mylonitic rocks originated in a normal sense-of-shear at about 20-30 km depth, where crystal-plastic processes where operative. This study also contradicts

Davies (1980) where he concludes that convergent tectonics was the prime mechanism for elevating and folding the metabasites into the broad domed landform (see below).

The following text details the geological history of the Suckling-Dayman Massif and brings together the key observations presented in the preceding chapters. The evolution is divided into four stages and is presented as schematic cross sections in Figure 7.1. The sections do not represent a single location but rather bring together observations from across the massif to compile the overall evolution of the Suckling and Dayman domes.

Stage1: Continental crust of the Australian plate margin (including protoliths to high-T metamorphic rocks that today comprise much of the Owen Stanley Range and the cores of the D'Entrecasteaux Islands MCC) followed Late Cretaceous oceanic crust down into a north-dipping Palaeogene subduction system (Davies, 1980; Davies and Jaques, 1984). The resulting arc-continent collision thickened the continental crust by thrusting the Papuan Ultramafic Belt (PUB) over the continental rocks in the Eocene (Fig. 7.1, stage 1; Davies, 1980; Davies and Jaques, 1984). This led to the deep subduction (>100 km) of some continental crust (Baldwin *et al*., 2005). The deeply subducted continental rocks are represented by the Kagi Metamorphics in Figure 7.1 but likely include other geologic units along strike.

Though the exposed subducted continental rocks were metamorphosed at high-T (Davies and Jaques, 1984, Davies and Warren, 1988; Hill and Baldwin, 1993; Baldwin *et al*., 2004), the exposed subducted Late Cretaceous oceanic crust varies from virtually unmetamorphosed rock (e.g. Kutu Volcanics, Fig. 7.1) through prehnite-pumpellyite facies to pumpellyite-actinolite facies (e.g. Suckling-Dayman Massif; Davies, 1980). The subducted Late Cretaceous oceanic crust is greenschist facies immediately below the basal contact of the PUB (Davies, 1980). All metabasite samples examined in this study come from the greenschist facies group of rocks (Chapter 6).

The majority of the Suckling Dayman Massif is pumpellyite-actinolite facies schist (Davies, 1980) and this assemblage indicates the massif has been exhumed from a depth

of 20-30 km. These metamorphic assemblages are noted in Figure 7.1 (stage 1) at appropriate points along the subducting slab.

Stage2: The timing of when the subduction system stalled and a transition to an extensional tectonic setting took place remains unclear. However, seafloor spreading in the Woodlark Basin had begun by 6 Ma suggesting that the transition from convergence to extension took place prior to this time (Taylor *et al*., 1999). In addition, Baldwin *et al*. (2004) report the timing of eclogite facies metamorphism of the subducted continental crust at 4.3 Ma prior to its exhumation in the extensional setting on the D'Entrecasteaux Islands. These results indicate that extension in this region began at least as early as the Miocene.

Regardless of when extension in this region began, the development of MCC extends from the D'Entrecasteaux Islands through to the Papuan Peninsula (Suckling-Dayman Massif). It is generally agreed (Davies and Jaques, 1984; Davies and Warren, 1988; Little *et al*., 2007) that the pre-existing thrust subduction boundary was reactivated in the extensional tectonic setting, such that the bounding shear zones of the MCC simply reversed the previous thrust motion (note that the kinematic arrow in Figure 7.1, stage 2 has reversed from stage 1). Any large displacement on low-angle normal faults results in isostatic uplift and warping of the lower plate into a broad antiform in response to tectonic denudation (Spencer, 1984). This is the dominant mechanism that controls the domed shape of MCC and is used here to define a developing domed shape for the exhuming lower plate of the Suckling-Dayman massif (Fig. 7.1, stage 2). The analysis of STRM data on the lowermost north flank of the Dayman Dome identified a change in dip of the metabasite dip slope from ~21° to ~18° N (Chapter 2). This orientation matches the average S1 orientation that dips 17° to 20° N (Chapter 5). The change in dip up the lower north flank identified in SRTM data is consistent with doming of the massif.

The kinematic analysis of the shear zone presented in Chapter 5 indicates that during this early stage of uplift the greenschist facies metabasite rocks underwent general shear deformation with a kinematic vorticity number (W_k) between 0.34 and 0.56. The pure

shear dominated flow may have been caused by buoyancy of continental crust from below (e.g. Kagi Metamorphics; Fig. 7.1, stage 2; Little *et al*., 2007) and/or the weight of a thick overburden (e.g. PUB; Fig. 7.1, stage 2; Bailey & Eyster, 2003). The orientation of structural lineaments identified in aerial photographs (Chapter 2) and structural megamullions identified in SRTM data (Chapter 2) correlates with the NNE-plunging orientation of mineral stretching lineations (L1; Chapter 5). This NNE extension direction best matches that predicted by the oldest recorded Eulerian pole (0.53-3.6 Ma; Table 2.1) for Woodlark Basin seafloor spreading, indicating that the pure shear dominated flow is older than 0.52 Ma. In fact, it is shown below that this deformation is older than 3.3 Ma. The corrugated non-planar morphology (megamullions) of the Dayman Dome is a feature observed in many detachment faults (e.g. Dinter & Royden, 1993; Okay & Satir, 2000; Little *et al*., 2007) including those called oceanic core complexes (Blackman *et al*., 1998).

Chapter 6 relates the rare presence of the blue amphibole riebeckite in shallowly dipping D2 shear zones to oxidising fluids rather than a change in P-T conditions. This interpretation may indicate that the 'glaucophane' identified by Davies (1980) may not necessarily indicate high-P conditions. L2 defined by aligned riebeckite characterises an unusual east-directed transport direction that is difficult to explain using the published Eularian poles of Taylor *et al*. (1999). The east-directed transport direction was only observed on the east-dipping flank of the Dayman Dome and this observation may indicate that the dip direction of the dome shape dominated over the overall tectonic extension direction in controlling the D2 transport direction on differently dipping flanks of the domes. The timing of the steeply dipping narrow D2 shear zones relative to the shallowly dipping riebeckite fabrics remains unclear as no cross cutting relationships were observed. However, their ductile nature places them within the 'stage 2' evolution sequence.

Stage 3: Davies (1980) reports that the emergence of the subducted oceanic crust from beneath the PUB took place in the Middle Miocene on the basis of extensive sedimentary rocks to the north of the massif (Fig. 7.1, stage 3). Sedimentation continued into the

Pliocene (Davies, 1980) with deposition of the Gwoira Conglomerate onto the north flank of the developing domes (Biman dip slopes in particular). Whitney and Dilek (1997) and Dinter and Royen (1993) report the deposition of sediment onto the flanks of actively exhuming MCC in Turkey and Greece respectively. The petrography of the lithic clasts in the Gwoira Conglomerate (Chapter 4) suggests they were sourced from metabasite units as opposed to ultramafic sources such as the PUB. Fluvial sediment characteristics, such as rounded and oxidised clasts (Chapter 4) suggest the metabasite source was subaerially exposed. The presence of shallow marine fossils indicates transgression of the sea and deposition of the Gwoira Conglomerate on a newly developed shelf (Fig. 7.1, stage 3).

Davies and Warren (1988) report a gravity low that may be due to a concentration of felsic material below the metabasite carapace of the Suckling-Dayman Massif. The felsic material may include the Kagi Metamorphics (as depicted in Figure 7.1) and intrusions such as the granite and monzonite that intrude metabasite rocks south of Mt Suckling (Fig. 1.2). The felsic rock may contribute to buoyancy-driven uplift of the massif (e.g. Davies & Smith, 1971). The granite and monzonite is undeformed and contact metamorphic assemblages including andalusite suggest it was emplaced at less than 12 km depth (Fig. 7.1, stage 3). The LA-ICP-MS ^{206}Pb-^{238}U age of one sample of granite is 3.3 ± 0.1 Ma (pers. comm. Melissa Murphy, 2008) and indicates the cessation of greenschist facies ductile shearing by this time.

A thinning lithosphere is generally compensated by a rising asthenosphere at depth and partial melting of the rising asthenosphere may have produced the mafic dykes that cut S1 at the Biniguni River (Chapter 5). A rising asthenosphere is also consistent with partial melting of the deep crust to produce the granite and monzonite units. The post-S1 timings of both the mafic dykes and, granite and monzonite units, suggests that there may exist a relationship between the two.

Assuming the mafic dykes intruded in a vertical orientation, their steep SW dip suggests subtle rotation. This observation is consistent with continued flexure of the mylonite zone to the present day to form the domed shape of the massif.

The cessation of ductile D1 and D2 deformation by the time of the mafic and felsic intrusions implies that brittle faults and fault zones must have controlled the final stages of exhumation of the Suckling-Dayman Massif. The scarcity of brittle to semi-brittle fault zones such as the D3 fault zone identified at the Pumani River (Chapter 5) suggests that any brittle carapace over the ductile D1 shear zone is largely eroded. Where exposed, brittle structures display a variably oriented, but commonly down dip, slickenside lineation that rarely matches the NNW transport direction predicted by the 0-0.5 Ma Woodlark-Australia Euler pole (Taylor *et al*., 1999; Table 2.1). Prehnite in the D3 mineral assemblage indicates a much lower pressure of metamorphism (Chapter 6) and is consistent with evolution of exhumation from ductile to brittle conditions.

Stage 4: At some stage since the Pliocene deposition of the Gwoira Conglomerate, it has been tilted toward the SE (Chapter 4). The SE dip of the Gwoira Conglomerate implies rotation about NE-SW oriented horizontal axis. This axis lies perpendicular to the NNW extension direction predicted by the 0-0.52 Ma Australia-Woodlark Euler pole (Taylor et al., 1999; Table 2.1). Therefore, the rotation of the Gwoira Conglomerate bedding from horizontal to the SE dip is inferred to be younger than 0.52 Ma. MCC are typically characterised by a low-angle detachment fault that separates a footwall of ductilely deformed metamorphic and intrusive rocks from a hanging wall of unmetamorphosed sedimentary units that have been tilted and displaced along normal faults. Domino-like rotation of normal faults, movement along a fault with listric geometry at depth, bowing of a low-angle fault due to footwall uplift or a combination of all of these may have uplifted and tilted hanging wall strata of the Gwoira Conglomerate.

Figure 7.1, stage 4 also shows the development of young faults (such as the Keveri Fault System and Onuam Fault), erosion of the metabasite domes and other units to the present day surface and shedding of Quaternary and Tertiary sediments mainly toward the north. The lack of drainage incision of the lowermost north flanks of the Dayman Dome suggests that exhumation of the dome is continuing today. It is therefore predicted that deeply subducted continental rocks (e.g. Kagi Metamorphics, Fig. 7.1, stage 4) may one day be exposed.

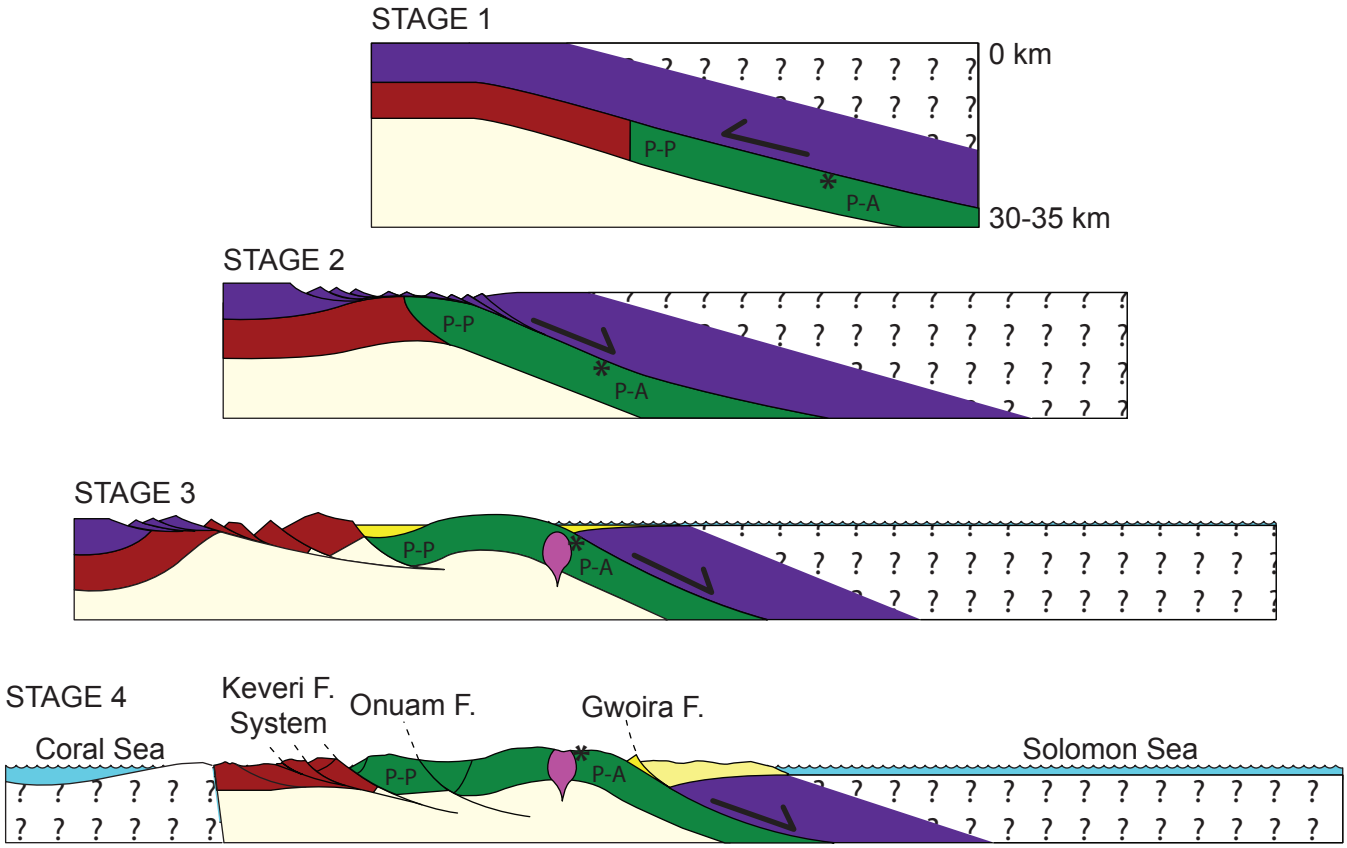

Undifferentiated Quaternary and Tertiary Volcanic and Sedimentary Rocks

Gwoira Conglomerate
(conglomerate, poorly sorted sandstone and siltstone)

Undifferentiated Tertiary Felsic Plutonics
(granite; granodiorite, monzonite; microdiorite, micromonzonite porphyry)

Kutu Volcanics
(basalt lava and pillow lava; minor tuff, limestone)

Goropu Metabasalt (including Bonenau Schist Member)
(variably schistose meta-basalt, -dolerite, -gabbro and -limestone; hornfels)

Papuan Ultramafic Belt (PUB)
(gabbro and ultramafic rock)

Kagi Metamorphics
(continental crust, garnet-bearing gneiss, biotite and chlorite schist)

Figure 7.1 Schematic cross sections of the evolution of the Suckling-Dayman Massif from Palaeogene arc-continent collision (stage 1) to Miocene to present day continental extension (stages 2-4). P-P = prehnite-pumpellyite faceies; P-A = pumpellyite-actinolite facies.

7.2 Conclusions

Following the objectives of the project listed in Section 1.5, this study has interpreted a dominant NNE trend to regional lineaments observed in aerial photography and STRM data, and correlated this with detailed field analysis of mineral stretching lineations (L1) in the main MCC bounding shear zone. The hanging wall sedimentary sequences of the Gwoira Conglomerate were shown to be in fault contact with metabasite footwall across D3 brittle fault zones. The metamorphic relationship across these fault zones is one of juxtaposition of greenschist facies mylonite rocks and unmetamorphosed sedimentary rocks. The mylonite shear zone is extensional with top down to the NNE normal sense-of-shear. Kinematic vorticity analyses show that the mylonite fabrics evolved in a pure shear dominated flow regime. The age of cross cutting granite and monzonite intrusions indicate that the mylonitic fabrics developed early in the evolution of the region and older than 3.3 Ma. Ductile shear zone fabrics evolved into brittle fault zone fabrics with exhumation. Metamorphic mineral assemblages of the ductile mylonite rocks record greenschist facies conditions. Pumpellyite-actinolite facies assemblages in the core of domes indicate peak metamorphic pressures of 6-9.5 kbar, indicating exhumation of the domes from 20-30 km depth. The broad field observations and detailed laboratory analyses of this study have been synthesised into a tectonic model for the evolution of the Suckling-Dayman Massif.

7.3 Directions for Further Research

Future studies of the Sucking-Dayman Massif would benefit from:

1) Exploration of the relative contributions of isostacy and buoyancy contrasts in the development of the domed landforms utilising modern geodynamical computer modelling;
2) Gravity surveys across the domed landforms to explore for low density crust at depth that may control buoyancy contrasts;
3) A search for brittle structures that controlled the final exhumation of the metabasite domes;

4) Investigating for layered shear zones such as those described by Wawrzenitz and Krohe (1998), Bestman *et al*. (2000), and Bailey and Eyster (2003) that contain layers of protomylonite, mylonite and ultramylonite in MCC;
5) Further kinematic vorticity analyses to explore for an evolution from pure shear dominated to simple shear dominated flow as documented by Bailey and Eyster (2003);
6) Examine the 'glaucophane'- and lawsonite-bearing samples of Davies (1980) to better determine the peak metamorphic pressure experienced by the subducted slab;
7) More extensive examination of the foraminifera microfossil assemblages in the Gwoira Conglomerate to determine the age of deposition; and
8) Geochronology of the felsic igneous rocks and structural fabrics to determine the absolute timing of deformation and magmatism.

References

- Baily C. M. and Eyster E. L., 2003. General Shear Deformation in Pinaleño Mountains Metamorphic Core Complex, Arizona. *Journal of Structural Geology*, vol. 25, p. 1883-1892.
- Baldwin S. L. and Ireland T. R., 2005. A Tale of Two Eras: Pliocene-Pleistocene Unroofing of Cenosoic and Late Archean Zircons from Active Metamorphic Core Complexes, Salomon Sea, Papua New Guinea. *Geology,* vol. 23, n. 11, p. 1023-1026.
- Baldwin S. L., Lister G. S., Hill E. J., Foster D. A. and McDougall I., 1993. Thermochronologic Constraints on the Tectonic Evolution of the Active Metamorphic Core Complexes, D'Entrecasteaux Islands, Papua New Guinea. *Tectonics*, vol. 12, n. 3, p. 611-628.
- Beiersdorfer R. E. and Day H. W., 1995. Mineral Paragenesis of Pumpellyite in Low-Grade Mafic Rocks. *Geological Society of America Special Paper*, 296.
- Bestmann M., Kunze K. and Matthews A., 2000. Evolution of Calcite Marble shear Zone Complex on Thassos Island, Greece: Microstructural and Textural Fabrics and their Kinematic Significance. *Journal of Structural Geology*, vol. 22, p. 1789-1807.
- Blackman D. K., Cann J. R., Janssen B. and Smith D. K., 1998. Origin of Extensional Core Complexes: Evidence from the Mid-Atlantic Ridge at Atlantis Fracture Zone. *Journal of Geophysical Research*, vol. 103, n. B9, p. 21,315-21,333.
- Bobyarchick, A.R., 1986. The Eigenvalues of Steady Flow in

  Mohr Space. *Tectonophysics*, 122, p.35-51.
- Brown E. H., 1977. The Crossite Content of Ca-Amphibole as a Guide to Pressure of Metamorphism. *Journal of Petrology*, vol. 18, n. 1, p. 53-72.
- Coombs D. S., Nakamura Y. and Vuagnat M., 1976. Pumpellyite-Actinolite Facies Schist of the Taveyenne Formation near Loeche, Valais, Switzerland. *Journal of Petrology*, vol. 17, n. 4, p. 440-471.
- Coussot, P. and Meunier, M., 1996. Recognition, Classification and Mechanical Description of Debris Flow. *Earth-Science Review*, 40, 209-227.
- Davies H. L. 1980. Folded Thrust Fault and Associated Metamorphics in the Suckling-Dayman Massif, Papua New Guinea. *American Journal of Science*, vol. 280-A, p. 171-191.
- Davies H. L. and Jaques A. L. 1984. Emplecement of Ophiolite in Papua New Guinea. Special *Publication of Geological Society of London*, vol. 13, p. 341-350.
- Davies H. L. and Smith I. E. 1971. Geology of Eastern Papua. *Geological Society of America Bulletin*, vol. 82, p. 3299-3312.
- Davies H. L. and Smith I. E. 1974. 1:250000 Geological Series-Explanatory Notes. Tufi-Cape Nelson, Papua New Guinea, sheet SC/55-8, 4 International Series. *Australian Government Publishing Service*, Canberra.

- Davies H. L. and Warren R. G. 1988. Origin of Eclogite-Bearing, Domed, Layered Metamorphic Complexes ("Core Complexes") in the D'Entrecasteaux Islands, Papua New Guinea. *Tectonics*, vol. 7, n. 1, p. 1-21.
- Dinter D. A. and Royden L., 1993. Late Cenozoic Extension in the Northeastern Greece: Strymon Valley Detachment System and Rhodope Metamorphic Core Complex. *Geology*, vol. 21, p. 45-48.
- Fisher, R. V., 1971. Features of Coarse-Grained, High-Concentration Fluids and Their Deposits. *Journal of Sedimentary Petrology*, vol., 41, n. 4, p. 916-927.
- Fossen H. and Tikoff B., 1993. The Deformation Matrix for Simultaneous Simple Shearing, Pure Shearing and Volume Change, and its Application to Transpression-Transtension Tectonics. *Journal of Structural Geology,* vol. 15, n. 3-5, p. 413-422.
- Gifkins C.C., Allen R.L. and McPhie J., 2005. Apparent welding textures in altered pumice-rich rocks, *J. Volcanol. Geotherm. Res*. vol. 142, p. 29–47.
- Hey M. H., 1954. A New Review of Chlorite: *Mineralogical Magazine*, vol. 30, p. 277-292.
- Hill E. J. 1994. Geometry and Kinematics of the Shear Zones Formed During Continental Extension in the Eastern Papua New Guinea. *Journal of Structural Geology*, vol. 16, n. 8, p. 1093-1105.
- Hill E. J. and Baldwin S. L. 1993. Exhumation of High-Pressure Metamorphic Rocks During Crustal Extension in the D'Entrecasteaux Region, Papua New Guinea. *Journal of Metamorphic Geology*, vol. 11, p. 261-277.
- Jun G., Guoqi H., Maosong L., Xuchang X., Yaoqing T., Jun W. and Min Z., 1995. The Mineralogy, Petrology, Metamorphic PTDt Trajectory and Exhumation Mechanism of Blueschist, South Tianshan, Northwestern China. *Tectonophysics*, vol. 250, p. 151-168.
- Leake, B.E., Woolley, A.R., Arps, C.E.S., Birch, W.D., Gilbert, M.C., Grice, J.D., Hawthorne, F.C., Kato, A., Kisch, H.J., Krivovchev, V.G., Linthout, K., Laird, J., Mandarino, J.A., Maresch, W.V., Nickel, E.H., Rock, N.M.S., Schumacher, J.C., Smith, D.C., Stephenson, N.C.N., Ungaretti, L., Whittaker, E.J.W. & Youzhi, G., 1997. Nomenclature of amphiboles: report of the subcommittee on amphiboles of the International Mineralogical Association, Commission on New Minerals and Mineral Names. *Canadian Mineralogist*, vol. 35, p. 219–246.
- Leake, B.E., Woolley, A.R., Birch, W.D., Burke, E.A.J., Ferraris, G., Grice, J.D., Hawthorne, F.C., Kisch, H.J., Krivovchev, V.G., Schumacher, J.C., Stephenson, N.C.N. & Whittaker, E.J.W., 2004. Nomenclature of amphiboles: additions and revisions to the International Mineralogical Association's amphibole nomenclature. *Mineralogical Magazine*, vol. 68 n. 1, p. 209-215.
- Lister G. S. and Williams P. E., 1983. The Partitioning of Deformation in Flowing rock Masses. *Tectonophysics*, vol. 92, p. 1-33.
- Little T. A., Baldwin S. L., Fitzgerald P. G. and Monteleone B., 2007. Continental Rifting and Metamorphyc Core Complex Formation Ahead of the Woodlark Spreading Ridge, D'Entrecasteaux Island, Papua New Guinea. *Tectonics*, vol. 26, TC1002, doi: 10.1029/2005TC001911.
- Lowe, D.R., 1976. Subaqueous Liquified and Fluidized Sediment Flow and Their Deposit. *Sedimentology*, 23(3): 285-308.

- Mann P. and Taylor F. W., 2002. Emergent Late Quaternary Coral Reefs of Eastern Papua New Guinea Constrain the Regional Pattern of Oceanic Ridge Propagation. Eos Transactions AGU, 83 (47), Fall Meeting Supplement, Abstract T52C-1206.
- Martinez, F., Goodliffe A.M. and Taylor B., 2001. Metamorphic Core Complex Formation by Density Inversion and Lower-crust Extrusion. *Nature*, vol. 411, 21 June 2001.
- Means W. D., Hobbs B. E., Lister G. S. and Williams P. F., 1980. Vorticity and non-coaxiality in Progressive Deformations. *Journal of Structural Geology*, vol. 2, p. 371-378.
- Middleton, G.V. & Hampton, M.A., 1976. Subaqueous Sediment Transport and Deposition by Sediment Gravity Flow. In: D.J. Stanley and D.J.P. Swift (Editors), *Marine Sediment Transport and Environment Management*, vol. 11. Wiley, New York, p. 197-218.
- Morad S. and Aldahan A.A., 1982. Authigenesis of Titanium Minerals in Two Proterozoic Sedimentary Rocks from Southern and Central Sweden. *Journal of Sedimentary Research*, vol. 52, n. 4, p. 1295-1305.
- Neumann T., Ostermaier M., Kramar U. and Simon R., 2006. Formation of Framboidal Pyrite in Estuarine Sediments of the Acterwasser Lagoon, SW Baltic Sea, and Implication on Trace Metal Mobility. *Geophysical Research*, vol. 8, 01163, 2006.
- Okay A. I. and Satir M., 2000. Coeval Plutonism and Metamorphism in the Latest Oligocene Metamorphic Core Complex in Northwest Turkey. *Geological Magazine*, vol. 137, n. 5, p. 495-516.
- Ollier C. D. and Pain C. F., 1981. Active Gneiss Domes in Papua new Guinea, New Tectonic Landforms. *Zeitschrift Für Geomorphologie* N. F., vol. 25, n. 2, p. 133-145.
- Passchier C. W., 1986. Flow in Natural Shear Zones - the Consequences of Spinning Flow Regimes. *Earth and Planetary Science Letters*, vol. 77, issue 1, p. 70-80.
- Simpson C. and De Paord G., 1993. Strain and Kinematic Analysis in General Shear Zones. *Journal of Structural Geology,* vol. 15, n.1, p. 1-20.
- Sturm R., 2002. PX-NOM – an Interactive Spreadsheet Program for the Computation of Pyroxene Analyses Derived from the Electron Microprobe. *Computers and Geosciences*, vol. 28, p. 473-483.
- Taylor B., Goodliffe A.M. and Martinez, F., 1999. How Continents Break up: Insights from Papua New Guinea. *Journal of Geophysical Research*, vol. 104, n. B4, p. 7497-7512.
- Wawrzenitz N. and Krohe A., 1998. *Tectonophysics*, vol. 285, p. 301-332.
- Wells M. L. and Allmendinger R. W., 1990. An Early History of Pure Shear in the Upper Plate of the Raft River Metamorphic Core Complex: Black Pine Mountains, Southern Idaho. *Journal of Structural Geology*, vol. 12, n. 7, p. 851-867.
- Whitney D. L. and Dilek Y., 1997. Core Complex Development in Central Anatolia, Turkey. *Geology*, vol. 25, n. 11, p. 1023-1026.

Appendices

Appendix A: Aerial Photographs and SRTM Structural Measurements

STRUCTURAL LINEAMENTS										
Aerial Photograph										SRTM
Suckling		Dayman							Biman-Dipslope	Dayman
44.3	193.9	143.9	93.5	97.8	1.7	326.6	195.9	16.2	2.0	133.0
42.6	200.9	142.8	21.5	30.5	4.7	182.5	176.2	17.8	4.0	124.0
40.2	184.6	171.5	12.7	32.4	4.6	201.4	188.6	16.9	2.2	122.0
43.4	180.0	148.5	29.7	30.0	1.5	190.8	195.0	18.9	5.4	70.0
40.9	180.0	196.0	72.2	26.4	1.9	212.7	190.8	10.5	14.1	62.0
41.0	91.5	185.1	105.0	12.9	0.0	216.4	200.3	4.1	27.5	35.0
38.8	96.7	166.0	70.4	48.9	0.0	224.5	201.9	353.2	13.1	40.0
46.5	88.0	142.2	75.8	101.9	0.0	191.7	199.7	320.0	14.7	46.0
49.4	93.7	166.3	68.1	103.6	7.4	178.6	198.6		11.2	24.0
38.9	109.0	135.2	93.1	20.6	22.9	190.8	203.2		8.7	20.0
35.3	222.2	182.1	18.4	25.4	27.2	180.0	195.2		3.8	34.0
41.0	235.6	166.4	81.7	32.6	5.7	183.4	192.9		8.6	29.0
40.2	222.2	148.2	23.7	21.0	12.2	294.8	16.9		10.7	39.0
38.5	226.4	143.4	21.7	98.2	4.4	280.6	11.2		5.3	131.0
37.4	231.9	131.2	83.9	19.4	15.8	281.2	16.2		0.0	141.0
47.7	233.4	134.6	76.0	12.7	92.4	323.2	24.3		17.6	132.0
38.3	218.3	167.4	6.8	12.7	16.9	332.1	25.8		1.0	125.0
38.3	216.4	165.0	4.0	5.4	19.2	281.5	23.6		5.1	124.0
43.3	206.5	147.7	14.0	356.5	22.1	288.6	12.6		2.6	2.0
47.8	204.6	139.1	10.0	130.2	355.2	287.3	14.5		351.3	2.0
31.2	210.5	130.2	12.5	104.3	0.0	309.9	17.8		353.3	0.0
42.7	199.7	134.8	11.2	27.3	8.0	277.6	20.9		3.6	16.0
36.3	215.1	149.1	11.3	38.3	6.1	294.2	22.2		354.0	15.0
34.9	206.2	167.3	26.8	56.9	4.7	312.0	25.0		4.0	14.0
225.1	212.5	125.4	14.8	126.4	4.0	307.8	27.7		2.7	14.0
229.0	203.9	126.2	15.6	113.8	6.5	300.9	31.3		2.3	12.0
224.9	211.5	119.3	20.1	39.3	12.7	5.1	25.2		45.4	10.0
221.3	217.0	115.0	106.6	36.4	9.6	29.0	20.5			11.0
215.2	215.1	118.3	101.5	46.2	102.5	218.9	14.6			9.0
216.1	173.4	129.3	105.7	42.4	7.2	214.6	19.4			22.0
206.7	176.0	107.3	105.9	36.3	21.6	217.9	37.2			17.0
211.7	176.3	125.0	97.5	37.9	19.3	217.7	46.3			13.0
210.1	195.5	127.2	101.6	59.8	16.6	231.1	27.3			1.0
214.4	188.6	120.5	50.9	10.6	319.1	217.4	9.0			358.0
199.1	187.6	125.2	104.3	8.6	315.8	222.8	21.4			357.0
207.8	158.9	105.8	20.6	5.5	322.8	221.9	344.6			0.0
224.8	150.2	103.6	90.1	4.4	301.3	219.6	34.2			355.0
229.8	164.1	40.4	23.2	0.0	297.9	335.2	26.3			357.0
231.1		34.5	21.2	9.4	305.2	332.8	22.9			356.0
196.3		93.2	29.8	3.6	303.2	219.1	30.8			358.0
212.5		93.8	36.9	3.6	329.2	203.1	17.1			
219.1		109.9	38.9	5.6	331.2	200.6	20.9			
216.6		106.8	125.5	21.5	315.0	213.1	22.4			
223.3		101.4	26.6	0.0	302.4	205.5	23.3			
189.6		26.0	107.3	15.5	304.0	218.7	25.6			
164.0		106.0	94.7	0.0	305.5	213.1	21.8			
199.3		106.8	54.3	18.8	314.2	215.2	11.1			
190.9		104.5	41.3	11.0	287.5	210.5	11.2			
		90.3	99.2	14.9	316.5	196.2	19.4			
			98.9	8.0	310.8	203.1	17.7			

Appendix B: Sample Locations, Lithologies and Catalogue Numbers

Sample	MU Number	Location	Lithology	Oriented Sample (X)	Polished	Cover-slip	Easting m (AGD66)	Northing m (AGD66)	Error (m±)
0601A	61807	Dare Cr.	Breccia		UNSW		076 9932	891 9166	5
0601B	61808	Dare Cr.	Palaeo		UNSW				
0601C	61809	Dare Cr.	Palaeo						
0601D	61810	Dare Cr.	Palaeo		UNSW				
0602A	61811	Pumani/Sisipoa R.	Sandstone		UNSW		N/A	N/A	N/A
0602B	61812	Pumani/Sisipoa R.	Breccia		UNSW				
0602C	61813	Pumani/Sisipoa R.	Clast from Breccia		UNSW				
0603	61814	Pumani/Sisipoa R.	Fault Breccia	X	UNSW		076 8367	892 0964	17
0604	61815	Pumani/Sisipoa R.	Basalt (shear z)	X		UNSW	076 7926	892 1346	17
0605	61816	Biyawap Cr.	Basalt (shear z)	X		UNSW	076 7635	892 1544	10
0606	61817	Dare Cr.	Sandstone		UNSW		076 9916	891 9306	N/A
0607	61818	Dare Cr.	Breccia		UNSW		076 9872	891 9414	15
0608	61819	Dare Cr.	Breccia		UNSW		076 9755	891 9324	20
0608A	61820	Dare Cr.	Palaeo						
0609	61821	Dare Cr.	Breccia		UNSW		076 9725	891 9264	24
0610	61822	Dare Cr.	Sandstone		UNSW		076 9595	891 9298	
0611A	61823	Dare Cr.	Breccia				076 9433	891 9248	N/A
0611B	61824	Dare Cr.	Clast from Breccia						
0612A	61825	Dare Cr.	Breccia		UNSW		076 9253	891 9266	N/A
0612B	61826	Dare Cr.	Breccia		UNSW				
0613	61827	Dare Cr.	Breccia				076 9131	891 9122	8
0614	61828	Dare Cr.	Breccia		UNSW		076 9109	891 9078	9
0615	61829	Dare Cr.	Sandst to Breccia		UNSW		076 9109	891 9078	9
0616	61830	Dare Cr.	Breccia		UNSW		076 9077	891 8982	6
0617A	61831	Dare Cr.	Concretion		UNSW		076 9003	891 8856	17
0617B	61832	Dare Cr.	Shell in mudstone						
0617C	61833	Dare Cr.	Cleavage ?		UNSW				
0618A	61834	Urawa Cr.	Sandstone		UNSW		077 1624	891 8086	N/A
0618B	61835	Urawa Cr.	Sandstone						
0618C	61836	Urawa Cr.	Sandstone						
0619	61837	Kwekweme Cr.	Sandstone		UNSW		N/A	N/A	N/A
0620	61838	Kwekweme Cr.	Sandstone		UNSW		077 0733	891 8680	N/A
0621	61839	Nowandowan R.	Heavy Mineral				N/A	N/A	N/A
0622	61840	Dare Cr.	Heavy Mineral				N/A	N/A	N/A
0623	61841	Pumani R.	Heavy Mineral				N/A	N/A	N/A
0624A	61842	Dare Cr.	Float		UNSW		077 0742	892 0092	N/A
0624B	61843	Dare Cr.	Float		UNSW				
0624C	61844	Dare Cr.	Float		UNSW				
0624I	61845	Dare Cr.	Float			MU			
0625	61846	Pumani R.	Heavy Mineral				N/A	N/A	N/A
0626	61847	Nowandowan R.	Float				N/A	N/A	N/A
0627	61848	Aro Cr.	Fault Zone	X		UNSW	077 0739	892 0090	15
0628	61849	Aro Cr.	Fault Zone		UNSW		077 6885	892 3096	12
0628A	61850	Aro Cr.	Fault Zone	X	UNSW				
0629	61851	Aro Cr.	Shear Zone	X		UNSW	076 6944	892 2794	10
0630	61852	Yatap Cr.	Shear Zone	X		UNSW	076 7319	892 2412	N/A

Sample	MU Number	Location	Lithology	Oriented Sample (X)	Polished	Cover-slip	Easting m (AGD66)	Northing m (AGD66)	Error (m±)
0631A	61853	Enowibidi Cr.	Sandstone		UNSW		N/A	N/A	N/A
0631B	61854	Enowibidi Cr.	Sandstone		UNSW		N/A	N/A	N/A
0660A	61855	Biniguni R.	Metabasite	X	UNSW		074 8979	892 9534	11
0660B	61856	Biniguni R.	Metabasite						
0661A	61857	Biniguni R.	Dyke						
0661B	61858	Biniguni R.	Dyke						
0661C	61859	Biniguni R.	Dyke		UNSW				
0661D	61860	Biniguni R.	Metabasite	X		UNSW			
0662A	61861	Mai'iu R.	Granite				074 9742	893 0630	9
0662B	61862	Mai'iu R.	Float						
0662C	61863	Mai'iu R.	Float						
0662D	61864	Mai'iu R.	Granite						
0663	61865	Mai'iu R.	Heavy Mineral						
0664	61866	Biniguni R.	Shear Zone	X	UNSW		074 8979	892 9534	N/A
0665	61867	Biniguni R.	Dyke						
0666	61868	Gwariu R.	Heavy Mineral						
0667	61869	Gwariu R.	Float				075 1533	892 9082	N/A
0668A	61870	Gwariu R.	Metabasite		UNSW		075 1781	892 8992	N/A
0668B	61871	Gwariu R.	Sill						
0668C	61872	Gwariu R.	Metabasite	X		UNSW			
0669	61873	Yuga Cr.	Metabasite	X		MU	075 1182	892 9122	20
0670	61874	Koraton Cr.	Metabasite	X		UNSW	075 0841	892 9162	20
0671A	61875	Gwariu R.	Float		MU		075 1533	892 9082	N/A
0671B	61876	Gwariu R.	Float		MU				
0671C	61877	Gwariu R.	Float		MU				
0671D	61878	Gwariu R.	Float		MU				
0672	61879	Bebegi Cr.	Metabasite(Green	X		MU	074 9447	892 9390	21
0673	61880	Yange Cr.	Fault Zone		UNSW		074 9443	892 9392	N/A
0674	61881	Wange Cr.	Metabasite(Green	X		UNSW	074 9878	892 9384	N/A
0675	61882	Goraedu Cr.	Metabasite(Green	X	UNSW		074 9962	892 9364	N/A
0676	61883	Yutmae Cr.	Metabasite(Green	X		UNSW	075 0013	892 9374	N/A
0677A	61884	Ampae Cr.	Metabasite(Gr/Bl)		UNSW		074 6654	892 9890	N/A
0677B	61885	Ampae Cr.	Metabasite(Gr/Bl)	X		MU			
0677C	61886	Ampae Cr.	Metabasite(Gr/Bl)	X		MU			
0677D	61887	Ampae Cr.	Metabasite(Gr/Bl)	X		MU			
0677E	61888	Ampae Cr.	Metabasite(Gr/Bl)	X		UNSW			
0677F	61889	Ampae Cr.	Metabasite(Gr/Bl)						
0677G	61890	Ampae Cr.	Metabasite(Gr/Bl)	X		UNSW			
0677H	61891	Ampae Cr.	Metabasite(Gr/Bl)	X		UNSW			
0677I	61892	Ampae Cr.	Metabasite(Gr/Bl)	X		UNSW			
0678	61893	Mai'iu R.	Heavy Mineral				N/A	N/A	N/A
0679	61894	Waremu Cr.	Metabasite(Gr/Bl)				074 7208	892 9838	N/A

Sample	Easting m (AGD66)	Northing m (AGD66)
0601A	769932	8919166
0603	768367	8920964
0604	767926	8921346
0605	767635	8921544
0606	769916	8919306
0607	769872	8919414
0608	769755	8919324
0609	769725	8919264
0610	769595	8919298
0611A	769433	8919248
0612A	769253	8919266
0613	769131	8919122
0614	769109	8919078
0615	769109	8919078
0616	769077	8918982
0617A	769003	8918856
0618A	771624	8918086
0620	770733	8918680
0624A	770742	8920092
0627	766885	8923096
0628	766914	8923006
0629	766944	8922794
0630	767319	8922412
0660A	748979	8929534
0662A	749742	8930630
0664	748979	8929534
0667	751533	8929082
0668A	751781	8928992
0669	751182	8929122
0670	750841	8929162
0671A	751533	8929082
0672	749447	8929390
0673	749443	8929392
0674	749878	8929384
0675	749962	8929364
0676	750013	8929374
0677A	746654	8929890
0679	747208	8929838

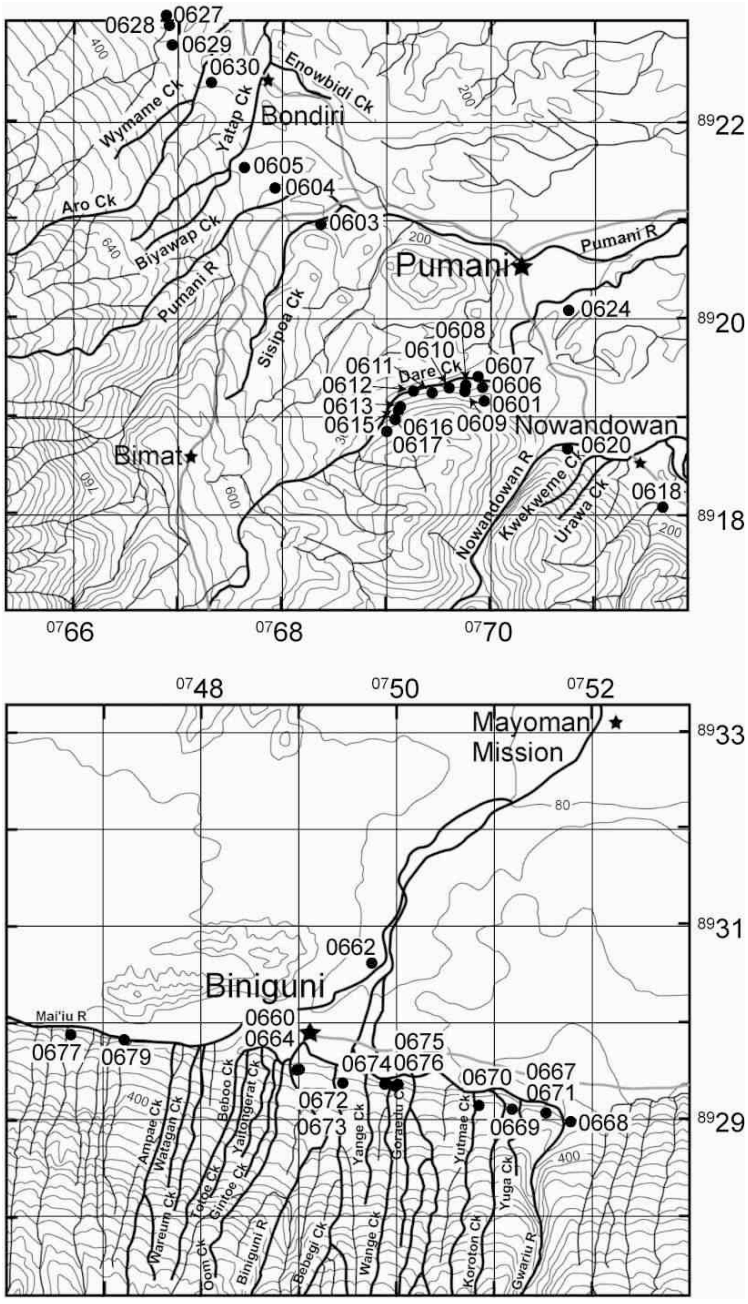

Appendix C: Electron Microprobe (EMP) Data

Comment	0602A 1.1	0602A 1.2	0602A 1.3	0602A 1.4	0602A 6.2	0602A 5.8	0602A 4.6	0602A 4.8	0602A 6.5	0602A 6.7	0602A 6.9	0602A 6.10	0602A 6.8	0602A 2.1	0602A 5.7	0602A 2.2	0602A 3.4	0602A 4.1	0602A 4.2	0602A 4.3	0602A 5.9
Mineral	chl	chl	chl	chl	pmp	pmp	pmp	pmp	pmp	pmp	pmp	pmp	pmp	pmp	pmp	pmp	prh	prh	prh	prh	prh
SiO_2	35.00	35.75	34.90	34.15	36.76	35.97	42.85	37.61	35.54	34.45	36.93	36.65	37.00	42.08	53.92	35.16	42.44	43.54	43.57	42.91	41.17
TiO_2	0.00	0.00	0.01	0.02	0.02	0.01	0.02	0.01	0.23	9.26	0.00	0.02	0.00	0.05	0.00	0.03	0.08	0.05	0.03	0.01	0.02
Al_2O_3	12.56	12.41	12.41	13.17	22.88	20.97	27.51	27.88	20.61	16.66	22.81	22.57	22.52	17.29	15.51	18.69	20.32	21.66	22.43	23.81	23.90
Cr_2O_3	0.00	0.00	0.02	0.02	0.02	0.05	0.04	0.01	0.01	0.02	0.00	0.00	0.03	0.00	0.00	0.00	0.00	0.00	0.03	0.00	0.00
Fe_2O_3	0.00	0.00	0.00	0.00	1.39	4.34	0.00	4.23	0.00	0.00	0.00	1.70	0.00	0.00	0.00	0.00	5.80	2.84	2.06	0.67	0.00
FeO	11.80	11.84	12.05	14.00	7.00	8.50	1.35	0.00	9.60	7.66	7.94	7.00	7.98	13.05	7.85	19.99	0.00	0.00	0.00	0.40	1.65
MnO	0.08	0.13	0.13	0.13	0.10	0.18	0.01	0.13	0.23	0.14	0.08	0.06	0.06	0.13	0.13	0.25	0.06	0.01	0.00	0.01	0.07
MgO	25.77	26.10	26.39	24.76	1.52	0.24	0.08	0.00	3.48	3.07	1.62	1.45	1.59	0.39	0.66	1.50	0.00	0.00	0.00	0.50	0.07
CaO	0.27	0.34	0.25	0.30	22.60	22.34	19.99	22.76	21.07	22.05	22.37	22.56	22.63	19.82	16.26	15.63	26.62	26.71	26.75	25.47	25.69
Na_2O	0.08	0.06	0.06	0.02	0.06	0.05	1.72	0.04	0.05	0.11	0.04	0.02	0.05	0.04	0.01	0.03	0.04	0.05	0.04	0.02	0.13
K_2O	0.04	0.01	0.02	0.02	0.01	0.01	0.01	0.02	0.01	0.01	0.00	0.01	0.00	0.01	0.02	0.02	0.01	0.00	0.01	0.00	0.02
Total	85.61	86.64	86.24	86.60	92.37	92.65	93.60	92.67	90.84	93.42	91.80	92.04	91.88	92.85	94.35	91.31	95.38	94.86	94.92	93.79	92.73
num ox	28.00	28.00	28.00	28.00	12.24	12.24	12.24	12.24	12.24	12.24	12.24	12.24	12.24	12.24	12.24	12.24	22.00	22.00	22.00	22.00	22.00
Si	6.95	7.01	6.90	6.80	3.04	3.02	3.30	2.99	3.02	2.87	3.07	3.04	3.08	3.49	4.12	3.09	5.98	6.09	6.07	6.01	5.89
Ti	0.00	0.00	0.00	0.00	0.00	0.00	0.00	0.00	0.01	0.58	0.00	0.00	0.00	0.00	0.00	0.00	0.01	0.01	0.00	0.00	0.00
Al	2.94	2.87	2.89	3.09	2.23	2.08	2.50	2.61	2.07	1.63	2.23	2.21	2.21	1.69	1.40	1.94	3.38	3.57	3.68	3.93	4.03
Cr	0.00	0.00	0.00	0.00	0.00	0.00	0.00	0.00	0.00	0.00	0.00	0.00	0.00	0.00	0.00	0.00	0.00	0.00	0.00	0.00	0.00
Fe^{3+}	0.00	0.00	0.00	0.00	0.09	0.27	0.00	0.25	0.00	0.00	0.00	0.11	0.00	0.00	0.00	0.00	0.62	0.30	0.22	0.07	0.00
Fe^{2+}	1.96	1.94	1.99	2.33	0.48	0.60	0.09	0.00	0.68	0.53	0.55	0.49	0.55	0.90	0.50	1.47	0.00	0.00	0.00	0.05	0.20
Mn	0.01	0.02	0.02	0.02	0.01	0.01	0.00	0.01	0.02	0.01	0.01	0.00	0.00	0.01	0.01	0.02	0.01	0.00	0.00	0.00	0.01
Mg	7.63	7.63	7.77	7.34	0.19	0.03	0.01	0.00	0.44	0.38	0.20	0.18	0.20	0.05	0.07	0.20	0.00	0.00	0.00	0.10	0.02
Ca	0.06	0.07	0.05	0.06	2.00	2.01	1.65	1.94	1.92	1.97	1.99	2.01	2.02	1.76	1.33	1.47	4.02	4.00	3.99	3.82	3.94
Na	0.03	0.02	0.02	0.01	0.01	0.01	0.26	0.01	0.01	0.02	0.01	0.00	0.01	0.01	0.00	0.00	0.01	0.01	0.01	0.01	0.04
K	0.01	0.00	0.00	0.01	0.00	0.00	0.00	0.00	0.00	0.00	0.00	0.00	0.00	0.00	0.00	0.00	0.00	0.00	0.00	0.00	0.00
Total	19.60	19.57	19.66	19.66	8.05	8.04	7.81	7.82	8.17	7.99	8.06	8.04	8.06	7.91	7.43	8.19	14.02	13.98	13.98	13.99	14.12

Comment	0602A 5.10	0602A 4.4	0602A 3.1	0602A 3.2	0602A 6.3	0602A 3.3	0602A 3.5	0602A 3.6	0602A 4.5	0602A 4.7	0602A 4.9	0602A 5.6	0602A 6.4	0602A 5.1	0602A 5.2	0602A 5.3	0602A 5.4	0602A 5.5	0602A 1.5
Mineral	prh	ilm	ep	ep	ep	cpx	cpx	cpx	ab	ab	ab	plag	ab	glass	glass	glass	glass	glass	?
SiO_2	44.35	1.03	37.64	37.59	37.60	51.17	51.09	51.85	68.76	69.45	67.87	62.49	68.19	41.69	37.85	44.31	37.87	38.91	8.77
TiO_2	0.00	48.57	0.10	0.04	0.05	0.48	0.94	0.38	0.00	0.02	0.00	0.44	0.01	1.15	0.72	0.91	0.55	0.97	12.02
Al_2O_3	23.96	0.08	21.34	21.65	23.48	3.22	3.23	2.73	20.32	20.50	20.44	23.43	20.40	15.98	18.84	9.63	18.91	19.66	0.90
Cr_2O_3	0.00	0.06	0.02	0.00	0.00	0.51	0.03	0.64	0.01	0.00	0.00	0.02	0.00	0.01	0.04	0.01	0.03	0.00	0.48
Fe_2O_3	0.14	0.00	16.17	15.73	13.13	0.00	0.00	0.00	0.00	0.00	0.00	0.00	0.00	0.00	0.00	0.00	0.00	0.00	0.00
FeO	0.00	46.37	0.00	0.00	0.00	6.35	10.60	6.06	0.04	0.01	0.02	1.93	0.27	6.98	8.18	8.79	9.13	7.20	62.76
MnO	0.01	2.62	0.22	0.13	0.06	0.17	0.25	0.14	0.00	0.00	0.00	0.06	0.00	0.16	0.13	0.31	0.13	0.15	0.04
MgO	0.00	0.05	0.00	0.00	0.00	16.35	16.43	16.74	0.00	0.00	0.00	0.93	0.02	6.78	3.68	9.30	2.99	3.59	0.00
CaO	26.58	0.82	23.30	23.35	23.60	20.91	17.39	20.96	0.87	0.53	0.93	3.30	0.44	21.35	22.61	22.92	22.59	21.96	8.03
Na_2O	0.03	0.01	0.02	0.00	0.02	0.25	0.24	0.26	11.41	11.67	11.29	7.68	11.73	0.07	0.05	0.11	0.07	0.09	0.03
K_2O	0.00	0.00	0.01	0.00	0.00	0.00	0.00	0.02	0.06	0.01	0.07	1.57	0.13	0.00	0.00	0.01	0.00	0.02	0.01
Total	95.08	99.62	98.83	98.51	97.93	99.42	100.19	99.78	101.46	102.20	100.63	101.84	101.20	94.17	92.10	96.30	92.27	92.53	93.03
num ox	22.00	3.00	25.00	25.00	25.00	6.00	6.00	6.00	8.00	8.00	8.00	8.00	8.00	13.00	13.00	13.00	13.00	13.00	0.00
Si	6.11	0.03	6.01	6.01	5.99	1.90	1.90	1.91	2.96	2.97	2.95	2.74	2.95	3.56	3.35	3.76	3.36	3.39	0.00
Ti	0.00	0.93	0.01	0.01	0.01	0.01	0.03	0.01	0.00	0.00	0.00	0.01	0.00	0.07	0.05	0.06	0.04	0.06	0.00
Al	3.89	0.00	4.02	4.08	4.41	0.14	0.14	0.12	1.03	1.03	1.05	1.21	1.04	1.61	1.97	0.96	1.98	2.02	0.00
Cr	0.00	0.00	0.00	0.00	0.00	0.01	0.00	0.02	0.00	0.00	0.00	0.00	0.00	0.00	0.00	0.00	0.00	0.00	0.00
Fe^{3+}	0.01	0.00	1.94	1.89	1.57	0.00	0.00	0.00	0.00	0.00	0.00	0.00	0.00	0.00	0.00	0.00	0.00	0.00	0.00
Fe^{2+}	0.00	0.99	0.00	0.00	0.00	0.20	0.33	0.19	0.00	0.00	0.00	0.07	0.01	0.50	0.61	0.62	0.68	0.52	0.00
Mn	0.00	0.06	0.03	0.02	0.01	0.01	0.01	0.00	0.00	0.00	0.00	0.00	0.00	0.01	0.01	0.02	0.01	0.01	0.00
Mg	0.00	0.00	0.00	0.00	0.00	0.90	0.91	0.92	0.00	0.00	0.00	0.06	0.00	0.86	0.48	1.18	0.40	0.47	0.00
Ca	3.92	0.02	3.99	4.00	4.03	0.83	0.69	0.83	0.04	0.02	0.04	0.16	0.02	1.95	2.15	2.08	2.15	2.05	0.00
Na	0.01	0.00	0.01	0.00	0.00	0.02	0.02	0.02	0.95	0.97	0.95	0.65	0.99	0.01	0.01	0.02	0.01	0.01	0.00
K	0.00	0.00	0.00	0.00	0.00	0.00	0.00	0.00	0.00	0.00	0.00	0.09	0.01	0.00	0.00	0.00	0.00	0.00	0.00
Total	13.94	2.04	16.00	16.00	16.02	4.02	4.02	4.02	5.00	5.00	5.00	5.00	5.02	8.57	8.62	8.71	8.62	8.54	0.00

Comment	0602A 1.6	0602A 1.7	0602A 2.3	0602A 6.1	0602A 6.6	0602A 5.11		0628 1.1	0628 1.2	0628 1.3	0628 1.4	0628 1.5+	0628 1.5+	0628 1.5+	0628 1.5+	0628 1.5+	0628 1.5+	0628 1.5+	0628 1.5+	0628 1.5+	
Mineral	?	?	?	?	?	Qtz		chl	chl	ep	ep	ep	ep	ep	ep	ep	ab	ab	ab	ab	
SiO_2	14.45	3.03	0.09	32.23	35.04	97.79		27.96	27.78	37.05	37.26	34.42	36.57	36.91	37.33	37.46	68.68	69.63	70.82	70.42	
TiO_2	42.35	24.41	1.71	1.17	0.57	0.00		0.07	0.03	0.07	0.04	0.84	0.07	0.11	0.04	0.15	0.02	0.02	0.05	0.03	
Al_2O_3	2.41	0.34	0.32	12.99	17.86	0.18		16.66	17.03	20.97	21.36	19.49	19.71	21.41	19.95	21.56	19.70	19.87	19.72	20.19	
Cr_2O_3	0.01	0.03	0.10	0.05	0.00	0.02		0.03	0.00	0.00	0.03	0.02	0.01	0.01	0.03	0.00	0.00	0.01	0.03	0.00	
Fe_2O_3	0.00	0.00	0.00	0.00	0.00	0.00		0.00	0.00	15.65	16.09	19.43	17.63	16.01	17.83	15.88	0.00	0.00	0.00	0.00	
FeO	25.47	64.83	0.51	22.69	16.48	0.07		29.59	29.54	0.90	0.00	0.90	0.00	0.00	0.00	0.00	0.34	0.23	0.34	0.21	
MnO	2.78	0.02	0.03	0.19	0.24	0.00		0.43	0.45	0.16	0.14	0.26	0.23	0.15	0.20	0.18	0.02	0.01	0.03	0.00	
MgO	0.40	0.00	1.51	4.95	5.11	0.00		13.69	14.12	0.00	0.00	3.49	0.00	0.00	0.22	0.00	0.03	0.01	0.07	0.00	
CaO	10.56	3.37	7.58	4.74	14.93	0.20		0.19	0.12	23.08	23.23	16.53	22.22	22.83	22.12	22.92	0.02	0.04	0.21	0.04	
Na_2O	0.03	0.01	0.18	0.03	0.06	0.00		0.01	0.01	0.01	0.00	0.02	0.01	0.00	0.00	0.01	12.03	11.86	11.60	11.81	
K_2O	0.03	0.01	0.06	0.25	0.10	0.01		0.05	0.08	0.00	0.01	0.01	0.00	0.00	0.01	0.00	0.03	0.10	0.09	0.13	
Total	98.49	96.05	12.10	79.28	90.39	98.26		88.69	89.16	97.88	98.15	95.40	96.47	97.43	97.73	98.17	100.87	101.77	102.95	102.83	
num ox	0.00	0.00	0.00	0.00	0.00	0.00		36.00	36.00	25.00	25.00	25.00	25.00	25.00	25.00	25.00	8.00	8.00	8.00	8.00	
Si	0.00	0.00	0.00	0.00	0.00	0.00		7.67	7.57	5.99	5.99	5.72	6.01	5.97	6.05	6.01	2.98	2.99	3.00	2.99	
Ti	0.00	0.00	0.00	0.00	0.00	0.00		0.01	0.01	0.01	0.00	0.10	0.01	0.01	0.01	0.02	0.00	0.00	0.00	0.00	
Al	0.00	0.00	0.00	0.00	0.00	0.00		5.38	5.47	4.00	4.05	3.82	3.82	4.08	3.81	4.08	1.01	1.01	0.99	1.01	
Cr	0.00	0.00	0.00	0.00	0.00	0.00		0.01	0.00	0.00	0.00	0.00	0.00	0.00	0.00	0.00	0.00	0.00	0.00	0.00	
Fe^{3+}	0.00	0.00	0.00	0.00	0.00	0.00		0.00	0.00	1.91	1.95	2.43	2.18	1.95	2.17	1.92	0.00	0.00	0.00	0.00	
Fe^{2+}	0.00	0.00	0.00	0.00	0.00	0.00		6.79	6.74	0.12	0.00	0.13	0.00	0.00	0.00	0.00	0.01	0.01	0.01	0.01	
Mn	0.00	0.00	0.00	0.00	0.00	0.00		0.10	0.10	0.02	0.02	0.04	0.03	0.02	0.03	0.02	0.00	0.00	0.00	0.00	
Mg	0.00	0.00	0.00	0.00	0.00	0.00		5.59	5.74	0.00	0.00	0.86	0.00	0.00	0.05	0.00	0.00	0.00	0.00	0.00	
Ca	0.00	0.00	0.00	0.00	0.00	0.00		0.06	0.04	4.00	4.00	2.94	3.91	3.96	3.84	3.94	0.00	0.00	0.01	0.00	
Na	0.00	0.00	0.00	0.00	0.00	0.00		0.01	0.00	0.00	0.00	0.01	0.00	0.00	0.00	0.00	1.01	0.99	0.95	0.97	
K	0.00	0.00	0.00	0.00	0.00	0.00		0.02	0.03	0.00	0.00	0.00	0.00	0.00	0.00	0.00	0.00	0.01	0.00	0.01	
Total	0.00	0.00	0.00	0.00	0.00	0.00		25.63	25.70	16.05	16.01	16.05	15.98	16.00	15.96	15.98	5.02	5.00	4.98	4.99	

Comment	0661C 1.2	0661C 1.12	0661C 1.14	0661C 1.15	0661C 1.16	0661C 1.25+	0661C 1.3	0661C 1.6	0661C 1.22	0661C 1.23	0661C 1.24+	0661C 1.4	0661C 1.18	0661C 1.19	0661C 1.5	0661C 1.20	0661C 1.21	0661C 1.7	0661C 1.8	0661C 1.8
Mineral	ab	ab	ab	ab	ab	ab	mu	mu	mu	mu	mu	chl	chl	chl	ep	ep	ep	hb	hb	cpx
SiO_2	69.09	70.44	69.31	69.89	70.08	68.23	45.18	53.72	54.70	55.95	52.24	33.19	31.01	30.56	37.54	37.68	37.46	38.67	39.92	49.01
TiO_2	0.00	0.00	0.01	0.02	0.00	0.01	0.89	0.07	0.01	0.06	0.04	0.02	0.01	0.01	0.76	0.08	0.10	2.06	2.80	1.17
Al_2O_3	20.19	20.21	19.82	20.21	20.21	19.46	29.95	21.94	21.43	22.32	20.48	17.40	16.89	16.37	22.67	23.98	21.81	12.77	10.59	4.17
Cr_2O_3	0.01	0.01	0.00	0.01	0.00	0.00	0.02	0.00	0.00	0.01	0.00	0.02	0.01	0.03	0.00	0.00	0.00	0.00	0.01	0.02
Fe_2O_3	0.00	0.00	0.00	0.00	0.00	0.00	0.00	0.00	0.00	0.00	0.00	0.00	0.00	0.00	0.00	0.00	0.00	0.00	0.00	0.00
FeO	0.02	0.13	0.07	0.04	0.02	0.40	6.38	4.35	3.05	3.38	4.37	15.52	16.56	16.56	12.29	10.82	13.59	23.20	23.17	10.65
MnO	0.01	0.02	0.01	0.00	0.00	0.02	0.03	0.02	0.06	0.07	0.06	0.21	0.25	0.24	0.07	0.08	0.21	0.48	0.32	0.26
MgO	0.02	0.00	0.01	0.01	0.01	0.75	1.26	5.40	5.59	5.65	7.03	21.38	22.98	22.80	0.00	0.00	0.00	5.43	6.19	11.56
CaO	0.22	0.02	0.04	0.12	0.21	0.63	0.02	0.09	0.08	0.07	0.17	0.06	0.14	0.21	22.94	22.67	21.81	11.32	11.14	22.06
Na_2O	11.65	11.82	12.04	11.57	11.57	11.16	0.61	0.07	0.05	0.04	0.03	0.01	0.02	0.01	0.01	0.03	0.01	1.79	1.64	0.59
K_2O	0.11	0.05	0.04	0.18	0.18	0.51	10.07	10.46	10.64	10.64	10.18	1.26	0.16	0.02	0.02	0.02	0.05	2.21	2.09	0.01
Total	101.34	102.71	101.35	102.05	102.27	101.17	94.42	96.13	95.64	98.19	94.60	89.07	88.02	86.81	96.30	95.35	95.05	97.93	97.89	99.51
num ox	8.00	8.00	8.00	8.00	8.00	8.00	12.00	12.00	12.00	12.00	12.00	36.00	36.00	36.00	13.00	13.00	13.00	24.00	24.00	24.00
Si	2.98	2.99	2.99	2.99	2.99	2.96	3.41	3.91	3.97	3.96	3.88	8.35	7.95	7.95	3.23	3.24	3.28	6.35	6.54	7.46
Ti	0.00	0.00	0.00	0.00	0.00	0.00	0.05	0.00	0.00	0.00	0.00	0.00	0.00	0.00	0.05	0.00	0.01	0.25	0.34	0.13
Al	1.03	1.01	1.01	1.02	1.02	1.00	2.66	1.88	1.84	1.86	1.79	5.16	5.10	5.02	2.30	2.43	2.25	2.47	2.05	0.75
Cr	0.00	0.00	0.00	0.00	0.00	0.00	0.00	0.00	0.00	0.00	0.00	0.00	0.00	0.01	0.00	0.00	0.00	0.00	0.00	0.00
Fe^{3+}	0.00	0.00	0.00	0.00	0.00	0.00	0.00	0.00	0.00	0.00	0.00	0.00	0.00	0.00	0.00	0.00	0.00	0.00	0.00	0.00
Fe^{2+}	0.00	0.00	0.00	0.00	0.00	0.01	0.40	0.26	0.19	0.20	0.27	3.27	3.55	3.60	0.88	0.78	0.99	3.19	3.17	1.36
Mn	0.00	0.00	0.00	0.00	0.00	0.00	0.00	0.00	0.00	0.00	0.00	0.04	0.05	0.05	0.01	0.01	0.02	0.07	0.04	0.03
Mg	0.00	0.00	0.00	0.00	0.00	0.05	0.14	0.59	0.61	0.60	0.78	8.02	8.78	8.84	0.00	0.00	0.00	1.33	1.51	2.62
Ca	0.01	0.00	0.00	0.01	0.01	0.03	0.00	0.01	0.01	0.01	0.01	0.02	0.04	0.06	2.11	2.09	2.04	1.99	1.96	3.60
Na	0.97	0.97	1.01	0.96	0.96	0.94	0.09	0.01	0.01	0.01	0.00	0.00	0.01	0.01	0.00	0.00	0.00	0.57	0.52	0.17
K	0.01	0.00	0.00	0.01	0.01	0.03	0.97	0.97	0.99	0.96	0.96	0.41	0.05	0.01	0.00	0.00	0.01	0.46	0.44	0.00
Total	5.00	4.99	5.01	4.99	4.98	5.02	7.74	7.64	7.60	7.59	7.71	25.27	25.53	25.54	8.58	8.55	8.60	16.68	16.57	16.12

Comment	0661C 1.10	0661C 1.1	0661C 1.17	0661C 1.24+	0661C 1.24+	0661C 1.25+	0661C 1.25+	0661C 1.25+	0661C 1.25+	0661C 1.25+	0661C 1.26+	0661C 1.26+	0661C 1.26+	0661C 1.26+	0661C 1.26+	0661C 1.26+	0661C 1.26+	0661C 3.1	0661C 3.2	0661C 1.11	0661C 1.13
Mineral	cpx	cpx	cpx	cpx	cpx	cpx	cpx	cpx	cpx	cpx	cpx	cpx	cpx	cpx	cpx	cpx	cpx	cpx	cpx	Qtz	Qtz
SiO_2	48.35	49.63	48.79	50.83	51.28	46.16	50.09	50.79	50.81	50.90	50.46	50.48	50.55	50.45	50.98	51.88	53.73	49.80	53.23	91.18	96.99
TiO_2	1.08	1.30	0.87	0.76	0.64	1.41	0.96	0.83	0.96	0.76	1.13	1.24	0.98	0.89	0.95	0.45	0.15	0.49	0.28	0.00	0.03
Al_2O_3	4.24	3.51	4.31	2.97	2.80	5.44	3.33	3.19	3.45	3.27	3.24	3.33	3.70	3.71	3.51	3.19	7.76	2.55	1.31	4.29	0.31
Cr_2O_3	0.01	0.01	0.00	0.00	0.00	0.02	0.00	0.01	0.00	0.00	0.00	0.03	0.02	0.00	0.00	0.00	0.01	0.01	0.83	0.00	0.03
Fe_2O_3	0.00	0.00	0.00	0.00	0.00	0.00	0.00	0.00	0.00	0.00	0.00	0.00	0.00	0.00	0.00	0.00	0.00	0.00	0.00	0.00	0.00
FeO	12.36	7.34	11.90	9.01	8.47	14.28	7.73	7.33	7.36	8.11	7.63	7.39	7.51	7.57	7.61	7.66	8.37	12.53	3.85	0.03	0.04
MnO	0.27	0.19	0.23	0.23	0.26	0.28	0.17	0.19	0.19	0.16	0.18	0.18	0.20	0.18	0.16	0.22	0.19	0.40	0.12	0.01	0.00
MgO	10.63	14.60	10.37	13.31	13.43	8.26	14.15	14.90	14.56	13.59	14.26	14.54	14.12	14.24	14.09	12.99	12.93	9.74	17.99	0.00	0.01
CaO	21.58	21.25	21.77	22.10	22.03	21.89	21.81	21.21	21.67	22.27	21.72	21.31	21.69	21.41	21.79	21.54	10.22	21.67	20.82	0.02	0.00
Na_2O	0.66	0.54	0.83	0.57	0.73	0.94	0.54	0.54	0.54	0.57	0.52	0.53	0.59	0.54	0.57	1.28	3.21	1.20	0.42	2.52	0.01
K_2O	0.01	0.01	0.05	0.07	0.05	0.01	0.00	0.02	0.00	0.02	0.00	0.00	0.00	0.01	0.01	0.02	0.51	0.02	0.01	0.03	0.07
Total	99.19	98.38	99.12	99.86	99.70	98.67	98.78	99.01	99.55	99.66	99.14	99.04	99.36	99.00	99.68	99.23	97.07	98.42	98.87	98.07	97.49
num ox	24.00	6.00	6.00	6.00	6.00	6.00	6.00	6.00	6.00	6.00	6.00	6.00	6.00	6.00	6.00	6.00	6.00	6.00	6.00	2.00	2.00
Si	7.44	1.88	1.87	1.91	1.92	1.81	1.89	1.90	1.89	1.90	1.89	1.89	1.89	1.89	1.90	1.94	1.99	1.93	1.96	0.95	1.00
Ti	0.13	0.04	0.03	0.02	0.02	0.04	0.03	0.02	0.03	0.02	0.03	0.03	0.03	0.03	0.03	0.01	0.00	0.01	0.01	0.00	0.00
Al	0.77	0.16	0.20	0.13	0.12	0.25	0.15	0.14	0.15	0.14	0.14	0.15	0.16	0.16	0.15	0.14	0.34	0.12	0.06	0.05	0.00
Cr	0.00	0.00	0.00	0.00	0.00	0.00	0.00	0.00	0.00	0.00	0.00	0.00	0.00	0.00	0.00	0.00	0.00	0.00	0.02	0.00	0.00
Fe^{3+}	0.00	0.00	0.00	0.00	0.00	0.00	0.00	0.00	0.00	0.00	0.00	0.00	0.00	0.00	0.00	0.00	0.00	0.00	0.00	0.00	0.00
Fe^{2+}	1.59	0.23	0.38	0.28	0.27	0.47	0.24	0.23	0.23	0.25	0.24	0.23	0.23	0.24	0.24	0.24	0.26	0.41	0.12	0.00	0.00
Mn	0.03	0.01	0.01	0.01	0.01	0.01	0.01	0.01	0.01	0.01	0.01	0.01	0.01	0.01	0.01	0.01	0.01	0.01	0.00	0.00	0.00
Mg	2.44	0.82	0.59	0.74	0.75	0.48	0.80	0.83	0.81	0.76	0.80	0.81	0.79	0.80	0.78	0.72	0.71	0.56	0.99	0.00	0.00
Ca	3.56	0.86	0.90	0.89	0.88	0.92	0.88	0.85	0.87	0.89	0.87	0.86	0.87	0.86	0.87	0.86	0.41	0.90	0.82	0.00	0.00
Na	0.20	0.04	0.06	0.04	0.05	0.07	0.04	0.04	0.04	0.04	0.04	0.04	0.04	0.04	0.04	0.09	0.23	0.09	0.03	0.05	0.00
K	0.00	0.00	0.00	0.00	0.00	0.00	0.00	0.00	0.00	0.00	0.00	0.00	0.00	0.00	0.00	0.00	0.02	0.00	0.00	0.00	0.00
Total	16.15	4.03	4.04	4.03	4.03	4.06	4.03	4.02	4.02	4.02	4.02	4.02	4.02	4.02	4.02	4.02	3.97	4.04	4.01	1.05	1.00

Comment	0605 1.1+	0605 1.1+	0605 1.1+	0605 1.1+	0605 1.6	0605 1.5	0605 1.2+	0605 1.1+	0605 1.1+	0605 1.1+	0605 1.1+	0605 1.1+	0605 1.1+	0605 1.1+	0605 1.1+	0605 1.1+	0605 1.9	0605 1.1+	0605 1.1+	0605 1.1+	0605 1.1+	0605 1.1+
Mineral	ep	ep	ep	ep	ep	ep	ep	ab	ab	ab	ab	ab	ab	ab	ab	ab	ab	ab	ab	ab	chl	chl
SiO_2	37.56	37.60	37.86	37.42	37.44	37.02	37.99	69.15	69.26	68.67	69.00	67.42	66.68	71.22	66.84	63.24	69.55	79.87	68.06	58.18	27.82	28.31
TiO_2	0.06	0.01	0.04	0.03	0.03	0.16	0.07	0.03	0.01	0.00	0.01	0.04	0.01	0.04	0.14	1.54	0.05	0.07	0.05	0.23	0.16	0.07
Al_2O_3	21.78	21.20	21.82	20.95	20.76	20.69	20.03	19.86	19.60	19.62	19.63	18.86	19.47	17.54	19.54	18.31	19.76	13.22	19.38	18.94	17.52	17.44
Cr_2O_3	0.00	0.00	0.02	0.00	0.03	0.03	0.00	0.01	0.00	0.01	0.00	0.00	0.00	0.00	0.00	0.00	0.00	0.00	0.03	0.00	0.00	0.00
Fe_2O_3	16.15	16.52	15.67	16.89	16.47	16.29	18.84	0.00	0.00	0.00	0.00	0.00	0.00	0.00	0.00	0.00	0.00	0.00	0.00	0.00	0.00	0.00
FeO	0.00	0.50	0.00	0.60	0.20	0.25	0.00	1.40	0.44	0.48	0.72	0.50	3.46	1.25	2.53	3.53	0.14	0.59	2.42	8.62	29.06	28.49
MnO	0.20	0.28	0.21	0.18	0.20	0.21	0.18	0.02	0.08	0.00	0.01	0.00	0.07	0.04	0.04	0.04	0.04	0.04	0.05	0.13	0.42	0.47
MgO	0.00	0.00	0.00	0.00	0.00	0.21	2.02	0.46	0.02	0.04	0.09	0.08	1.28	0.44	1.18	1.38	0.00	0.05	0.86	3.67	13.68	12.99
CaO	22.93	22.56	22.73	22.81	22.70	21.59	18.77	0.07	0.03	0.09	0.37	0.09	0.10	0.04	0.54	1.32	0.05	0.21	0.03	0.25	0.23	1.48
Na_2O	0.01	0.02	0.00	0.00	0.00	0.09	0.58	11.93	12.02	11.90	12.03	11.39	10.72	10.40	10.79	10.12	12.17	8.05	10.98	7.39	0.04	0.00
K_2O	0.00	0.00	0.00	0.05	0.10	0.12	0.02	0.08	0.03	0.04	0.03	0.06	0.03	0.11	0.14	0.04	0.11	0.05	0.14	1.05	0.04	0.02
Total	97.07	97.03	96.77	97.24	96.27	95.04	96.62	103.00	101.51	100.84	101.90	98.45	101.83	101.08	101.74	99.52	101.85	102.16	101.99	98.47	88.96	89.27
num ox	25.00	25.00	25.00	25.00	25.00	25.00	25.00	8.00	8.00	8.00	8.00	8.00	8.00	8.00	8.00	8.00	8.00	8.00	8.00	8.00	28.00	28.00
Si	5.99	6.02	6.04	5.99	6.04	6.04	6.06	2.96	2.99	2.98	2.97	3.00	2.91	3.07	2.91	2.85	2.99	3.33	2.95	2.72	5.89	5.97
Ti	0.01	0.00	0.00	0.00	0.00	0.02	0.01	0.00	0.00	0.00	0.00	0.00	0.00	0.00	0.00	0.05	0.00	0.00	0.00	0.01	0.02	0.01
Al	4.10	4.00	4.11	3.96	3.95	3.98	3.77	1.00	1.00	1.00	1.00	0.99	1.00	0.89	1.00	0.97	1.00	0.65	0.99	1.04	4.37	4.34
Cr	0.00	0.00	0.00	0.00	0.00	0.00	0.00	0.00	0.00	0.00	0.00	0.00	0.00	0.00	0.00	0.00	0.00	0.00	0.00	0.00	0.00	0.00
Fe^{3+}	1.94	1.99	1.88	2.04	2.00	2.00	2.26	0.00	0.00	0.00	0.00	0.00	0.00	0.00	0.00	0.00	0.00	0.00	0.00	0.00	0.00	0.00
Fe^{2+}	0.00	0.07	0.00	0.08	0.03	0.03	0.00	0.05	0.02	0.02	0.03	0.02	0.13	0.05	0.09	0.13	0.00	0.02	0.09	0.34	5.15	5.03
Mn	0.03	0.04	0.03	0.02	0.03	0.03	0.02	0.00	0.00	0.00	0.00	0.00	0.00	0.00	0.00	0.00	0.00	0.00	0.00	0.00	0.08	0.08
Mg	0.00	0.00	0.00	0.00	0.00	0.05	0.48	0.03	0.00	0.00	0.01	0.01	0.08	0.03	0.08	0.09	0.00	0.00	0.06	0.26	4.32	4.08
Ca	3.92	3.87	3.89	3.91	3.92	3.77	3.21	0.00	0.00	0.00	0.02	0.00	0.00	0.00	0.03	0.06	0.00	0.01	0.00	0.01	0.05	0.33
Na	0.00	0.01	0.00	0.00	0.00	0.03	0.18	0.99	1.01	1.00	1.01	0.98	0.91	0.87	0.91	0.88	1.01	0.65	0.92	0.67	0.02	0.00
K	0.00	0.00	0.00	0.01	0.02	0.02	0.00	0.00	0.00	0.00	0.00	0.00	0.00	0.01	0.01	0.00	0.01	0.00	0.01	0.06	0.01	0.01
Total	15.98	15.99	15.96	16.01	15.99	15.98	16.00	5.04	5.02	5.02	5.03	5.00	5.04	4.92	5.04	5.05	5.02	4.67	5.02	5.12	19.91	19.85

Comment	0605 1.1+	0605 1.1+	0605 1.3	0605 1.8	0605 1.10	0605 1.2	0605 1.2+	0605 1.2+	0605 1.2+	0605 1.2+	0605 1.2+	0605 1.2+	0605 1.2+	0605 2.1	0605 2.2	0605 2.3	0605 1.4	0605 1.6	0605 1.4	0605 1.1+	0605 1.3	0605 1.2	0605 1.12	0605 1.11	0605 2.5
Mineral	chl	chl	chl	chl	chl	gl	gl	gl	gl	gl	gl	gl	gl	gl	gl	gl	tit	tit	tit	tit	tit	mu	mu	mu	mu
SiO_2	28.30	31.25	27.57	26.80	26.76	52.90	46.62	48.09	56.60	49.02	53.64	58.82	48.59	53.93	54.24	54.12	30.45	22.61	31.00	30.72	19.59	46.92	46.75	51.94	51.27
TiO_2	0.04	0.06	0.05	0.03	0.18	0.03	0.01	0.03	0.00	0.03	0.01	0.02	0.02	0.06	0.00	0.01	36.27	53.38	34.15	33.95	57.74	0.04	0.00	0.07	0.02
Al_2O_3	16.94	17.36	16.99	17.87	17.48	4.00	6.23	5.50	2.74	4.88	2.50	2.41	5.46	3.07	2.50	2.29	1.75	1.03	3.52	3.07	2.48	21.16	19.84	21.27	21.32
Cr_2O_3	0.02	0.01	0.01	0.00	0.00	0.00	0.00	0.00	0.02	0.00	0.00	0.00	0.04	0.00	0.01	0.00	0.00	0.00	0.00	0.04	0.01	0.00	0.01	0.00	0.02
Fe_2O_3	0.00	0.00	0.00	0.00	0.00	3.99	7.22	6.52	2.81	5.54	6.08	24.25	6.14	6.66	12.38	12.97	0.00	0.00	0.00	0.00	0.00	13.82	12.87	8.13	11.00
FeO	29.35	27.66	30.83	30.38	31.53	21.35	19.55	20.85	19.00	20.20	20.50	0.00	19.45	21.80	17.30	17.00	2.68	0.83	2.90	3.83	4.32	0.00	0.00	0.00	0.00
MnO	0.46	0.42	0.46	0.43	0.48	0.17	0.28	0.24	0.22	0.20	0.17	0.23	0.24	0.17	0.19	0.14	0.02	0.00	0.00	0.06	0.06	0.16	0.13	0.05	0.11
MgO	12.97	12.45	12.04	12.90	12.24	7.51	8.96	8.24	7.54	8.69	6.70	6.05	8.75	5.33	4.84	4.80	0.19	0.00	0.43	0.86	1.21	5.53	5.78	4.04	5.03
CaO	0.20	0.15	0.20	0.10	0.14	1.82	1.97	1.83	3.38	2.51	2.48	1.89	2.36	1.08	0.54	0.35	27.26	21.46	27.11	25.59	14.86	0.22	0.09	0.11	0.18
Na_2O	0.41	0.94	0.05	0.04	0.02	5.19	4.15	4.46	3.96	4.46	5.88	4.66	3.88	6.86	7.13	7.06	0.03	0.03	0.01	0.01	0.04	0.05	0.07	0.07	0.11
K_2O	0.04	0.02	0.09	0.01	0.02	0.04	0.04	0.04	0.04	0.05	0.06	0.03	0.05	0.05	0.01	0.01	0.06	0.04	0.02	0.02	0.05	8.14	8.48	10.30	9.16
Total	88.74	90.31	88.28	88.58	88.85	96.60	94.30	95.15	96.03	95.02	97.42	95.93	94.35	98.35	97.89	97.44	98.71	99.38	99.14	98.17	100.37	94.65	92.75	95.16	97.11
						97.00	95.02	95.80	96.32	95.58	98.03	98.36	94.97	99.01	99.13	98.74									
num ox	28.00	28.00	28.00	28.00	28.00	23.00	23.00	23.00	22.05	23.00	23.00	23.00	23.00	23.00	23.00	23.00	5.00	5.00	5.00	5.00	5.00	22.00	22.00	22.00	22.00
Si	6.02	6.41	5.95	5.75	5.77	7.92	7.22	7.40	8.00	7.51	8.00	8.20	7.47	8.00	7.99	8.00	1.01	0.75	1.02	1.02	0.64	6.42	6.53	6.98	6.78
Ti	0.01	0.01	0.01	0.01	0.03	0.00	0.00	0.00	0.00	0.00	0.00	0.00	0.00	0.01	0.00	0.00	0.91	1.33	0.85	0.85	1.43	0.00	0.00	0.01	0.00
Al	4.25	4.20	4.32	4.52	4.44	0.71	1.14	1.00	0.46	0.88	0.44	0.40	0.99	0.54	0.43	0.40	0.07	0.04	0.14	0.12	0.10	3.41	3.27	3.37	3.32
Cr	0.00	0.00	0.00	0.00	0.00	0.00	0.00	0.00	0.00	0.00	0.00	0.00	0.01	0.00	0.00	0.00	0.00	0.00	0.00	0.00	0.00	0.00	0.00	0.00	0.00
Fe^{3+}	0.00	0.00	0.00	0.00	0.00	0.45	0.84	0.75	0.30	0.64	0.68	2.54	0.71	0.74	1.37	1.44	0.00	0.00	0.00	0.00	0.00	1.42	1.35	0.82	1.09
Fe^{2+}	5.23	4.75	5.57	5.45	5.68	2.67	2.53	2.68	2.25	2.59	2.56	0.00	2.50	2.70	2.13	2.10	0.07	0.02	0.08	0.11	0.12	0.00	0.00	0.00	0.00
Mn	0.08	0.07	0.08	0.08	0.09	0.02	0.04	0.03	0.03	0.03	0.02	0.03	0.03	0.02	0.02	0.02	0.00	0.00	0.00	0.00	0.00	0.02	0.02	0.01	0.01
Mg	4.12	3.81	3.87	4.13	3.93	1.68	2.07	1.89	1.59	1.99	1.49	1.26	2.00	1.18	1.06	1.06	0.01	0.00	0.02	0.04	0.06	1.13	1.20	0.81	0.99
Ca	0.04	0.03	0.05	0.02	0.03	0.29	0.33	0.30	0.51	0.41	0.40	0.28	0.39	0.17	0.09	0.06	0.97	0.76	0.96	0.91	0.52	0.03	0.01	0.02	0.03
Na	0.17	0.37	0.02	0.02	0.01	1.51	1.25	1.33	1.08	1.33	1.70	1.26	1.16	1.97	2.04	2.02	0.00	0.00	0.00	0.00	0.00	0.01	0.02	0.02	0.03
K	0.01	0.00	0.03	0.00	0.01	0.01	0.01	0.01	0.01	0.01	0.01	0.01	0.01	0.01	0.00	0.00	0.00	0.00	0.00	0.00	0.00	1.42	1.51	1.77	1.55
Total	19.93	19.66	19.90	19.99	19.99	15.25	15.42	15.39	14.22	15.39	15.30	13.97	15.26	15.34	15.13	15.09	3.05	2.90	3.06	3.06	2.88	13.87	13.92	13.80	13.80

Comment	0605 2.6	0605 1.1+	0605 1.1+	0605 1.1	0605 1.1+	0605 1.1+	0605 1.1+	0605 1.1+	0605 1.1+	0605 1.1+	0605 1.1+	0605 1.1+	0605 1.2+	0605 1.7	0605 2.4	0605 1.2+	0605 1.1+	0605 1.1+	0605 1.1+	0605 1.1+	0605 1.1+	0605 1.1+	0605 1.1+	0605 1.1+
Mineral	mu	qtz	qtz	?	?	?	?	?	?	?	?	?	?	?	?	?	?	?	?	?	?	?	?	?
SiO_2	52.88	95.11	99.19	42.84	90.61	86.08	37.40	18.46	72.38	62.39	59.12	52.30	73.77	13.92	52.23	64.13	41.80	41.03	43.75	31.19	32.61	36.55	35.36	34.38
TiO_2	0.03	0.04	0.00	0.04	0.22	0.01	0.04	16.65	9.09	0.03	0.04	13.28	7.03	0.03	0.02	0.37	1.85	0.45	0.22	0.17	0.16	0.04	0.21	0.03
Al_2O_3	14.77	2.13	0.09	20.10	1.88	3.42	17.48	0.92	2.85	18.35	18.34	13.16	5.39	8.20	3.33	15.57	19.52	17.68	18.50	16.16	17.09	18.67	17.46	18.47
Cr_2O_3	0.00	0.00	0.00	0.00	0.00	0.01	0.00	0.00	0.00	0.00	0.00	0.01	0.00	0.01	0.00	0.01	0.00	0.01	0.00	0.01	0.01	0.00	0.00	0.00
Fe_2O_3	13.53	0.00	0.00	17.90	0.00	0.00	0.00	0.00	0.00	0.00	0.00	0.00	0.00	0.00	3.49	0.00	0.00	0.00	0.00	0.00	0.00	0.00	0.00	0.00
FeO	1.80	0.76	0.30	0.00	2.55	4.82	19.89	1.13	3.87	5.16	8.75	3.90	3.53	17.34	22.70	100.67	95.23	18.36	17.98	28.89	27.54	21.07	25.60	25.42
MnO	0.09	0.00	0.01	0.13	0.01	0.06	0.25	0.18	0.07	0.09	0.13	0.07	0.09	0.20	0.22	0.03	0.16	0.22	0.25	0.39	0.35	0.26	0.33	0.48
MgO	4.41	0.41	0.00	5.95	0.92	1.60	8.69	0.00	1.49	2.04	3.56	1.22	1.15	5.74	7.64	2.35	3.74	8.37	8.03	13.01	12.14	10.08	11.48	10.87
CaO	0.74	0.05	0.05	3.27	0.78	1.56	0.17	39.82	6.86	0.12	0.23	9.75	7.12	27.08	4.18	1.37	10.56	0.55	0.31	0.70	0.22	0.10	0.29	0.13
Na_2O	2.09	0.04	0.01	0.04	0.03	0.02	0.05	0.07	0.25	8.61	8.46	6.71	3.97	0.02	4.15	8.93	0.04	0.09	2.56	0.10	1.59	0.04	1.97	2.23
K_2O	6.89	0.95	0.00	5.81	0.04	0.03	4.51	0.03	0.20	0.48	0.98	0.09	0.05	0.03	0.08	1.00	4.54	4.67	3.45	0.06	0.07	3.81	0.28	0.40
Total	95.88	99.49	99.65	94.29	97.02	97.62	88.48	77.27	97.06	97.28	99.61	100.48	102.09	72.59	97.69	100.67	95.23	91.43	95.05	90.68	91.78	90.62	92.98	92.42
num ox	22.00	23.00	8.00	22.00	25.00	8.00		25.00	23.00	23.00	23.00	2.00			23.00	25.00	25.00	28.00	28.00	28.00	28.00	28.00	28.00	28.00
Si	7.16	11.16	3.99	5.98	11.97	3.69		4.30	9.42	8.27	7.88	0.62	0.00	0.00	7.83	6.29	4.74	7.89	8.02	6.42	6.57	7.23	6.92	6.78
Ti	0.00	0.00	0.00	0.00	0.02	0.00		2.91	0.89	0.00	0.00	0.12	0.00	0.00	0.00	0.03	0.16	0.06	0.03	0.03	0.02	0.01	0.03	0.00
Al	2.36	0.29	0.00	3.30	0.29	0.17		0.25	0.44	2.87	2.88	0.18	0.00	0.00	0.59	1.80	2.61	4.01	4.00	3.92	4.06	4.35	4.03	4.30
Cr	0.00	0.00	0.00	0.00	0.00	0.00		0.00	0.00	0.00	0.00	0.00	0.00	0.00	0.00	0.00	0.00	0.00	0.00	0.00	0.00	0.00	0.00	0.00
Fe^{3+}	1.38	0.00	0.00	1.88	0.00	0.00		0.00	0.00	0.00	0.00	0.00	0.00	0.00	0.39	0.00	0.00	0.00	0.00	0.00	0.00	0.00	0.00	0.00
Fe^{2+}	0.20	0.07	0.01	0.00	0.28	0.17		0.22	0.42	0.57	0.98	0.04	0.00	0.00	2.85	8.26	9.03	2.95	2.76	4.98	4.64	3.48	4.19	4.20
Mn	0.01	0.00	0.00	0.02	0.00	0.00		0.03	0.01	0.01	0.01	0.00	0.00	0.00	0.03	0.00	0.02	0.04	0.04	0.07	0.06	0.04	0.06	0.08
Mg	0.89	0.07	0.00	1.24	0.18	0.10		0.00	0.29	0.40	0.71	0.02	0.00	0.00	1.71	0.34	0.63	2.40	2.19	3.99	3.65	2.97	3.35	3.20
Ca	0.11	0.01	0.00	0.49	0.11	0.07		9.93	0.96	0.02	0.03	0.12	0.00	0.00	0.67	0.14	1.28	0.11	0.06	0.15	0.05	0.02	0.06	0.03
Na	0.55	0.01	0.00	0.01	0.01	0.00		0.03	0.06	2.21	2.19	0.15	0.00	0.00	1.20	1.70	0.01	0.03	0.91	0.04	0.62	0.02	0.75	0.85
K	1.19	0.14	0.00	1.03	0.01	0.00		0.01	0.03	0.08	0.17	0.00	0.00	0.00	0.02	0.13	0.66	1.15	0.81	0.02	0.02	0.96	0.07	0.10
Total	13.84	11.76	4.01	13.95	12.87	4.22		17.69	12.52	14.44	14.85	1.25	0.00	0.00	15.29	18.69	19.13	18.64	18.81	19.62	19.69	19.08	19.45	19.54

Comment	0605 1.1+	0605 1.2+	0605 1.1+	0605 1.5		0672 1.1	0672 1.2	0672 1.3	0672 1.5	0672 1.9	0672 1.9+	0672 1.9+	0672 1.9+	0672 1.9+	0672 1.9+	0672 1.9+	0672 1.9+	0672 1.9+	0672 1.9+	0672 1.9+	0672 1.9+	0672 1.9+	0672 1.1	0672 1.1
Mineral	?	?	?	?		ep	ep	ep	ep	ep	ep	ep	ep	ep	ep	ep	ep	ep	ep	ep	ep	ep	act t	act t
SiO_2	42.95	38.72	38.98	35.55		38.04	38.53	38.38	38.37	38.55	38.11	38.21	38.72	38.48	38.78	38.88	37.56	38.56	38.43	38.71	37.92	44.32	42.72	54.09	54.11
TiO_2	0.02	0.02	0.04	0.17		0.02	0.09	0.09	0.15	0.14	0.11	0.12	0.08	0.09	0.10	0.13	0.13	0.12	0.05	0.05	0.08	0.08	0.01	0.00	0.03
Al_2O_3	18.26	16.66	18.45	18.97		24.00	26.65	26.13	25.76	27.01	25.22	26.16	25.65	26.42	26.54	26.81	23.91	26.26	24.96	25.55	24.40	18.35	22.77	1.76	1.80
Cr_2O_3	0.00	0.00	0.00	0.00		0.00	0.03	0.01	0.04	0.03	0.00	0.00	0.01	0.00	0.01	0.00	0.01	0.05	0.01	0.00	0.04	0.02	0.00	0.03	0.01
Fe_2O_3	0.00	0.00	0.00	0.00		13.08	9.32	10.26	10.54	8.62	11.21	10.65	11.12	9.76	9.44	9.47	11.53	10.02	11.99	11.12	12.43	12.76	5.71		
FeO	20.59	23.06	23.52	24.37		0.00	0.00	0.00	0.00	0.00	0.00	0.00	0.00	0.00	0.00	0.00	0.00	0.00	0.00	0.00	0.00	0.00	0.00	16.01	15.76
MnO	0.30	0.33	0.36	0.37		0.12	0.12	0.10	0.22	0.13	0.07	0.06	0.16	0.12	0.08	0.22	0.13	0.13	0.09	0.08	0.14	0.22	0.23	0.36	0.31
MgO	8.65	9.36	10.17	9.50		0.00	0.00	0.00	0.00	0.00	0.00	0.00	0.00	0.00	0.00	0.00	0.21	0.00	0.00	0.00	0.10	4.64	3.18	13.51	13.71
CaO	0.07	0.40	0.15	0.13		23.43	23.77	23.62	23.54	23.87	23.74	23.67	23.35	23.72	23.75	23.36	22.98	23.65	23.56	23.77	22.96	19.78	19.16	11.96	11.89
Na_2O	4.52	2.84	3.60	0.05		0.00	0.01	0.00	0.00	0.02	0.01	0.01	0.01	0.00	0.00	0.02	0.06	0.02	0.03	0.00	0.00	0.14	1.48	0.56	0.57
K_2O	0.82	0.10	0.04	3.24		0.01	0.01	0.01	0.00	0.00	0.00	0.00	0.01	0.00	0.00	0.00	0.00	0.00	0.00	0.00	0.00	0.03	0.01	0.08	0.07
Total	96.18	91.48	95.31	92.35		97.38	97.57	97.57	97.57	97.51	97.34	97.81	97.99	97.62	97.75	97.94	95.37	97.81	97.92	98.16	96.81	99.07	94.70	98.36	98.25
num ox	28.00	28.00	28.00	28.00		25.00	25.00	25.00	25.00	25.00	25.00	25.00	25.00	25.00	25.00	25.00	25.00	25.00	25.00	25.00	25.00	25.00	25.00	23.00	23.00
Si	7.83	7.55	7.30	7.01		6.00	6.00	5.99	6.00	6.00	5.99	5.96	6.03	6.00	6.03	6.03	6.03	6.00	6.01	6.02	6.00	6.75	6.71	7.85	7.84
Ti	0.00	0.00	0.01	0.02		0.00	0.01	0.01	0.02	0.02	0.01	0.01	0.01	0.01	0.01	0.01	0.02	0.01	0.01	0.01	0.01	0.01	0.00	0.00	0.00
Al	3.93	3.83	4.08	4.41		4.46	4.90	4.81	4.75	4.96	4.67	4.81	4.71	4.86	4.86	4.90	4.52	4.82	4.60	4.68	4.55	3.30	4.22	0.30	0.31
Cr	0.00	0.00	0.00	0.00		0.00	0.00	0.00	0.00	0.00	0.00	0.00	0.00	0.00	0.00	0.00	0.00	0.01	0.00	0.00	0.00	0.00	0.00	0.00	0.00
Fe^{3+}	0.00	0.00	0.00	0.00		1.55	1.09	1.21	1.24	1.01	1.33	1.25	1.30	1.14	1.10	1.10	1.39	1.17	1.41	1.30	1.48	1.46	0.68	0.00	0.00
Fe^{2+}	3.14	3.76	3.68	4.02		0.00	0.00	0.00	0.00	0.00	0.00	0.00	0.00	0.00	0.00	0.00	0.00	0.00	0.00	0.00	0.00	0.00	0.00	1.94	1.91
Mn	0.05	0.05	0.06	0.06		0.02	0.02	0.01	0.03	0.02	0.01	0.01	0.02	0.02	0.01	0.03	0.02	0.02	0.01	0.01	0.02	0.03	0.03	0.04	0.04
Mg	2.35	2.72	2.84	2.79		0.00	0.00	0.00	0.00	0.00	0.00	0.00	0.00	0.00	0.00	0.00	0.05	0.00	0.00	0.00	0.02	1.05	0.74	2.92	2.96
Ca	0.01	0.08	0.03	0.03		3.96	3.97	3.95	3.94	3.98	4.00	3.96	3.89	3.96	3.96	3.88	3.95	3.95	3.94	3.96	3.89	3.23	3.23	1.86	1.85
Na	1.60	1.07	1.31	0.02		0.00	0.00	0.00	0.00	0.01	0.00	0.00	0.00	0.00	0.00	0.00	0.02	0.01	0.01	0.00	0.00	0.04	0.45	0.16	0.16
K	0.19	0.02	0.01	0.82		0.00	0.00	0.00	0.00	0.00	0.00	0.00	0.00	0.00	0.00	0.00	0.00	0.00	0.00	0.00	0.00	0.01	0.00	0.01	0.01
Total	19.10	19.09	19.31	19.18		15.99	15.99	15.99	15.99	16.00	16.00	16.00	15.96	15.99	15.98	15.96	16.00	15.99	15.99	15.98	15.98	15.88	16.06	15.09	15.08

Comment	0672 1.1	0672 1.1	0672 1.1	0672 1.1	0672 1.1	0672 1.1	0672 1.1	0672 1.1	0672 1.1	0672 1.1	0672 1.1	0672 1.1	0672 1.1	0672 1.1	0672 1.1	0672 1.1	0672 1.1	0672 1.1	0672 1.1	0672 1.1	0672 1.8	0672 1.9+	0672 1.9+	0672 1.9+	0672 1.9+
Mineral	act t	act t	act t	act t	act t	act t	act t	act t	act t	act t	act t	act t	act t	act t	act t	act t	act t	act t	act t	act t	act	act	act	act	act
SiO_2	53.83	53.52	54.13	53.49	52.99	53.62	53.16	53.29	54.05	53.45	54.13	53.57	53.12	54.51	53.42	53.88	54.12	54.38	54.01	55.98	49.87	54.20	54.30	54.76	54.04
TiO_2	0.02	0.01	0.02	0.03	0.00	0.01	0.02	0.02	0.07	0.07	0.03	0.04	0.06	0.00	0.04	0.04	0.02	0.02	0.06	0.03	0.01	0.01	0.05	0.03	0.08
Al_2O_3	1.58	2.10	1.45	1.95	1.99	1.53	1.97	1.64	1.52	2.55	1.75	2.05	2.52	1.20	2.48	2.11	1.92	1.56	1.92	1.20	6.39	1.84	0.90	1.56	1.59
Cr_2O_3	0.00	0.02	0.00	0.04	0.02	0.00	0.00	0.02	0.00	0.00	0.03	0.01	0.02	0.00	0.00	0.00	0.00	0.02	0.00	0.00	0.06	0.00	0.01	0.01	0.00
Fe_2O_3																									
FeO	15.19	16.03	15.70	17.12	18.35	18.59	18.01	17.40	16.32	15.93	15.37	16.47	16.18	15.31	15.79	16.01	15.60	15.67	16.12	14.98	16.43	15.62	16.81	15.19	15.22
MnO	0.34	0.35	0.33	0.37	0.40	0.31	0.29	0.30	0.36	0.36	0.39	0.38	0.32	0.40	0.38	0.41	0.28	0.34	0.33	0.33	0.34	0.37	0.35	0.31	0.32
MgO	13.91	13.30	13.66	12.57	11.71	11.64	11.99	12.47	12.89	13.30	13.77	13.03	13.01	14.30	13.41	13.36	13.71	13.78	13.53	14.46	12.13	13.83	13.08	13.98	13.70
CaO	12.20	12.40	12.42	12.46	12.46	12.46	12.38	12.42	12.25	12.21	12.56	12.22	12.00	12.22	12.07	12.03	12.04	12.01	11.82	12.00	12.48	12.13	12.48	12.10	12.13
Na_2O	0.44	0.40	0.41	0.37	0.27	0.21	0.30	0.38	0.43	0.54	0.39	0.54	0.65	0.38	0.63	0.60	0.54	0.47	0.56	0.52	0.26	0.51	0.18	0.56	0.53
K_2O	0.05	0.08	0.08	0.12	0.12	0.08	0.10	0.11	0.09	0.08	0.07	0.08	0.10	0.04	0.09	0.07	0.07	0.06	0.07	0.03	0.03	0.07	0.04	0.06	0.07
Total	97.55	98.22	98.21	98.51	98.33	98.45	98.22	98.05	97.98	98.51	98.49	98.39	97.98	98.35	98.29	98.52	98.31	98.31	98.42	99.54	98.01	98.58	98.21	98.56	97.67
num ox	23.00	23.00	23.00	23.00	23.00	23.00	23.00	23.00	23.00	23.00	23.00	23.00	23.00	23.00	23.00	23.00	23.00	23.00	23.00	23.00	23.00	23.00	23.00	23.00	23.00
Si	7.85	7.79	7.86	7.80	7.79	7.87	7.81	7.82	7.88	7.75	7.83	7.80	7.75	7.88	7.76	7.81	7.84	7.87	7.83	7.95	7.31	7.83	7.92	7.89	7.87
Ti	0.00	0.00	0.00	0.00	0.00	0.00	0.00	0.00	0.01	0.01	0.00	0.00	0.01	0.00	0.00	0.00	0.00	0.00	0.01	0.00	0.00	0.00	0.01	0.00	0.01
Al	0.27	0.36	0.25	0.33	0.35	0.27	0.34	0.28	0.26	0.44	0.30	0.35	0.43	0.20	0.42	0.36	0.33	0.27	0.33	0.20	1.10	0.31	0.15	0.27	0.27
Cr	0.00	0.00	0.00	0.00	0.00	0.00	0.00	0.00	0.00	0.00	0.00	0.00	0.00	0.00	0.00	0.00	0.00	0.00	0.00	0.00	0.01	0.00	0.00	0.00	0.00
Fe^{3+}	0.00	0.00	0.00	0.00	0.00	0.00	0.00	0.00	0.00	0.00	0.00	0.00	0.00	0.00	0.00	0.00	0.00	0.00	0.00	0.00	0.00	0.00	0.00	0.00	0.00
Fe^{2+}	1.85	1.95	1.91	2.09	2.26	2.28	2.21	2.14	1.99	1.93	1.86	2.00	1.98	1.85	1.92	1.94	1.89	1.90	1.95	1.78	2.01	1.89	2.05	1.83	1.85
Mn	0.04	0.04	0.04	0.05	0.05	0.04	0.04	0.04	0.05	0.04	0.05	0.05	0.04	0.05	0.05	0.05	0.03	0.04	0.04	0.04	0.04	0.05	0.04	0.04	0.04
Mg	3.02	2.88	2.96	2.73	2.57	2.55	2.62	2.73	2.80	2.87	2.97	2.83	2.83	3.08	2.90	2.89	2.96	2.97	2.92	3.06	2.65	2.98	2.84	3.00	2.97
Ca	1.91	1.93	1.93	1.95	1.96	1.96	1.95	1.95	1.92	1.90	1.95	1.91	1.88	1.89	1.88	1.87	1.87	1.86	1.84	1.83	1.96	1.88	1.95	1.87	1.89
Na	0.13	0.11	0.12	0.10	0.08	0.06	0.09	0.11	0.12	0.15	0.11	0.15	0.18	0.11	0.18	0.17	0.15	0.13	0.16	0.14	0.08	0.14	0.05	0.16	0.15
K	0.01	0.01	0.02	0.02	0.02	0.01	0.02	0.02	0.02	0.01	0.01	0.02	0.02	0.01	0.02	0.01	0.01	0.01	0.01	0.01	0.01	0.01	0.01	0.01	0.01
Total	15.08	15.09	15.08	15.09	15.08	15.03	15.07	15.10	15.05	15.11	15.08	15.11	15.12	15.07	15.12	15.10	15.08	15.06	15.09	15.02	15.17	15.09	15.03	15.06	15.07

Comment	0672 1.9+	0672 1.6	0672 1.7	0672 1.9+	0672 1.9+	0672 1.9+	0672 1.9+	0672 1.9+	0672 1.9+	0672 1.9+	0672 1.9+	0672 1.9+	0672 1.9+	0672 1.9+	0672 1.9+	0672 1.9+	0672 1.9+	0672 1.9+	0672 1.9+	0672 1.9+	0672 1.9+	0672 1.9+
Mineral	act	ab	ab	ab	ab	ab	ab	ab	ab	ab	ab	ab	ab	ab	ab	ab	ab	ab	ab	ab	chl	chl
SiO_2	53.64	69.92	69.97	71.10	70.08	69.65	69.20	68.02	69.45	69.01	69.78	69.87	70.08	69.90	70.32	69.88	66.87	70.38	69.42	70.00	28.68	26.85
TiO_2	0.07	0.00	0.01	0.02	0.00	0.00	0.03	0.05	0.02	0.03	0.02	0.02	0.02	0.02	0.02	0.02	0.00	0.01	0.00	0.00	0.02	0.00
Al_2O_3	2.07	20.00	20.11	19.64	20.15	19.64	19.73	17.65	19.67	19.43	19.76	19.65	20.20	19.98	20.04	19.86	20.06	20.07	19.81	20.08	18.19	19.01
Cr_2O_3	0.04	0.00	0.00	0.00	0.02	0.01	0.03	0.00	0.00	0.00	0.01	0.00	0.02	0.00	0.05	0.00	0.00	0.00	0.02	0.01	0.01	0.00
Fe_2O_3																						
FeO	15.66	0.12	0.15	0.16	0.15	0.32	0.30	2.25	0.20	0.14	0.23	0.62	0.38	0.10	0.12	0.17	0.77	0.29	0.27	0.38	26.72	27.54
MnO	0.32	0.00	0.00	0.00	0.01	0.00	0.00	0.03	0.03	0.01	0.00	0.00	0.00	0.02	0.00	0.00	0.06	0.02	0.00	0.01	0.35	0.46
MgO	13.29	0.00	0.00	0.02	0.00	0.02	0.00	1.63	0.02	0.02	0.01	0.32	0.00	0.00	0.00	0.03	0.00	0.00	0.01	0.02	13.25	14.18
CaO	11.91	0.05	0.03	0.06	0.16	0.05	0.15	1.79	0.06	0.06	0.05	0.41	0.12	0.07	0.03	0.03	1.44	0.13	0.05	0.21	2.76	0.12
Na_2O	0.64	12.04	11.97	11.86	12.06	12.17	12.15	11.23	12.00	12.02	12.04	11.95	12.17	11.97	12.22	11.77	11.72	11.97	12.24	12.12	0.35	0.03
K_2O	0.07	0.07	0.12	0.09	0.09	0.17	0.03	0.09	0.01	0.08	0.05	0.06	0.14	0.05	0.02	0.08	0.05	0.09	0.05	0.08	0.02	0.00
Total	97.72	102.21	102.37	102.94	102.72	102.04	101.62	102.73	101.46	100.81	101.96	102.91	103.12	102.11	102.82	101.84	100.97	102.96	101.87	102.91	90.34	88.18
num ox	23.00	8.00	8.00	8.00	8.00	8.00	8.00	8.00	8.00	8.00	8.00	8.00	8.00	8.00	8.00	8.00	8.00	8.00	8.00	8.00	28.00	28.00
Si	7.82	2.99	2.99	3.01	2.98	2.99	2.98	2.95	2.99	2.99	2.99	2.98	2.98	2.99	2.99	3.00	2.93	2.99	2.98	2.98	5.94	5.69
Ti	0.01	0.00	0.00	0.00	0.00	0.00	0.00	0.00	0.00	0.00	0.00	0.00	0.00	0.00	0.00	0.00	0.00	0.00	0.00	0.00	0.00	0.00
Al	0.36	1.01	1.01	0.98	1.01	0.99	1.00	0.90	1.00	0.99	1.00	0.99	1.01	1.01	1.00	1.00	1.03	1.01	1.00	1.01	4.44	4.75
Cr	0.00	0.00	0.00	0.00	0.00	0.00	0.00	0.00	0.00	0.00	0.00	0.00	0.00	0.00	0.00	0.00	0.00	0.00	0.00	0.00	0.00	0.00
Fe^{3+}	0.00	0.00	0.00	0.00	0.00	0.00	0.00	0.00	0.00	0.00	0.00	0.00	0.00	0.00	0.00	0.00	0.00	0.00	0.00	0.00	0.00	0.00
Fe^{2+}	1.91	0.00	0.01	0.01	0.01	0.01	0.01	0.08	0.01	0.01	0.01	0.02	0.01	0.00	0.00	0.01	0.03	0.01	0.01	0.01	4.63	4.88
Mn	0.04	0.00	0.00	0.00	0.00	0.00	0.00	0.00	0.00	0.00	0.00	0.00	0.00	0.00	0.00	0.00	0.00	0.00	0.00	0.00	0.06	0.08
Mg	2.89	0.00	0.00	0.00	0.00	0.00	0.00	0.11	0.00	0.00	0.00	0.02	0.00	0.00	0.00	0.00	0.00	0.00	0.00	0.00	4.09	4.48
Ca	1.86	0.00	0.00	0.00	0.01	0.00	0.01	0.08	0.00	0.00	0.00	0.02	0.01	0.00	0.00	0.00	0.07	0.01	0.00	0.01	0.61	0.03
Na	0.18	1.00	0.99	0.97	1.00	1.01	1.02	0.94	1.00	1.01	1.00	0.99	1.00	0.99	1.01	0.98	0.99	0.99	1.02	1.00	0.14	0.01
K	0.01	0.00	0.01	0.00	0.00	0.01	0.00	0.00	0.00	0.00	0.00	0.00	0.01	0.00	0.00	0.00	0.00	0.00	0.00	0.00	0.00	0.00
Total	15.09	5.01	5.00	4.98	5.01	5.02	5.02	5.07	5.01	5.02	5.01	5.02	5.02	5.00	5.01	4.99	5.06	5.00	5.02	5.02	19.91	19.93

Comment	0672 1.9+	0672 1.9+	0672 1.4	0672 1.9+	0672 1.9+	0672 1.9+	0672 1.9+	0672 1.9+		0676 1.1	0676 1.1	0676 1.1	0676 1.1	0676 1.1	0676 1.1	0676 1.1	0676 1.1	0676 1.8+	0676 1.8+	0676 1.8+	0676 1.8+	0676 1.8+	0676 1.8+	0676 1.8+
Mineral	chl	chl	tit	tit	tit	?	?	qtz		ep	ep	ep	ep	ep	ep	ep	ep	ep	ep	ep	ep	ep	ep	ep
SiO_2	28.33	26.67	31.19	30.09	32.06	49.53	63.61	99.88		34.79	37.94	37.97	38.11	37.90	38.03	37.78	37.67	37.64	37.58	37.26	37.85	37.69	37.49	37.27
TiO_2	0.01	0.04	35.55	30.49	35.11	0.00	0.03	0.00		0.09	0.08	0.11	0.05	0.06	0.06	0.09	0.09	0.08	0.09	1.83	0.05	0.08	0.06	0.06
Al_2O_3	17.50	19.70	2.70	4.62	2.93	8.15	11.18	0.01		20.78	23.25	23.14	22.98	22.75	23.55	21.78	21.83	21.72	22.05	20.44	21.25	22.80	21.61	21.76
Cr_2O_3	0.00	0.01	0.00	0.00	0.00	0.01	0.00	0.00		0.01	0.00	0.01	0.01	0.00	0.00	0.00	0.01	0.02	0.02	0.00	0.03	0.02	0.00	0.01
Fe_2O_3										17.47	14.25	13.92	14.50	14.37	13.59	16.20	16.00	15.97	15.42	15.44	16.89	14.84	16.36	16.36
FeO	27.74	27.22	1.49	5.87	1.30	16.10	7.47	0.08		0.00	0.00	0.00	0.00	0.00	0.00	0.00	0.00	0.00	0.00	0.00	0.00	0.00	0.00	0.00
MnO	0.34	0.40	0.03	0.09	0.00	0.28	0.12	0.02		0.20	0.15	0.08	0.12	0.15	0.13	0.26	0.27	0.10	0.08	0.11	0.08	0.11	0.10	0.23
MgO	15.06	13.88	0.22	2.35	0.01	12.30	6.61	0.00		2.68	0.00	0.00	0.00	0.00	0.00	0.00	0.00	0.09	0.00	0.00	0.00	0.00	0.00	0.00
CaO	0.11	0.10	27.17	23.29	26.69	7.33	6.03	0.00		19.85	23.27	23.45	23.51	23.27	23.35	23.11	23.01	22.78	22.88	23.12	23.26	23.39	23.18	23.06
Na_2O	0.03	0.04	0.17	0.03	0.33	0.32	6.95	0.01		0.03	0.01	0.00	0.00	0.02	0.01	0.00	0.00	0.01	0.02	0.00	0.00	0.01	0.00	0.00
K_2O	0.00	0.01	0.02	0.01	0.00	2.14	0.03	0.00		0.01	0.00	0.01	0.00	0.01	0.00	0.00	0.00	0.01	0.01	0.00	0.00	0.00	0.00	0.01
Total	89.11	88.08	98.55	96.85	98.43	96.17	102.02	99.99		94.16	97.53	97.29	97.84	97.08	97.36	97.59	97.29	96.82	96.60	96.66	97.72	97.46	97.16	97.12
num ox	28.00	28.00	5.00	5.00	5.00	28.00	12.00	23.00		25.00	25.00	25.00	25.00	25.00	25.00	25.00	25.00	25.00	25.00	25.00	25.00	25.00	25.00	25.00
Si	5.93	5.65	1.03	1.02	1.05	8.94	4.33	11.49		5.74	5.99	6.01	6.01	6.02	6.01	6.00	6.00	6.01	6.01	5.98	6.01	5.97	5.98	5.95
Ti	0.00	0.01	0.88	0.78	0.87	0.00	0.00	0.00		0.01	0.01	0.01	0.01	0.01	0.01	0.01	0.01	0.01	0.01	0.22	0.01	0.01	0.01	0.01
Al	4.32	4.92	0.10	0.18	0.11	1.74	0.90	0.00		4.04	4.33	4.32	4.27	4.26	4.39	4.08	4.10	4.09	4.16	3.87	3.98	4.26	4.07	4.10
Cr	0.00	0.00	0.00	0.00	0.00	0.00	0.00	0.00		0.00	0.00	0.00	0.00	0.00	0.00	0.00	0.00	0.00	0.00	0.00	0.00	0.00	0.00	0.00
Fe^{3+}	0.00	0.00	0.00	0.00	0.00	0.00	0.00	0.00		2.17	1.69	1.66	1.72	1.72	1.62	1.93	1.92	1.92	1.86	1.86	2.02	1.77	1.96	1.97
Fe^{2+}	4.86	4.82	0.04	0.17	0.04	2.43	0.42	0.01		0.00	0.00	0.00	0.00	0.00	0.00	0.00	0.00	0.00	0.00	0.00	0.00	0.00	0.00	0.00
Mn	0.06	0.07	0.00	0.00	0.00	0.04	0.01	0.00		0.03	0.02	0.01	0.02	0.02	0.02	0.04	0.04	0.01	0.01	0.02	0.01	0.02	0.01	0.03
Mg	4.70	4.38	0.01	0.12	0.00	3.31	0.67	0.00		0.66	0.00	0.00	0.00	0.00	0.00	0.00	0.00	0.02	0.00	0.00	0.00	0.00	0.00	0.00
Ca	0.03	0.02	0.96	0.84	0.94	1.42	0.44	0.00		3.51	3.94	3.98	3.97	3.96	3.95	3.93	3.92	3.90	3.92	3.98	3.96	3.97	3.96	3.95
Na	0.01	0.02	0.01	0.00	0.02	0.11	0.92	0.00		0.01	0.00	0.00	0.00	0.01	0.00	0.00	0.00	0.00	0.01	0.00	0.00	0.00	0.00	0.00
K	0.00	0.00	0.00	0.00	0.00	0.49	0.00	0.00		0.00	0.00	0.00	0.00	0.00	0.00	0.00	0.00	0.00	0.00	0.00	0.00	0.00	0.00	0.00
Total	19.91	19.89	3.04	3.11	3.03	18.49	7.68	11.51		16.16	15.99	15.99	15.99	15.99	15.99	15.99	15.99	15.97	15.97	15.93	15.98	16.00	16.00	16.01

Comment	0676 1.8+	0676 1.8+	0676 1.8+	0676 1.8+	0676 1.8+	0676 1.8+	0676 1.8+	0676 1.8+	0676 1.8+	0676 1.8+	0676 1.8+	0676 1.8+	0676 1.8+	0676 1.8+	0676 1.8+	0676 1.8+	0676 1.8+	0676 1.8+	0676 1.8+	0676 1.8+	0676 1.8+	0676 1.8+	0676 1.2	0676 1.3	0676 1.4
Mineral	ep	ep	ep	ep	ep	ep	ep	ep	ep	ep	ep	ep	ep	ep	ep	ep	ep	ep	ep	ep	ep	ep	amp	amp	amp
SiO_2	37.74	37.85	37.90	37.83	37.39	37.86	37.53	38.06	37.48	37.53	38.00	37.74	37.41	37.91	37.72	37.21	37.72	37.45	37.48	37.26	37.30	37.96	53.31	53.90	54.64
TiO_2	0.04	0.12	0.08	0.08	0.08	0.05	0.09	0.10	0.17	0.08	0.12	0.07	0.09	0.11	0.18	0.30	2.15	0.11	0.05	1.00	0.12	0.04	0.05	0.02	0.03
Al_2O_3	21.56	23.05	22.22	23.22	21.96	22.20	21.61	22.82	21.63	21.71	22.51	22.75	21.60	22.40	20.62	21.50	20.30	21.51	21.58	21.05	21.48	22.74	2.04	2.16	1.53
Cr_2O_3	0.03	0.02	0.16	0.32	0.01	0.00	0.00	0.03	0.00	0.09	0.01	0.00	0.00	0.08	0.03	0.02	0.04	0.01	0.01	0.04	0.03	0.00	0.03	0.00	0.03
Fe_2O_3	16.46	14.59	15.38	13.73	15.74	15.56	16.45	14.76	15.84	16.17	14.47	14.41	15.82	15.12	17.75	15.37	15.72	16.31	16.47	15.82	16.20	14.53	1.59	1.12	1.31
FeO	0.00	0.00	0.00	0.00	0.00	0.00	0.00	0.00	0.00	0.00	0.00	0.00	0.00	0.00	0.00	0.00	0.00	0.00	0.00	0.00	0.00	0.00	13.60	15.60	17.10
MnO	0.12	0.16	0.14	0.08	0.12	0.10	0.05	0.16	0.09	0.23	0.17	0.18	0.15	0.13	0.10	0.15	0.15	0.17	0.19	0.19	0.12	0.16	0.32	0.34	0.27
MgO	0.00	0.00	0.00	0.00	0.79	0.00	0.00	0.00	0.00	0.00	0.08	0.00	0.00	0.05	0.00	0.00	0.00	0.00	0.00	0.00	0.00	0.00	14.38	13.28	12.25
CaO	23.19	23.25	23.00	23.14	21.99	23.30	23.14	23.11	23.17	22.96	22.95	23.20	23.09	22.66	22.75	22.88	23.24	23.01	22.94	23.06	23.01	23.09	9.78	9.22	7.91
Na_2O	0.00	0.01	0.01	0.02	0.03	0.00	0.01	0.03	0.00	0.02	0.05	0.02	0.02	0.01	0.01	0.00	0.02	0.00	0.00	0.03	0.01	0.01	1.53	2.57	3.26
K_2O	0.00	0.01	0.00	0.02	0.00	0.00	0.00	0.00	0.00	0.00	0.00	0.01	0.01	0.01	0.00	0.00	0.00	0.00	0.01	0.00	0.00	0.00	0.04	0.08	0.04
Total	97.49	97.60	97.35	97.08	96.53	97.54	97.23	97.59	96.78	97.17	96.91	96.94	96.61	96.97	97.38	95.89	97.77	96.95	97.09	96.88	96.65	97.08	96.51	98.18	98.23
num ox	25.00	25.00	25.00	25.00	25.00	25.00	25.00	25.00	25.00	25.00	25.00	25.00	25.00	25.00	25.00	25.00	25.00	25.00	25.00	25.00	25.00	25.00	23.00	23.00	23.00
Si	6.00	5.98	6.01	6.00	5.98	6.00	5.98	6.01	6.00	5.99	6.04	6.01	6.00	6.03	6.02	6.01	5.99	5.99	5.99	5.97	5.98	6.03	7.80	7.82	7.95
Ti	0.00	0.01	0.01	0.01	0.01	0.01	0.01	0.01	0.02	0.01	0.01	0.01	0.01	0.01	0.02	0.04	0.26	0.01	0.01	0.12	0.01	0.01	0.01	0.00	0.00
Al	4.04	4.29	4.16	4.34	4.14	4.15	4.06	4.25	4.08	4.08	4.22	4.27	4.08	4.20	3.88	4.09	3.80	4.06	4.06	3.98	4.06	4.26	0.35	0.37	0.26
Cr	0.00	0.00	0.02	0.04	0.00	0.00	0.00	0.00	0.00	0.01	0.00	0.00	0.00	0.01	0.00	0.00	0.00	0.00	0.00	0.00	0.00	0.00	0.00	0.00	0.00
Fe^{3+}	1.97	1.74	1.84	1.64	1.89	1.86	1.97	1.75	1.91	1.94	1.73	1.73	1.91	1.81	2.13	1.87	1.88	1.96	1.98	1.91	1.96	1.74	0.18	0.12	0.14
Fe^{2+}	0.00	0.00	0.00	0.00	0.00	0.00	0.00	0.00	0.00	0.00	0.00	0.00	0.00	0.00	0.00	0.00	0.00	0.00	0.00	0.00	0.00	0.00	1.66	1.89	2.08
Mn	0.02	0.02	0.02	0.01	0.02	0.01	0.01	0.02	0.01	0.03	0.02	0.02	0.02	0.02	0.01	0.02	0.02	0.02	0.03	0.03	0.02	0.02	0.04	0.04	0.03
Mg	0.00	0.00	0.00	0.00	0.19	0.00	0.00	0.00	0.00	0.00	0.02	0.00	0.00	0.01	0.00	0.00	0.00	0.00	0.00	0.00	0.00	0.00	3.13	2.87	2.66
Ca	3.95	3.94	3.91	3.93	3.77	3.96	3.95	3.91	3.97	3.92	3.91	3.96	3.97	3.86	3.89	3.96	3.96	3.94	3.93	3.96	3.95	3.93	1.53	1.43	1.23
Na	0.00	0.00	0.00	0.01	0.01	0.00	0.00	0.01	0.00	0.01	0.01	0.00	0.01	0.00	0.00	0.00	0.01	0.00	0.00	0.01	0.00	0.00	0.43	0.72	0.92
K	0.00	0.00	0.00	0.00	0.00	0.00	0.00	0.00	0.00	0.00	0.00	0.00	0.00	0.00	0.00	0.00	0.00	0.00	0.00	0.00	0.00	0.00	0.01	0.02	0.01
Total	15.99	15.99	15.97	15.98	16.00	15.99	15.99	15.98	15.99	15.99	15.98	15.99	16.00	15.95	15.96	15.98	15.91	15.99	15.99	15.97	15.99	15.97	15.15	15.30	15.30

Comment	0676 1.8+	0676 1.8+	0676 1.8+	0676 1.8+	0676 1.8+	0676 1.8+	0676 1.8+	0676 1.8+	0676 1.5	0676 1.8+	0676 1.8+	0676 1.8+	0676 1.8+	0676 1.8+	0676 1.8+	0676 1.8+	0676 1.8+	0676 1.8+	0676 1.8+	0676 1.8+	0676 1.8+
Mineral	amp	amp	act	act	act	act	act	tit	ab	ab	ab	ab	ab	ab	ab	ab	ab	ab	ab	ab	ab
SiO_2	53.30	55.31	51.69	53.33	52.41	53.75	55.59	34.59	69.74	69.43	69.06	69.89	69.76	69.58	68.96	67.83	69.17	69.77	70.40	68.74	70.16
TiO_2	0.02	0.03	0.12	0.07	0.11	0.11	0.02	31.75	0.00	0.03	0.03	0.00	0.01	0.02	0.03	0.06	0.03	0.01	0.00	0.03	0.01
Al_2O_3	3.81	2.43	2.73	2.24	3.28	1.84	0.88	1.32	19.71	19.70	19.80	19.91	19.75	19.93	19.63	19.07	19.47	19.69	20.09	19.54	20.04
Cr_2O_3	0.08	0.01	0.02	0.00	0.17	0.07	0.04	0.03	0.00	0.02	0.00	0.02	0.00	0.00	0.00	0.02	0.00	0.03	0.00	0.00	0.01
Fe_2O_3	2.30	1.03	0.59	0.82	0.70	0.27	0.39	0.00	0.00	0.00	0.00	0.00	0.00	0.00	0.00	0.00	0.00	0.00	0.00	0.00	0.00
FeO	14.20	14.40	17.10	14.65	16.10	15.10	14.30	3.65	0.23	0.31	0.43	0.27	0.42	0.28	0.34	1.17	0.44	0.15	0.25	0.18	0.32
MnO	0.29	0.31	0.36	0.31	0.35	0.35	0.31	0.09	0.01	0.00	0.00	0.00	0.00	0.01	0.01	0.03	0.00	0.00	0.00	0.00	0.00
MgO	13.02	13.30	11.98	13.99	12.75	13.90	14.75	2.49	0.03	0.00	0.07	0.01	0.01	0.00	0.02	0.93	0.00	0.00	0.01	0.00	0.00
CaO	7.86	8.17	11.17	11.40	11.26	12.10	11.50	24.91	0.02	0.10	0.08	0.09	0.08	0.05	0.07	0.46	0.05	0.03	0.07	0.14	0.05
Na_2O	2.15	2.91	1.20	0.88	1.25	0.69	0.94	0.18	11.93	12.16	11.97	12.14	12.26	12.06	12.08	11.40	12.36	12.11	11.85	12.01	11.97
K_2O	0.03	0.05	0.19	0.07	0.22	0.11	0.05	0.01	0.04	0.09	0.07	0.07	0.02	0.06	0.16	0.02	0.01	0.09	0.06	0.03	0.11
Total	96.83	97.85	97.09	97.67	98.52	98.26	98.74	99.03	101.71	101.84	101.51	102.39	102.31	102.00	101.29	100.99	101.53	101.88	102.73	100.68	102.67
num ox	23.00	23.00	23.00	23.00	23.00	23.00	23.00	5.00	8.00	8.00	8.00	8.00	8.00	8.00	8.00	8.00	8.00	8.00	8.00	8.00	8.00
Si	7.75	7.96	7.68	7.76	7.63	7.79	7.95	1.13	3.00	2.99	2.98	2.99	2.99	2.99	2.98	2.96	2.99	2.99	2.99	2.99	2.99
Ti	0.00	0.00	0.01	0.01	0.01	0.01	0.00	0.78	0.00	0.00	0.00	0.00	0.00	0.00	0.00	0.00	0.00	0.00	0.00	0.00	0.00
Al	0.65	0.41	0.48	0.38	0.56	0.31	0.15	0.05	1.00	1.00	1.01	1.00	1.00	1.01	1.00	0.98	0.99	1.00	1.01	1.00	1.01
Cr	0.01	0.00	0.00	0.00	0.02	0.01	0.00	0.00	0.00	0.00	0.00	0.00	0.00	0.00	0.00	0.00	0.00	0.00	0.00	0.00	0.00
Fe^{3+}	0.25	0.11	0.07	0.09	0.08	0.03	0.04	0.00	0.00	0.00	0.00	0.00	0.00	0.00	0.00	0.00	0.00	0.00	0.00	0.00	0.00
Fe^{2+}	1.73	1.73	2.12	1.78	1.96	1.83	1.71	0.10	0.01	0.01	0.02	0.01	0.02	0.01	0.01	0.04	0.02	0.01	0.01	0.01	0.01
Mn	0.04	0.04	0.05	0.04	0.04	0.04	0.04	0.00	0.00	0.00	0.00	0.00	0.00	0.00	0.00	0.00	0.00	0.00	0.00	0.00	0.00
Mg	2.82	2.85	2.65	3.03	2.77	3.00	3.14	0.12	0.00	0.00	0.00	0.00	0.00	0.00	0.00	0.06	0.00	0.00	0.00	0.00	0.00
Ca	1.23	1.26	1.78	1.78	1.76	1.88	1.76	0.87	0.00	0.00	0.00	0.00	0.00	0.00	0.00	0.02	0.00	0.00	0.00	0.01	0.00
Na	0.61	0.81	0.35	0.25	0.35	0.19	0.26	0.01	0.99	1.01	1.00	1.01	1.02	1.00	1.01	0.96	1.04	1.01	0.98	1.01	0.99
K	0.01	0.01	0.04	0.01	0.04	0.02	0.01	0.00	0.00	0.00	0.00	0.00	0.00	0.00	0.01	0.00	0.00	0.01	0.00	0.00	0.01
Total	15.09	15.19	15.22	15.13	15.22	15.13	15.08	3.07	5.00	5.02	5.02	5.02	5.02	5.01	5.03	5.03	5.03	5.01	4.99	5.02	5.00

Comment	0676 1.8+	0676 1.8+	0676 1.8+	0676 1.8+	0676 1.8+	0676 1.8+	0676 1.8+	0676 1.8+	0676 1.8+	0676 1.8+	0676 1.6	0676 1.7	0676 1.8+	0676 1.8+		0677H 1.1	0677C 1.2	0677 E	0677 C	0677 C	0677 H	0677 H	0677 B
Mineral	ab	ab	chl	chl	chl	chl	chl	chl	chl	chl	qtz	?	?	?		ep	ep	ep	ep	ep	ep	ep	ep
SiO_2	69.51	69.49	29.04	28.90	27.44	28.56	28.83	28.33	29.42	27.78	97.44	58.46	46.82	59.40		40.88	37.48	39.38	37.11	38.3	37.57	38.02	38.07
TiO_2	0.02	0.00	0.01	0.04	0.03	0.03	0.04	0.02	0.04	0.01	0.00	0.15	0.08	0.07		0.031	0.032	0.047	0.078	0.042	0.064	0.058	0.093
Al_2O_3	19.63	19.25	17.08	17.24	17.16	18.25	16.45	17.77	16.54	17.50	1.47	9.25	11.48	15.60		24.52	24.18	21.71	24.5	24.62	23.21	23.55	23.08
Cr_2O_3	0.01	0.00	0.05	0.00	0.01	0.09	0.01	0.05	0.03	0.04	0.01	0.03	0.00	0.01		0	0.021	0.115	0	0	0	0	0.041
Fe_2O_3	0.00	0.00	0.00	0.00	0.00	0.00	0.00	0.00	0.00	0.00						6.215	6.754	13.87	6.773	5.685	14.06	13.52	12.98
FeO	0.29	0.62	24.65	22.89	25.56	23.60	24.23	24.19	23.97	25.96	0.13	8.57	14.42	6.57		0	0	0	0	0	0	0	0
MnO	0.00	0.00	0.36	0.42	0.42	0.37	0.39	0.39	0.36	0.42	0.02	0.19	0.22	0.08		0.191	0.267	0.168	0.331	0.213	0.113	0.111	0.15
MgO	0.00	0.26	16.83	17.91	16.12	17.87	17.23	17.08	17.16	16.46	0.01	6.96	7.93	3.91		2.076	2.614	2.867	3.111	2.42	0	0	0.001
CaO	0.03	0.31	0.31	0.22	0.15	0.14	0.32	0.22	0.38	0.07	0.02	5.78	16.87	8.21		20.61	22.3	17.58	20.59	22.22	23.34	23.45	22.83
Na_2O	12.22	11.85	0.05	0.07	0.05	0.01	0.03	0.05	0.04	0.01	0.95	5.35	0.57	7.53		1.297	0.141	0.061	0.104	0.293	0.022	0	0.005
K_2O	0.03	0.07	0.00	0.02	0.01	0.00	0.02	0.02	0.02	0.00	0.00	0.12	0.04	0.05		0.011	0.01	1.375	0.011	0	0	0.013	0
Total	101.74	101.84	88.38	87.71	86.94	88.91	87.53	88.11	87.96	88.26	100.04	94.84	98.44	101.44		95.22	93.12	95.77	91.93	93.23	96.98	97.37	95.94
num ox	8.00	8.00	28.00	28.00	28.00	28.00	28.00	28.00	28.00	28.00	25.00	25.00	23.00	8.00		25	25	25	25	25	25	25	25
Si	2.99	2.99	6.03	6.00	5.85	5.86	6.05	5.90	6.12	5.84	12.27	8.98	6.87	2.73		6.436	6.101	6.263	6.088	6.198	5.972	6.006	6.086
Ti	0.00	0.00	0.00	0.01	0.00	0.00	0.01	0.00	0.01	0.00	0.00	0.02	0.01	0.00		0.004	0.004	0.006	0.01	0.005	0.008	0.007	0.011
Al	1.00	0.98	4.19	4.22	4.32	4.42	4.07	4.36	4.06	4.33	0.22	1.68	1.98	0.85		4.552	4.64	4.07	4.739	4.696	4.35	4.386	4.35
Cr	0.00	0.00	0.01	0.00	0.00	0.01	0.00	0.01	0.00	0.01	0.00	0.00	0.00	0.00		0	0.003	0.014	0	0	0	0	0.005
Fe^{3+}	0.00	0.00	0.00	0.00	0.00	0.00	0.00	0.00	0.00	0.00	0.00	0.00	0.00	0.00		0.736	0.827	1.66	0.836	0.692	1.682	1.607	1.561
Fe^{2+}	0.01	0.02	4.28	3.97	4.56	4.05	4.25	4.21	4.17	4.56	0.01	1.10	1.77	0.25		0	0	0	0	0	0	0	0
Mn	0.00	0.00	0.06	0.07	0.08	0.06	0.07	0.07	0.06	0.07	0.00	0.02	0.03	0.00		0.025	0.037	0.023	0.046	0.029	0.015	0.015	0.02
Mg	0.00	0.02	5.21	5.54	5.13	5.47	5.39	5.30	5.32	5.15	0.00	1.59	1.73	0.27		0.487	0.634	0.679	0.761	0.584	0	0	3E-04
Ca	0.00	0.01	0.07	0.05	0.04	0.03	0.07	0.05	0.08	0.02	0.00	0.95	2.65	0.40		3.477	3.889	2.996	3.619	3.852	3.975	3.969	3.91
Na	1.02	0.99	0.02	0.03	0.02	0.01	0.01	0.02	0.02	0.00	0.23	1.59	0.16	0.67		0.396	0.044	0.019	0.033	0.092	0.007	0	0.001
K	0.00	0.00	0.00	0.01	0.00	0.00	0.01	0.00	0.01	0.00	0.00	0.02	0.01	0.00		0.002	0.002	0.279	0.002	0	0	0.003	0
Total	5.02	5.02	19.88	19.90	19.99	19.92	19.92	19.93	19.85	19.99	12.74	15.97	15.22	5.18		16.12	16.18	16.01	16.13	16.15	16.01	15.99	15.95

Comment	0677C 1.1	0677C	0677E	0677E	0677C	0677H	0677H 1.2	0677E	0677E	0677C	0677C	0677H	0677H	0677H	0677E	0677B	0677C	0677H	0677B	0677B	0677H
Mineral	act	act	act	act	act	act	Kfs	ab	ab	ab	ab	ab	ab	ab	tit	tit	tit	tit	chl	chl	chl
SiO_2	55.20	54.49	56.79	54.41	54.96	47.09	63.65	68.23	69.01	69.90	70.18	69.73	69.51	69.84	30.86	31.31	33.97	32.07	26.77	26.76	26.44
TiO_2	0.00	1.01	0.00	0.02	0.14	0.13	0.04	0.00	0.00	0.01	0.00	0.00	0.00	0.01	33.66	39.39	31.16	36.16	0.12	0.21	0.02
Al_2O_3	0.85	1.24	1.47	1.82	1.66	6.60	18.38	19.37	19.66	19.76	19.51	19.06	19.82	19.99	3.44	0.89	5.42	2.63	19.45	17.72	19.21
Cr_2O_3	0.00	0.00	0.00	0.00	0.00	0.03	0.02	0.02	0.01	0.00	0.01	0.00	0.01	0.02	0.04	0.00	0.03	0.00	0.00	0.01	0.01
Fe_2O_3	0.00	0.00	0.00	0.00	0.00	0.00	0.00	0.00	0.00	0.00	0.00	0.00	0.00	0.00	0.00	0.00	0.00	0.00	0.00	0.00	0.00
FeO	12.45	11.82	12.93	12.40	11.85	20.36	0.55	0.16	0.00	0.05	0.09	0.71	0.04	0.09	3.62	0.76	1.23	1.03	27.61	28.32	28.97
MnO	0.31	0.27	0.28	0.34	0.26	0.35	0.00	0.00	0.02	0.03	0.00	0.04	0.00	0.01	0.04	0.01	0.00	0.01	0.41	0.43	0.46
MgO	15.99	15.67	14.22	15.90	15.97	14.28	0.30	0.10	0.01	0.00	0.00	0.37	0.00	0.00	1.92	0.00	0.43	0.00	14.18	13.73	13.52
CaO	12.45	13.03	11.51	12.56	12.87	8.00	0.22	0.12	0.02	0.06	0.05	0.45	0.03	0.07	24.43	28.22	23.31	27.89	0.13	0.21	0.03
Na_2O	0.32	0.28	0.55	0.40	0.37	0.26	0.37	11.89	11.80	11.96	12.06	11.71	12.04	11.99	0.02	0.00	0.04	0.19	0.06	0.05	0.02
K_2O	0.03	0.04	0.06	0.06	0.04	0.04	15.46	0.03	0.07	0.05	0.03	0.06	0.07	0.04	0.23	0.00	1.96	0.01	0.01	0.01	0.00
Total	97.60	97.84	97.82	97.91	98.14	97.14	98.98	99.93	100.62	101.82	101.95	102.14	101.51	102.07	98.25	100.57	97.54	99.97	88.73	87.43	88.70
num ox	23.00	23.00	23.00	23.00	23.00	23.00	8.00	8.00	8.00	8.00	8.00	8.00	8.00	8.00	5.00	5.00	5.00	5.00	28.00	28.00	28.00
Si	7.93	7.81	8.10	7.81	7.84	7.05	2.97	2.99	2.99	3.00	3.01	3.00	2.99	2.99	1.02	1.01	1.11	1.04	5.64	5.77	5.62
Ti	0.00	0.11	0.00	0.00	0.02	0.01	0.00	0.00	0.00	0.00	0.00	0.00	0.00	0.00	0.84	0.96	0.77	0.88	0.02	0.03	0.00
Al	0.14	0.21	0.25	0.31	0.28	1.17	1.01	1.00	1.01	1.00	0.99	0.97	1.01	1.01	0.13	0.03	0.21	0.10	4.83	4.50	4.81
Cr	0.00	0.00	0.00	0.00	0.00	0.00	0.00	0.00	0.00	0.00	0.00	0.00	0.00	0.00	0.00	0.00	0.00	0.00	0.00	0.00	0.00
Fe^{3+}	0.00	0.00	0.00	0.00	0.00	0.00	0.00	0.00	0.00	0.00	0.00	0.00	0.00	0.00	0.00	0.00	0.00	0.00	0.00	0.00	0.00
Fe^{2+}	1.50	1.42	1.54	1.49	1.41	2.55	0.02	0.01	0.00	0.00	0.00	0.03	0.00	0.00	0.10	0.02	0.03	0.03	4.86	5.10	5.15
Mn	0.04	0.03	0.03	0.04	0.03	0.04	0.00	0.00	0.00	0.00	0.00	0.00	0.00	0.00	0.00	0.00	0.00	0.00	0.07	0.08	0.08
Mg	3.42	3.35	3.02	3.40	3.40	3.19	0.02	0.01	0.00	0.00	0.00	0.02	0.00	0.00	0.09	0.00	0.02	0.00	4.45	4.41	4.28
Ca	1.92	2.00	1.76	1.93	1.97	1.28	0.01	0.01	0.00	0.00	0.00	0.02	0.00	0.00	0.87	0.98	0.82	0.97	0.03	0.05	0.01
Na	0.09	0.08	0.15	0.11	0.10	0.07	0.03	1.01	0.99	0.99	1.00	0.98	1.00	1.00	0.00	0.00	0.00	0.01	0.02	0.02	0.01
K	0.01	0.01	0.01	0.01	0.01	0.01	0.92	0.00	0.00	0.00	0.00	0.00	0.00	0.00	0.01	0.00	0.08	0.00	0.00	0.00	0.00
Total	15.04	15.02	14.86	15.10	15.06	15.39	5.00	5.02	5.00	5.00	5.00	5.01	5.01	5.00	3.07	3.01	3.05	3.03	19.94	19.96	19.97

Comment	0677H	0677B	0677B	0677E	0677C	0677B	0677H		0677G 1.7+	0677G 1.2+	0677G 1.2+	0677G 1.2+	0677G 1.2+	0677G 1.2+	0677G 1.2+	0677G 1.2+	0677G 1.2+	0677G 1.2+	0677G 1.7+	0677G 1.7+	0677G 1.7+	0677G 1.7+
Mineral	chl	qtz	qtz	cc	?	?	?		ep	ep	ep	ep	ep	ep	ep	ep	ep	ep	ep	ep	ep	ep
SiO_2	27.61	99.83	100.59	0.34	33.56	35.62	30.31		37.78	37.95	37.68	37.53	38.27	37.56	37.90	38.18	38.01	38.04	38.70	39.21	38.48	38.32
TiO_2	0.00	0.02	0.00	0.00	16.60	13.34	13.85		1.38	0.00	0.04	0.03	0.10	0.12	0.07	0.07	0.03	0.07	0.06	0.14	0.12	0.09
Al_2O_3	16.90	0.01	0.01	0.11	14.64	16.11	11.18		23.28	22.45	21.84	21.71	23.93	20.65	23.72	24.02	23.98	22.65	24.53	24.46	25.07	24.85
Cr_2O_3	0.00	0.00	0.00	0.03	0.02	0.01	0.00		0.02	0.00	0.00	0.00	0.03	0.00	0.00	0.00	0.00	0.00	0.00	0.02	0.01	0.02
Fe_2O_3	0.00	0.00	0.00	0.00	0.00	0.00	0.00		13.11	14.88	15.81	15.58	13.10	17.54	13.43	12.03	12.78	14.80	11.94	11.53	11.54	11.98
FeO	28.33	0.14	0.07	0.40	7.96	8.63	18.55		0.00	0.00	0.00	0.00	0.00	0.00	0.00	0.00	0.00	0.00	0.00	0.00	0.00	0.00
MnO	0.36	0.00	0.00	0.06	0.10	0.10	0.30		0.13	0.24	0.04	0.12	0.11	0.08	0.06	0.11	0.09	0.10	0.17	0.19	0.18	0.08
MgO	13.67	0.00	0.00	0.00	2.34	0.00	8.14		0.92	0.00	0.00	0.00	0.00	0.00	0.00	0.00	0.00	0.00	0.00	0.00	0.00	0.00
CaO	0.05	0.00	0.01	54.21	22.19	24.71	11.04		20.51	23.00	23.24	23.06	23.35	23.20	23.35	23.21	23.52	23.33	23.28	22.70	23.53	23.45
Na_2O	0.04	0.01	0.01	0.01	0.03	0.01	0.28		0.31	0.03	0.02	0.03	0.04	0.03	0.02	0.06	0.02	0.01	0.00	0.44	0.01	0.00
K_2O	0.01	0.00	0.01	0.00	0.06	0.00	0.02		0.00	0.01	0.00	0.00	0.01	0.00	0.01	0.01	0.01	0.00	0.00	0.01	0.00	0.01
Total	86.99	100.01	100.69	55.16	97.50	98.53	93.66		96.13	97.08	97.09	96.50	97.63	97.42	97.21	96.49	97.16	97.54	97.49	97.54	97.78	97.60
num ox	28.00	2.00	2.00	0.00	0.00	0.00	0.00		25.00	25.00	25.00	25.00	25.00	25.00	25.00	25.00	25.00	25.00	25.00	25.00	25.00	25.00
Si	5.97	1.00	1.00	0.00	0.00	0.00	0.00		6.00	6.03	6.01	6.02	6.02	6.00	5.99	6.06	6.01	6.02	6.07	6.13	6.02	6.01
Ti	0.00	0.00	0.00	0.00	0.00	0.00	0.00		0.16	0.00	0.01	0.00	0.01	0.01	0.01	0.01	0.00	0.01	0.01	0.02	0.01	0.01
Al	4.30	0.00	0.00	0.00	0.00	0.00	0.00		4.36	4.21	4.10	4.10	4.44	3.89	4.42	4.49	4.47	4.22	4.54	4.51	4.62	4.59
Cr	0.00	0.00	0.00	0.00	0.00	0.00	0.00		0.00	0.00	0.00	0.00	0.00	0.00	0.00	0.00	0.00	0.00	0.00	0.00	0.00	0.00
Fe^{3+}	0.00	0.00	0.00	0.00	0.00	0.00	0.00		1.57	1.78	1.90	1.88	1.55	2.11	1.60	1.44	1.52	1.76	1.41	1.36	1.36	1.41
Fe^{2+}	5.12	0.00	0.00	0.00	0.00	0.00	0.00		0.00	0.00	0.00	0.00	0.00	0.00	0.00	0.00	0.00	0.00	0.00	0.00	0.00	0.00
Mn	0.07	0.00	0.00	0.00	0.00	0.00	0.00		0.02	0.03	0.01	0.02	0.02	0.01	0.01	0.01	0.01	0.01	0.02	0.02	0.02	0.01
Mg	4.40	0.00	0.00	0.00	0.00	0.00	0.00		0.22	0.00	0.00	0.00	0.00	0.00	0.00	0.00	0.00	0.00	0.00	0.00	0.00	0.00
Ca	0.01	0.00	0.00	0.00	0.00	0.00	0.00		3.49	3.92	3.97	3.96	3.93	3.97	3.96	3.95	3.98	3.95	3.91	3.80	3.94	3.94
Na	0.02	0.00	0.00	0.00	0.00	0.00	0.00		0.10	0.01	0.01	0.01	0.01	0.01	0.01	0.02	0.01	0.00	0.00	0.13	0.00	0.00
K	0.00	0.00	0.00	0.00	0.00	0.00	0.00		0.00	0.00	0.00	0.00	0.00	0.00	0.00	0.00	0.00	0.00	0.00	0.00	0.00	0.00
Total	19.89	1.00	1.00	0.00	0.00	0.00	0.00		15.92	15.98	15.99	15.99	15.98	16.00	15.99	15.98	16.00	15.98	15.95	15.98	15.98	15.98

Comment	0677G 1.7+	0677G 1.7+	0677G 1.7+	0677G 1.7+	0677G 1.7+	0677G 1.7+	0677G 1.7+	0677G 1.7+	0677G 1.7+	0677G 1.7+	0677G 1.7+	0677G 1.7+	0677G 1.7+	0677G 1.7+	0677G 1.7+	0677G 1.7+	0677G 1.7+	0677G 1.7+	0677G 1.7+	0677G 1.7+	0677G 1.7+	0677G 1.7+	0677G 1.7+
Mineral	ep	ep	ep	ep	ep	ep	ep	ep	ep	ep	ep	ep	ep	ep	ep	ep	ep	ep	ep	ep	ep	ep	act
SiO_2	37.71	38.52	38.75	38.01	38.75	37.99	38.30	37.63	38.14	38.13	38.35	38.01	37.60	37.99	37.73	37.99	38.28	38.40	40.95	35.94	40.34	40.16	53.58
TiO_2	0.04	0.14	0.15	0.07	0.08	0.02	0.10	0.04	0.06	0.11	0.13	0.10	0.10	0.04	0.05	0.08	0.07	0.07	0.05	0.07	0.09	0.08	0.01
Al_2O_3	21.53	24.50	24.03	24.54	21.70	22.13	24.35	21.40	24.55	24.90	24.89	25.38	22.09	23.30	21.54	22.03	24.77	25.17	23.68	23.98	24.21	24.96	2.17
Cr_2O_3	0.02	0.02	0.01	0.03	0.00	0.02	0.02	0.00	0.04	0.05	0.00	0.00	0.04	0.00	0.02	0.03	0.03	0.06	0.03	0.00	0.00	0.02	0.02
Fe_2O_3	16.59	12.57	12.07	12.48	14.70	15.76	12.65	16.61	12.55	11.65	11.74	11.28	15.53	14.00	16.65	15.53	11.96	11.29	12.73	16.27	12.30	11.27	0.00
FeO	0.00	0.00	0.00	0.00	0.00	0.00	0.00	0.00	0.00	0.00	0.00	0.00	0.00	0.00	0.00	0.00	0.00	0.00	0.00	0.00	0.00	0.00	16.55
MnO	0.10	0.17	0.12	0.19	0.07	0.15	0.16	0.14	0.12	0.10	0.16	0.15	0.20	0.08	0.15	0.08	0.17	0.15	0.17	0.29	0.16	0.15	0.36
MgO	0.00	0.00	0.24	0.00	0.18	0.00	0.00	0.00	0.00	0.00	0.00	0.00	0.00	0.00	0.00	0.00	0.00	0.00	0.00	2.84	0.00	0.00	13.02
CaO	23.17	23.16	23.25	23.37	22.78	23.13	23.38	22.98	23.30	23.42	23.63	23.64	23.00	23.16	23.20	23.16	23.56	23.42	21.57	18.10	22.01	22.36	12.06
Na_2O	0.01	0.00	0.03	0.00	0.03	0.00	0.02	0.00	0.01	0.03	0.01	0.01	0.02	0.04	0.00	0.06	0.00	0.02	1.49	0.05	0.80	0.84	0.56
K_2O	0.00	0.00	0.00	0.00	0.00	0.01	0.00	0.02	0.01	0.00	0.00	0.00	0.02	0.03	0.00	0.00	0.00	0.00	0.01	0.01	0.01	0.01	0.08
Total	97.50	97.82	97.42	97.45	96.82	97.63	97.72	97.16	97.55	97.22	97.74	97.44	97.05	97.24	97.68	97.42	97.64	97.44	99.41	95.92	98.69	98.71	98.42
num ox	25.00	25.00	25.00	25.00	25.00	25.00	25.00	25.00	25.00	25.00	25.00	25.00	25.00	25.00	25.00	25.00	25.00	25.00	25.00	25.00	25.00	25.00	23.00
Si	6.00	6.03	6.08	5.98	6.16	6.02	6.01	6.00	5.99	6.00	6.01	5.97	5.99	6.01	5.99	6.03	6.00	6.02	6.28	5.73	6.22	6.19	7.79
Ti	0.00	0.02	0.02	0.01	0.01	0.00	0.01	0.00	0.01	0.01	0.02	0.01	0.01	0.00	0.01	0.01	0.01	0.01	0.01	0.01	0.01	0.01	0.00
Al	4.04	4.52	4.45	4.55	4.06	4.13	4.51	4.03	4.55	4.62	4.60	4.70	4.15	4.35	4.03	4.12	4.58	4.65	4.28	4.51	4.40	4.53	0.37
Cr	0.00	0.00	0.00	0.00	0.00	0.00	0.00	0.00	0.01	0.01	0.00	0.00	0.00	0.00	0.00	0.00	0.00	0.01	0.00	0.00	0.00	0.00	0.00
Fe^{3+}	1.99	1.48	1.43	1.48	1.76	1.88	1.49	1.99	1.48	1.38	1.38	1.33	1.86	1.67	1.99	1.85	1.41	1.33	1.47	1.95	1.43	1.31	0.00
Fe^{2+}	0.00	0.00	0.00	0.00	0.00	0.00	0.00	0.00	0.00	0.00	0.00	0.00	0.00	0.00	0.00	0.00	0.00	0.00	0.00	0.00	0.00	0.00	2.01
Mn	0.01	0.02	0.02	0.03	0.01	0.02	0.02	0.02	0.02	0.01	0.02	0.02	0.03	0.01	0.02	0.01	0.02	0.02	0.02	0.04	0.02	0.02	0.04
Mg	0.00	0.00	0.06	0.00	0.04	0.00	0.00	0.00	0.00	0.00	0.00	0.00	0.00	0.00	0.00	0.00	0.00	0.00	0.00	0.68	0.00	0.00	2.82
Ca	3.95	3.88	3.91	3.94	3.88	3.93	3.93	3.93	3.92	3.95	3.97	3.98	3.93	3.93	3.95	3.94	3.96	3.93	3.55	3.09	3.64	3.69	1.88
Na	0.00	0.00	0.01	0.00	0.01	0.00	0.01	0.00	0.00	0.01	0.00	0.00	0.01	0.01	0.00	0.02	0.00	0.01	0.44	0.02	0.24	0.25	0.16
K	0.00	0.00	0.00	0.00	0.00	0.00	0.00	0.00	0.00	0.00	0.00	0.00	0.00	0.01	0.00	0.00	0.00	0.00	0.00	0.00	0.00	0.00	0.02
Total	15.99	15.95	15.97	15.99	15.93	15.98	15.98	15.98	15.98	15.99	15.99	16.01	15.99	15.99	15.99	15.98	15.99	15.98	16.06	16.03	15.97	16.01	15.10

Comment	0677G 1.7+	0677G 1.5	0677G 1.6	0677G 1.7+	0677G 1.7+	0677G 1.7+	0677G 1.3	0677G 1.4	0677G 1.7+	0677G 1.7+	0677G 1.7+	0677G 1.7+	0677G 1.7+	0677G 1.7+	0677G 1.7+	0677G 1.7+	0677G 1.7+	0677G 1.7+	0677G 1.7+	0677G 1.7+
Mineral	act	act	act	act	ab	ab	ab	ab	ab	ab	ab	ab	ab	ab	ab	ab	ab	ab	ab	ab
SiO_2	54.85	54.48	54.31	53.81	69.56	69.25	70.21	69.33	69.26	69.53	69.23	70.82	69.78	69.73	70.05	69.29	70.43	70.90	69.48	69.60
TiO_2	0.83	0.00	0.03	0.01	0.02	0.02	0.00	0.00	0.00	0.01	0.04	0.01	0.03	0.01	0.02	0.02	0.00	0.00	0.04	0.02
Al_2O_3	1.56	1.19	1.31	1.40	19.81	19.70	19.93	19.84	19.60	19.74	19.82	20.24	19.74	19.84	19.86	19.82	20.09	20.26	19.95	19.97
Cr_2O_3	0.01	0.00	0.00	0.00	0.00	0.01	0.00	0.01	0.00	0.03	0.02	0.00	0.00	0.00	0.01	0.02	0.00	0.01	0.01	0.01
Fe_2O_3	0.00	0.34	0.00	0.00	0.00	0.00	0.00	0.00	0.00	0.00	0.00	0.00	0.00	0.00	0.00	0.00	0.00	0.00	0.00	0.00
FeO	15.33	15.50	16.22	16.93	0.28	0.35	0.06	0.08	0.29	0.45	0.30	0.10	0.28	0.27	0.32	0.17	0.17	0.08	0.26	0.25
MnO	0.40	0.30	0.37	0.36	0.00	0.00	0.00	0.00	0.00	0.04	0.01	0.02	0.00	0.00	0.00	0.02	0.02	0.00	0.01	0.03
MgO	13.13	13.90	13.36	12.68	0.01	0.01	0.00	0.00	0.01	0.00	0.00	0.00	0.00	0.02	0.00	0.02	0.00	0.00	0.01	0.05
CaO	12.27	12.20	12.28	12.31	0.09	0.31	0.07	0.07	0.16	0.09	0.19	0.07	0.18	0.12	0.07	0.14	0.08	0.10	0.12	0.19
Na_2O	0.80	0.41	0.34	0.32	11.80	11.76	11.97	11.96	12.04	11.94	12.17	12.16	11.98	11.99	12.04	12.24	11.81	12.05	11.98	12.24
K_2O	0.04	0.06	0.04	0.06	0.04	0.03	0.05	0.04	0.04	0.05	0.04	0.04	0.04	0.11	0.03	0.04	0.05	0.06	0.07	0.08
Total	99.22	98.34	98.26	97.88	101.60	101.44	102.30	101.34	101.40	101.88	101.82	103.46	102.03	102.09	102.41	101.77	102.64	103.45	101.95	102.43
num ox	23.00	23.00	23.00	23.00	8.00	8.00	8.00	8.00	8.00	8.00	8.00	8.00	8.00	8.00	8.00	8.00	8.00	8.00	8.00	8.00
Si	7.87	7.89	7.89	7.88	2.99	2.99	3.00	2.99	2.99	2.99	2.98	2.99	2.99	2.99	2.99	2.98	3.00	2.99	2.98	2.98
Ti	0.09	0.00	0.00	0.00	0.00	0.00	0.00	0.00	0.00	0.00	0.00	0.00	0.00	0.00	0.00	0.00	0.00	0.00	0.00	0.00
Al	0.26	0.20	0.22	0.24	1.00	1.00	1.00	1.01	1.00	1.00	1.01	1.01	1.00	1.00	1.00	1.01	1.01	1.01	1.01	1.01
Cr	0.00	0.00	0.00	0.00	0.00	0.00	0.00	0.00	0.00	0.00	0.00	0.00	0.00	0.00	0.00	0.00	0.00	0.00	0.00	0.00
Fe^{3+}	0.00	0.04	0.00	0.00	0.00	0.00	0.00	0.00	0.00	0.00	0.00	0.00	0.00	0.00	0.00	0.00	0.00	0.00	0.00	0.00
Fe^{2+}	1.84	1.88	1.97	2.07	0.01	0.01	0.00	0.00	0.01	0.02	0.01	0.00	0.01	0.01	0.01	0.01	0.01	0.00	0.01	0.01
Mn	0.05	0.04	0.05	0.04	0.00	0.00	0.00	0.00	0.00	0.00	0.00	0.00	0.00	0.00	0.00	0.00	0.00	0.00	0.00	0.00
Mg	2.81	3.00	2.89	2.77	0.00	0.00	0.00	0.00	0.00	0.00	0.00	0.00	0.00	0.00	0.00	0.00	0.00	0.00	0.00	0.00
Ca	1.89	1.89	1.91	1.93	0.00	0.01	0.00	0.00	0.01	0.00	0.01	0.00	0.01	0.01	0.00	0.01	0.00	0.00	0.01	0.01
Na	0.22	0.12	0.10	0.09	0.98	0.98	0.99	1.00	1.01	0.99	1.02	1.00	1.00	1.00	1.00	1.02	0.97	0.99	1.00	1.02
K	0.01	0.01	0.01	0.01	0.00	0.00	0.00	0.00	0.00	0.00	0.00	0.00	0.00	0.01	0.00	0.00	0.00	0.00	0.00	0.00
Total	15.03	15.06	15.04	15.05	5.00	5.00	5.00	5.01	5.02	5.01	5.02	5.00	5.01	5.01	5.01	5.03	4.99	5.00	5.01	5.03

Comment	0677G 1.7+	0677G 1.7+	0677G 1.7+	0677G 1.7+	0677G 1.7+	0677G 1.7+	0677G 1.7+	0677G 1.7+	0677 G 1.1	0677G 1.7+	0677G 1.7+	0677G 1.7+	0677G 1.7+	0677G 1.7+	0677G 1.7+	0677G 1.7+	0677G 1.7+	0677G 1.7+
Mineral	ab	ab	ab	ab	ab	ab	tit	tit	tit	qtz	qtz	qtz	qtz	?	?	?	?	?
SiO_2	69.27	67.81	66.77	68.07	64.07	62.93	30.94	34.78	30.95	99.99	100.37	100.02	100.45	84.43	48.90	44.10	42.71	61.14
TiO_2	0.00	0.04	2.34	0.00	0.02	4.49	39.51	34.54	36.67	0.00	0.01	0.00	0.00	0.01	0.04	0.10	15.26	0.01
Al_2O_3	19.80	16.40	18.51	18.45	15.34	15.79	0.77	1.56	2.36	0.01	0.00	0.01	0.01	10.45	20.36	17.26	2.45	21.26
Cr_2O_3	0.00	0.02	0.00	0.00	0.01	0.00	0.02	0.00	0.00	0.02	0.01	0.01	0.00	0.00	0.01	0.02	0.04	0.00
Fe_2O_3	0.00	0.00	0.00	0.00	0.00	0.00	0.00	0.00	0.00									
FeO	0.34	3.49	0.26	1.15	4.36	1.83	0.72	2.71	1.31	0.14	0.07	0.05	0.16	0.28	9.32	11.96	11.22	4.44
MnO	0.00	0.04	0.00	0.02	0.09	0.04	0.04	0.10	0.02	0.01	0.01	0.02	0.00	0.00	0.11	0.24	0.26	0.03
MgO	0.01	2.74	0.00	0.99	3.41	1.32	0.00	0.71	0.00	0.02	0.01	0.00	0.00	0.00	0.00	4.59	7.41	0.08
CaO	0.10	2.80	1.99	1.09	4.54	4.96	28.30	24.75	27.84	0.02	0.01	0.02	0.06	0.07	13.81	19.95	18.15	7.42
Na_2O	12.04	10.27	11.62	11.34	9.20	10.25	0.02	0.10	0.10	0.02	0.00	0.01	0.00	6.88	4.32	0.15	0.28	8.81
K_2O	0.04	0.03	0.05	0.03	0.05	0.06	0.01	0.08	0.01	0.01	0.00	0.01	0.01	0.01	0.02	0.01	0.06	0.02
Total	101.60	103.62	101.54	101.14	101.08	101.66	100.33	99.32	99.26	100.21	100.49	100.14	100.69	102.13	96.87	98.38	97.83	103.22
num ox	8.00	8.00	8.00	8.00	8.00	8.00	5.00	5.00	5.00	8.00	8.00	8.00	23.00	25.00	8.00	25.00	8.00	23.00
Si	2.98	2.94	2.91	2.97	2.88	2.81	1.01	1.13	1.02	4.00	4.00	4.00	11.49	10.86	2.43	7.00	2.23	7.80
Ti	0.00	0.00	0.08	0.00	0.00	0.15	0.97	0.84	0.91	0.00	0.00	0.00	0.00	0.00	0.00	0.01	0.60	0.00
Al	1.01	0.84	0.95	0.95	0.81	0.83	0.03	0.06	0.09	0.00	0.00	0.00	0.00	1.58	1.19	3.23	0.15	3.20
Cr	0.00	0.00	0.00	0.00	0.00	0.00	0.00	0.00	0.00	0.00	0.00	0.00	0.00	0.00	0.00	0.00	0.00	0.00
Fe^{3+}	0.00	0.00	0.00	0.00	0.00	0.00	0.00	0.00	0.00	0.00	0.00	0.00	0.00	0.00	0.00	0.00	0.00	0.00
Fe^{2+}	0.01	0.13	0.01	0.04	0.16	0.07	0.02	0.07	0.04	0.00	0.00	0.00	0.02	0.03	0.39	1.59	0.49	0.47
Mn	0.00	0.00	0.00	0.00	0.00	0.00	0.00	0.00	0.00	0.00	0.00	0.00	0.00	0.00	0.00	0.03	0.01	0.00
Mg	0.00	0.18	0.00	0.06	0.23	0.09	0.00	0.03	0.00	0.00	0.00	0.00	0.00	0.00	0.00	1.09	0.58	0.02
Ca	0.00	0.13	0.09	0.05	0.22	0.24	0.99	0.86	0.98	0.00	0.00	0.00	0.01	0.01	0.74	3.39	1.02	1.01
Na	1.01	0.86	0.98	0.96	0.80	0.89	0.00	0.01	0.01	0.00	0.00	0.00	0.00	1.71	0.42	0.04	0.03	2.18
K	0.00	0.00	0.00	0.00	0.00	0.00	0.00	0.00	0.00	0.00	0.00	0.00	0.00	0.00	0.00	0.00	0.00	0.00
Total	5.02	5.07	5.03	5.04	5.11	5.07	3.01	3.01	3.04	4.00	4.00	4.00	11.51	14.20	5.18	16.39	5.11	14.69

Appendix D: Field Structural Measurements

S1

Strike	Dip	Dip-dir	Strike	Dip	Dip-dir	Strike	Dip	Dip-dir	Strike	Dip	Dip-dir	Strike	Dip	Dip-dir
	Ampae		128.5 /	25 /	N	64.5 /	38 /	NW	121.5 /	15 /	N	105.5 /	24 /	S
291.5 /	31 /	N	123.5 /	19 /	N	351.5 /	12 /	N	120.5 /	35 /	N	104.5 /	44 /	S
294.5 /	33 /	N	122.5 /	23 /	N		Biniguni		277.5 /	17 /	N	21.5 /	65 /	W
296.5 /	35 /	N	126.5 /	24 /	N	84.5 /	13 /	NE	317.5 /	16 /	NE	152.5 /	37 /	SW
298.5 /	34 /	N	134.5 /	24 /	N	147.5 /	22 /	NE	322.5 /	20 /	NE	93.5 /	31 /	S
285.5 /	21 /	N	126.5 /	18 /	N	112.5 /	20 /	NE	302.5 /	20 /	NE	145.5 /	23 /	SW
288.5 /	22 /	N	129.5 /	24 /	N	117.5 /	12 /	NE	320.5 /	18 /	NE	52.5 /	18 /	NW
293.5 /	25 /	N	110.5 /	27 /	N	307.5 /	21 /	NE	318.5 /	14 /	NE	160.5 /	41 /	W
297.5 /	26 /	N	88.5 /	13 /	N	312.5 /	22 /	NE	329.5 /	15 /	NE	111.5 /	17 /	S
306.5 /	20 /	N	120.5 /	27 /	N	305.5 /	17 /	NE	314.5 /	18 /	NE	147.5 /	33 /	SW
284.5 /	25 /	N	112.5 /	26 /	N	317.5 /	20 /	NE	295.5 /	23 /	NE	178.5 /	40 /	W
283.5 /	17 /	N	128.5 /	25 /	N	311.5 /	25 /	NE	307.5 /	19 /	NE	131.5 /	15 /	SW
277.5 /	15 /	N	97.5 /	21 /	N	251.5 /	33 /	N	305.5 /	10 /	NE	92.5 /	36 /	S
295.5 /	26 /	N	77.5 /	14 /	N	277.5 /	24 /	N	326.5 /	12 /	NE	115.5 /	17 /	S
323.5 /	24 /	N	104.5 /	29 /	N	313.5 /	35 /	N	309.5 /	13 /	NE	31.5 /	63 /	W
279.5 /	21 /	N	131.5 /	22 /	N	232.5 /	10 /	NW	353.5 /	6 /	E	241.5 /	60 /	NW
330.5 /	23 /	NE	143.5 /	15 /	NE	261.5 /	14 /	NW		Gintoe		83.5 /	31 /	S
303.5 /	21 /	N	171.5 /	17 /	NE	241.5 /	17 /	NW	242.5 /	29 /	N	139.5 /	16 /	SW
312.5 /	20 /	N	120.5 /	17 /	N	68.5 /	16 /	NE	307.5 /	24 /	N	36.5 /	22 /	NW
269.5 /	19 /	N	115.5 /	24 /	N	163.5 /	19 /	NE	311.5 /	25 /	N	143.5 /	34 /	SW
277.5 /	26 /	N	116.5 /	16 /	N	148.5 /	15 /	NE		Goraedu		103.5 /	30 /	S
309.5 /	11 /	N	94.5 /	5 /	N	126.5 /	24 /	NE	329.5 /	16 /	NE	154.5 /	40 /	SW
297.5 /	15 /	N	109.5 /	17 /	N	96.5 /	29 /	N	307.5 /	19 /	NE	177.5 /	42 /	W
281.5 /	11 /	N	132.5 /	21 /	N	90.5 /	17 /	N	171.5 /	40 /	NE	76.5 /	12 /	S
301.5 /	14 /	N	69.5 /	14 /	N	63.5 /	30 /	N	281.5 /	23 /	NE	106.5 /	38 /	S
257.5 /	14 /	N	129.5 /	10 /	N	78.5 /	19 /	N	128.5 /	47 /	NE	133.5 /	36 /	SW
323.5 /	11 /	N	98.5 /	23 /	N	83.5 /	28 /	N	83.5 /	24 /	N	39.5 /	41 /	W
286.5 /	17 /	N	97.5 /	15 /	N	302.5 /	9 /	N	140.5 /	31 /	NE	50.5 /	52 /	NW
280.5 /	11 /	N	85.5 /	15 /	N	73.5 /	14 /	N	299.5 /	14 /	NE	125.5 /	19 /	S
300.5 /	15 /	N	88.5 /	16 /	N	118.5 /	35 /	N	122.5 /	35 /	NE	144.5 /	17 /	SW
268.5 /	16 /	N	92.5 /	25 /	N	92.5 /	25 /	N	232.5 /	30 /	NE	42.5 /	22 /	NW
290.5 /	18 /	N	118.5 /	21 /	N	89.5 /	19 /	N	133.5 /	32 /	NE	144.5 /	41 /	SW
269.5 /	19 /	N	76.5 /	23 /	N	95.5 /	16 /	N	124.5 /	23 /	NE	101.5 /	19 /	S
280.5 /	20 /	N	123.5 /	10 /	N	113.5 /	25 /	N	309.5 /	19 /	NE	144.5 /	27 /	SW
313.5 /	15 /	N	89.5 /	26 /	N	110.5 /	28 /	N	120.5 /	25 /	NE	83.5 /	22 /	S
282.5 /	16 /	N	156.5 /	19 /	N	72.5 /	11 /	N	117.5 /	20 /	NE	80.5 /	29 /	S
302.5 /	16 /	N	112.5 /	11 /	N	186.5 /	14 /	E	322.5 /	20 /	NE	100.5 /	39 /	S
314.5 /	16 /	N	113.5 /	25 /	N	137.5 /	18 /	NE		Gwariu		25.5 /	54 /	W
311.5 /	16 /	N		Bebegi		124.5 /	8 /	NE	284.5 /	78 /	S	179.5 /	30 /	W
310.5 /	14 /	N	257.5 /	35 /	NW	98.5 /	10 /	N	276.5 /	54 /	S	84.5 /	38 /	S
288.5 /	22 /	N	281.5 /	32 /	N	108.5 /	20 /	N	257.5 /	33 /	S	78.5 /	39 /	N
307.5 /	25 /	N	282.5 /	45 /	N	84.5 /	8 /	N	309.5 /	24 /	SW	52.5 /	33 /	NW
297.5 /	23 /	N	65.5 /	42 /	NW	60.5 /	11 /	NW	307.5 /	21 /	SW	53.5 /	54 /	NW
298.5 /	23 /	N	271.5 /	41 /	N	69.5 /	10 /	N	309.5 /	27 /	SW	136.5 /	45 /	SW
257.5 /	49 /	N	68.5 /	51 /	NW	122.5 /	19 /	N	327.5 /	21 /	SW	136.5 /	39 /	SW
10.5 /	31 /	E	265.5 /	45 /	NW	119.5 /	15 /	N	113.5 /	35 /	SW	129.5 /	37 /	SW
206.5 /	36 /	W	73.5 /	39 /	NW	131.5 /	16 /	N	112.5 /	42 /	SW	84.5 /	36 /	S
302.5 /	17 /	N	267.5 /	29 /	N	118.5 /	13 /	N	117.5 /	40 /	S		Koroton	
302.5 /	15 /	N	72.5 /	34 /	NW	72.5 /	10 /	N	237.5 /	18 /	NW	275.5 /	19 /	N
317.5 /	21 /	NE	254.5 /	35 /	NW	82.5 /	5 /	N	84.5 /	35 /	NW	60.5 /	39 /	N
304.5 /	27 /	N	92.5 /	47 /	N	65.5 /	11 /	N	134.5 /	33 /	SW	57.5 /	33 /	N
97.5 /	85 /	N	268.5 /	50 /	N	99.5 /	20 /	N	133.5 /	46 /	S	72.5 /	27 /	N
138.5 /	23 /	NE	66.5 /	24 /	NW	83.5 /	23 /	N	126.5 /	59 /	SW	100.5 /	22 /	N
125.5 /	22 /	N	104.5 /	47 /	N	85.5 /	31 /	N	134.5 /	61 /	SW	86.5 /	18 /	N
101.5 /	23 /	N	58.5 /	51 /	NW	90.5 /	22 /	N	94.5 /	13 /	S	77.5 /	11 /	N
108.5 /	30 /	N	53.5 /	4 /	NW	92.5 /	24 /	N	31.5 /	10 /	E	75.5 /	21 /	N
104.5 /	20 /	N	81.5 /	35 /	NW	115.5 /	13 /	N	80.5 /	14 /	S	113.5 /	17 /	N
107.5 /	9 /	N		Beboo			Biniguni		142.5 /	27 /	SW	71.5 /	23 /	N
156.5 /	16 /	NE	252.5 /	33 /	NW	141.5 /	22 /	NE	110.5 /	24 /	S	281.5 /	21 /	N

S1

Strike	Dip	Dip-dir
292.5 /	29 /	N
141.5 /	22 /	NE
Oom		
268.5 /	24 /	N
Totoe		
277.5 /	7 /	N
232.5 /	10 /	N
Wange		
300.5 /	22 /	NE
84.5 /	19 /	N
307.5 /	20 /	NE
95.5 /	16 /	N
291.5 /	25 /	N
82.5 /	25 /	NW
257.5 /	31 /	NW
278.5 /	35 /	N
287.5 /	23 /	NE
319.5 /	28 /	NE
322.5 /	23 /	NE
254.5 /	13 /	N
278.5 /	13 /	N
Wareum		
243.5 /	32 /	N
Wotagan		
272.5 /	10 /	N
266.5 /	12 /	N
277.5 /	16 /	N
Yaitongerat		
276.5 /	19 /	N
Yange		
317.5 /	23 /	NE
312.5 /	19 /	NE
316.5 /	25 /	NE
319.5 /	34 /	NE
317.5 /	21 /	NE
83.5 /	30 /	N
64.5 /	35 /	NW
315.5 /	22 /	NE
295.5 /	31 /	NE
307.5 /	30 /	NE
119.5 /	32 /	NE
301.5 /	30 /	NE
123.5 /	26 /	NE
90.5 /	23 /	NE
313.5 /	18 /	NE
15.5 /	21 /	NW
315.5 /	17 /	NE
58.5 /	28 /	NW
161.5 /	17 /	SW
317.5 /	62 /	SW
Yuga		
155.5 /	35 /	NE
57.5 /	37 /	NW
54.5 /	31 /	NW
254.5 /	26 /	NW
74.5 /	17 /	NW
127.5 /	20 /	NE
254.5 /	21 /	N
112.5 /	17 /	N
142.5 /	20 /	NE
323.5 /	21 /	NE
251.5 /	26 /	N
130.5 /	20 /	NE
117.5 /	16 /	N
268.5 /	24 /	N
295.5 /	38 /	N
242.5 /	30 /	N
46.5 /	28 /	NW
52.5 /	44 /	NW
110.5 /	33 /	N
62.5 /	30 /	NW
69.5 /	29 /	NW
93.5 /	21 /	N
120.5 /	12 /	N
133.5 /	25 /	NE
107.5 /	23 /	N
86.5 /	15 /	N
Yutmae		
301.5 /	23 /	NE
295.5 /	36 /	NE
297.5 /	30 /	NE
118.5 /	13 /	NE
313.5 /	49 /	NE
298.5 /	50 /	NE
129.5 /	23 /	NE
287.5 /	14 /	NE
127.5 /	14 /	NE
310.5 /	34 /	NE
Aro		
167.5 /	25 /	N
147.5 /	8 /	NE
162.5 /	21 /	NE
150.5 /	20 /	NE
147.5 /	26 /	NE
165.5 /	24 /	NE
156.5 /	31 /	NE
154.5 /	35 /	NE
160.5 /	23 /	NE
117.5 /	27 /	NE
130.5 /	22 /	NE
154.5 /	28 /	NE
169.5 /	28 /	NE
Biyawap		
292.5 /	50 /	NE
Wymame		
287.5 /	25 /	NE
46.5 /	24 /	NE
118.5 /	23 /	NE
115.5 /	12 /	NE
283.5 /	20 /	NE
317.5 /	20 /	NE
Yatap		
201.5 /	31 /	E
27.5 /	31 /	E

S2

Strike	Dip	Dip-dir
Aro		
202.5 /	27 /	SE
197.5 /	5 /	SE
177.5 /	26 /	E
182.5 /	36 /	E
11.5 /	35 /	E
182.5 /	28 /	E
Biyawap		
10.5 /	36 /	E
12.5 /	37 /	E
363.5 /	37 /	E
25.5 /	33 /	E
15.5 /	25 /	E
362.5 /	37 /	E
19.5 /	50 /	E
17.5 /	37 /	E
12.5 /	31 /	E
17.5 /	41 /	E
22.5 /	40 /	E
22.5 /	27 /	E
25.5 /	21 /	E
19.5 /	28 /	E
10.5 /	36 /	E
292.5 /	50 /	E
12.5 /	37 /	E
363.5 /	37 /	E
25.5 /	33 /	E
15.5 /	25 /	E
362.5 /	37 /	E
19.5 /	50 /	E
17.5 /	37 /	E
12.5 /	31 /	E
17.5 /	41 /	E
22.5 /	40 /	E
22.5 /	27 /	E
25.5 /	21 /	E
19.5 /	28 /	E
Biyawap		
183.5 /	25 /	E
16.5 /	25 /	E

L1

Plunge	Trend
Ampae	
33 /	24.5
32 /	30.5
26 /	18.5
34 /	21.5
22 /	23.5
21 /	24.5
24 /	23.5
26 /	22.5
19 /	18.5
24 /	11.5
16 /	14.5
16 /	21.5
15 /	8.5
24 /	19.5
20 /	17.5
20 /	33.5
20 /	30.5
19 /	28.5
21 /	7.5
16 /	19.5
25 /	17.5
12 /	13.5
15 /	17.5
13 /	22.5
15 /	12.5
12 /	18.5
14 /	33.5
15 /	17.5
11 /	22.5
15 /	30.5
17 /	16.5
17 /	17.5
17 /	14.5
13 /	19.5
19 /	7.5
8 /	12.5
17 /	17.5
18 /	27.5
16 /	29.5
15 /	28.5
12 /	30.5
22 /	15.5
25 /	16.5
23 /	11.5
20 /	15.5
10 /	350.5
15 /	349.5
17 /	353.5
24 /	349.5
19 /	348.5
8 /	345.5
1 /	349.5
17 /	346.5
17 /	347.5
12 /	338.5
18 /	351.5
15 /	345.5
14 /	338.5
13 /	344.5
18 /	346.5
14 /	344.5
21 /	344.5
18 /	342.5
16 /	349.5
17 /	354.5
14 /	347.5
26 /	345.5
18 /	343.5
15 /	21.5
8 /	14.5
16 /	5.5
20 /	342.5
14 /	352.5
5 /	358.5
14 /	355.5
20 /	11.5
15 /	351.5
11 /	359.5
22 /	4.5
15 /	7.5
14 /	8.5
16 /	348.5
24 /	357.5
18 /	352.5
22 /	357.5
8 /	345.5
26 /	0.5
12 /	2.5
11 /	350.5
21 /	3.5
Bebegi	
37 /	7.5
38 /	11.5
21 /	10.5
48 /	10.5
15 /	42.5
37 /	25.5
32 /	8.5
23 /	30.5
36 /	356.5
26 /	4.5
39 /	14.5
Beboo	
3 /	32.5
Biniguni	
8 /	31.5
12 /	19.5
16 /	25.5
17 /	25.5
13 /	53.5
11 /	60.5
7 /	40.5
9 /	32.5
11 /	44.5
8 /	24.5
11 /	34.5
14 /	48.5
11 /	24.5
9 /	25.5
11 /	23.5
15 /	34.5
20 /	17.5
18 /	17.5
18 /	358.5
14 /	32.5
12 /	37.5
13 /	31.5
9 /	26.5
10 /	25.5
31 /	37.5
19 /	29.5
18 /	36.5
17 /	44.5
24 /	28.5
26 /	3.5
6 /	35.5
9 /	46.5
16 /	36.5
9 /	38.5
10 /	13.5
7 /	17.5
9 /	20.5
5 /	355.5
8 /	14.5
18 /	22.5
11 /	27.5
9 /	357.5
8 /	12.5
6 /	5.5
4 /	357.5
14 /	337.5
15 /	32.5
21 /	8.5
30 /	22.5
19 /	7.5
14 /	32.5
12 /	35.5
16 /	39.5
14 /	17.5
33 /	19.5
9 /	32.5
16 /	57.5
20 /	54.5
17 /	64.5
18 /	52.5
15 /	56.5
15 /	57.5
19 /	43.5
17 /	49.5
20 /	45.5
11 /	29.5
14 /	33.5
15 /	31.5
7 /	48.5
Gintoe	
17 /	13.5
22 /	16.5
25 /	11.5
Gwariu	
15 /	164.5
5 /	301.5
17 /	193.5
34 /	326.5
2 /	153.5
36 /	325.5
Koroton	
19 /	39.5
13 /	45.5
9 /	42.5
7 /	29.5
14 /	10.5
23 /	17.5
21 /	13.5
24 /	6.5
23 /	15.5
Oom	
26 /	2.5
Totoe	
5 /	351.5
12 /	352.5
Wareum	
24 /	16.5
Wotagan	
15 /	357.5
Yaitongerat	
20 /	42.5
Yange	
25 /	352.5
Yuga	
16 /	8.5
32 /	9.5
21 /	13.5
20 /	17.5
17 /	18.5
17 /	27.5
10 /	17.5
28 /	21.5
23 /	22.5
19 /	10.5
Aro	
19 /	29.5
9 /	30.5
4 /	28.5
8 /	33.5
3 /	33.5
1 /	31.5
Biyawap	
26 /	18.5
Urawa	
22 /	162.5
33 /	149.5
Wymame	
12 /	51.5
21 /	36.5
19 /	27.5
Yatap	
6 /	247.5

L2

Plunge	Trend
Aro	
22 /	87.5
21 /	73.5
Biyawap	
31 /	115.5
31 /	115.5
26 /	119.5
37 /	97.5
37 /	117.5
28 /	98.5
35 /	107.5
9 /	113.5
10 /	108.5
46 /	119.5
20 /	97.5
31 /	115.5
31 /	115.5
37 /	97.5
37 /	117.5
28 /	98.5
35 /	107.5
9 /	113.5
10 /	108.5
46 /	119.5
20 /	97.5

DYKE

Strike	Dip	Dip-dir
Biniguni Dyke		
315.5 /	57 /	SW
221.5 /	64 /	SW
152.5 /	54 /	SW
144.5 /	77 /	SW
149.5 /	67 /	SW
150.5 /	55 /	SW
165.5 /	85 /	SW
127.5 /	65 /	SW
143.5 /	75 /	SW

S0

Strike	Dip	Dip-dir
	Aro	
312.5 /	35 /	NE
186.5 /	26 /	E
	Dare	
241.5 /	55 /	NW
62.5 /	58 /	NW
43.5 /	44 /	W
29.5 /	54 /	W
220.5 /	51 /	NW
42.5 /	90 /	SW
134.5 /	20 /	SW
149.5 /	22 /	SW
151.5 /	15 /	SW
132.5 /	25 /	SW
	Enowibidi	
15.5 /	24 /	E
35.5 /	28 /	E
35.5 /	26 /	E
	Kwekweme	
7.5 /	18 /	E
9.5 /	34 /	E
21.5 /	43 /	E
	Nowandowan	
132.5 /	78 /	NE
	Pumani	
94.5 /	18 /	S
80.5 /	29 /	S
94.5 /	30 /	S
	Urawa	
347.5 /	15 /	NE
177.5 /	20 /	NE
37.5 /	25 /	E
47.5 /	37 /	SE

FAULT PLANE			SLICKENSIDE	
Strike	Dip	Dip-dir	Plunge	Trend
Ampae			Ampae	
77.5 /	68 /	S	15 /	51.5
291.5 /	89 /	N	Aro	
299.5 /	86 /	N	17 /	191.5
Biniguni			68 /	161.5
267.5 /	72 /	S	Dare	
231.5 /	19 /	NW	18 /	315.5
282.5 /	47 /	N	29 /	347.5
297.5 /	71 /	S	Kwekweme	
241.5 /	77 /	NW	37 /	203.5
233.5 /	70 /	NW		
313.5 /	57 /	NE		
Gwariu				
101.5 /	24 /	N		
Wange				
186.5 /	50 /	E		
161.5 /	48 /	E		
174.5 /	51 /	E		
Aro				
247.5 /	15 /	SE		
62.5 /	64 /	SE		
Dare				
139.5 /	87 /	N		
117.5 /	75 /	N		
171.5 /	77 /	W		
125.5 /	60 /	N		
Kwekweme				
93.5 /	41 /	SE		
Nowandowan				
363.5 /	40 /	E		
217.5 /	40 /	E		

S1(from Davies and Smith, 1974)

Strike	Dip	Dip-dir	Strike	Dip	Dip-dir
Suckling-Dayman			240	60	NW
25	30	SE	300	35	NE
30	20	SE	210	40	W
35	20	SE	160	40	SW
355	15	E	155	45	SW
320	15	NE	130	70	SW
275	15	N	150	45	SW
260	10	NNW	80	35	S
265	30	N	80	40	S
140	35	SW	75	15	S
280	30	N	55	30	SE
270	10	N	60	50	SE
20	10	W	60	60	SE
120	10	SW	95	30	S
215	10	NW	85	45	S
200	20	W	110	30	S
220	20	NW	45	30	NW
40	30	SE	40	70	SE
70	10	SE	75	70	S
125	25	SW	45	40	SE
100	20	S	100	55	S
310	15	N	155	45	SW
200	15	NW	80	30	S
180	10	W	90	20	S
35	90		50	30	SE
155	35	SW	0	25	E
260	30	N	5	25	E
310	15	NE	45	15	SE
340	15	E	50	50	SE
260	15	N	260	20	N
280	20	N	320	30	NE
275	20	N	215	60	W
320	15	NE	280	35	NE
250	15	NW	190	40	W
270	15	N	165	45	W
265	20	N	90	45	S
260	25	N	80	60	S
270	20	N	90	25	S
300	30	N	330	30	NE
295	20	N	45	30	SE
305	35	NE	40	50	SE
310	25	NE	40	30	SE
10	7	E	35	25	SE
310	40	NE	40	15	SE
280	50	N			
265	50	N			
280	25	N			
10	10	N			
30	80	E			
250	10	N			
270	35	N			
20	15	E			

Appendix E: Vorticity Measurements

X	Z	X/Z	Angle (°)	Sense of Shear	Mantled Porphyroclast Type
			Sample 0677G		
47	9	5.2	-3	Top-to-the-left	σ
27	11	2.45	8	Top-to-the-right	σ
61	33	1.84	-9	Top-to-the-left	σ
28	20	1.4	33	Top-to-the-right	σ
39	23	1.7	53	Top-to-the-left	σ
25	16	1.56	-22	Top-to-the-left	σ
64	20	3.2	15	Top-to-the-right	σ
58	19	30	2	Top-to-the-right	σ
19	11	1.72	58	Top-to-the-right	σ
13	9	1.44	-29	Top-to-the-left	σ
20	13	1.53	-12	Top-to-the-left	σ
10	8	1.25	58	Top-to-the-right	δ
110	60	1.83	18	Top-to-the-right	σ
32	14	2.28	18	Top-to-the-right	σ
38	15	2.53	-42	Top-to-the-left	σ
70	40	1.75	-72	Top-to-the-left	σ
65	55	1.18	-38	Top-to-the-left	σ
18	9	2	-16	Top-to-the-left	σ
17	8	2.12	6	Top-to-the-right	σ
40	19	2.1	-74	Top-to-the-left	σ
12	9	1.33	-16	Top-to-the-left	σ
15	10	1.5	14	Top-to-the-right	σ
			Sample 0677G		
10	6	1.7	20	Top-to-the-right	σ
15	7	2.1	13	Top-to-the-right	σ
16	7	2.3	14	Top-to-the-right	σ
82	31	2.6	17	Top-to-the-right	σ
10	7	1.4	15	Top-to-the-right	σ
7	4	1.7	20	Top-to-the-right	σ
18	6	3	-18	Top-to-the-left	σ
13	10	1.3	6	Top-to-the-right	σ
10	6	1.7	17	Top-to-the-right	σ
12	8	1.5	-24	Top-to-the-left	σ
11	7	1.6	-10	Top-to-the-left	σ
7	3	2.3	-6	Top-to-the-left	σ
7	3	2.3	32	Top-to-the-right	σ
5	4	1.2	-68	Top-to-the-right	σ
6	4	1.5	82	Top-to-the-right	σ
16	8	2	70	Top-to-the-right	σ
7	4	1.7	-27	Top-to-the-left	σ
60	45	1.3	-52	Top-to-the-left	σ
50	17	2.9	-5	Top-to-the-left	σ
90	30	3	26	Top-to-the-right	σ
22	10	2.2	-35	Top-to-the-left	σ